Etude d'architecture multicellulaire avec le microenvironnement contrôlé

Qingzong Tseng

UNIVERSITÉ DE GRENOBLE

Thesis

For the degree of

Doctor of Philosophy

Université de Grenoble

Specialty : **Physics for life science**

Presented by

Qingzong TSENG

Supervised by **Manuel THERY**

prepared in the laboratory **Physics of the cytoskeleton and morphogenesis, LPCV**
within **the graduate school of Physics**

Study of multicellular architecture with controlled microenvironment

Thesis defended the **1st of July 2011**,
in front of the committee:

Mr. Bruno GOUD
Institut Curie, France
Mr. Carl-Philipp HEISENBERG
Institute of Science and Technology, Austria
Mr. Fernando MARTIN-BELMONTE
Centro de Biología Molecular Severo Ochoa, Spain
Ms. Corinne ALBIGES-RIZO
Institut Albert Bonniot, France
Mr. Marc BILLAUD
Institut Albert Bonniot, France
Mr. Manuel THERY
Commissariat à l'Energie Atomique et aux Energies Alternatives, France

UNIVERSITÉ DE GRENOBLE

THÈSE

Pour obtenir le grade de

DOCTEUR DE L'UNIVERSITÉ DE GRENOBLE

Spécialité : **Physique pour les sciences du vivant**

Arrêté ministériel : 7 août 2006

Présentée par

Qingzong TSENG

Thèse dirigée par **Manuel THERY**

préparée au sein du **Physique du cytosquelette et de la morphogenèse,** Laboratoire physiologie cellulaire & végétale **dans l'École Doctorale de Physique**

Étude d'Architecture Multicellulaire dans un Microenvironnement Contrôlé

Thèse soutenue publiquement le **1ère juillet 2011**
devant le jury composé de :

Mme. Corinne ALBIGES-RIZO
CNRS, Institut Albert Bonniot (Président)
M. Carl-Philipp, HEISENBERG
Institute of Science and Technology, Austria (Rapporteur)
M. Fernando MARTIN-BELMONTE
Centro de Biología Molecular Severo Ochoa, Spain (Rapporteur)
M. Bruno, GOUD
CNRS, Institut Curie (Membre)
M. Marc BILLAUD
CNRS, Institut Albert Bonniot (Membre)
M. Manuel THERY
CEA, Insititut de Recherches en Technologies et Sciences pour le Vivant (Membre)

Abstract

This thesis dissertation is comprised of three major parts. The first part devotes to all the technological developments that have been realized in my thesis study. These developments in microfabrication, in image acquisition and analysis, and in the traction force analysis had solved various problems we have encountered during our study of epithelial architecture.

The second part describes the study of the spatial organization of the adhesion systems in epithelia. From their polarity, their functioning, to their remodeling, the epithelial architecture is deeply linked with the adhesion systems. With the capability to well define the location of cell-matrix interaction, we examined how the intercellular adhesion was organized according to the cell-matrix adhesion. Our results highlighted the instructive role of cell-matrix adhesion in organizing the intercellular adhesion. This organization subsequently governed the internal polarity which was indicated by the centrosome positioning. During epithelial remodeling, both the adhesion system and internal polarity were subjected to modification. Nevertheless they could be regulated differently depending on the context of remodeling.

The last part is focused on the physical aspect of the epithelial architecture. Apart from the biochemical signaling network, mechanical force is also a substantial ingredient in morphogenesis. Together with our techniques in micropatterning the soft gel, the development of software for traction force microscope, and our knowledge of cell-cell positioning, we were able to analyze precisely the mechanical property of the multicellular architecture. We found that the cellular contractility was modulated by the spatial organization of the adhesion system. It permitted us to complete the current physical model of epithelial geometry with an anisotropic term for contractility. This new physical model could effectively account for the cell positioning on various matrix geometries.

Résumé

Ce manuscrit de thèse est composé de trois parties dédiées aux développements technologiques nécessaires à l'étude de la polarité et des contraintes mécaniques dans les cellules épithéliales.

La première partie décrit les développements technologiques et méthodologiques qui ont été réalisés en micro-fabrication et traitement de surface, acquisition et analyse d'image, et mesure des forces de traction.

La deuxième partie décrit l'étude de l'organisation spatiale du système d'adhérence des cellules épithéliales. De la régulation de leur polarité à celle de leur fonction, l'architecture des cellules épithéliales est profondément liée à leur système d'adhérence. Nous avons utilisé les micropatrons adhésifs pour contrôler la géométrie de la matrice extra-cellulaire pour examiner l'effet de l'adhérence des cellules avec la matrice sur la position des zones d'adhérence intercellulaire. Nos résultats montrent que l'organisation spatiale de l'adhérence cellule-matrice joue un rôle déterminant sur celle de l'adhérence intercellulaire. Ils montrent également que cette organisation dirige ensuite la position du centrosome et l'orientation de l'ensemble de la polarité interne. Lors d'une réorganisation spatiale de l'épithélium, comme c'est le cas au cours de la transition épithélium-mésenchyme, les systèmes d'adhérence et la polarité interne subissent tous les deux de profondes modifications. Néanmoins, les cellules semblent capables de les réguler de façon indépendante selon le type de stimulus qui induit la réorganisation.

La dernière partie est une analyse des paramètres physiques impliqués dans l'architecture épithéliale. En parallèle des régulations biochimiques, les contraintes mécaniques jouent également un rôle fondamental dans la régulation des processus morphogenétiques. L'association de l'ensemble de nos développements technologiques (patterning de substrat déformable, logiciel de détection et de mesure de force, contrôle du positionnement des cellules) nous a permis d'analyser précisément les propriétés mécaniques des architectures multicellulaires. Nous avons découvert que l'organisation spatiale du système adhérence était un régulateur majeur de l'intensité et de la répartition des forces intra-cellulaires. Cette observation nous a permis de proposer une modification du modèle actuel de distribution des contraintes dans un épithélium qui prend en compte l'anisotropie des forces inter-cellulaires en réponse à l'hétérogénéité de la matrice extra-cellulaire. Ce nouveau modèle physique permet de rendre compte des positions adoptées par les cellules en réponse aux différentes géométries de la matrice extra-cellulaire.

For Dominique Chauvat, a great teacher in ENS Cachan.

Without his passion and patience I won't be able to embrace physics today.

Acknowledgments

First and foremost, I would like to thank my wife Yuming. She accompanied me through every hard day. Without her relentless support during the last five years, the life in a foreign country would have been much more difficult.

I owe my gratitude to my thesis supervisor Manuel Théry. He is more like a friend than a boss. He always encouraged me no matter how the result was. He shared with me his enthusiasm and knowledge in science without reserve. He left me great freedom in my work so that I could have opportunities to develop new techniques and learn new things.

Martial Balland, a great friend in science and climbing. He enlightened me on the traction force microscopy. The scientific discussion with him both in the lab and on the cliff made science more exciting.

François Amblard, my supervisor of master's thesis, for his guidance and mentorship. He introduced me to the field of biophysics.

Laurent Blanchoin, the “chef” of our lab, with his support we could focus more on science and worry less about administrative works and budget issue. He was also the propeller of the lab that moved everyone forward. I also want to thank all the people in our lab, only with their help and support I could have finish my thesis work smoothly. Christophe Guerin, Jérémie Gaillard and Cécile Prunier, they kept the lab well organized and did a lot of common works for us.. Anne-Cécile Reymann and Cristian Suarez helped me many times on administrative work which was difficult for a foreign student like me.

Odile Filhol-Cochet for all her help in cell culture, reagents and her knowledge in EMT. Alexandre Deshière, he helped me make the fluorescent protein constructs and made the lentivirus for us. Eve Duchemin-Pelletier, she kindly kept the cells for my experiment and helped make the most boring video microscope experiments.

The CYTOO cell architect for their material support. Maria-Luisa Calvo-Munoz and Joanne Young, they helped me on the micropatterned substrate and the videomicroscope.

The Biopuce lab for their sharing of equipment, working bench, and the cell culture room.

Last but not least, thanks to my family in Taiwan for their remote but spiritual support.

Table of contents

1 General Introduction

One of the most striking features of the multicellular organism is the specialization and orchestration of individual cells to form complex tissues and organs. How this highly ordered organization is achieved during the development process and how it is maintained during the lifespan of the organism have always been fascinating topics.

Epithelia can be considered as the most primordial tissue. It emerged early in ancient metazoans such as sponges and cnidarians(Nichols et al., 2006). Coherent adhesion between cells and cellular polarity, i.e. asymmetrical distribution of cellular components, are the crucial features of epithelia. They made possible the compartmentalization of animal body and directional transportation of substances, and afterward, the development of a more complex body plan (Cereijido et al., 2004).

In complex metazoans, the epithelia participate in various functions such as digestion, reproduction, excretion, and hormonal signaling. There is also a wide morphological diversity in epithelial tissue. They are capable of forming highly ordered pattern such as the drosophila lens cells and the elaborated tubular structures in our kidney. The mechanism of epithelia morphogenesis and pattern formation is not only an intriguing topics in biology but also in physics.

Epithelial morphogenesis processes are widely studied by using embryos of insects, amphibian, or fishes. They are living examples with integral natural machineries of morphgenesis. Furthermore, the extensive genetic toolbox for those model organisms facilitated the deciphering of the molecular network behind epithelial morphogenesis. However, the inherited complexity of the *in vivo* system make it difficult to control many experimental parameters, not to mention the cost, the labor, and the ethic issues for the study of mammalian embryos.

Cell culture exists as a simplified experimental system. Even though cells are maintained in a context rather different than in the real tissue, we can gain more control over the system. Furthermore, it greatly reduces the inconveniences of manipulating, imaging, and maintaining living organisms.

Micropatterned ECM protein appeared to be a good way to further manipulate the cell-matrix interaction and cell shapes for cultured cells. As those parameters can be maintained as constant, cell-to-cell variability is minimized and statistical analysis become more reliable.

The objective of present study is to examine the epithelial architecture in a controlled microenvironment. With a precise localization of cell-matrix and cell-cell adhesions, we would like to gain a different perspective on both the biochemical signaling network and the mechanical properties of the epithelial morphogenesis. Novel experimental methods were developed during this study to deal with specific questions. Therefore, I will first dedicate the next chapter to all these technological developments. Afterward, it will be more focused on biological system. The study of the epithelial adhesion systems and polarity is presented in Chapter 3. In Chapter 4, it is the study of the mechanical aspect of epithelial architecture.

2 Tools for the small world

The advances in biology are often following the breakthrough of techniques. The invention of PCR and discovery of thermal-stable polymerases, had boosted the study of molecular biology. The improvements in light microscope and the fluorescent proteins facilitate the observation of cellular machinery in dynamic. Many questions that were difficult to answer in the past time become straightforward with the help of new tools.

The use of micro-fabrication techniques in cell biology could be dated more than 20 years ago (Watt et al., 1988) .However it is until recent years that micro-fabrication equipments become more accessible, and these techniques started to make impact on the community. One of the commonly used micro-fabrication techniques is to micro-pattern adhesive ECM proteins on the substrate for adherent cells. With the micropatterned substrates, the shape of the cell become reproducible. Thus the localization of organelles can be more precisely described. Statistical description can be more easily applied to the protein localization. In addition, we acquires more control over the physical properties of the cell(Théry, 2010).

Micropatterning also allowed us to create a regularized cell array on the substrate, so that the positioning of each sample on the coverslip is predictable and well-aligned. This made the automatic image acquisition and image analysis more amenable. All these aspects allowed us to extract more and more information from a single experiment.

It has been often argued that the use of micropattern is just creating an experimental artifact. Nevertheless we should not forget that the cells cultured in a plastic petri dish is no more closer to physiological context. Conventional cell culture has been used for decades to keep cells alive out of their native tissue and let researchers to gain more control over the whole system. In this circumstance, micropatterned substrate can be regarded as an improvement on cell culture where we gain further control over the cell-ECM interaction and take a step forward in rebuild tissue-like environment.

In this chapter, I will first detail the techniques that I have ameliorated or developed for the micropattern fabrication on both rigid and soft substrates. Afterward, I will also present the computer routines that I have developed to enable automatic image

acquisition and analysis. At the end, I will focus on the programming of force calculation from traction force microscopy experiments.

2.1 Micropatterning ECM protein on glass coverslip

The most widely used method to create micropatterned ECM protein is the micro-contact printing. The greatest advantage of this method is that once the photoresist master (mold) for the stamp which contains the desired patterns is made, no more micro-fabrication equipment and special chemistry are required. The stamp could be made and used in every ordinary biology laboratory. However, the micro-contact printing itself is not a well reproducible process. The absorption of protein on the stamp is dependent on the nature of the protein going to be printed. The transfer of protein to the substrate depends critically upon the quality of the contact between the stamp and the substrate(Théry et al., 2009). Moreover, it is difficult to create large arrays of homogeneous micropatterns by micro-contact printing, thus prevents further automation in the image acquisition and analysis steps.

Alternatively, direct photolithography is also a simple way to produce micropatterned substrates(Fink et al., 2007). Shortly, substrate was coated with photoactivable molecules. UV light was then send through a mask to selectively activate defined regions. This chemical contrast between illuminate and non-illuminated region could subsequently be used to create adhesive and non-adhesive patterns on the substrate. Depending on the chemistry used and the resolution required, the light source could be a common hand held UV lamp for DNA gel and the mask could be a transparency printed by an office printer. In addition, direct photolithography is capable to pattern the whole coverslip homogeneously. This opens up a way to easily automatize the image acquisition process.

Oxygen plasma cleaned glass coverslip coated with poly-L-lysine-grafted-polyethylene glycol (PLL-g-PEG) has been shown to be an ideal substrate for direct UV lithography. The PLL-g-PEG coated surface is highly repellent to protein and cell by nature. Upon deep UV illumination, the polymer chains is oxidized and the illuminated region becomes adhesive. As a result, adhesive micropatterns could be generated on the whole coverslip just in a few steps(Azioune et al., 2009).

Still, several inconveniences should be noted. First, relatively expensive deep UV light source and photomask made from quartz are required. Second, the linkage between PLL-g-PEG and glass is somehow not strong enough that some cell types exerting strong

forces could tear off the patterns or grow into non-adhesive regions. To circumvent this problem, glass coverslips were first coated with a thin (<50nm) layer of polystyrene before coating with PLL-g-PEG(Azioune et al., 2010). The dense polymer network of polystyrene improves the binding of PLL-g-PEG but generates a low fluorescent background in UV and green channel.

The detailed experimental protocol can be found in AnnexeB.1 .

2.2 Soft substrate

Tissue cells have a well defined elastic property *in vivo* (Figure2.1). It could very with aging, or with pathological condition. Mechanical property of cellular microenvironment should play an important role in tissue morphogenesis and homeostasis. For example, it has been shown that stem cell lineage specification can be guided by matrix elasticity (Engler et al., 2006). The morphology and behavior of differentiated tissue cells also varies with substrate rigidity (Pelham et al., 1997; Discher et al., 2005). Despite decades of practice of cell culture on rigid plastic and glass, the quest for a more *in vivo* like cell culture system has never ended.

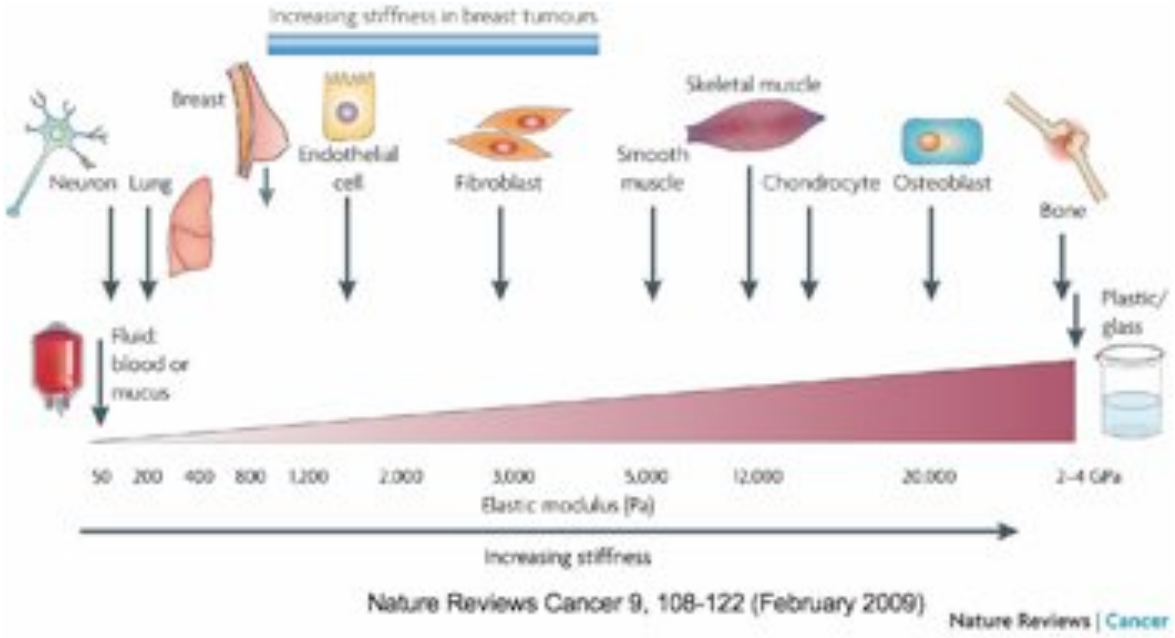

Figure 2.1: The rigidity spectrum of tissue cells

3D cell culture comes out to be more relevant to *in vivo* tissue environment, regarding to their rigidity, matrix composition and dimensionality for adhesion. However, the difficulties in manipulation, imaging, and amenability to high throughput analysis of 3D culture make the 2D system still routinely used most laboratory(Keely et al., 2007). Moreover, the control of rigidity and the ECM protein composition are more demanding for the 3D matrix system. Considering the basement membranes are thin and basically 2D, epithelial cells *in vivo* resting on a flat basement membrane can be approximated by

adhering to a compliant 2D substrate(Yamada et al., 2007 a). In addition to their physiological rigidity, compliant substrates enable the measurement of traction forces that cells exerted on them (see section 2.5).

Currently, the most extensively used 2D compliant substrates are made of polyacrylamide hydrogel or silicon elastomer, PolyDiMethylSiloxane (PDMS). They are easy to prepare and their elastic modulus can be fine tuned around a wide range covering most *in vivo* tissue elastic properties. However, the polyacrylamide gel has several important advantages over PDMS: (i) The elastic modulus of the gel can go down to tens of Pascal which is extremely difficult to produce by PDMS. (ii)The porous nature of the polyacrylamide gel provides a more physiological environment for cell culture. (iii) Its optical properties and minimal thickness permits the observation of immunofluorescence at high magnifications (Pelham et al., 1997).

Considering the aspects mentioned above, micropatterning ECM protein on the polyacrylamide soft gel could be a major step towards a experimental system where we could control simultaneously the mechanical and geometrical properties of the microenvironment. Nevertheless, the hydrogel properties and intrinsic repellent surface of polyacrylamide gel make it unsuitable to conventional methods like micro-contact printing. Several attempts have been made to address this problem, either by using a silicon sheet as stencil to confine the location of photoactivators (Wang et al., 2002; Parker et al., 2002), or by a long and complex chemistry to modify the gel surface to make it susceptible to micro-contact printing(Damljanović et al., 2005).

Inspired by the protocol of patterning PDMS by deep UV(Azioune et al., 2010), I developed simple and efficient way to pattern ECM proteins on polyacrylamide gel. This protocol exploit the repellent nature of the polyacrylamide gel surface, and the use of deep UV will render it favorable to covalent protein conjugation. Nevertheless, the effectiveness of UV activation is strongly dependent on gel surface properties. Only when the UV light is shined to the gel when it is still attached to the surface where it polymerized against, the activation is effective. It is possible that the gel surface polymer chain adopt different configurations upon contact with air, water, or solid(Gautam et al., 2000). Nevertheless, what is the exact physio-chemical modification of polyacrylamide upon deep UV illumination remains unclear. Because theoretically, oxidation of amide bond does not create a carboxylate group for subsequent chemical crosslinking by EDC (1-Ethyl-3-[3-dimethylaminopropyl]carbodiimide Hydrochloride).

Another critical step during the patterning of polyacrylamide gel is the surface properties of the quartz mask (or plate) on which the acrylamide polymerized. The successfulness of the patterning strongly depends on the hydrophobicity of the surface. Since the gel is much easier to detach from a hydrophobic surface(Radola, 1980), the thin patterned gel surface is less likely to be damaged during the detachment step.

This part of study has led to two patent applications. The detailed experimental protocol can be found in AnnexeB.3 .

2.3 Automated image acquisitions

The idea of automated microscope has emerged along with the needs of cell based high content screening(Neumann et al., 2006, 2010). Despite of the existence of some commercial instruments for over ten years, it is still not a common practice in most cell biology laboratories. In fact, even without the need for high-throughput screening, an automated microscope will still greatly speed up the image acquisition routine.

The regularized cell geometry and array-like cell positioning on the micropatterned substrate make the automated image acquisition amenable to ordinary cell biology laboratories. Traditionally, each microscope slide was only used to take several images to capture some characteristic phenotypes. Even with an attempt of image quantification, in most cases, only a limited sample images were collected due to the variability of cell number and cell shape in each observation field.

A micropatterned substrate allowed us to exploit the whole surface of the slide with a regular distance between each sample and controlled cell number and geometry. Image acquisition is no longer just looking for a few charming images over the whole slide but rather a statistical survey of a large population. In low magnification images, the location of cell can be pinpointed and subsequent analysis can be automated. For acquiring high magnification images, instead of going through the array of cells one by one with the joystick and wait for a rather lengthy multi-channels Z-stack acquisition before passing to the next sample, the whole acquisition procedure can be automatized quite easily with a motorized stage.

In order to implement the automated image acquisition in our laboratory, I have developed several computer tools. They were either written as Metamorph journals for image acquisition or as ImageJ plugins for image analysis. The detailed description of them could be found at the annexe section. Briefly, the whole automated acquisition procedure was started from positioning the sample at the center of the field of view (AnnexeA.1). Then, the stage calibration was performed to correct the rotation of the sample, so that the acquisition could go on to the position of next sample accurately(AnnexeA.2). During the acquisition, the focus drift was corrected by an autofocus algorithm(AnnexeA.3) without manuel intervention. With the microscope well-focused and positioned at each sample, we could choose to make full acquisition on the

whole slide which might take up a huge storage space, or make preliminary screening on-the-fly so that only positions containing the sample of interests will be acquired(AnnexeA.4).

2.4 Image processing & analysis

Since the arriving of the era of digital imaging, the practice of digital image processing becomes indispensable. It not only helps to render the acquired raw image more clean and clear, but most importantly it helps us to extract more information from the images, for example the improvement of resolution by deconvolution or the reconstruction and visualization of three dimensional volume. While the digital imaging facilitated the visualization and quantification of biological events, it also brings up new challenges for evaluating an unprecedented quantity of data. Currently, most of the image analysis and quantification are still done manually, which is both time consuming and susceptible to personal bias. Therefore, there is an exigency for developing automatized computer routines.

In this section, I will focus on my development of image processing and analysis routines related to the micropatterned cells.

Template matching

A precise localization of the micropatterns on the acquired images is the first step for all the micropattern related image processing routines. Either for a single pattern on a high magnification image or multiple patterns on a low magnification image, a robust template matching/feature detection method allowed us to automatize subsequent processing and analysis steps.

The standard approach to do feature detection in computer vision is by comparing the correlation between two images (cross-correlation). In mathematics, it is an operation of shifting a given function *A* and multiplying by another function *B*. The resulting correlation function *R* will peak at the position where the shift of *A* will give maximum overlap between *A* and *B* (Figure2.2). In digital image processing, each image could be regarded as a 2D function *I*(x,y), where *I* is the signal intensity value at pixel position x and y. Based on the same principle, the best match between pattern A and image B can be obtained by calculating the correlation function between them. Since the correlation function is calculated more efficiently in the Fourier domain, both images are first converted into frequency domain by fast Fourier transformation to get the 2D correlation function (Figure2.3). The coordinates of the brightest point (highest peak) in the correlation image *R* will give us the required shift of image *A* to have the best overlap between *A* and *B*, which is equivalent to finding the exact position of the pattern *A* on image *B*.

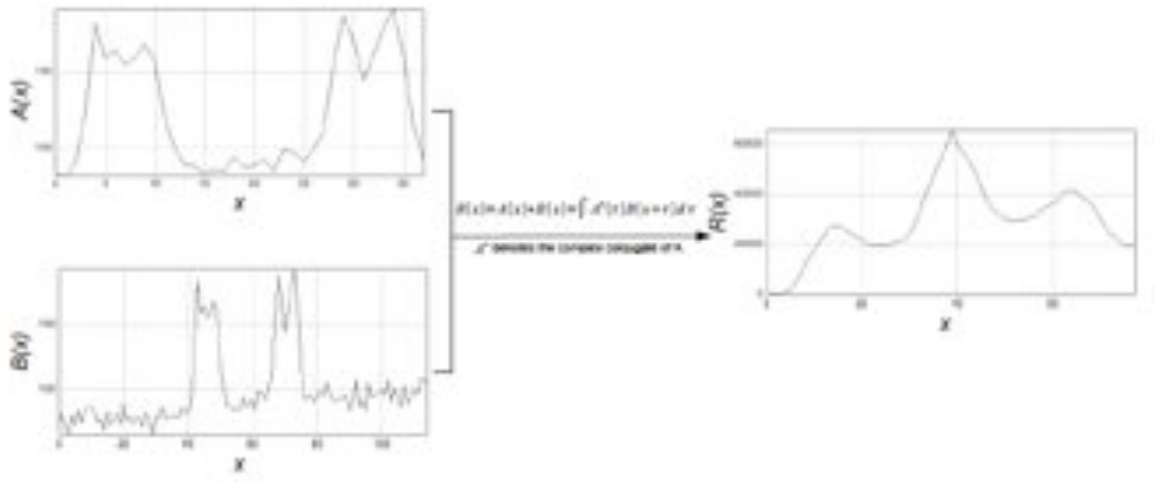

Figure 2.2: Cross-correlation between function A(x) and B(x)

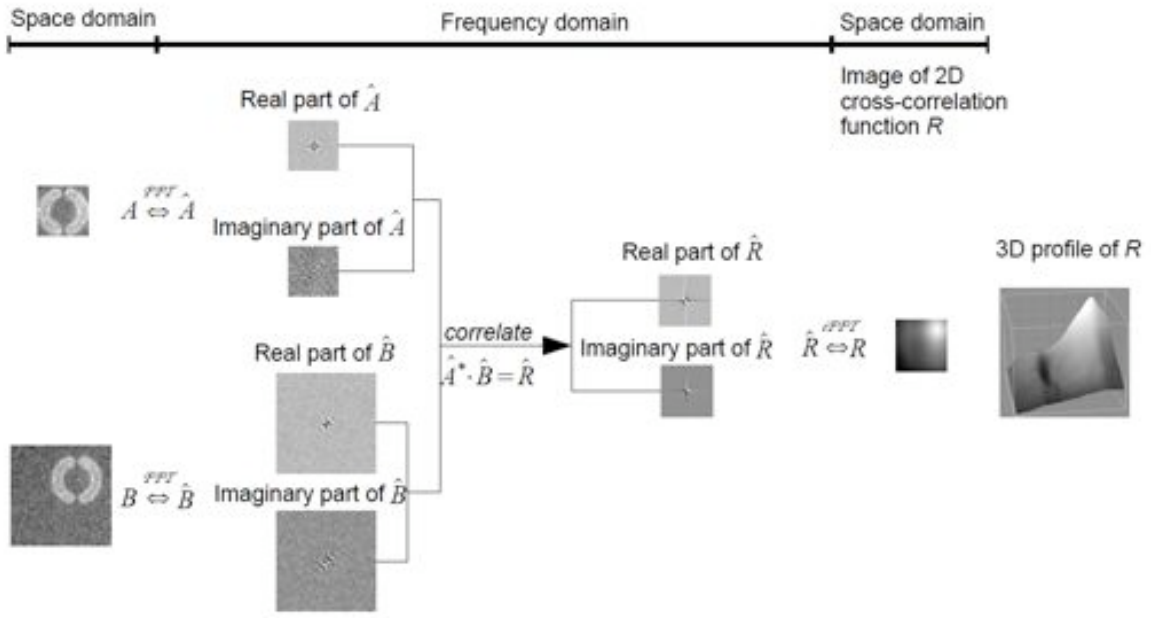

Figure 2.3: 2D cross-correlation between two images

If image *B* contains several identical patterns of *A*, we will have multiple peaks in the correlation image *R*. By locating the coordinates of each peak in *R*, we can find the exact position of each pattern on image *B* (Figure2.4).

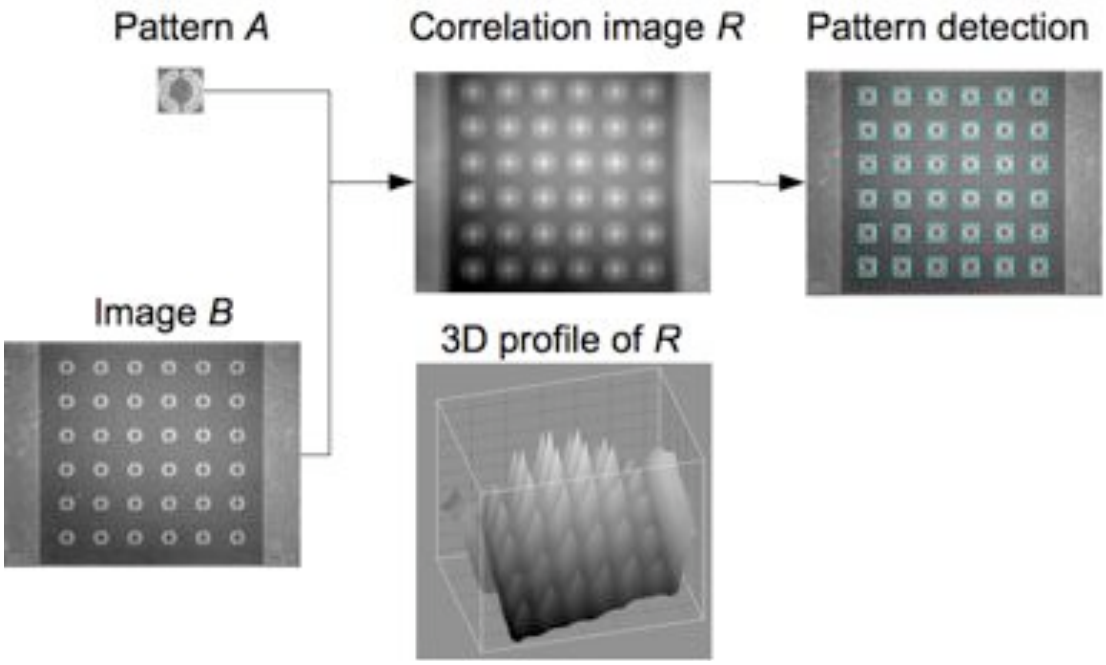

Figure 2.4: Multiple pattern detection by cross-correlation

However, the standard template matching by cross-correlation can fail when the correlation between the pattern and the exact match region on the image is less than the correlation between pattern and a bright spot (Figure2.5). Normalized correlation coefficient is a variant of cross-correlation where both the local and global intensities are normalized. By implementing this normalized form of cross-correlation in frequency domain, the above difficulties can be overcome without sacrificing efficiency(Lewis, 1995).

Another useful application of this template matching algorithm is to do image registration. Time-lapse images are frequently suffered from stage drifting or jigger. By selecting a landmark feature in the image, we can use template matching to align the slices within a time-lapse stack with ease. It was also used to align each immunofluorescent images before doing statistical analysis.

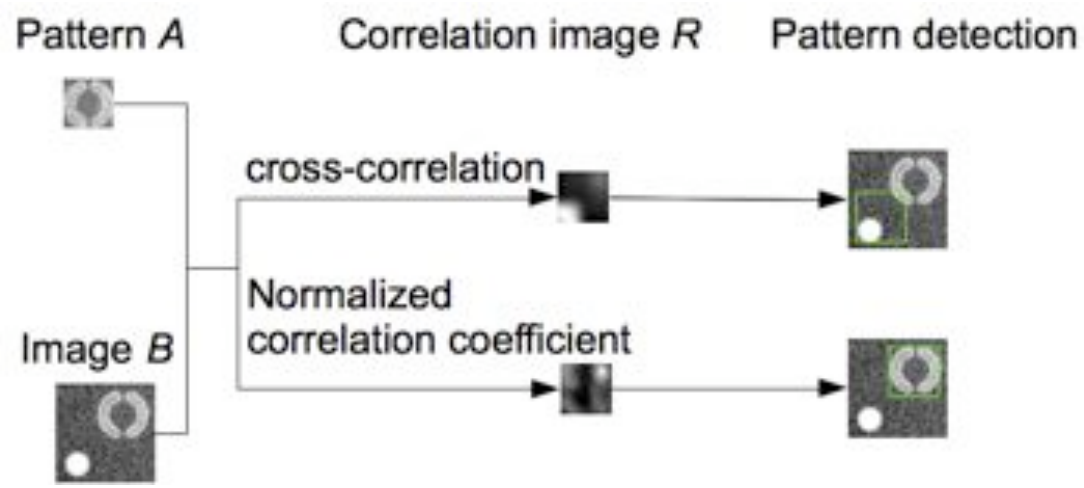

Figure 2.5: Limitation of unnormalized algorithm.

This part of work has given rise to two ImageJ plugins: *Template Matching*, and *Align slices in stack*. They can be downloaded online:

http://sites.google.com/site/qingzongtseng/template-matching-ij-plugin

Nuclear segmentation

After locating the position of micropatterns, the raw image can be cropped into sub-images with one micropattern per image. As mentioned in sectionError: Reference source not found, the number of cells occupying each micropattern cannot be precisely controlled under current method. Therefore, a classifying procedure is required either during the image acquisition or within the image processing steps.

Before proceeding to any further analysis, the first step is to separate the pixels representing the nucleus from those corresponding to the background. Thresholding is the simplest way to carry out this task on fluorescent labelled objects. Since the labelled nucleus will be presented by pixels with higher intensity, the grayscale nucleus image can be turned into binary image based on a given threshold intensity value which separates pixels of nucleus from pixels of background. In this binary image, we are able to assess the shape, the size and the number of existing objects, and thus determine the number of nuclei per pattern.

In the simplest scenario, nuclei are well separated from each others and the number of nuclei could be determined by counting the binary objects. However, very often nuclei are touching each other or the blurring of nuclear fluorescent signals are overlapped. Before attempting to explicitly separate each nuclei by further processing the image, we can already perform a rough classification based on the total area and circularity of the object which could be composed of one, two, or more nuclei. For example in Figure2.6, no single nucleus is found with circularity below 0.6 and area greater than 300 μm^2.

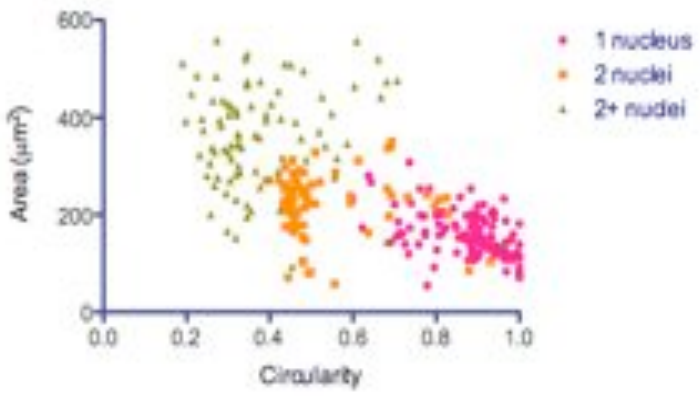

Figure2.6: Determine the number of nuclei by shape factors.

In addition to the above method based on the overall shape factor and area, it is possible to break up touching nuclei by watershed algorithm and then perform shape analysis on each segmented object (Grier, 2006). Another way to improve the nuclear segmentation process is to filter the grayscale image before the thresholding and binarization steps. The Mexican hat filter (Laplacian of Gaussian, LOG) is a commonly used filter to enhance circular object from a noisy background(Sage et al., 2005). By choosing a kernel adapted to the nuclear size, nuclear signals can be largely enhanced from background noise and fluorescent blurring(Figure2.7).

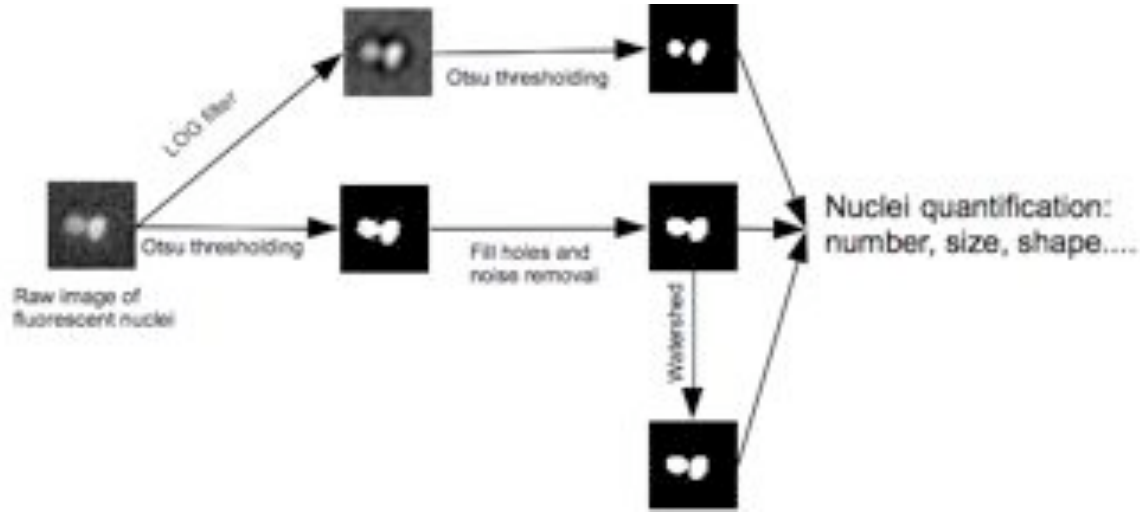

Figure 2.7: Image binarization and segmentation

Mitosis detection in time-lapse series

The detection of mitosis event in time-lapse image series has several potential applications, for example the measurement of cell division axis or the duration of cell cycle. We can also use it to refine the analysis to daughter cells originated from the same cell.

Since the nucleus is subjected to a dramatic reorganization during mitosis, the change of shape and variation of fluorescent intensity can serve as good indicators of mitosis. As shown in Figure2.8, changes in Feret diameter, roundness, and fluorescent contrast (StdDev/Mean) manifest specific profiles at the moment where mitosis happened. After surveying 12 time-lapse series and compare the evolution of these parameters before

and after the moment one nucleus becomes two nuclei (t=0), we can pick out the parameters which are rather invariable from cell to cell and thus could be used as general criteria for mitosis detection. For example, a sharp increase in Feret diameter and fluctuation in fluorescent contrast can be used to detect first division from one nucleus to two nuclei (Figure2.9), while the increase in roundness and area are useful for the detection of second division from two to three nuclei (Figure2.10). Combining these criteria with the number of nuclei presented in the image, cell division can be identified accurately.

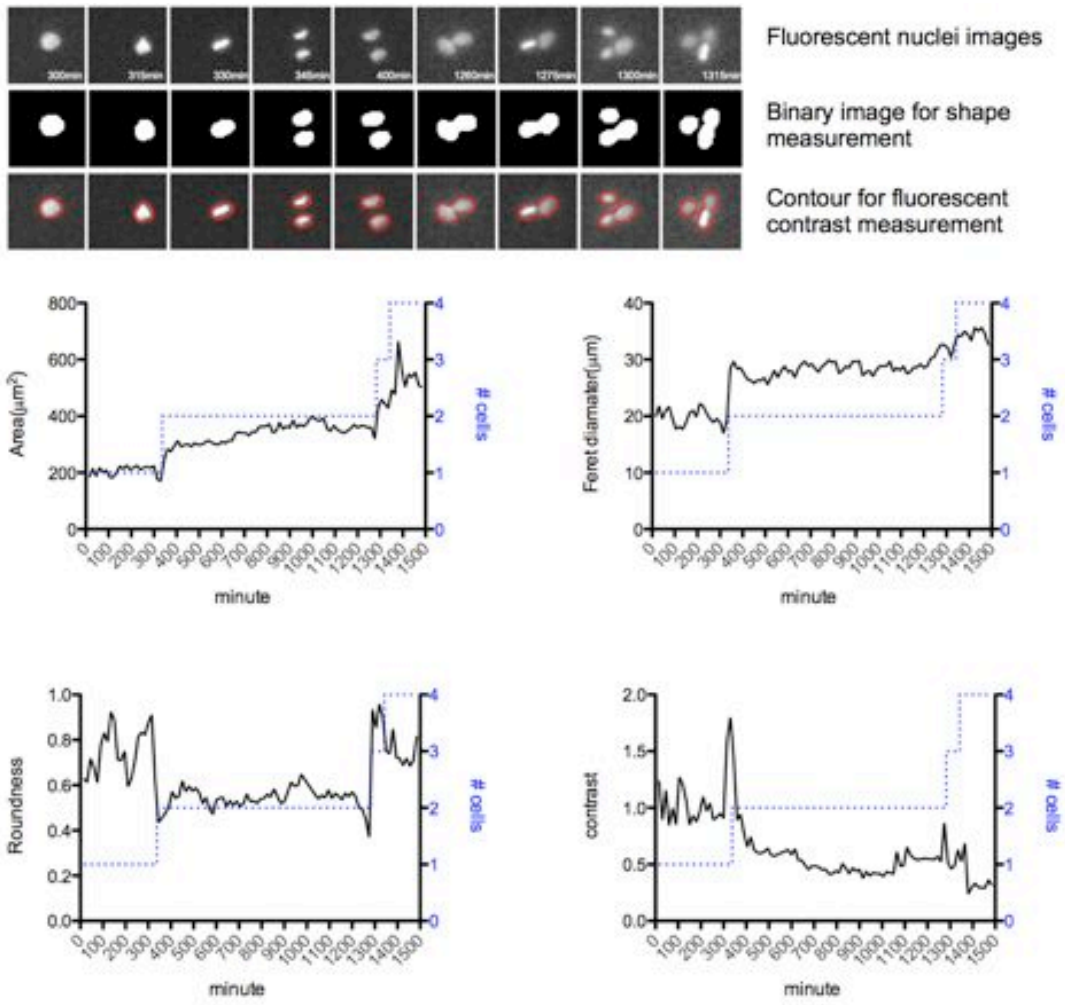

Figure 2.8: Change of shape factor during 1st and 2nd mitosis events.

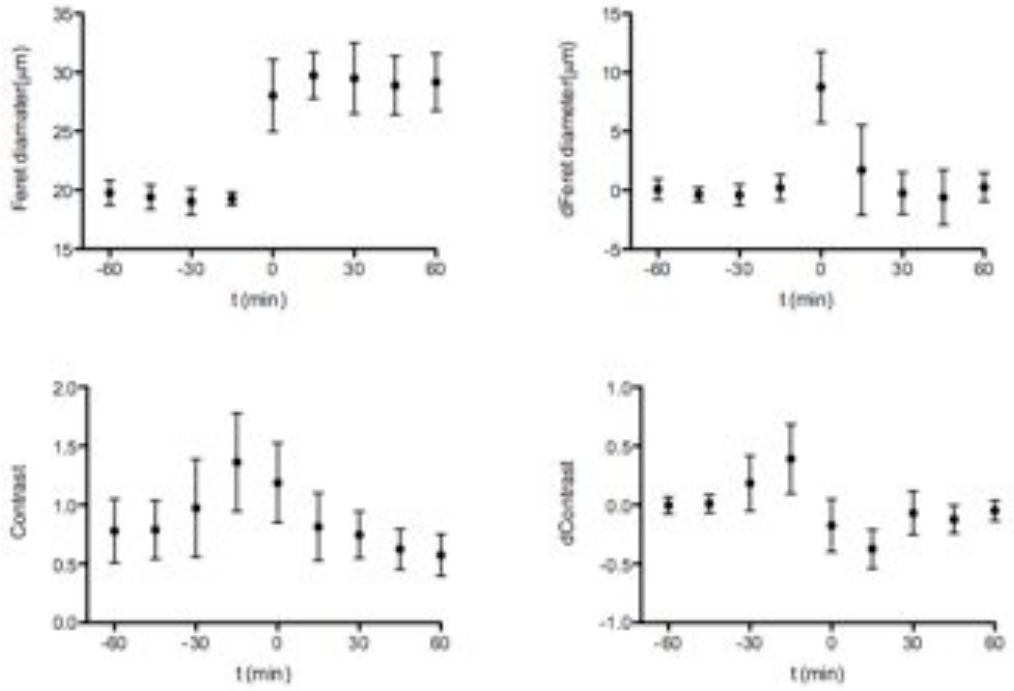

Figure 2.9: The shape factor change around the 1st mitosis event. Averaged from 12 different time-lapse movies

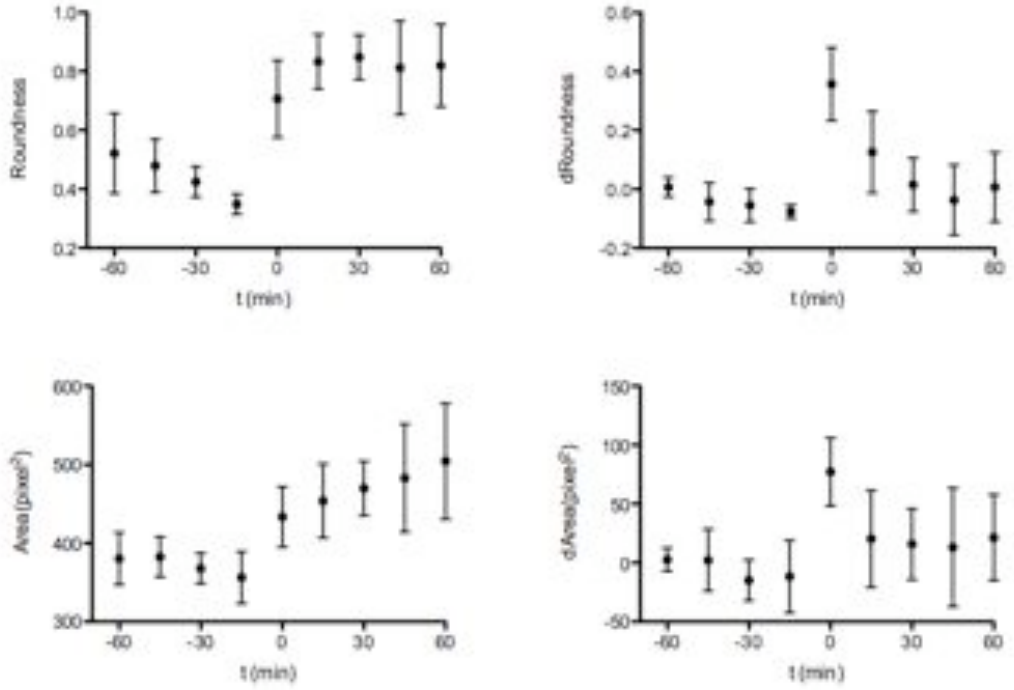

Figure 2.10: The shape factor change around the 2nd mitosis event. Averaged from 12 different time-lapse movies

Statistic analysis of protein localization

With a constrained cell geometry on micropattern, localization of cellular proteins by immunofluorescent labeling becomes more comparable from cell to cell. We can easily make statistical analysis on protein localization by making a virtual cell where each pixel value correspond to the mean or standard deviations of intensities of the same pixel from all the samples (Figure2.11). This could reveal subtile variations which are not readily perceivable on individual immunofluorescent image.

A prerequisite to do such analysis is the perfect alignment of cells from each image, so that the same pixel would correspond to the same cellular localization for all the images. If the micropatterns are fluorescent labelled, the alignment can simply be done by aligning the pattern using the template matching method mentioned previously. Otherwise, phase contrast image or cell contour labeling can also be used for alignment but with reduced precision.

We should also aware that the averaged value could be severely biased if there existed some extreme values in our images such as non-specific fluorescent background or inconsistent imaging conditions. To avoid such biases, one can normalize the fluorescent intensity within each image so that each pixel represents a relative percentage rather than an absolute value.

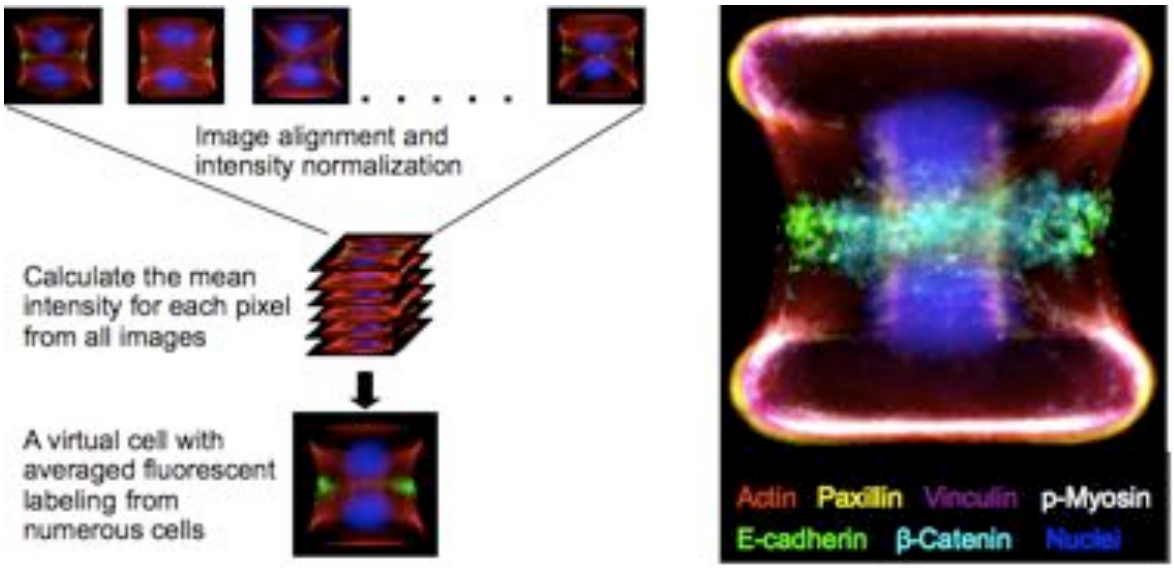

Figure 2.11: Multiple averaged staining on a virtual cell.

2.5 Traction Force measurement

Mechanical force is known to play an important role in the regulation of various cellular process, such as adhesion, migration, differentiation, and multicellular homeostasis. As a result, measuring the traction forces that cell exert on their surrounding ECM turns to be a tool to probe how mechanical forces is modulated within the cell (ref?).

The traction force measurement was first pioneered by Harris et al. who put cells on silicon thin film and used the wrinkling of the film as a qualitative indicator of cellular traction force(Harris et al., 1980). Today, the traction force can be quantified more precisely and with resolutions down to single focal adhesion. This improvement is largely owing to advances in calculation algorithm and computing capacities, while the basic experimental setup remains rather simple and straightforward: a compliant substrate on which the deformation made by cellular traction can be measured. A commonly used substrate for traction force microscope is made by polyacrylamide gel embedded with fluorescent beads as fiducial markers. The availability, ease of preparation and tunable rigidity over a wide range corresponding to physiologic tissue condition make it a ideal choice for traction force microscope (TFM) experiments.

The TFM could be divided into two main stages. The first stage is the measuring of the displacement field, which is done by taking one image of the fluorescent beads while the cell is attaching to the substrate, and another image of the beads after detaching the cell. The displacement field is obtained by tracking the beads on the images with and without cell. The second stage is the force reconstruction from the displacement field by solving an ill-posed inverse elasticity problem (Figure2.12). In the following part, I will address on my work of ameliorating the method of bead tracking, and the implementation of force calculation algorithms in the public domain image processing software---ImageJ.

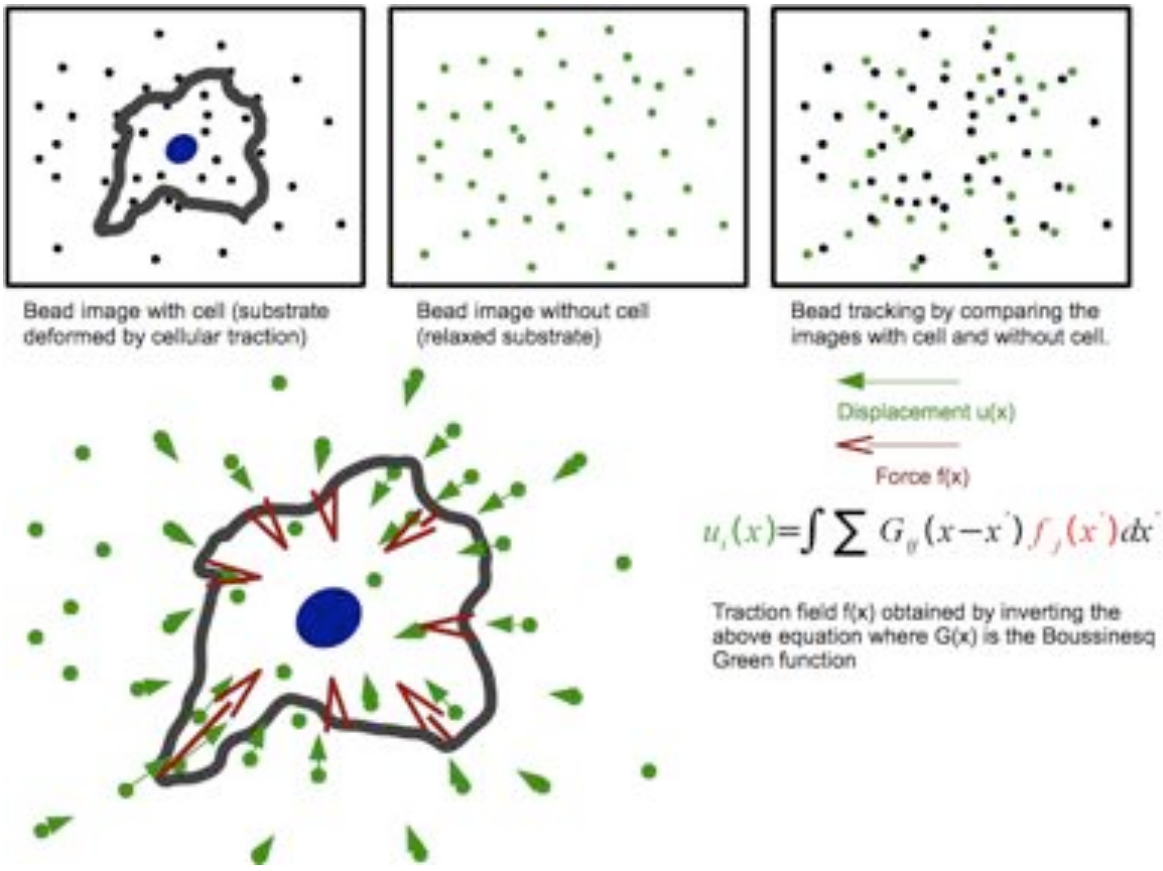

Figure 2.12: General scheme of the traction force microscopy (TFM)

Bead tracking

The bead tracking in TFM are based on two routines commonly used in fluid mechanics: namely Particle image velocimetry(PIV) and Particle tracking velocimetry(PTV). The PTV tracks individual beads according to their proximity, shape, and intensity. In the PIV, images are divided into subregions called interrogation windows and the displacement field is established by the cross-correlation between two windows. The accuracy of PTV is limited by insufficient distinctness of single bead and the lack of information from their surrounding displacement vectors. On the contrary, PIV compares images of interrogation window which usually contain more than one bead. As a result, PIV gains in accuracy owing to the increased information available for feature tracking, but losses in resolution since the displacement field is spatially averaged over the interrogation window which is usually larger than the bead density.

Considering the amenability to automation and the requirement of traction force resolution in my study, iterative PIV was selected as my bead tracking routine. However, conventional PIV uses a cross-correlation algorithm that compares only interrogation windows with equal dimension. The tracking would fail if the shift between two windows were too important and the correlation between them became too weak. This problem could be partially circumvented by using an iterative PIV scheme. In this case, large interrogation windows are used first, and the measured displacements serve to preshift the smaller interrogation windows in the subsequent iteration so that a large displacement is more likely to be captured. Nevertheless, above solution relies on the accuracy of the preshift. When the actual displacement vectors encompassed by the interrogation window are quite diverge, the measured displacement will only be a average of those vectors. Consequently, the smaller window in the next iteration may inherit a false preshift which does not represent the actual displacement, and lead to a cross-correlation between windows containing irrelevant features(Figure2.13).

A more proper solution to get around this difficulties is to perform iterative PIV by using the cross-correlation between an interrogation window and a larger search window. This type of cross-correlation is also described as “template matching”(See section2.4). Since the search is done against a larger window, even the preshift given by the previous PIV is inaccurate, the best match representing by a significant correlation peak will still be presented in the cross-correlation result. In this configuration, the previous PIV on large interrogation window only served as a guidance for searching the correlation peak(Figure2.13).

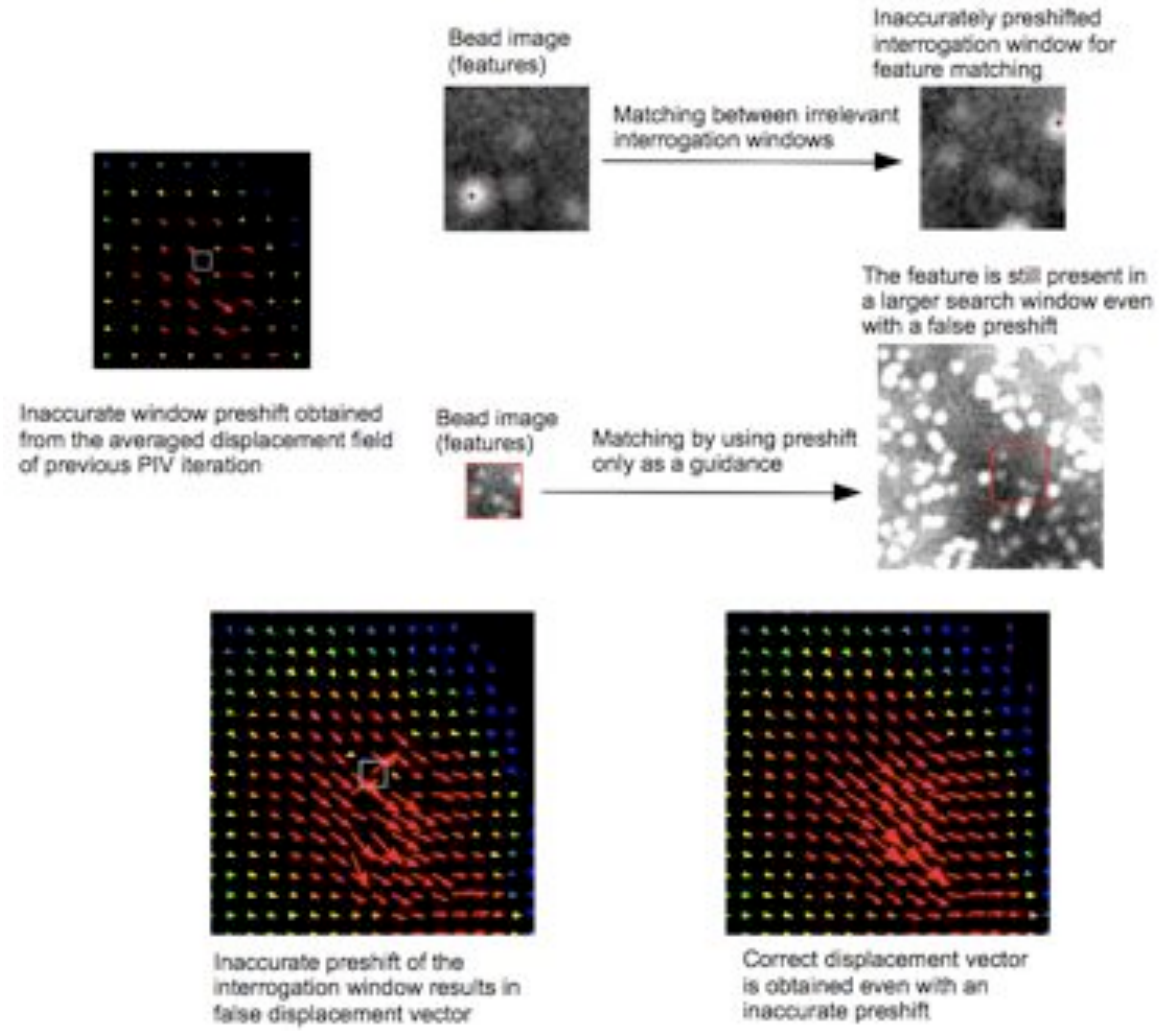

Figure 2.13: Amelioration of iterative PIV by using a larger search window.

When the interrogation window gets smaller, PIV will eventually encounter the same problem as PTV since the available features in each interrogation window become less and less. This problem is manifested by a less distinct peak value as well as multiple similar peaks in the correlation map (i.e. the 2D correlation function). Quite usually in a region where large and inhomogeneous displacements occurred, the correlation map tended to be very noisy and it became difficult to determine the best match only by the maximum peak value. In this situation, one could choose to eliminate the vector obtained with low correlation value and interpolate it by surrounding vectors later on. On the other hand, the best match could be determined not only by the maximum correlation value but also by the sharpness of the peak and take into account the displacement vector measured in previous iteration (Figure2.14).

An additional precaution should be made when the bead tracking is performed on the micropatterned polyacrylamide gel. The fluorescent beads under the pattern are strongly bleached during the UV activation step(Figure2.15), therefore the normalized algorithm of cross-correlation should be used in order to avoid false matching toward bright beads(See section2.4). Figure2.15 compared the displacement fields of micropatterned cells measured by conventional iterative PIV and the improved PIV used in current study.

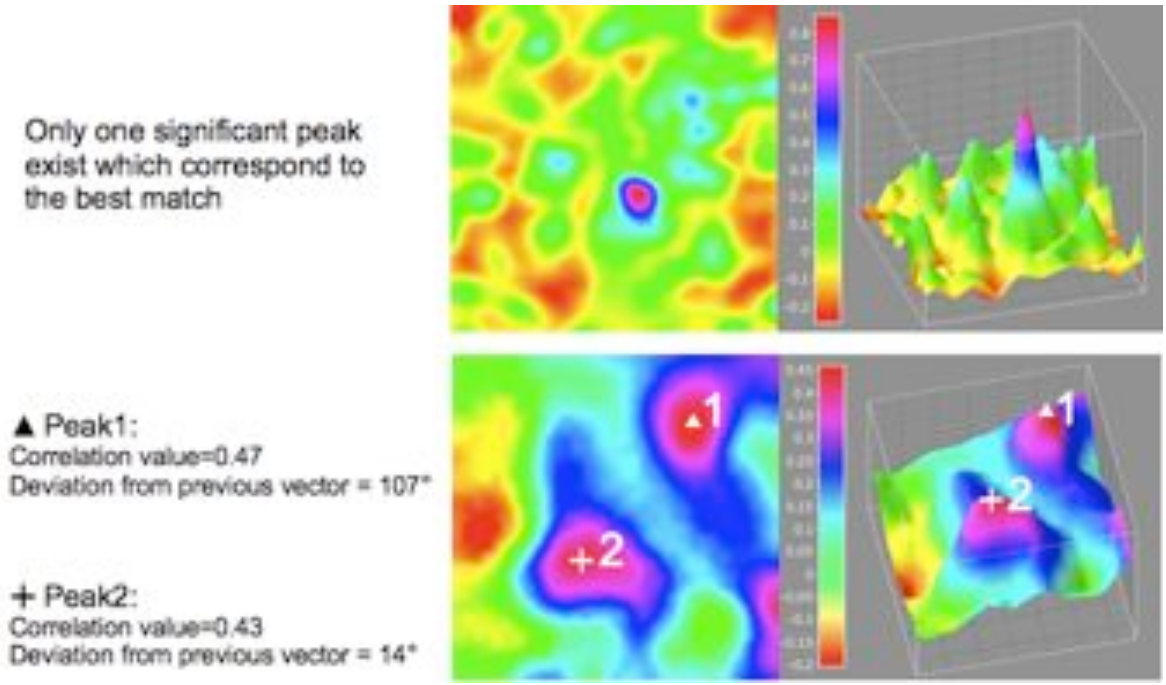

Figure 2.14: Finding the best match with both the correlation value and the displacement vector measure in previous iteration.

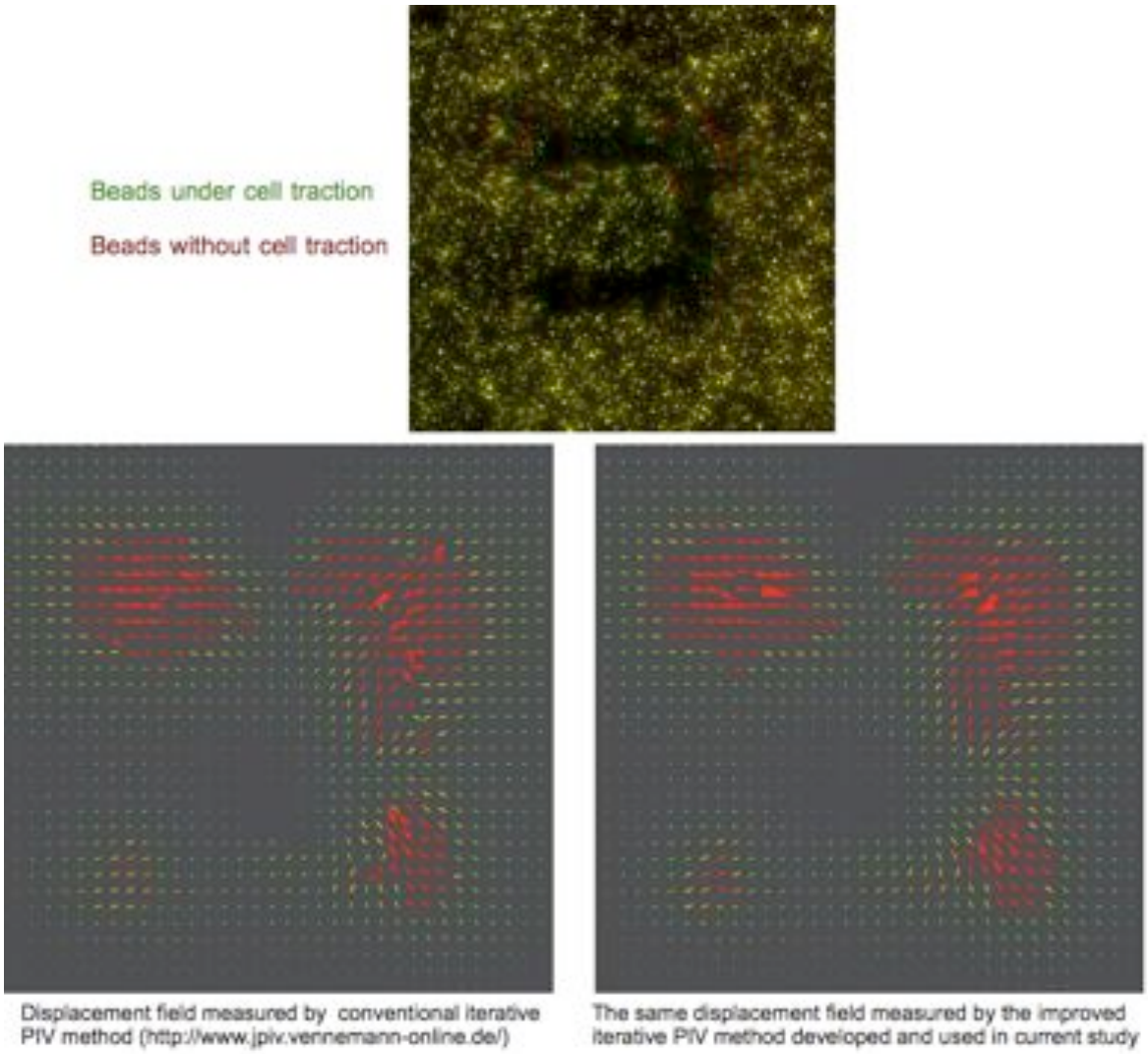

Figure 2.15: Comparing the displacement field obtained from conventional PIV and the improved PIV method in current study.

Traction force reconstruction

Considering the deformation(displacement) parallel to the gel surface caused by cellular traction is far smaller than the thickness of the gel, the gel can thus be approximated as a semi-infinite half space. The displacement $u(x_1, x_2)$ on the surface of this half space is described as the convolution between the point forces $f(x_1', x_2')$ and the elastic Green's tensor function $G_{ij}(x_1 - x_1', x_2 - x_2')$, where the subscript index i,j take on values from 1 to 2 assuming that the force and displacement orthogonal to the gel surface

is negligible (Equation1). The explicit expression of this Green's tensor is the so called Boussinesq solution(Landau, 2006). As a result, the solution for the force field requires the deconvolution of the displacement field with the Green's function.

$$u_i(x)=\int \sum_j G_{ij}(x-x')f_j(x')dx' \quad \text{.....Equation 1}$$

In the Fourier space, the convolution becomes a simple multiplication, and the relation in Equation1 can be rewrite as in Equation2, where subscript k stand for the mode (i.e number of basis function) in the frequency domain.

$$\tilde{u}_{ik}=\left\{\sum_j \tilde{G}_{ij}\tilde{f}_j\right\}_k \quad \text{.....Equation 2}$$

Where $\tilde{f}$ is the force field in the Fourier space, $\tilde{u}$ is the displacement field in Fourier space, and $\tilde{G}$ is the elastic Green's function in Fourier space expressed as following:

$$\tilde{G}_k=\frac{2(1+\nu)}{Ek^3}\begin{pmatrix}(1-\nu)k^2+\nu k_y^2 & -\nu k_x k_y \\ -\nu k_x k_y & (1-\nu)k^2+\nu k_x^2\end{pmatrix} \quad \text{.....Equation 3}$$

Where E is the Young's elastic modulus, ν is the poisson ratio, and k is the corresponding wavevector in Fourier space.

Now the traction field in Fourier space can be calculated by Equation 4, where the $\tilde{G}_{ij}^{-1}$ denote the inversion of the 2D Green's tensor.

$$\tilde{f}_{ik}=\left\{\sum_j \tilde{G}_{ij}^{-1}\tilde{u}_j\right\}_k \quad \text{.....Equation 4}$$

According to Sabass et al., a regularization scheme can be implemented to above equation to give an efficient and reliable force reconstruction(Equation 5).

$$\tilde{f}_{ik}=\{\sum_{l,j}[\sum_m \tilde{G}_{ml}\tilde{G}_{mi}+\lambda^2 I]^{-1}\tilde{G}_{jl}\tilde{u}_j\}_k \quad \text{.....Equation 5}$$

As we can see from the above equations, the main difficulties for finding the force field from this ill-posed inverse problem is the lack of information on the exact localization of traction forces. Unless the exact location where cell exerted traction force is known(Balaban et al., 2001), the force field can only be estimated either from a regular

grid as in the Fourier transform traction cytometry(FTTC)(Butler et al., 2002) or from an adaptive mesh as in the boundary element method(BEM)(Dembo et al., 1999).

In the present study, FTTC was used to reconstruct the traction force from the displacement field. The displacement field measured by PIV is readily to be transformed into Fourier space since the displacement field is measured on a regular grid. This avoids further interpolation as the displacement field measured by PTV needs to be further remapped onto a regular grid which is in fact an averaging step compromising the resolution of the displacement field. Then the force field is calculated in the Fourier space. Finally the force field in real space is obtained by inverse Fourier-transformation.

Along with the bead tracking by PIV, the FTTC algorithm is implemented in JAVA computer language so that the whole TFM process from image processing, displacement field measurement to force calculation could be performed under ImageJ which is a common image processing software in public domain. This should largely facilitate the employment of TFM in most biological laboratories.

This software package for the traction force microscopy containing the PIV program, the FTTC program, and a program to draw the vector plot of the displacement and force field is available online:

https://sites.google.com/site/qingzongtseng/tfm

2.6 Discussions

Improving the efficiency of automated acquisition

Our current implementation of automated acquisition involved screening the sample of interests at high magnification. Although it could be done unattended during the night, it is still desirable to increase the efficiency of acquisition process. One of the possible improvement is to perform prescreening on low magnification images, since the filtering of empty positions (micropattern not occupied by cells) and basic discrimination of cell numbers can be done quite efficiently with low resolution images. After preliminary image analysis and locating the position of interest on the low magnification image, the program could switch to high magnification objectives and go directly to those positions containing the sample of interest.

The pros and cons of automated imaging process

The automatization of certain repetitive routines can largely reduce our working load and the human bias in measurement. Some large data collection and statistical analysis are even not feasible without automated routines. For example, the analysis of cell positioning presented in section3.2 involved thousands of measurement per experimental condition. The automatized acquisition process can also eliminated the bias from manual selection of sample.

Nevertheless, by automatizing the image acquisition procedure, we also loss the opportunity to observe other interesting events which were unforeseen at the beginning and might be eliminated by the computer through the screening process. For example, when we focus on the positioning of two cells on each micropattern, we might neglect some interesting behavior of three or four cells per micropattern since those images of more than two cells were automatically eliminated by the computer. However when we observe and select the sample by our eye, we have the chance to see many unexpected events. Observation is the beauty and essence of the “Old-school” biology.

Quality control of automated analysis

With the help of computer, huge amount of images are analyze and converted into numbers and graphs automatically. However, we could easily get lost in such facility since no more visual intervention was taking place to signal the abnormalities during the analysis. For example, the initial criteria for detecting cell numbers such as nuclear size, and shape factor defined for wild-type cell might be unadapted for mutant cells. If we were not aware of this, we could easily come up with a irrelevant analysis result from the computer which followed the give parameters with fidelity.

One indispensable practice to avoid such pitfall in automation is to implement a sort of quality control step. For example, randomly selected images from a large sample pool were displayed along with the analysis/measurement by the computer. So that we always verify the correctness of the automated analysis.

Limitations of presenting micropatterning techniques

Despite the large improvement brought to us by the direct lithography method, there are several issues required to be addressed here.

The quality of lithograph strongly depends on the distance between the sample and the mask. However, without special cleanroom facilities, it is difficult to control the contact pressure between the mask and the coverslip as well as avoiding dusts coming in between. As a result, micropattern reproducibility is still not perfect. This issue of reproducibility could also coming from the surface property of the mask. Our patterning technique relies on the electrostatic interaction between the passivation agent, PLL-g-PEG, and the coverslip surface. Bring the mask surface, which bore electrostatic reactivity as well, in direct contact with the PLL-g-PEG coated surface might compromise the coating quality.

3 ECM geometry and epithelial morphogenesis

The extracellular matrix was originally considered only as a support for cell growth and migration. However, a growing body of evidence now points to a more dynamic role for the extracellular matrix in tissue development and homeostasis. The signals provided by the extracellular matrix are crucial for epithelial polarity. The structural and mechanical properties of the extracellular matrix are at the same time guiding morphogenesis and being actively modulated by tissue cells.

In spite of those importance aspects of extracellular matrix, the detailed mechanism defining the active function of ECM in epithelial morphogenesis remains largely unexplored. This might be due to the lack of imaging techniques for the ECM structures or the lack of control over the cell-ECM interaction in conventional experimental systems. Hence, micropatterning the ECM protein (see section2.1) appears to be a good strategy allowed us to get further control over the spatial arrangement of cell-ECM interaction.

Here in this chapter, I will present our studies on how the cell-ECM adhesion can regulate intercellular junction; how the interplay between the two adhesion system governs the global epithelial geometry; and how the polarity of internal organelles coordinates with tissue morphology through the adhesion systems. With a minimum system composed of controlled cell-cell and cell-ECM interactions, we can better appreciate those processes and see how they are modified during epithelial remodeling.

3.1 Introduction

Epithelial tissues exhibit a wide variety of morphology. They could be multilayers of flattened cells as the stratified squamous epithelium found in our skin and esophagus. They could be a single layer of elongated cells as the simple columnar epithelium found in the inner surface of our digestive duct. They could also have a intermediate form where columnar or cuboidal cells growing upon another layer of epithelial cells (Figure3.1).

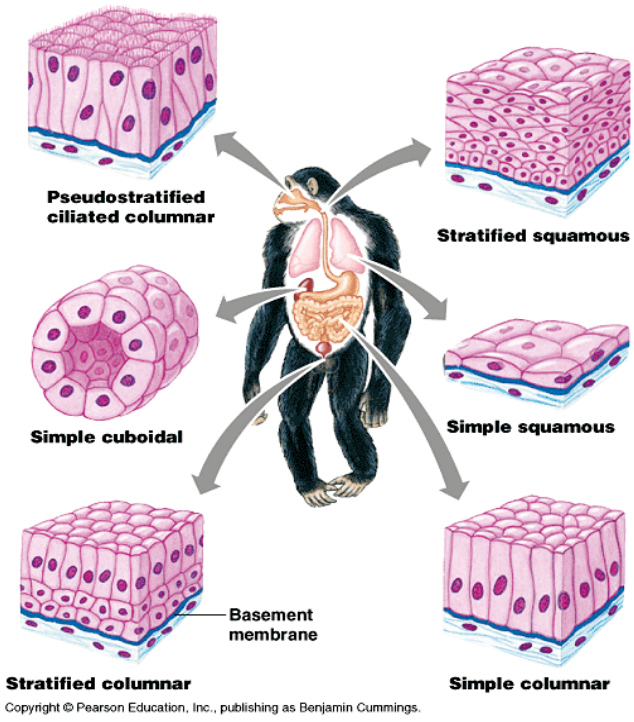

Figure 3.1: Different class of epithelium

Despite their differences in appearance, there are also common features shared by epithelial tissues. There is generally no blood vessel penetrating between epithelial cells, which means they are dependent of the underlying connective tissue for oxygens and nutrients. In between the epithelial cells and connective tissues we can found the extra-cellular matrix called basal lamina (or basement membrane). It functions as a supportive network to maintain epithelial tissues and plays a key role in tissue morphogenesis. The adhesion between epithelial cell and this extra-cellular matrix serves as the anchorage point and provides cues for growth, migration, and cellular polarity etc.(Rozario et al., 2010).

Another common feature of epithelia is that they are all tightly packed and bounded by well developed intercellular junctions. Thus the epithelia are capable of providing functional and physical separation between body compartments. The intercellular junctions not only maintain a physical coherence of the epithelial tissue, but also participate in a wide spectrum of signaling pathways which highlighted their importance in tissue homeostasis and morphogenesis(Perez-Moreno et al., 2003).

At the single cell level, epithelium is marked by its asymmetrical distribution of internal organelles and membrane component. The apical-basal polarization is responsible for the directional transportation of materials like the absorption of nutrients from the intestinal surface toward inner vessels and the secretion of milk toward the mammary lumen. This cellular polarity is also reflected in the spatial organization of epithelial adhesion systems. Different types of intercellular adhesion system are located sequentially along the apical-basal axis on the lateral face, with the cell-matrix adhesion located at the basal face (Figure3.2).

During morphogenetic events such as embryogenesis and wound repair, epithelium could undergo dramatic remodeling and adopt mesenchymal phenotype. Both epithelial polarity and junction organization are subjected to considerable modification. On the other hand, this epithelial to mesenchymal transition(EMT) has also been described in tumoral metastasis. In such pathologic condition, part of the cellular program of EMT is hijacked by malignant cell to establish an uncontrolled post-developmental plasticity(Thiery, 2003; Revenu et al., 2009; Thiery et al., 2009; Yang et al., 2008).

In the following introductory sections, I will start by reviewing individual adhesion complexes and then go on to discuss the crosstalk mechanism between them as well as how they get involved in the epithelial polarity. Apart from the apical-basal polarity which is more emphasized in epithelia, the centrosome positioning which is the basis for the polarity of internal organelles will also be addressed. At the end, I will deal with the reorganization of adhesion system and polarity during the epithelial-mesenchymal transition.

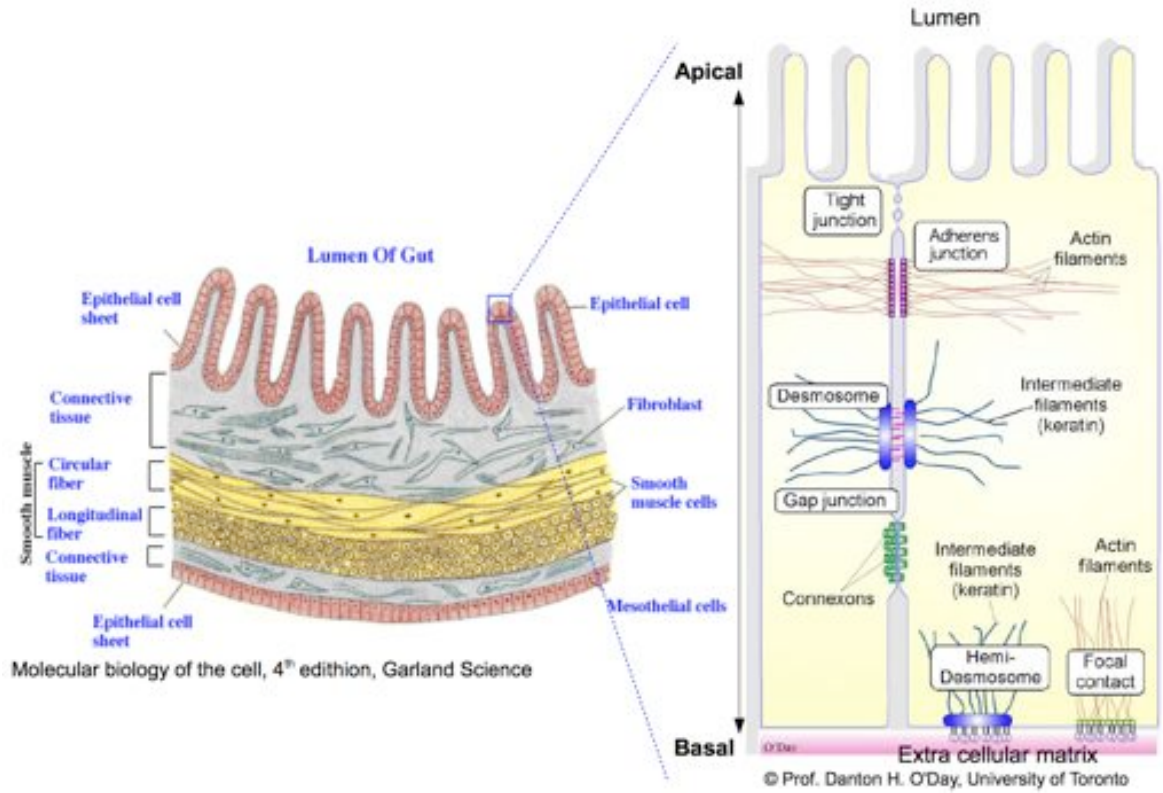

Figure 3.2: Scheme of epithelial architecture

Cell-Matrix adhesion

Physical linkage

The connections between epithelium and the underlying extra-cellular matrix are mediated by two types of integrin-dependant junctions: focal adhesion and hemidesmosomes. The focal adhesions are linked to the actin cytoskeletons while the hemidesmosomes are linked to the intermediate filaments (Figure3.3). The integrin family of receptors have roles in both physical linkage and chemical signal transduction. Upon engagement of ligands such as collagen, laminin, or fibronectin in the extra-cellular matrix, integrin undergoes conformation change or/and oligomerization which in turn allow further binding with downstream adaptors and kinases to initiate specific signaling pathway(Campbell et al., 2011).

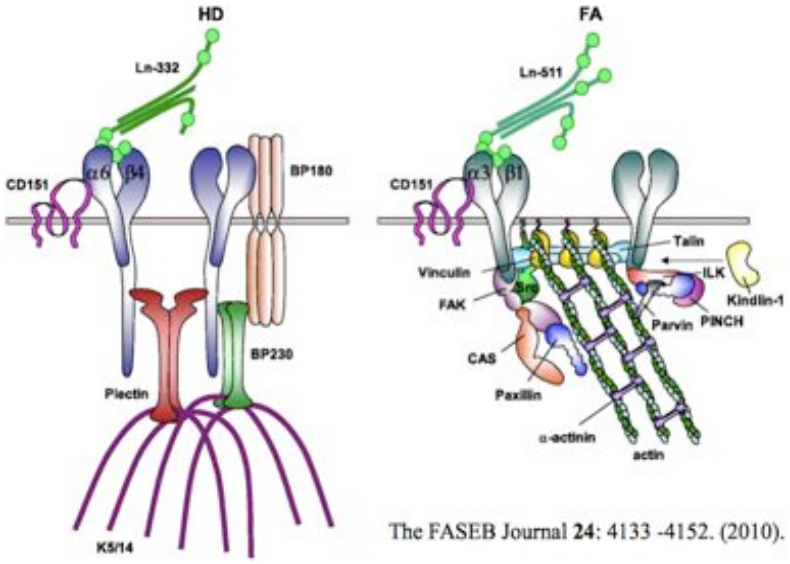

Figure 3.3: Junctional complexes of hemidesmosome and Focal adhesion.

Mechanosensitivity of ECM adhesion

Although both adhesion complexes have been described in epithelial tissue *in vivo* and *in vitro*, compared with the study of focal adhesion the adhesion through hemidesmosome remains poorly understood. Nevertheless, their connections with cytoskeleton network suggest they might have common role in tissue mechanical properties. The study on cultured cells and reconstituted biochemical systems has unveiled

the mechanism of mechanosensitivity in focal adhesion complex. The recruitment of adaptor proteins and activation of downstream signaling pathway can be modulated according to the mechanical properties of the matrix network in addition to the chemical difference of ligand (Geiger et al., 2009). Apart from those pioneer studies on fibroblast which develops prominent focal adhesions and might engages different set of integrin molecules then the epithelial cell *in vivo*, evidences have also confirmed similar mechanosensitivity of focal adhesion in 3D cultured epithelial cell(Wozniak et al., 2003) and hemidesmosome in worms(Zhang et al., 2011).

ECM remodeling

Recent studies have pointed up the fact that cells are not just passively sensing the extra-cellular matrix properties, but are capable of actively modulating the extra-cellular matrix structure through the cell-matrix adhesion(Davidson et al., 2004; Rozario et al., 2010; Haigo et al., 2011). This kind of mechanical and topological modulation could account for the experimental differences between cells cultured on 2D rigid substrate where matrix is flat and rigid, and cells cultured on 3D compliant substrate where matrix is soft and could be restructured upon the force exerted by cell. It is possible that the rigidity-dependent cell behavior can be partly explained by the modulability of substrate(Cukierman et al., 2001).

Based on recent advances, the cell-ECM interaction should now be regarded as a reciprocal process. Cell can sense both the chemical and physical stimuli from ECM ligand. Correspondingly, ECM proteins is being actively secreted and structured by cells. Therefore, the adhesion through integrin receptor is not simply an anchoring point, but rather a bridge to make mechanical continuity between intra- and extra-cellular environment.

Cell-cell junction

A multicellular assembly depends on the establishment and maintenance of connection between cells. In complex metazoan, this is accomplished by the intercellular junctions which, in contrast to the cell-matrix adhesion, are mainly mediated through homophilic interaction between transmembrane proteins.

In vertebrate epithelia, the major types of intercellular junctions are: gap junctions, which allow intercellular transportation of small cytosolic molecules; tight junctions, which are indispensable for establishing the epithelial barrier; the cadherin based adherens junctions and desmosomes which associate intercellular adhesions with cytoskeletons to modulate the tissue integrity and morphology.

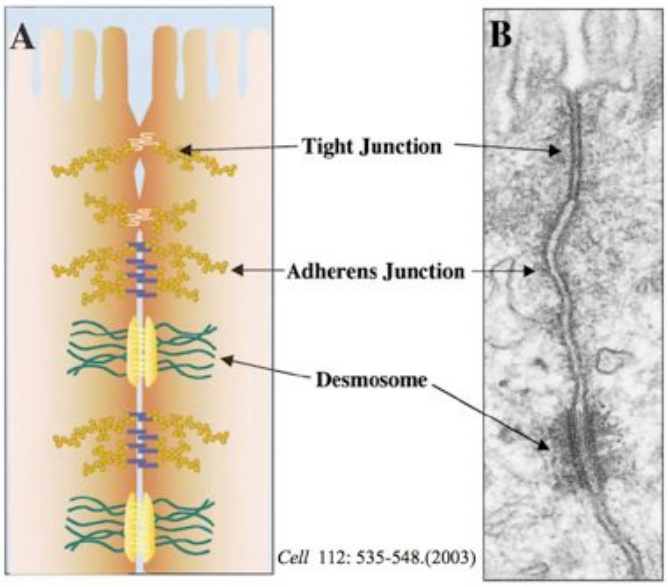

Figure 3.4: Spatial organization of cell-cell junction

The structure of adherens junction

Adherens junction is the first adhesion complex formed upon initial cell-cell contact and during embryogenesis. The omnipresence of adherens junction throughout the complex metazoan underlines its pivotal role in cell-cell adhesion. Moreover, the subsequent formation of tight junctions and desmosomes is also closely coupled with the adherens junction complex.

Epithelial adherens junctions are mainly formed by E-cadherin, which is the best studied member of the cadherin family. E-cadhrin is often considered as a major regulator of the epithelial phenotype. Its frequent downregulation in cancer is considered as a key event in metastasis. Like other cadherin family proteins, it is composed of five extracellular cadherin domains (ECs), the transmembrane domain, and the highly conserved cytoplasmic domain which allowed the binding of downstream effector proteins such as the catenins. By association with calcium ions, the extracellular cadherin domain undergoes homophilic interaction with the EC of the cadherin presented by the neighboring cell(trans- dimerization) (Figure 3.5). Although the exact structural mechanism of cadherin homophilic binding remains unclear, it has been shown that the binding strength is related to the conformation of trans- dimerization(Gumbiner, 2005; Chappuis-Flament et al., 2001). It is also possible that the mechanical load itself could modulate the binding conformation(Hong et al., 2011). On the other hand, cis- dimerization (dimerization of of cadherins of the same cell) or clustering could also be parameters to regulate the adhesion strength, considering the single trans- cadherin bonding is rather weak(Yap et al., 1997; Wu et al., 2010; Baumgartner et al., 2000).

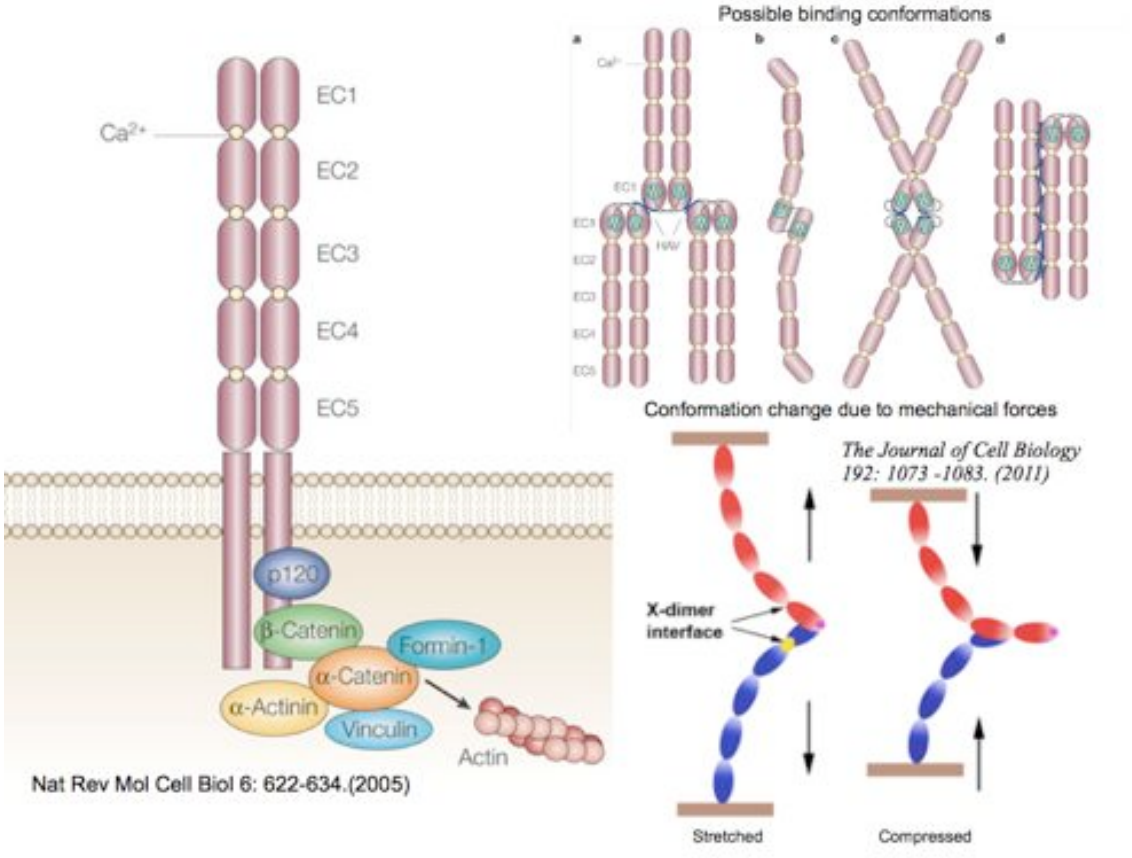

Figure 3.5: Adherens junction complex and different binding conformations

Signaling through the adherens junction

Besides supporting cell–cell adhesion by the extracellular domain of cadherin, the adherens junction also participates in signaling events, cellular polarity, and connection between actin cytoskeleton and cell-cell junction. All these functions are mediated through the cadherin cytoplasmic domains which further bind to other adaptor proteins, especially the catenin family proteins. The catenins can regulate the formation, stabilization, and turnover of the adherens junction(Perez-Moreno et al., 2006). The linkage of actin and microtubule cytoskeletons to adherens junctions is also ascribed to the catenins(Harris et al., 2010; Mège et al., 2006), though the exact mechanism of this linkage remains unclear(Nelson, 2008). In addition, diverse signaling processes are integrated through the catenins including the Rho family GTPases and the Wnt pathway(Braga et al., 2005; Nelson, 2008). As a consequnce, the cadherin-catenin complexes are capable of modulating intrinsic cellular behavior like polarity and mechanical property in response to extrinsic cues provided by the microenvironment.

The structure of tight junction

Tight junctions are located at the most apical end along the intercellular boundary. The adhesion is based on transmembrane proteins such as claudins and occludins which bind directly with their counterpart from neighboring cell. The tight sealing of the paracellular space is achieved by the polymerization of these transmembrane protein to form a molecular chain of barriers (Figure3.6).

The formation of tight junction

The invariable formation of tight junction apically to the adherens junction emphasizes the coupling between the two junction complexes. In both developing embryos and cultured cells, the formation of tight junction is dependent on the prior formation of adherens junction. It is possible that cadherin initiates intracellular signal to instruct the assembly to tight junctions, or tight junction use cadherin as scaffold for assembly(Mitic et al., 1998; Hartsock et al., 2008).

Signalings through the tight junction

The cytoplasmic part of the tight junction transmembrane protein interacts with various scaffold proteins. The resulting complex protein network plays pivotal role in polarity signaling pathway, and makes connection between tight junction and actin cytoskeleton (Figure3.6)(Shin et al., 2006). In addition to their ability to tight seal the intercellular spaces, tight junction also forms a barrier to segregate the apical membrane domain from the remaining basal-lateral membrane domain. Thus, tight junction is usually considered as a hallmark for fully polarized epithelial cells(Pollard et al., 2003).

Mechanic coupling of tight junction

In addition to their well-known functions in paracellular transportation and segregation of membrane domains, the interaction between actin cytoskeleton and tight junction components including ZO and Cingulin suggests they are potentially coupled to mechanical response. Studies on pulmonary epithelial cell have demonstrated the paracellular permeability could be modulated by mechanical stretching(Gonzalez-Mariscal et al., 2006).

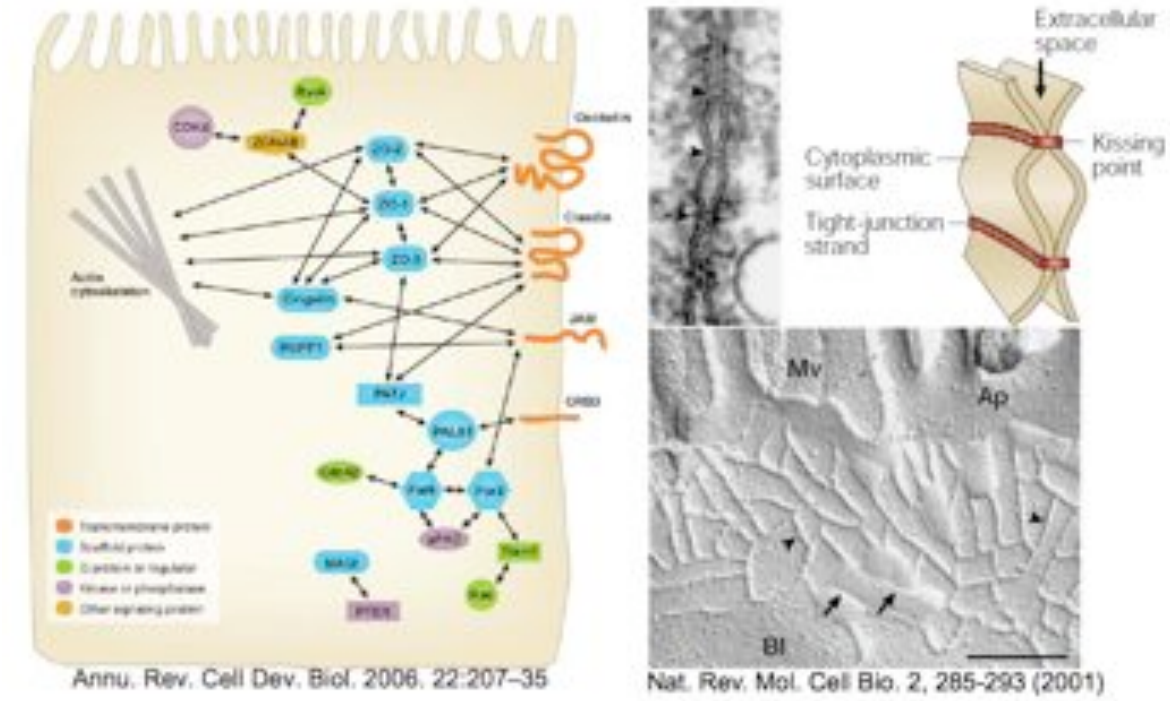

Figure 3.6: Tight junction complex

The structure of desmosomes

Desmosomes are another major class of intercellular junction found in vertebrate epithelia. Like the adherens junction, the intercellular adhesion of desmosomes are mediated by transmembrane cadherins: the Desmocollin and Desmoglein. In contrast to the classical cadherins, a mature desmosomal junction is composed of both homophilic and heterophilic interaction between Desmocollin and Desmoglein(Green et al., 2009). The cytoplasmic tail of desmosomal cadherin binds to catenin-like proteins which in turn bind to intermediate filaments(IF) (Figure3.7). As an analogy to the adherens junctions, the desmosomes make physical binding between neighboring cells and bridge the mechanical continuity by linking the IF cytoskeletons. This mechanical role is supported by the fact that dysfunction of desmosomal proteins will lead to skin and heart fragility.

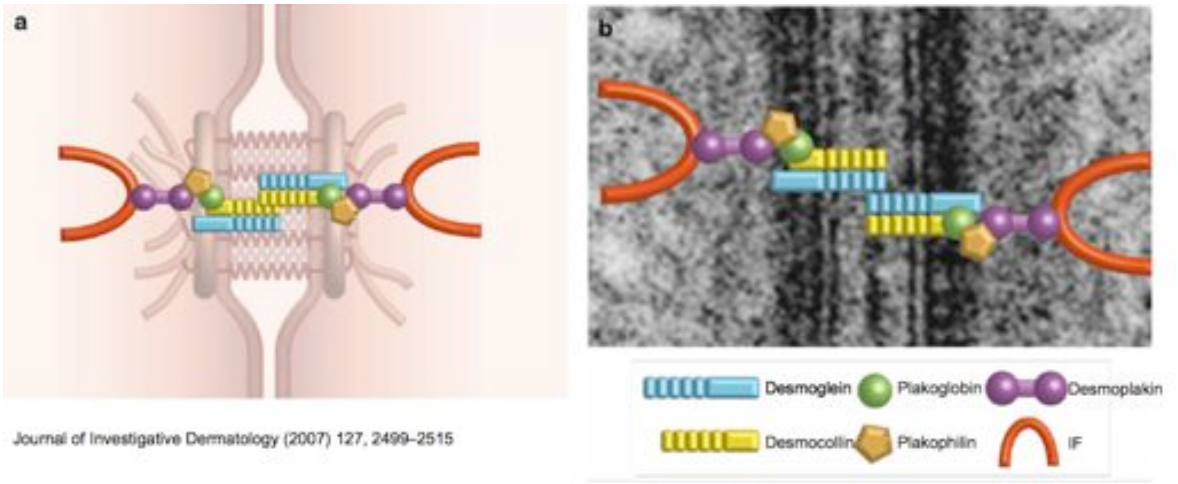

Figure 3.7: The structure of the desmosome complex

The formation of desmosomes

The formation of desmosomes is also believed to be associated with adherens junctions. Experiments suggest the existence of an initial association between E-cadherin and plakoglobin, the desmosomal catenin. Besides, this association is essential for subsequent desmosomes maturation (Garrod et al., 2002; Green et al., 2009). The appearance of desmosomal proteins at the cell-cell contact border can be seen rapidly after initial contact. This punctuate nascent junctions are then coalesced into more stable plaques linked with intermediated filament bundles(Pasdar et al., 1988). This maturation process

requires both intermediate filaments and actin filaments(Godsel et al., 2005). An alternating arrangement of adherens junctions and desmosomes was observed in cultured keratinocytes(Green et al., 1987).

Crosstalk between integrin and cadherin adhesions

Taking into account their connections with actin cytoskeleton and engagement of many common signaling effectors, the crosstalk between integrin and cadherin adhesion has been frequently mentioned. The crosstalk can be either mediated through their common regulatory signaling pathways, or directly by the mechanical coupling through their linkage with actin cytoskeleton(Weber et al., 2011).

Among their common signaling effectors, the Rho-family GTPase is one of the most studied in the framework of integrin-cadherin crosstalk. Integrin is well known for its implication in the Rho GTPase pathway(Huveneers et al., 2009), while the cadherin based cell-cell junction is also extensively interacting with the Rho family proteins(Watanabe et al., 2009). Evidently, Rho GTPase can be the direct mediator between the integrin and cadherin adhesion(Grosheva et al., 2001; Chu et al., 2004; Yano et al., 2004). Nonetheless, other signaling pathways like the tyrosine kinase Src or Ras family proteins were also implicated in this crosstalk (Wang et al., 2006; Retta et al., 2006).

Apart from the interaction via the signaling pathway, the two adhesion system could also directly communicate through the actin cytoskeleton. The mechanical force transduced through the actin network can act as a regulator for both integrin and cadherin adhesions if we consider their potential mechanosensitivities(Bershadsky et al., 2006). Indeed, recent studies have demonstrated such crosstalk through the contractility of actin network(de Rooij et al., 2005; Liu et al., 2010).

Apical-basal polarity and adhesion systems

The establishment of cell polarity (i.e. asymmetric distribution of cellular components), is indispensable for morphogenesis process and proper functioning of epithelia. For example, the direction of nutrient transportation across the intestinal epithelia follows the global tissue geometry, that is from lumen side toward the inner connective tissue of the gut. At the same time, the organization of single cell within the intestinal epithelia follows as well the global tissue geometry, with an asymmetric organization of organelles ensuring the directional transportation of nutrients from apical lumen side toward basal matrix side. Considering the fact that the polarity of individual cell complies with tissue morphology and this polarity is well coordinated between neighboring cells, it is plausible that polarity is triggered and regulated by cell-ECM and cell-cell adhesions(Yeaman et al., 1999).

Initiate apical-basal polarity via the adhesion systems

It has been shown that even in the absence of cell-cell adhesion, adhesion to ECM was sufficient to setup the apical-basal identity(Streuli et al., 1995; Nelson, 2009). The cell-ECM interaction is also critical for signaling the formation of apical membrane domain and luminal space in epithelial cyst formation(Yu et al., 2005; O'Brien et al., 2001; Bryant et al., 2008). The polarity complexes are found to be recruited to intercellular junction upon initial cell-cell contact(Ohno, 2001; Suzuki et al., 2002). In addition, the tight junctional protein ZO-1 is also presented at the early cadherin-based cell-cell junction(Itoh et al., 1997; Ando-Akatsuka et al., 1999), thus potentiate subsequent formation of tight junction which is a key signature of epithelial polarity(Shin et al., 2006).

Maintenance of epithelial polarity through adhesion systems

A more complete epithelial polarization requires the spatial segregation of membrane phospholipids, notably the PtdIns(3,4,5)P_3 and PtdIns(3,4)P_2. This is accomplished through distinct apical membrane localization of lipid phosphatase(Martin-Belmonte et al., 2007), which is in turn regulated by the polarity protein complexes associated with cell-cell junctions, especially the tight junctions(von Stein et al., 2005). In mature mammalian epithelia, key polarity regulators are mainly associated with tight

junctions, which itself is regulated by specific apical polarity proteins such as Par3, Par6, aPKC, etc.(Shin et al., 2006). Another important mediator between the adhesion complex and the polarity complex is the Rho family GTPase. Both the adhesion junction and polarity complex are mutually controlled by the activity of Rho family GTPases(Braga et al., 2005).

Epithelial centrosome positioning and polarity

In addition to the apical-basal arrangement of adhesion systems and segregation of membrane domains, another prominent signature of epithelial polarity is the asymmetric organization of internal organelles. This asymmetry is critical for the epithelial functioning such as absorption or excretion, as well as maintaining the apical-basal membrane segregation which requires a directional renewal of membrane components.

Centrosome and A-P polarity

The importance of centrosome in initiating cellular polarity has been demonstrated in the embryos of *Drosophila* and *C. elegans(Raff et al., 1989; Cowan et al., 2004)*. While in somatic cells, the centrosome position is tightly bounded with the nucleus and Golgi apparatus(Bornens, 1977; Saraste et al., 2007). This ensures the intracellular biosynthetic machinery being aligned with the endocytic pathway by the microtubule network(Bornens, 2008). Concomitantly, the resulting bidirectional trafficking is also coordinated with the apical-basal polarity(Rodriguez-Boulan et al., 2005). In non-dividing epithelia, the subapical positioning of centrosome is inherently linked to the ciliogenesis process(Nigg et al., 2009). The position of centrosome is therefore deeply linked with the cortical apicobasal polarity.

The mechanism of centrosome positioning

In many cell types, the centrosome is located near the cell center during the interphase. How this center position is maintained has been an intriguing topic since decades. Reconstituted system using purified proteins showed that the microtubule aster had a self-centering capability(Ndlec et al., 1997) It might be one of the centering mechanism of centrosome *in vivo*, that the microtubules act like rods pushing simultaneously against the rigid cell cortex. Later studies have further demonstrated that both pushing and pulling forces generated by microtubule polymerization or/and by the action of motor proteins are responsible for the active centering of centrosome(Burakov et al., 2003; Grill et al., 2005; Zhu et al., 2010). While these results rather focused on the fundamental mechanisms that kept the centrosome at the center, tissue cells are able to further modulate the centrosome position under different situations including migration,

wound healing, or neuron polarization(Ueda et al., 1997; Etienne-Manneville et al., 2001; de Anda et al., 2005; Gomes et al., 2005).

Centrosome positioning in epithelia

In polarized epithelial cell, the apical localization of centrosome is linked to the direction of vesicle trafficking and ciliogenesis. However, it is not very well addressed whether this apical centrosome is still actively maintained at the cell center. Considering the fact that a substantial number of non-centrosomal microtubules is presented in epithelia, the centrosome positioning mechanism might be different from the cell with only aster-like microtubule network. It has been shown in both living epidermis and cultured keratinocytes that microtubules were anchored to the desmosomes instead of to the centrosome(Lechler et al., 2007). Without such aster-like microtubule network emanating from the centrosome, the centrosome positioning could be very different from conventional view. Moreover, how these non-centrosomal microtubules are anchored near the apical membrane(Mogensen et al., 2000; Meng et al., 2008), and how they are released and transferred from the centrosome could be deeply associated with the epithelial polarity.

It is thus worth to examine the centrosome positioning in the polarized epithelia, and to ask whether this positioning is actively regulating the epithelial polarization process or is passively a consequence resulted from the polarization.

Adhesion and polarity during epithelial remodeling

During the embryonic development in most metazoan, epithelia undergo dramatic remodeling and become mesenchymal-like. This epithelial-mesenchymal transition (EMT) occurs at critical phases during embryogenesis. Owing to this transition, cells are able to detach from a coherent epithelial sheet and travel to specific locations in the embryo where they differentiate into other cell type.

Similar cellular behavior has also been observed in tumor metastasis where carcinoma cells disseminate from the site of primary tumor. During this process, carcinoma cell losses their epithelial traits and acquires mesenchymal phenotypes. Now, many evidences have shown that this process in tumor progression and the EMT in embryonic development share certain common pathways(Thiery et al., 2009). Thus it becomes a crucial issue to understand the mechanisms governing the EMT in both development and pathologic conditions.

Opposite to the process of epithelial junction formation and polarity establishment, EMT involves the loss epithelial polarity and reorganization of adhesion systems. One of the central features of EMT is the downregulation of E-cadherin. Since the E-cadherin-based adherens junction functions as a regulator for other adhesion system, it can be easily imagined a reorganization of adhesion systems accompanying the loss of E-cadherin molecule. In addition to this modification of adhesion system, transformation from epithelial apical-basal polarity to the mesenchymal front-rear polarity is another distinct feature of EMT.

Under pathologic condition, the alteration of both adhesion and polarity is routinely being described despite the hierarchical relationship between them remains unclear. While in development process, different extent of EMT might take place(Friedl, 2004). Epithelia can undergo efficient migration and maintaining cell-cell adhesion at the same time suggesting that the EMT process can be fine-tuned instead of being a binary switch(Revenu et al., 2009). Considering these intermediate situations, it is possible that during EMT the adhesion and polarity can be regulated separately while staying tightly coupled.

Motivations and objectives

The cell-cell adhesion and cell-matrix adhesion have profound influences on the epithelial morphogenesis. The interdependence and cross-regulation between the two adhesion systems is thus a vital issue in morphogenesis. Our current knowledge in this issue is mainly concluded from suppressing or enhancing individual component of the adhesion system. Despite the specificity, this approach is susceptible to omit some cooperative mechanism between each component.

In this study, I am attempting to directly manipulate the spatial organization the adhesion systems with the micropatterning technique. So that we can see how cells respond to the spatial arrangement of adhesion systems imposed on them. This approach allowed us to keep the whole adhesion machinery intact, and observe how they interact with each other in a native form. By the same approach, we also want to examine how the epithelial morphogenesis and remodeling process would react with different spatial arrangement of cell-cell adhesion and cell-matrix adhesion.

3.2 Intercellular junction and centrosome polarity regulated by ECM geometry – (Paper draft)

The paper draft presented here described how the cell-matrix adhesion regulated the stability of cell-cell junction as well as the internal polarity of cell.

The first part of the results demonstrated that there was a direct repulsion effect between integrin and cadherin adhesion, and this effect occurred in a very fast time scale. Consequently, cell-cell junction couldn't get stabilized when placed close to ECM. Cell-cell junction got stabilized when they were away from ECM where less membrane dynamics occurred.

Once the cell-cell junction got stabilized, internal polarity which was indicated by centrosome positioning also became oriented. We found a significant bias of centrosome position toward stabilized cell-cell junction. While cells with unstabilized intercellular junction had their centrosome positioned at the center of cell.

The last part of the paper showed that during epithelial remodeling such as EMT, the cortical polarity (indicated by the spatial segregation between different adhesion complex) and the internal polarity (indicated by centrosome positioning) could be regulated differently.

Spatial segregation of cell-ECM and cell-cell adhesions orients epithelial cell positioning and polarity

Qingzong Tseng[1], Eve Duchemin-Pelletier[2], Alexis Curtet[1], Alexandre Deshiere[2], Hervé Guillou[3], Odile Filhol-Cochet[2] and Manuel Thery[1]

[1] Laboratoire de Physiologie Cellulaire et Végétale, iRTSV, CEA/CNRS/UJF/INRA, 17 rue des martyrs, 38054, Grenoble, France.

[2] Laboratoire de Biologie du Cancer et de l'Infection, iRTSV, CEA/CNRS/UJF, 17 rue des martyrs, 38054, Grenoble, France.

[3] Laboratoire de Thermodynamique des Petits Systèmes, Institut Néel, 25 avenue des Martyrs, 38042, Grenoble, France

ABSTRACT

Multicellular assembly into a functional epithelium results from both cell spatial arrangement and cell polarization. The coupling of these two processes made their respective contributions to the construction and the destruction of epithelium architecture difficult to analyze. In addition, epithelium morphology depends on cell adhesion to both the extra-cellular matrix (ECM) and the neighboring cells. We developed a minimal model system to investigate these mechanisms in mammary epithelial cells. Original ECM micropatterns were used to geometrically constrain cell doublets while letting them the possibility to self-position their inter-cellular junction. Two complementary approaches in which ECM was locally added or removed demonstrated the existence of an active process that segregates cell-ECM and cell-cell adhesions. This segregation mechanism appeared to be a driving force for the positioning and stabilization of cell-cell junctions. The stability of the junction then induced centrosome reorientation toward the junction. Interestingly, epithelium disassembly during the TGFβ-induced epithelial-mesenchymal transition specifically affected the segregation of cell adhesions, and thus the positions of cell junctions, without perturbing the cell polarisation process. Cell polarisation in this context appeared to be fully dependent on Src tyrosine kinase activity. These results revealed the respective and independent contributions of cell adhesion and cell polarization to epithelium morphogenesis. The distinction of these two processes could profoundly change our appreciation of epithelium construction and deconstruction during physiological or pathological events.

INTRODUCTION

The coherence of epithelial assembly is maintained by distinct types of adhesion systems. The cadherin junction plays a major role in the linkage between cells while the integrin adhesion anchors cell to the extra-cellular matrix(ECM). Besides, both adhesion system also convey a wide spectrum of signal corresponding to external stimuli[1].Interestingly, the two adhesion systems share many similarities. For example, they both connect to the actin cytoskeleton and recruit common adapters, and they are both involved in a certain common signalling pathways. Indeed, there is a growing body of evidence showing that the crosstalk between integrin and cadherin is profoundly implicated in the epithelial morphogenesis[2]. However, apart from these similarities, they take distinct spatial localization *in vivo*[3,4], with cadherin based adheren junction near the apical part and integrin based adhesion at the basal face. It remains unclear whether this spatial segregation is resulted from a biochemical incompatibility between the two adhesion systems, or it is purely a consequence of epithelial polarization.

Although this spatial segregation and epithelial polarity could be reconstructed in cultured cells through self-organisation processes. It doesn't allow us to spatially manipulate each adhesion system. We could neither ask how one would be affected by another's localization, nor how the polarity would be modulated regarding to their localization.

Micropatterned substrate provided a system where the cell-ECM interaction could be well defined. It permit us to study how cell-cell adhesion interact with cell-ECM adhesion. With two MCF10A cells on a defined ECM geometry, we could have a minimum system composed of single cell-cell junction and a controlled cell-ECM adhesion.

RESULTS

Absence of ECM can stabilize cell-cell junction

We first studied how the localization of intercellular junction would be influenced by cell-matrix adhesion. About 50 to 100 Cell doublets were recorded by time-lapse microscopy for 24 hours. Thousands of time-lapse images were then analyzed automatically (Figure S1). The orientation of nucleus-nucleus axis implied the localization of cell-cell junction. The overall movement level of cell doublets was also quantified.

On an isotropic ECM microenvironment, two cells built their intercellular junction randomly without any preference and kept turning around each other as previously described(Figure 1A and C)[5]. However, epithelial cells *in vivo* actually encounter an anisotropic microenvironment with ECM contact only at certain location. It prompt us to ask whether the positioning of respective adhesion system would reflect this external heterogeneity. Thus we create gaps devoid of ECM on the [ring]-shaped ECM to mimic the sites of cell-cell adhesion *in vivo* where cells do not contact the matrix. On this heterogeneous ECM, cell doublets started to adopt stable orientations and position their cell-cell junction above the gap where the cell-matrix interaction was absent(Figure 2B and D). The same spatial exclusion effect was also observed by using different ECM proteins (Figure S2).

To understand how this exclusion happened dynamically, we expressed GFP tagged E-cadherin in MCF10A cells and recorded the junction movement on the [gapped-ring] pattern. We observed an active membrane ruffling near the cell-cell junction when the junction was positioned upon cell-ECM adhesion region. At the same time, the cell-cell junction also moved rapidly when it was located over the ECM adhesion region. Once the junction entered the gap devoid of ECM, the membrane ruffling was diminished and junction stopped moving(Figure 1E). We could also see the tension started to build up which was indicated by the straightness of junction[6], analogous to the stable cell-cell junction seen *in vivo*[7].

It has been previously suggested that active membrane protrusion mediated by Rac GTPase could modulate cel-cell junction stability[8], we thus treated cell doublets with a Rac specific inhibitor NSC23766. With Rac inactivation, cell-cell junction positioning

became insensitive to ECM localization (Figure 1F), which implies Rac played an active role in the spatial exclusion between the two adhesion systems.

Presence of ECM adhesion repulse cell-cell junction

To further confirm this spatial exclusion effect, a complementary approach would be testing whether the presence of matrix adhesion would drive away the cell-cell adhesion. Cell doublets adopted two stable configurations with intercellular junction positioned in the midline either horizontally or vertically when there exist two large region devoid of ECM(Figure2A left). However, when cell-ECM adhesion was introduced right under the horizontal midline, the cell-cell junction was much less preferred to be positioned there but rather at the vertical midline(Figure2A right). The exact junction positions were further confirmed by immunofluorescent labeling of the cell-cell junction(Figure2B).

We subsequently analyzed the movement of cell doublet on these two pattern. We found that cells moved faster when their junction lay above ECM than when it lay above ECM free regions. Adding ECM in the horizontal midline induced cell acceleration when the junction passed on it (Figure 2C). We concluded that cell-cell junction was destabilized above cell-ECM adhesion(Figure 2D). The junction stabilization was accentuated as the distance between the two adhesion systems getting increased (Figure S3A). Furthermore, the stabilizing effect associated to the spatial segregation of cell-ECM and cell-cell junction was sufficient to induce cell deformation and cell perimeter increase. (Figure S3B). Taken together, our results showed that the cell-cell junction was actively located away from cell-ECM adhesion and getting stabilized as the distance to ECM adhesion increased. This spatial segregation could be responsible to the polarization of the cell cortex into two adhesion domains with ECM adhesion at the basal face and intercellular adhesion near the apical pole of the lateral face.

Centrosome polarity is orientated toward stable cell-cell junction

A polarized epithelium is not only marked by the segregation of their adhesion system, but also an asymmetric distribution of internal organelles. Centrosome position could serve as an indicator for this internal polarity considering its function in organizing

the transportation of cytosolic materials[9]. The epithelium *in vivo* has their centrosome positioned subapically, proximal to the adheren junction and distal to the matrix adhesion[10]. This *in vivo* configuration could be reproduced in cell culture system as in the 3D acini[11]. Contrarily, during wound healing[12] or in cell group confined on ECM micropattern[13], the centrosome is rather positioned away from cell-cell junction.

These discrepancy made us wondering how the internal polarity is regulated by the cortical polarity. Thus we measured the centrosome position of cell doublets on [ring] and [gapped-ring] shaped ECM (Figure 3A). On the [ring]-shaped pattern, cell doublets kept turning and junctions were less stabilized, the majority of centrosomes were located near the center of nucleus. While on the [gapped-ring] pattern where the absence of ECM facilitated the stabilization of cell-cell junction, the majority of centrosomes were positioned toward the junction(Figure 3B and C). Moreover, after separating cell doublets that established their intercellular junction over the gap from those established their junction over the ECM, we could see a more pronounced centrosome polarity orientation toward those stabilized cell-cell junctions(Figure 3C and D). Statistical analysis confirmed this bias of centrosome polarity toward cell-cell junction(Figure3E). These results demonstrate centrosome is positioned toward a stable, non-moving, cell-cell junction. Epithelial morphogenesis appears to be based on spatial segregation of the two main adhesion systems. This segregation induces cell-cell junction stabilization, which in turn promotes centrosome polarity toward the junction.

Centrosome polarity is maintained in TGFβ-induced EMT but disrupted upon Src inhibition

The stability of cell-cell junction and cell polarization are two key elements of epithelial morphogenesis that are regulated during EMT[14]. Similar remodelling phenotypes has also been described during cancer metastasis[15]. In the classical experimental system such as 3D acini, EMT is characterized by the disruption of cell-cell junction and lost of epithelial polarity[16,17]. However, since the junction positioning and cell polarity is tightly coupled , it is difficult to identify their respective contribution during EMT. Epithelial cells aggregate and form mammary acini-like structures when cultured in matrigel (Figure 4A). WT cells form hollow structures with cell polarity oriented toward cell-cell junction away from the ECM surrounding the acinus. When EMT was induced by TGFβ treatment[18], cells

within acini got mispositioned. Nonetheless the orientation of polarity was difficult to analyse since cells had junctions all around. Positioning and polarization processes were difficult to distinguish. Our minimal model system set up a favourable circumstance to study these two processes during EMT.

We first found that TGFβ treated cells became randomly positioned on [gapped-ring] pattern (Figure 4B). This inferred that the the mechanism of spatial segregation between cell-ECM and cell-cell adhesions was no longer maintained. Surprisingly, TGFβ treated cells still maintained the capacity to orient their centrosome polarity toward junction(Figure 4C), albeit the junction was unable to be stabilized by the absence of ECM. We then wondered how the centrosome polarity was maintained in TGFβ treated cells.

Src tyrosine kinase has a pivotal role in the malignant transformation and epithelial plasticity[19,20]. Others has also reported Src intervene with the crosstalk between integrin-cadherin[21,22]. However, the mechanism that how (TGFβ-induced) EMT is mediated by Src remains ambiguous[23,24,25,26]. Hence, we first examined how the normal epithelial junction localization and centrosome polarity would be affect upon Src inhibition by a specific Src kinase inhibitor SU6656. Intriguingly, we found that Src inactivation did not perturb cell positioning (Figure 4B) but rather perturbed centrosome positioning (Figure 4C). We then further asked whether the capacity of maintaining centrosome polarity toward junction in TGFβ treated cells was mediated by Src as well. Inhibition of Src on TGFβ treated cells strongly perturbed their centrosome polarity, thus they had lost both epithelial junction localization and centrosome positioning(Figure 4B, C).

Interestingly, another EMT model by casein kinase knockout[27], showed disrupted junction localization and centrosome polarity even without Src inactivation(Figure S4). This remodelling of junction positioning and centrosome polarity was further confirmed on MCF10A acini. Most peripheral cells in TGFβ treated acini still seem to display oriented polarity toward acinus interior. Acini made of cells treated with TGFβ and SU6656 as well as those made of cells without CK2b consisted of mispositioned and mispolarized cells (Figure 4A and S4).

CONCLUSION

Geometric control of the adhesion systems allowed us to ask how one could be affected by another, and how internal polarity would be organized regarding to the localization of cortical adhesion systems. Despite of the amenability to large throughput analysis and ease of imaging, it should be noted that our minimum 2D system is insufficient to reproduce a *bona fide* apical-basal epithelial polarity as seen in 3D acini or confluent monolayer systems due to the topological limitation to form a closed barrier segregating different membrane domains.

The mechanism governing the epithelial morphogenesis inevitably involves in epithelial remodelling during EMT. While the extreme case of EMT is described as complete dissociation of junction and disruption of polarity resembled to tumor metastasis, different extent of EMT take place during development as well[28]. EMT induced by TGFβ might reflect this scenario in which the segregation between the two adhesion systems no longer exist but the capability to orient internal cell polarity was still maintained. Under this circumstance, epithelial cells could undergo dramatic remodelling, bringing cell-cell junctions closer to cell-ECM adhesions. At the same time, cells are still able to position their centrosome toward the junction, so that their internal polarity is coordinated with external adhesive cues. On the other hand, removing casein kinase or inhibition of Src kinase might engender a more pathological EMT where cells lose both the segregation of the two adhesion systems and the orientation of internal polarity. Src has been shown to be a main effector of TGFβ pathway. The prominent phenotype after Src upregulation is the dissociation of cell-cell junction and scattering of cells. While there is no direct evidence showing how Src could regulate centrosome positioning, it has been reported that p120 catenin, a major substrate of Src[29], associate with microtubules and localize with centrosome[30,31].

In summary, we propose a model (Figure 5) that the spatial segregation between the cell-ECM and cell-cell adhesions is not just a passive result of epithelial polarization, but instead participates actively in the formation and stability of a polarized epithelial adhesion systems. Subsequently, internal polarity is organized regarding to this polarized cortical polarity. During EMT, cells could alter their morphology via revoking this spatial segregation while the disruption of the internal polarity is context dependent.

REFERENCES

1. Papusheva, E. & Heisenberg, C. Spatial organization of adhesion: force-dependent regulation and function in tissue morphogenesis. *EMBO J* 29, 2753-2768 (2010).

2. Chen, X. & Gumbiner, B.M. Crosstalk between different adhesion molecules. *Current Opinion in Cell Biology* 18, 572-578 (2006).

3. Tyler, S. Epithelium—The Primary Building Block for Metazoan Complexity. *Integrative and Comparative Biology* 43, 55 -63 (2003).

4. Alberts, B. et al. *Molecular Biology of the Cell, Fourth Edition*. (Garland Science: 2002).

5. Huang, S., Brangwynne, C.P., Parker, K.K. & Ingber, D.E. Symmetry-breaking in mammalian cell cohort migration during tissue pattern formation: role of random- walk persistence. *Cell Motil. Cytoskeleton* 61, 201-213 (2005).

6. McLachlan, R.W. & Yap, A.S. Protein tyrosine phosphatase activity is necessary for E-cadherin-activated Src signaling. *Cytoskeleton (Hoboken)* 68, 32-43 (2011).

7. Rauzi, M., Verant, P., Lecuit, T. & Lenne, P. Nature and anisotropy of cortical forces orienting Drosophila tissue morphogenesis. *Nat. Cell Biol* 10, 1401-1410 (2008).

8. Yano, H. et al. Roles played by a subset of integrin signaling molecules in cadherin-based cell–cell adhesion. *The Journal of Cell Biology* 166, 283 -295 (2004).

9. Rodriguez-Boulan, E., Kreitzer, G. & Musch, A. Organization of vesicular trafficking In epithelia. *Nat Rev Mol Cell Biol* 6, 233-247 (2005).

10. Trier, J.S. STUDIES ON SMALL INTESTINAL CRYPT EPITHELIUM. *The Journal of Cell Biology* 18, 599 -620 (1963).

11. Underwood, J.M. et al. The ultrastructure of MCF-10A acini. *J. Cell. Physiol* 208, 141-148 (2006).

12. Euteneuer, U. & Schliwa, M. Mechanism of centrosome positioning during the wound response in BSC-1 cells. *The Journal of Cell Biology* 116, 1157 -1166 (1992).

13. Desai, R.A., Gao, L., Raghavan, S., Liu, W.F. & Chen, C.S. Cell polarity triggered by cell-cell adhesion via E-cadherin. *J Cell Sci* jcs.028183 (2009). doi:10.1242/jcs.028183

14. Nelson, W.J. Remodeling Epithelial Cell Organization: Transitions Between Front–Rear and Apical–Basal Polarity. *Cold Spring Harbor Perspectives in Biology* 1, (2009).

15. Thiery, J.P. Epithelial-mesenchymal transitions in tumour progression. *Nat Rev Cancer* 2, 442-454 (2002).

16. Feigin, M.E. & Muthuswamy, S. Polarity proteins regulate mammalian cell-cell junctions and cancer pathogenesis. *Curr Opin Cell Biol* 21, 694-700 (2009).

17. Viloria-Petit, A.M. et al. A role for the TGFβ-Par6 polarity pathway in breast cancer progression. *Proceedings of the National Academy of Sciences* 106, 14028 -14033 (2009).

18. Zavadil, J. & Böttinger, E.P. TGF-beta and epithelial-to-mesenchymal transitions. *Oncogene* 24, 5764-5774 (2005).

19. Thiery, J.P. Epithelial-mesenchymal transitions in development and pathologies. *Current Opinion in Cell Biology* 15, 740-746 (2003).

20. Debnath, J. & Brugge, J.S. Modelling glandular epithelial cancers in three- dimensional cultures. *Nat Rev Cancer* 5, 675-688 (2005).

21. Wang, Y. et al. Integrins regulate VE-cadherin and catenins: Dependence of this regulation on Src, but not on Ras. *Proceedings of the National Academy of Sciences of the United States of America* 103, 1774 -1779 (2006).

22. Martinez-Rico, C., Pincet, F., Thiery, J. & Dufour, S. Integrins stimulate E-cadherin-mediated intercellular adhesion by regulating Src-kinase activation and actomyosin contractility. *J Cell Sci* 123, 712-722 (2010).

23. Galliher, A.J. & Schiemann, W.P. Beta3 integrin and Src facilitate transforming growth factor-beta mediated induction of epithelial-mesenchymal transition in mammary epithelial cells. *Breast Cancer Res* 8, R42 (2006).

24. Cicchini, C. et al. TGF[beta]-induced EMT requires focal adhesion kinase (FAK) signaling. *Experimental Cell Research* 314, 143-152 (2008).

25. Maeda, M., Shintani, Y., Wheelock, M.J. & Johnson, K.R. Src Activation Is Not Necessary for Transforming Growth Factor (TGF)-β-mediated Epithelial to Mesenchymal Transitions (EMT) in Mammary Epithelial Cells. *Journal of Biological Chemistry* 281, 59 -68 (2006).

26. Piek, E., Moustakas, A., Kurisaki, A., Heldin, C. & ten Dijke, P. TGF-(beta) type I receptor/ALK-5 and Smad proteins mediate epithelial to mesenchymal transdifferentiation in NMuMG breast epithelial cells. *J Cell Sci* 112, 4557-4568 (1999).

27. Deshière, A., Theis-Febvre, N., Martel, V., Cochet, C. & Filhol, O. Protein kinase CK2 and cell polarity. *Mol. Cell. Biochem* 316, 107-113 (2008).

28. Revenu, C. & Gilmour, D. EMT 2.0: shaping epithelia through collective migration. *Current Opinion in Genetics & Development* 19, 338-342 (2009).

29. Reynolds AB et al. Identification of a new catenin: the tyrosine kinase substrate p120cas associates with E-cadherin complexes. *Mol Cell Biol* 14, 8333-8342 (1994).

30. Meng, W., Mushika, Y., Ichii, T. & Takeichi, M. Anchorage of Microtubule Minus Ends to Adherens Junctions Regulates Epithelial Cell-Cell Contacts. *Cell* 135, 948- 959 (2008).

31. Perez-Moreno, M., Song, W., Pasolli, H.A., Williams, S.E. & Fuchs, E. Loss of p120 catenin and links to mitotic alterations, inflammation, and skin cancer. *Proceedings of the National Academy of Sciences* 105, 15399 -15404 (2008).

MATERIALS AND METHODS

Immunofluorescent staining

Thirty hours after plating cells on micropatterned coverslip, cells were either extracted in cytoskeleton buffer (10mM MES, 138mM KCl, 3mM MgCl, 2mM EGTA, pH6.1)containing 0.5% TritonX-100, then fixed in 4% paraformaldehyde; or fixed directly by Methanol in -20°C for 6 minutes. Fixed cells were incubated with 1:1000 dilution of anti gamma-Tubulin (Abcam ab11317) antibody for centrosome staining, 1:200 dilution of anti alpha-Catenin(Calbiochem B52975)or 1:50 dilution of anti E-cadherin (Santa Cruz sc8426) for 1 hour, and then incubated with corresponding secondary antibodies for 30 min. All the antibodies were diluted in PBS containing 0.1% Tween, 3% BSA. After PBS washing, coverslips were mounted in Mowiol mounting medium.

Video microscopy and Image acquisitions

Time-lapse acquisitions were taken with an inverted microscope (Axiovert 200M; Carl Zeiss, Inc.). The temperature, CO_2, and humidity control were performed using a Box and Brick system (Life Imaging Services). Multiple positions were recorded using an XY motorized stage (Marzhauser) with a 15-min time frame over 48 h with a dry 10× phase-contrast objective. Fluorescence images were taken using an upright microscope (BX61; Olympus) with 100x (NA 1.4) oil immersion objectives mounted on a piezo ceramic (Physics Instruments). Both microscopes were controlled with Metamorph software (MDS Analytical Technologies).

Cell culture and kinase inhibition

The culture of MCF10A cells and the generation of ΔCK2β cell line was described previously[27]. Cells were seeded on patterned substrate at a density of $8x10^4/cm^2$. Cells not attaching to the adhesive region on the substrate were washed away 1 hours after seeding. TGFβ (R&D systems) was added at 2ng/mL to the culture medium 48hr before cell plating on micropattern and during time-lapse acquisition as well. After cell spreading on micropatterns, Hoechst 33342 was added at 5ng/mL to label nucleus during time-lapse

movie. 24 hours after plating cell, 10uM NSC23766 (Tocris) was added to medium for Rac inhibition or 5uM SU6656 (Calbiochem) for Src inhibition.

Automated nuclei tracking

Image field from each stage position was first segmented to 36 sub-region based on micropattern positions. Sub-regions were first screened for existence of nucleus by standard deviation of pixel intensities. Nucleus images were then convolved by a 9x9 mexican hat kernel. Binarized nuclei images were obtained by automatic thresholding and a median filter to remove isolated noise pixels. After a watershed segmentation, the number of nuclei was determined considering their size and shape factor as well. For the analysis without inhibitor, only subs-regions containing only one nucleus at the beginning were selected for subsequent mitosis detection. Based on the nucleus shape factor, intensity variation, and the number of nucleus detected, division from one cell to two cells could be detected. Then only after cell division, the orientations of nucleus-nucleus axis were recorded. The measurement went on until the end of the time-lapse series or the detection of the second mitosis event.

Micropatterned substrate fabrication

Glass coverslips were first spin-coated with adhesion promotor Ti Prime (MicroChemicals) and then with 0.5% polystyrene at 3000rpm. Polystyrene coated coverslips were oxidized through oxygen plasma (FEMTO;Diener Electronics) 10s at 30W before incubating with 0.1mg/mL PLL-PEG (Surface Solutions) in 10mM HEPES pH7.4 for 15min. Afterward, coverslips were insolated with deep UV (UVO cleaner, Jelight) through a photomask (TOPPAN) for 2min. Right after UV activation, coverslips were incubated with 20ug/mL of selected ECM protein (Sigma) and 10ug/mL of fluorescent fibrinogen conjugate (Invitrogen) solution in PBS for 30min. Coverslips were washed 3 times with sterile PBS before plating cells.

MCF10A acini and confocal imaging

$1x10^4$ cells were seeded in chamber slides coated with Growth factor reduced EHS ECM (Matrigel® BD Biosciences; with protein concentrations between 9 and 11 mg/ml) in assay medium (DMEM/F12 supplemented with 2% donor Horse serum, 10 µg/ml insulin, 0.5 µg/ml hydrocortisone, 100 ng/ml Cholera toxin, 5 ng/ml EGF (Peprotech, France). Assay medium was replaced every 3 days. When indicated, at day 6, cells were treated with 2ng/ml TGF for 50h.

3D cell structures were performed using a Leica TCS-SP2 laser scanning confocal apparatus coupled to a Leica DMIRBE microscope.

FIGURE LEGENDS

Figure 1

A- Phase contrast and nuclei images from time-lapse movie, with angular distribution histogram and movement analysis of cell doublets on [ring] (A) and [gapped-ring] (B) shaped micropattern. C- Examples of immunofluorescent staining of alpha-catenin and averaged images on [ring] (C) and [gapped-ring] (D). (E) High magnification time-lapse images of E-cadherin-GFP expressing cells on [gapped-ring] showing junction rotation and membrane ruffles (arrow) on ECM followed by junction stabilization and stretching in the gap. (F) Cells positions and movement analysis of cells on [gapped-ring] after Rac inhibition. Statistical test is a Kolmogorov-Smirnov test, ***=99% confidence in the difference between the two distributions.

Figure 2

(A) Cell doublet positioning on [cross] and [cross+bar] from video analyses. (B) Examples of immunofluorescent staining of E-cadherin and averaged images on [cross] (left) and [cross+bar] (right). (C) Movement analysis of cell doublets on [cross] and [cross+bar] showing proportion of moving frames in individual movies (left) and averaged angular speed for each position. Arrows indicate cell acceleration when the junction passes over ECM along diagonals on [cross] (red arrows), along diagonals and horizontal bar on [cross+bar] (blue arrow). (D) Scheme showing stable and unstable junction positioning in response to ECM geometry.

Figure 3

(A) Internal cell polarity orientation was quantified by measuring centrosome position with respect to the nucleus center and the orientation of the nucleus-nucleus axis, lengths were normalized with respect to nucleus radius. All centrosome positions, black dots, were plotted in this referential. Dashed line represents the approximate cell shape in this referential. Centrosomes positions were then classified in different regions: central (blue) or peripheral, toward cell-cell junction (red) or on the opposite side (green). (B) Immunofluorescent staining of centrosome (gamma-Tubulin in green), cell-cell junction (alpha-Catenin in red), nuclei (DNA in blue) and micropatterned ECM in gray ([ring] on

top [gapped-ring] in the bottom. (C) Centrosome positioning in each sub-cellular region when cells were plated on [ring] or [gapped-ring]. The positions on [gapped-ring] could be separated into those corresponding to stable or unstable cell doublets position with respect to ECM. (D) Scheme showing the stable and unstable cell doublets positions on [gapped-ring]. (E) Statistical comparison of centrosomes positions along the nucleus-nucleus axis. High x values correspond to large centrosome off-centering toward cell-cell junction. Statistical tests correspond to Student T test. *** = P<0,001.

Figure 4

(A) Immuno-fluorescence stainings on 7-days old MCF10A acini in Matrigel showing Golgi apparatus (red), nuclei (blue) and actin (green) in control conditions or in the presence of TGFbeta and Src tyrosine kinase inhibitor SU6656. (B) Cell position and centrosome orientation on [gapped-ring] illustrated by immuno-fluorescence staining of nuclei (DNA, blue), centrosome (gamma-tubulin, green) and cell-cell junction (alpha-catenin, red). Circular histograms show cell positions on [gapped-ring] in response to TGFbeta and/or Src tyrosine kinase inhibition by SU6656. Statistical tests are Kolmogorov-Smirnov tests, ***=99% confidence in the difference between the two distributions. (C) centrosome orientation in cells plated on [gapped-ring] in response to TGFbeta and/or Src tyrosine kinase inhibition by SU6656. Top histogram shows in color centrosome positioning in each sub-cellular regions. Bottom histogram represents centrosome positions along the nucleus-nucleus axis, toward the adjacent cell. Statistical tests correspond to Student T test. *** = P<0,001.

Figure 5

Schematic model showing the junction positioning and stabilization as well as centrosome positioning during epithelium maturation in the upper part followed by subsequent disruption of this geometry and polarity via different pathways in the lower part.

Figure S1

(A) Automated detection of mitosis event from fluorescent images of nuclei staining with Hoechst in 10x video-microscopy acquisitions and 15 minutes time-frame. Fluorescence

intensity increase during metaphase and object separation during anaphase are used to detect mitosis and determine the part of the movie in which daughter cell positions has to be analyzed. (B) Example of image thresholding and segmentation to detect nuclei positions and automatically record nucleus-nucleus orientation. (C) The measured angles of nucleus-nucleus axis orientation over time from all movies were pooled and plotted together in a circular histogram showing the angular distribution of cell doublets (right top graph). The histogram has been made circular for clarity but is identical modulo 180°. In addition, for each movie, the instantaneous angular speed is calculated at every time point. Comparison between measured value and personal visual appreciation of movement led to the determination of an arbitrary threshold of 0.3 degree/min above which cell position change was considered as a movement. For each movie, this ratio was used to calculate the proportion of moving frame. All these percentage (one per movie) were graphically represented with a "scatter plot" graphic (right bottom part).

Figure S2

(A) Instantaneous angular speed is plotted against nucleus-nucleus orientation on [ring] (blue) and [gapped-ring] to visualize speed variations depending on local ECM density. Error bars show 95% confidence interval on average speed value. Angular speed is lower when cell-cell orientation is around 0° (=180°) i.e. when the cell-cell junction pass above the ECM gap. (B) Angular distributions of nucleus-nucleus axis orientations measured on collagen or laminin coated [ring] and [gapped-ring]. Stabilization of the junction along the ECM gap occurred in both conditions.

Figure S3

(A) Length of the gap in [gapped-square] shaped micropatterns was increased on three different micropatterns to test the effect of the distance between cell-ECM adhesion and cell-cell junction on junction stability. Angular distributions of nucleus-nucleus axis orientations as well as the distributions of the proportions of moving frame in each movie demonstrated the stabilizing effect of the distance. (B) On [square] shaped micropatterns, cell doublets adopted two equivalent states with their junction oriented horizontally or vertically corresponding to the minimization of their perimeter. Cells positioning along diagonals, with elongated junctions along diagonals appeared unstable. Gaps were added

on the micropatterns to test whether the stabilization effect of cell-cell junction due to ECM removal could compensate the destabilization effect due to cell-cell junction and cell perimeter lengthening. Angular distributions of nucleus-nucleus axis orientations confirmed that ECM gap had such a strong stabilizing effect that they were sufficient to stabilize cell-cell positioning along diagonal and promote cell distortion. Images show F-actin (magenta), E-cadherin (white), nuclei (blue), and ECM (green) staining on [square] and [gapped-square].

Figure S4

Cell positioning and internal polarity orientation of CK2 knock-down cells on [gapped-ring]. (A) Angular distributions of nucleus-nucleus axis orientations. Statistical test is a Kolmogorov-Smirnov test, *** = 99% confidence in the difference between the two distributions. (B) Representation of centrosome position in different sub-cellular regions showed a reduction of orientations toward junctions and an increase of orientations in the opposite direction (top). Statistical comparison of centrosomes positions along the nucleus-nucleus axis (bottom). Statistical tests correspond to Student T test. * = P<0,01. C-Immuno-fluorescence stainings on 7-days old dCK2 MCF10A acini in Matrigel showing Golgi apparatus (red), nuclei (blue) and actin (green). Cells were mis-positioned and appeared also mis-oriented since some peripheral cells had their Golgi apparatus oriented outwards.

FIGURES

Figure 1 Cell-cell junction is stabilized away from ECM

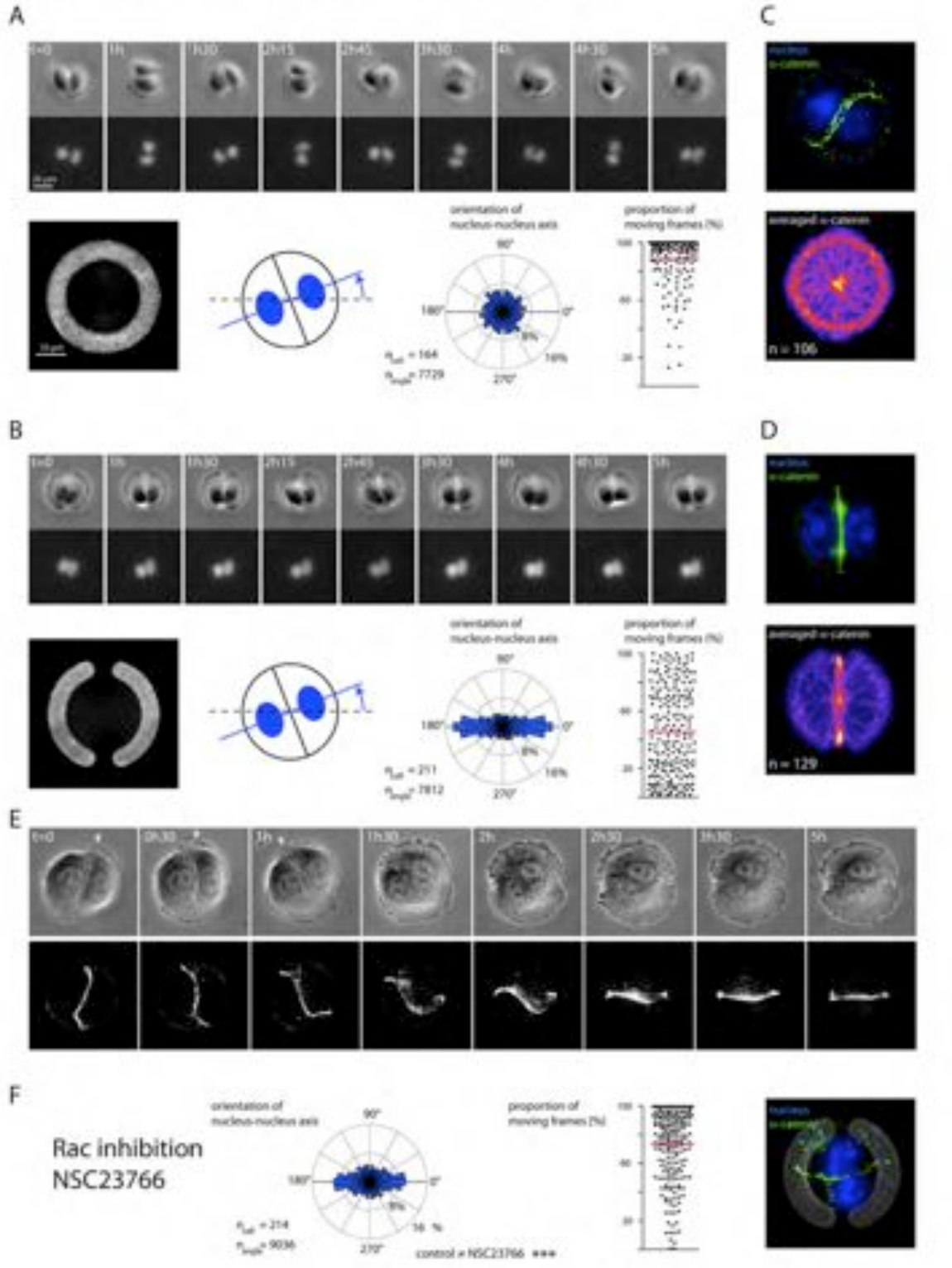

Figure 2: Contact with ECM destabilizes cell-cell junction

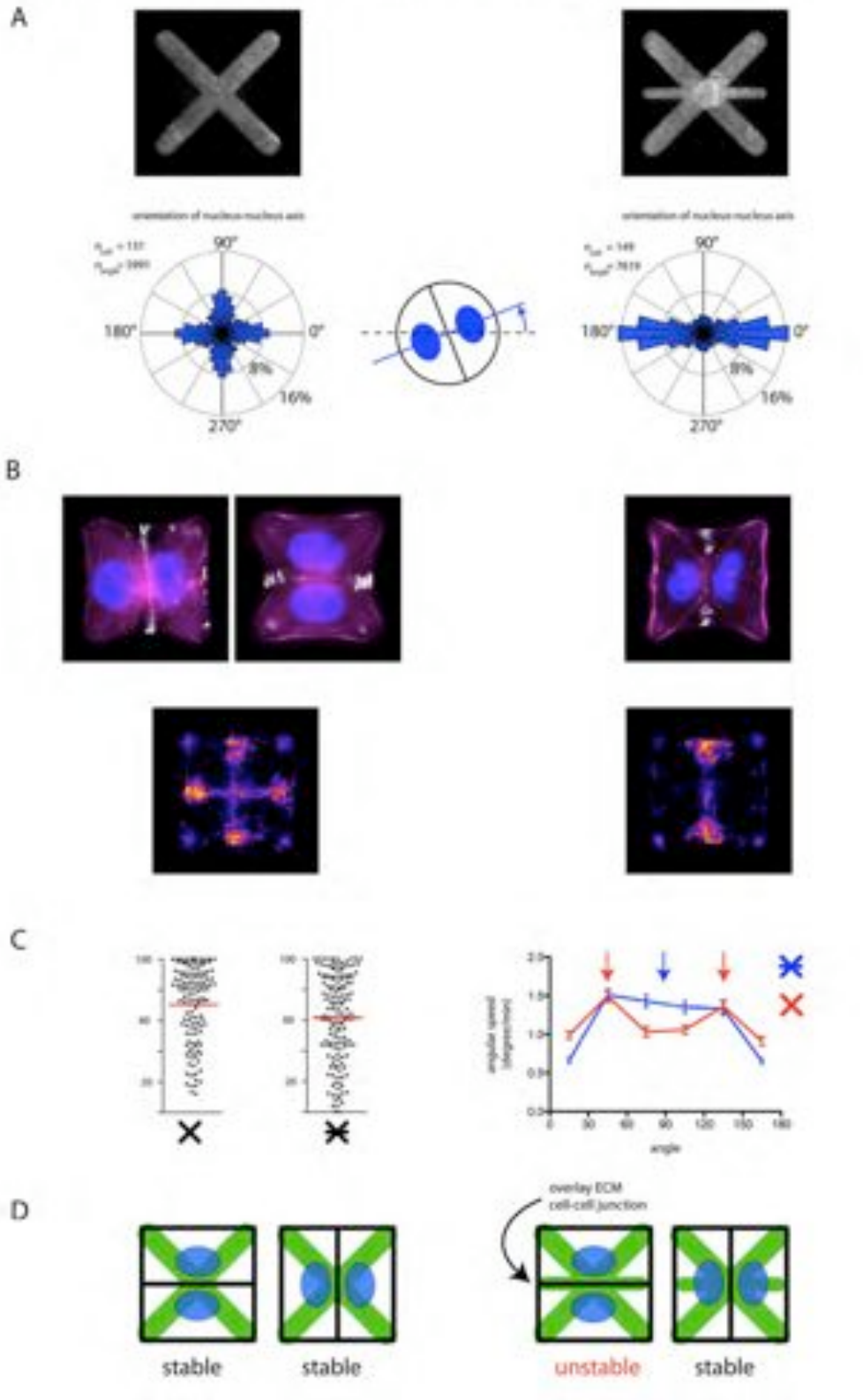

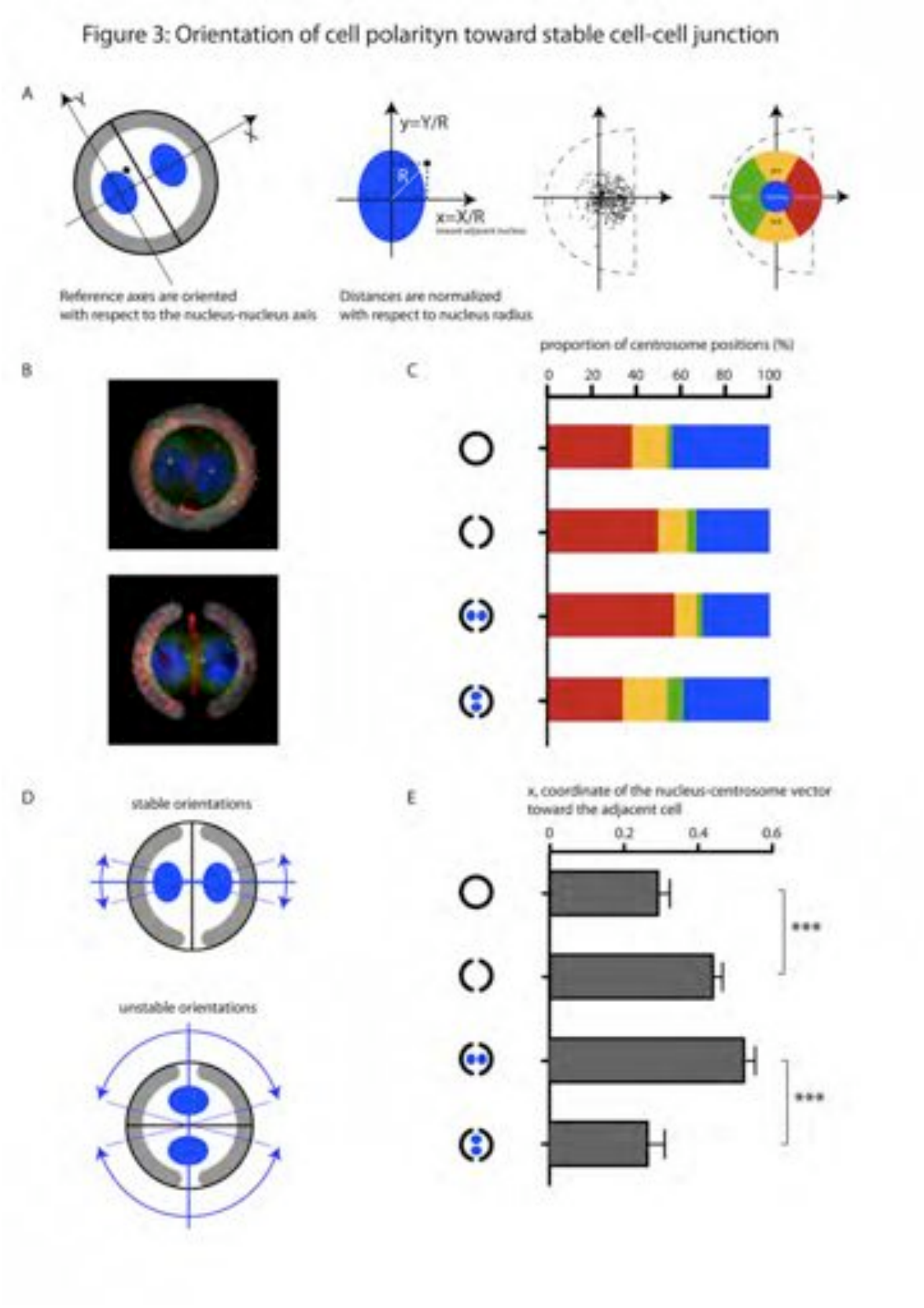
Figure 3: Orientation of cell polarityn toward stable cell-cell junction
A
Reference axes are oriented with respect to the nucleus-nucleus axis
y=Y/R
x=X/R
Distances are normalized with respect to nucleus radius
B
C
proportion of centrosome positions (%)
0
20
40
60
80
100
D
stable orientations
unstable orientations
E
x, coordinate of the nucleus-centrosome vector toward the adjacent cell
0
0.2
0.4
0.6
***
***

Figure 4 : Cell position and polarity during EMT-induced epithelial deconstruction

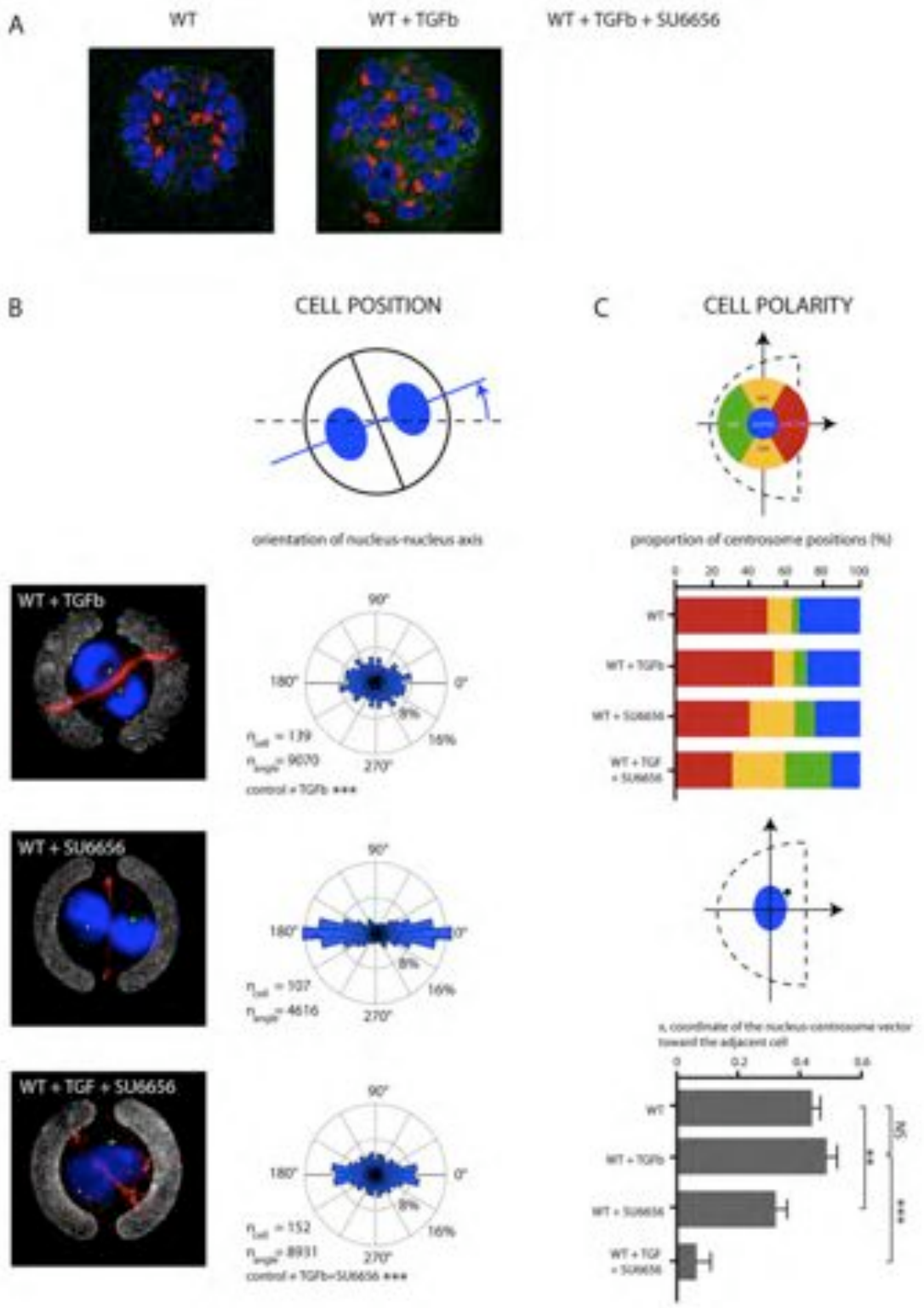

Figure 5 : Cell geometry and cell polarity in epithelium morphogenesis

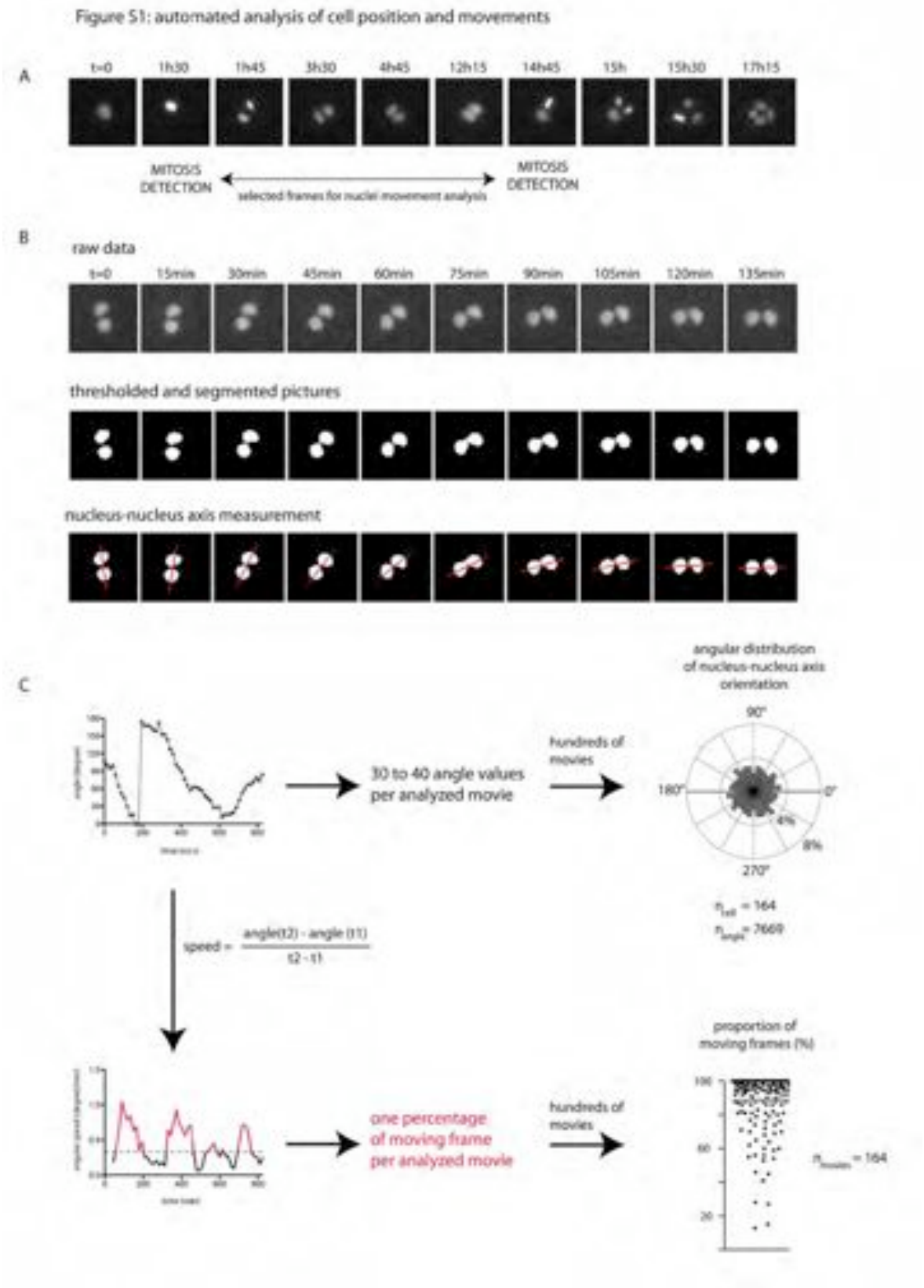
Figure S1: automated analysis of cell position and movements
A
t=0
1h30
1h45
3h30
4h45
12h15
14h45
15h
15h30
17h15
MITOSIS DETECTION
selected frames for nuclei movement analysis
MITOSIS DETECTION
B
raw data
t=0
15min
30min
45min
60min
75min
90min
105min
120min
135min
thresholded and segmented pictures
nucleus-nucleus axis measurement
C
30 to 40 angle values per analyzed movie
hundreds of movies
angular distribution of nucleus-nucleus axis orientation
90°
180°
0°
270°
4%
8%
speed = angle(t2) - angle (t1) / t2 - t1
one percentage of moving frame per analyzed movie
hundreds of movies
proportion of moving frames (%)
100
60
20

Figure S2: Stability of cell positioning in response to various ECM components

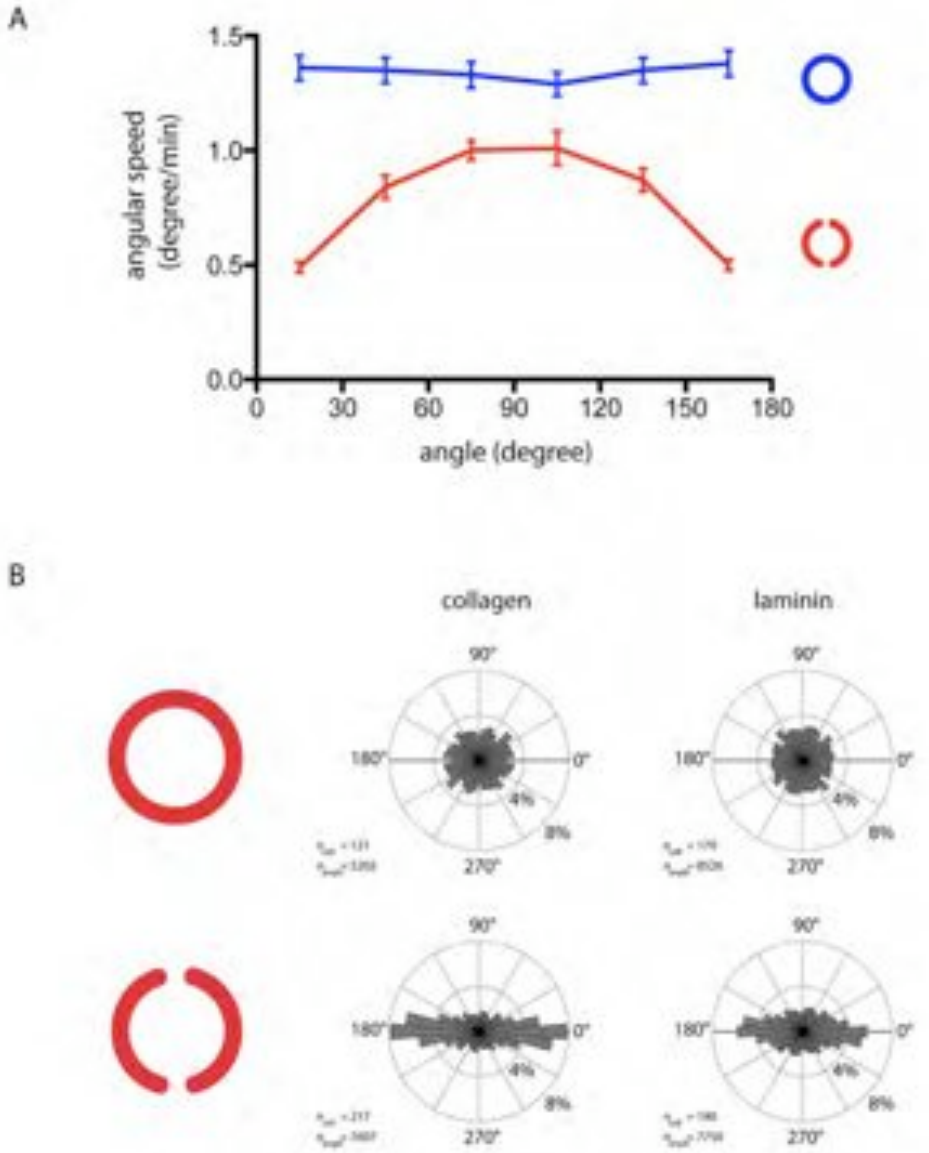

Figure S3 : influence of ECM geometry on cell-cell junction stabilization

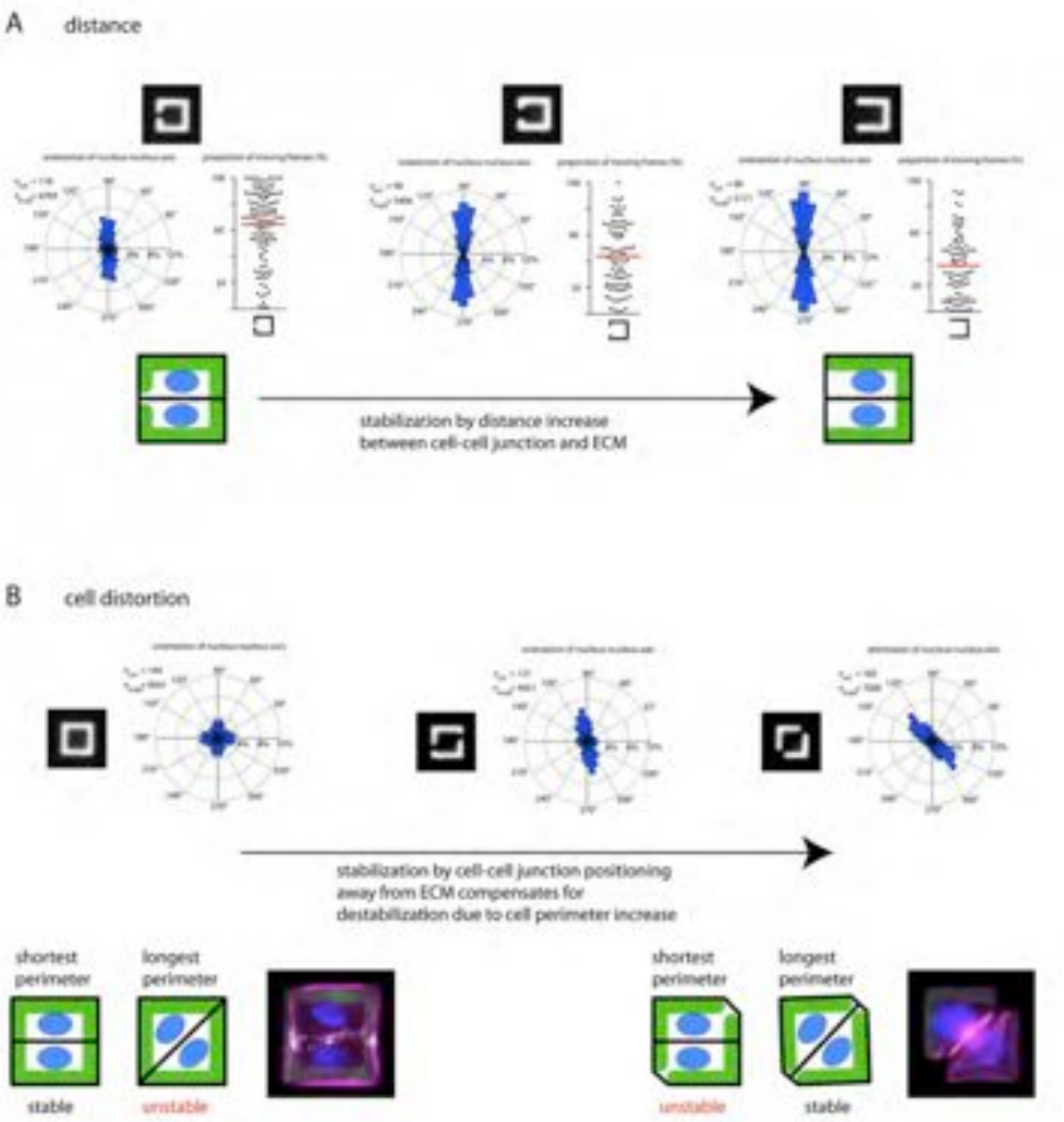

Figure S4 : CK2 knock-down perturb cell positioning and cell polarity

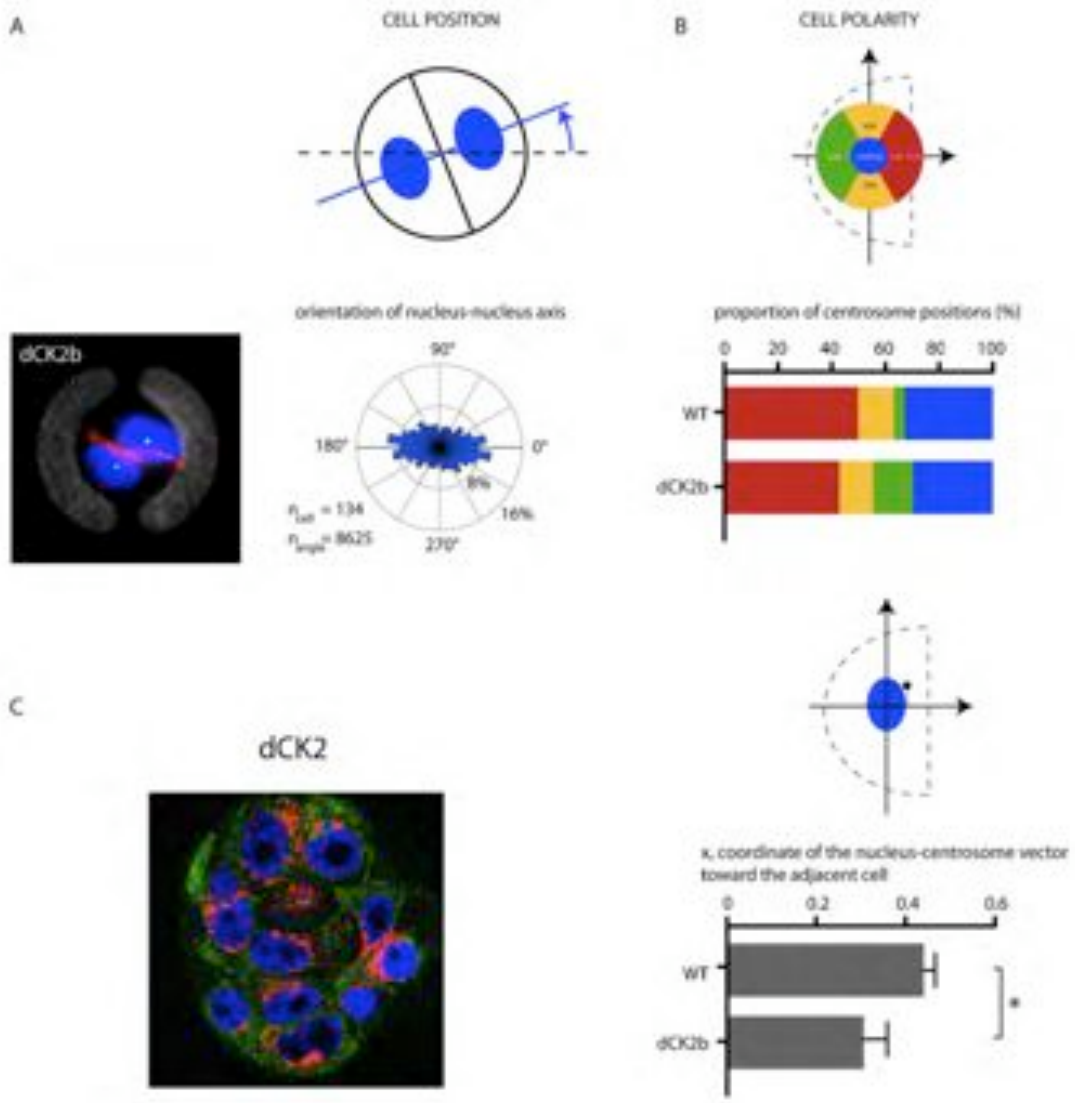

3.3 Spatial exclusion, contractility, and cell perimeter

Although our previous result suggested that the segregation between the integrin and cadherin adhesion system are owing to the membrane dynamic protrusions which were generated by the contact with ECM, there are still other important factors determining the positioning of cell junction. Here, I tried to further understand the mechanism of cell-cell junction positioning regarding to the ECM geometry.

Spatial exclusion is not due to biochemical incompatibility

If the segregation between the cadherin and integrin junction was purely due to direct biochemical incompatibility (i.e. mutual inhibition, binding competition... etc.), then the positioning of the cell-cell junction would be placed on wherever the region devoid of ECM was.

To test this hypothesis, MCF10A cell doublets were put on a series of rectangular-shaped ECM micropatterns. There were ECM gaps at different location on each pattern respectively (Figure3.8). After fixing the cell doublets and stained for E-cadherin, the position of cell-cell junction could be compared with the position of the ECM gap. The lower panel of the figure3.8 shows the averaged E-cadherin staining from 20 cell doublets for each pattern. When the ECM gap was placed symmetrically in the middle of the pattern, the intercellular junctions were somehow slightly more intense over the ECM gap. However when the gap moved toward the left, the junction didn't followed it. It means that only by inhibition of cell-matrix adhesion is not sufficient to guide the position of cell-cell adhesion. The junction positioning is also determined by other factors. For example, the symmetry of the cell shape could be one of the reasons that made the junction be preferentially placed in the midline.

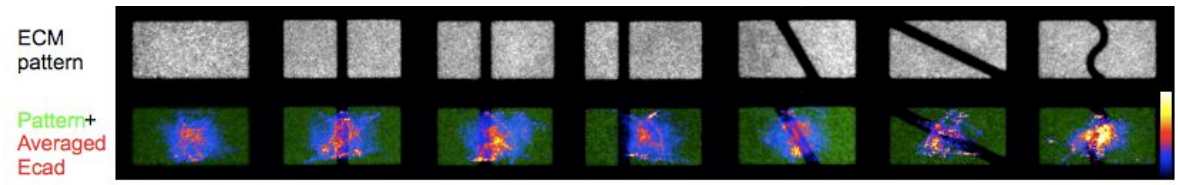

Figure 3.8: ECM geometries and corresponding junction positioning

In order to minimize the effect from the cell shape, cell doublets were put on the [I] -shape with a gap on the mid bar. In this case, the change of cell shape would be minimized since the bias of cell-cell junction due to the ECM gap would only occur at the middle part of the junction, while the shape of the 2 cell could still be approximately the same (Figure3.9). Surprisingly, the intercellular junctions were invariably placed near the horizontal midline, and insensitive to the presence of ECM gap as seen from the averaged E-cadherin staining in figure3.10. Rather than being contradictory to our previous result, we can rationalize that the spatial exclusion between the cell-cell and cell-ECM adhesion cannot be simply explained by direct biochemical incompatibility.

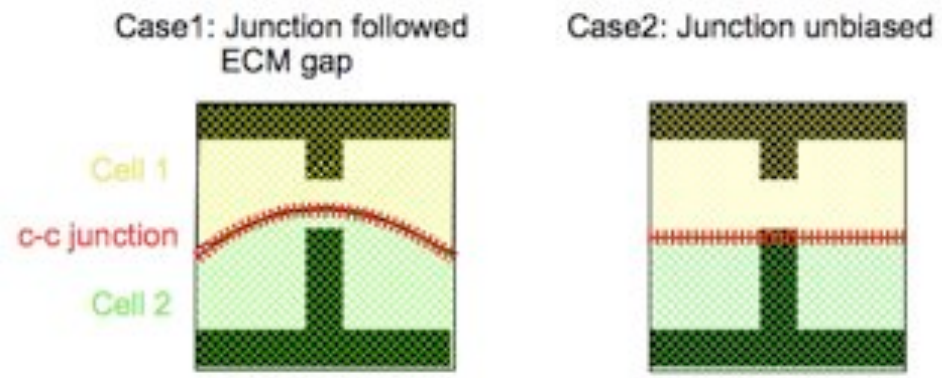

Figure 3.9: Scheme explaining two hypothetical configurations

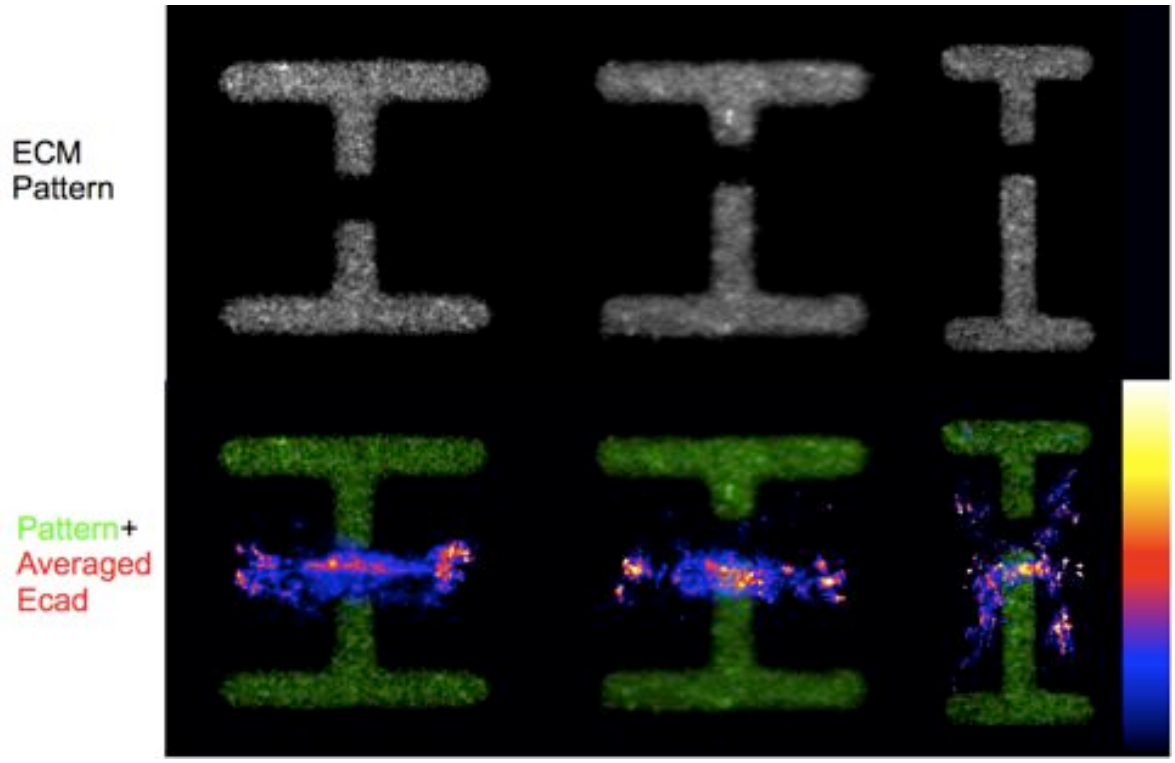

Figure 3.10: Cell-cell junction was not following the ECM gap.

Sensitive at the edge

The difference in the positioning of cell-cell junction on the [gapped-工] (Figure3.10) and the [gapped-ring] (see page70 Figure1D), made it somehow difficult to conclude the spatial exclusion between the cell-cell and cell-ECM adhesion. In order to clarify this confusion, we took another complementary strategy to survey the position of cell-cell junction. By measuring the nucleus-nucleus axis orientation from time-lapse images, we could efficiently survey a large amount of sample and probe the dynamics of the junction movement as the same time.

In figure3.11, we can see that the nucleus-nucleus orientations (perpendicular to cell-cell junction orientation) were unaffected when the ECM adhesion was introduced or removed at the central part (compare C0 with C1 ,C2). The cell-cell junction started to be oriented and cell movement started to stabilize only after the removal of ECM adhesion at the peripheries (compare C2 with C3). In addition, this effect was further enhanced after enlarging the region devoid of ECM (compare C3 with C4). The important transition right after suppressing the cell-ECM interaction at the cell peripheries suggests the periphery of the cell and the edge of the cell-cell junction are more sensitive to the cell-ECM adhesion than the center region.

To further define the limit between center and edge, we gradually introduced the ECM adhesion starting from the center part of the intercellular junction (Figure3.12). We can see that the extremities at the last one third of the intercellular junction were the regions most sensitive to the presence of cell-ECM interaction(Compare H6,H7 and H5,H6 in figure3.12).

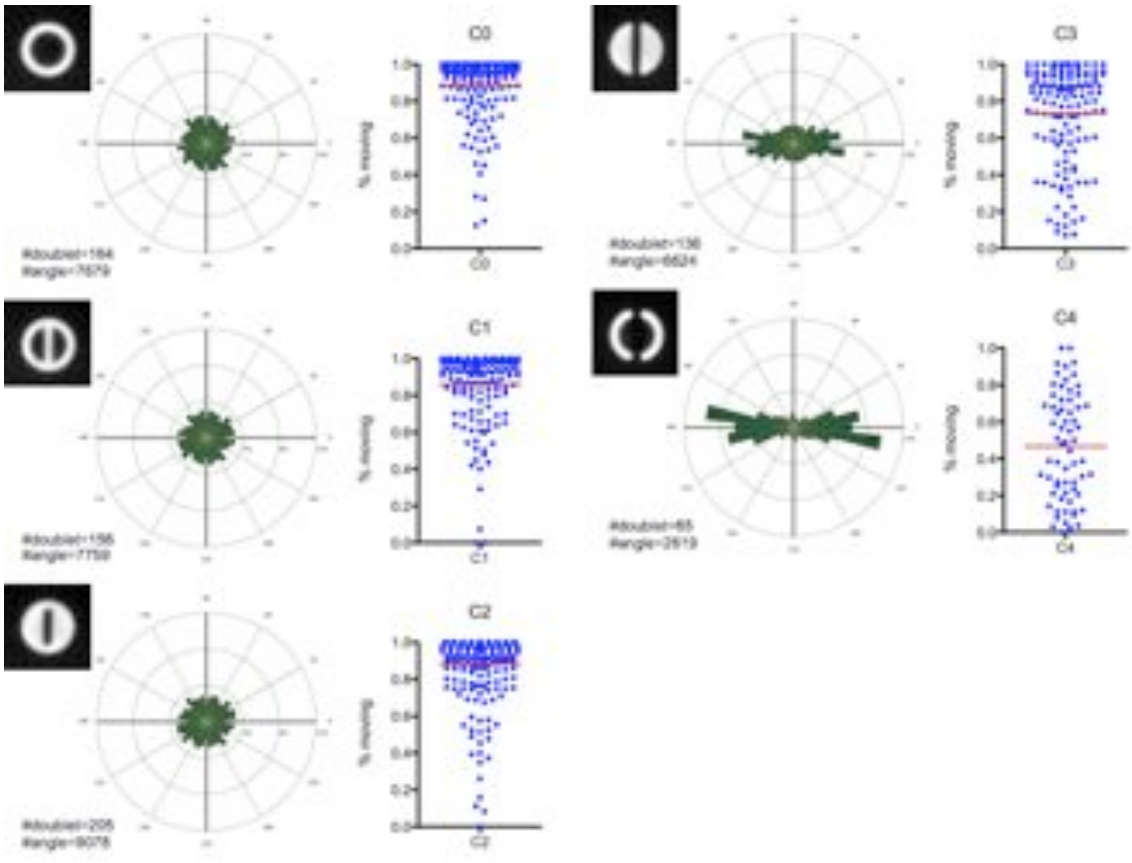

Figure 3.11: Removing ECM at the periphery has stronger effect on the cell-cell position

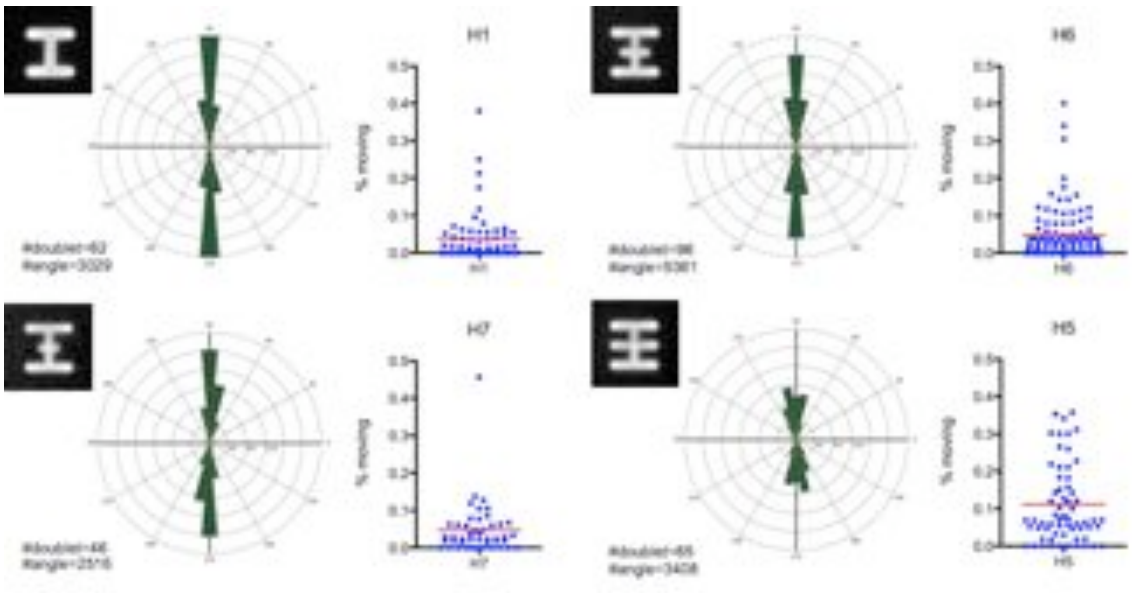

Figure 3.12: The last one third of the extremity of the cell-cell junction is the part most sensitive to the presence of ECM adhesion

Cell-cell junction is not simply blocked by the ECM gap

It could be argued that the preferred positioning of cell-cell junction above the ECM gap was not owing to the spatial exclusion between the two adhesion system, but only because of the discontinuity of the ECM adhesion at the periphery that made the cell movement difficult. So that the cell-cell junction was just “blocked” at the position lack of ECM.

To test this hypothesis, we used a series of ECM geometry allowing continuous cell-ECM adhesion(Figure3.13). Similar to previous result, cell doublet preferentially adopted a configuration with less cell-ECM adhesion at the extremities of the cell-cell junction. The cell doublet indeed moved more when there was continuous track instead of gaps on similar ECM profiles(compare the scatter plot between X4 in figure3.13 and H6 in figure3.12). Nonetheless the spatial exclusion between the two adhesions was still observed, excluding the hypothesis that the junction was simply blocked by the lack of ECM. In all the cases, the presence of ECM gap did contribute to the stability of the junction positioning (compare the [Square] in figure3.13 and H5 in figure3.12; and see also page77 figure S3A).

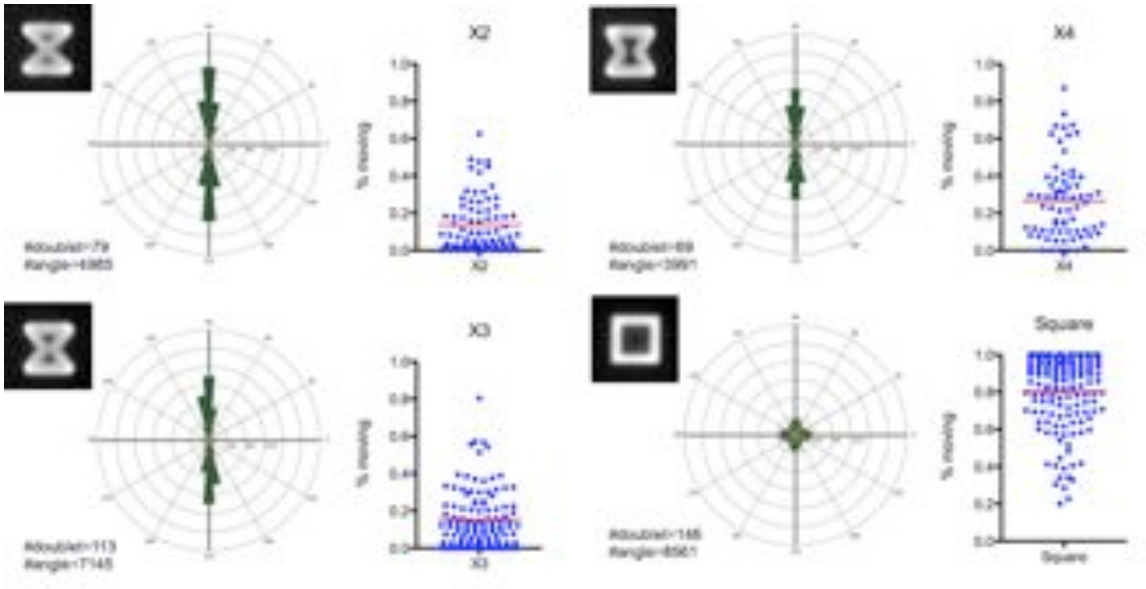

Figure 3.13:

Perimeters does matter

Previous studies on geometry of cell assembly have shown that cells adopted an arrangement that minimized the perimeter of the individual cell**(Hayashi et al., 2004; Käfer et al., 2007)**. We verified this argument on our system by elongating the cross-shaped pattern on which the doublets adopted two symmetric configurations (Figure3.14). As the shape elongate, one of the configurations became unfavorable. This supported the perimeter minimizing rule. Furthermore, by introducing the cell-ECM adhesion below the extremities of the cell-cell junction, we found that the expanse of perimeter increase override the spatial exclusion effect(c.f. X5, X6).

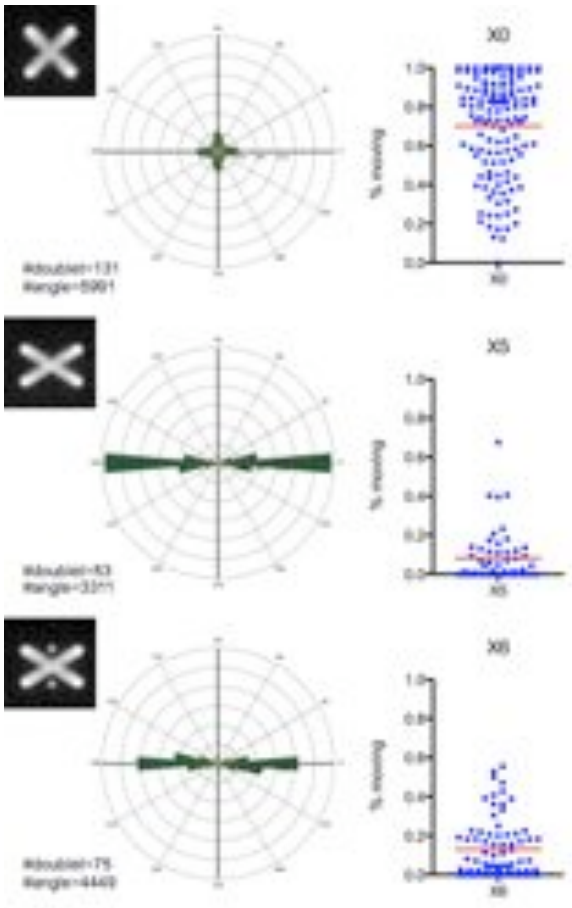

Figure 3.14:

Taken together, the spatial exclusion between the cell-cell and cell-ECM adhesion is a critical determinant for the cell positioning. This spatial exclusion was mainly resulted from the destabilization of cell-cell junction at the proximity of cell-ECM adhesion. The

destabilization is more effective at the extremities of the cell-cell junction where we found most E-cadherin were concentrated(Figure3.15) which has also been reported by others(Yamada et al., 2007 b). However there are still other factors such as cellular contractility(see Chapter4) and cell shape, that govern the epithelial geometry.

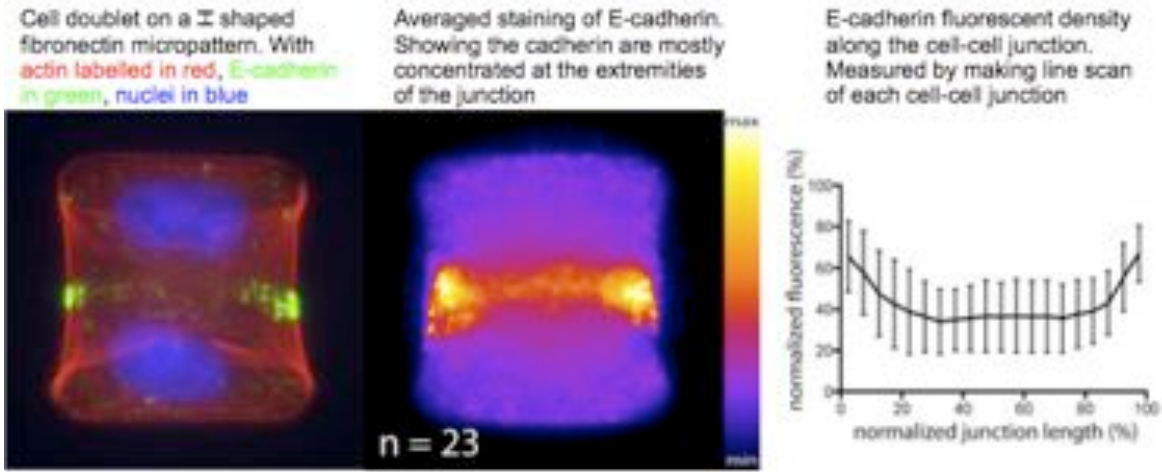

Figure 3.15: E-cadherins are more concentrated at the junction extremities.

3.4 More about centrosome positioning

Centrosome position in cell monolayer

Our previous result showed that the centrosome was positioned in proximity of the stabilized cell-cell junction for cell doublets(see page72, figure3C). We further wondered if this could also be observed in the epithelial monolayer. MCF10A cells were kept in confluence for 6 days, then fixed and stained for cell-cell junction, centrosome and nuclei (Figure3.16). On the left panel of Z-Y cross section, we can see that both α-catenin stained adherens junction and γ-tubulin stained centrosome were located at the apical part of the cell. In the X-Y plane, we can notice that many centrosomes positioned close to the cell-cell junction instead of being on top of the nuclear center(arrowheads in figure3.16). Further quantification are required to justify this observation, and it remains to be an open question about the nature of this interaction between centrosome and intercellular junction.

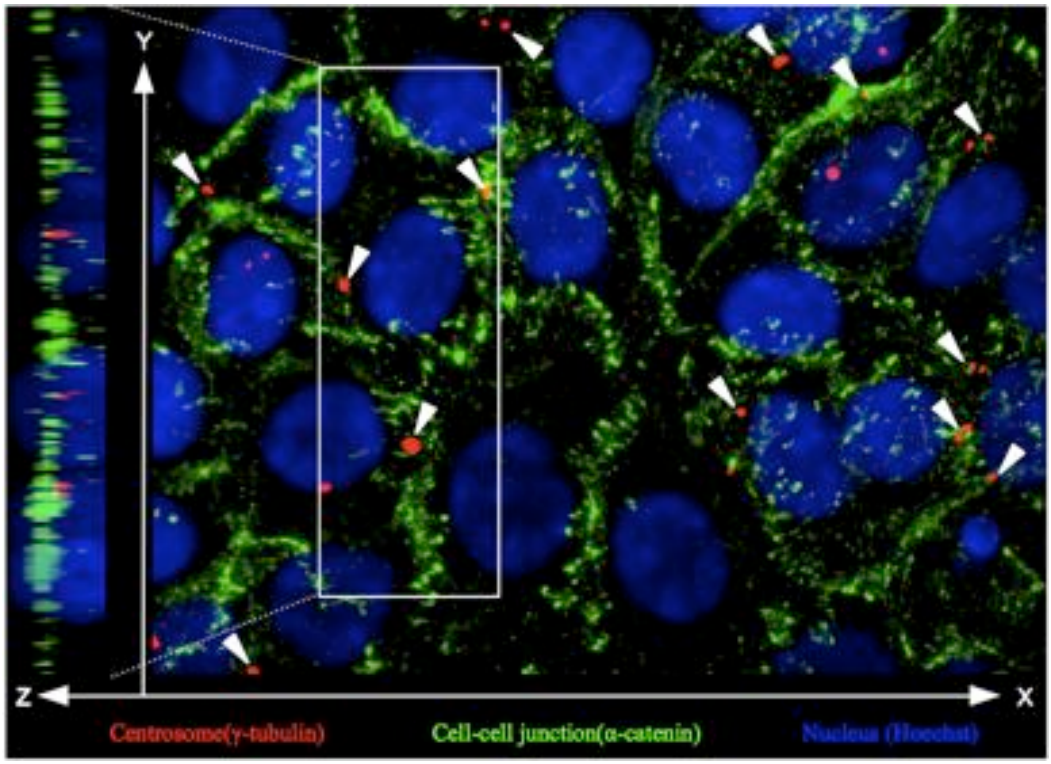

Figure 3.16: centrosome position in MCF10A monolayer

Cadherin junction stability and centrosome positioning

Since we have seen that the centrosome positioning toward the cell-cell junction was more pronounced when the junction was stabilized by the absence of cell-ECM adhesion, it is appealing to ask whether the centrosome positioning will be affected if we altered the composition of the cell-cell junction complex. Therefore, we compared the centrosome positioning between the wild type MCF10A cells and the cells overexpressing the exogenous E-cadherin-GFP. When the E-cadherin was overexpressed, we can see that the positioning of the junction upon the ECM gap was slightly increased. Strikingly, the centrosomes were positioned significantly closer to the cell-cell junction (Figure3.17). It suggests that the interaction between centrosome and adherens junction was further reinforced when there were more cadherin at the junction. Whether this is owing to a direct linkage between cadherin and centrosome or the increased amount of cadherin at the junction can recruit more adaptor proteins for this interaction still needs further investigation.

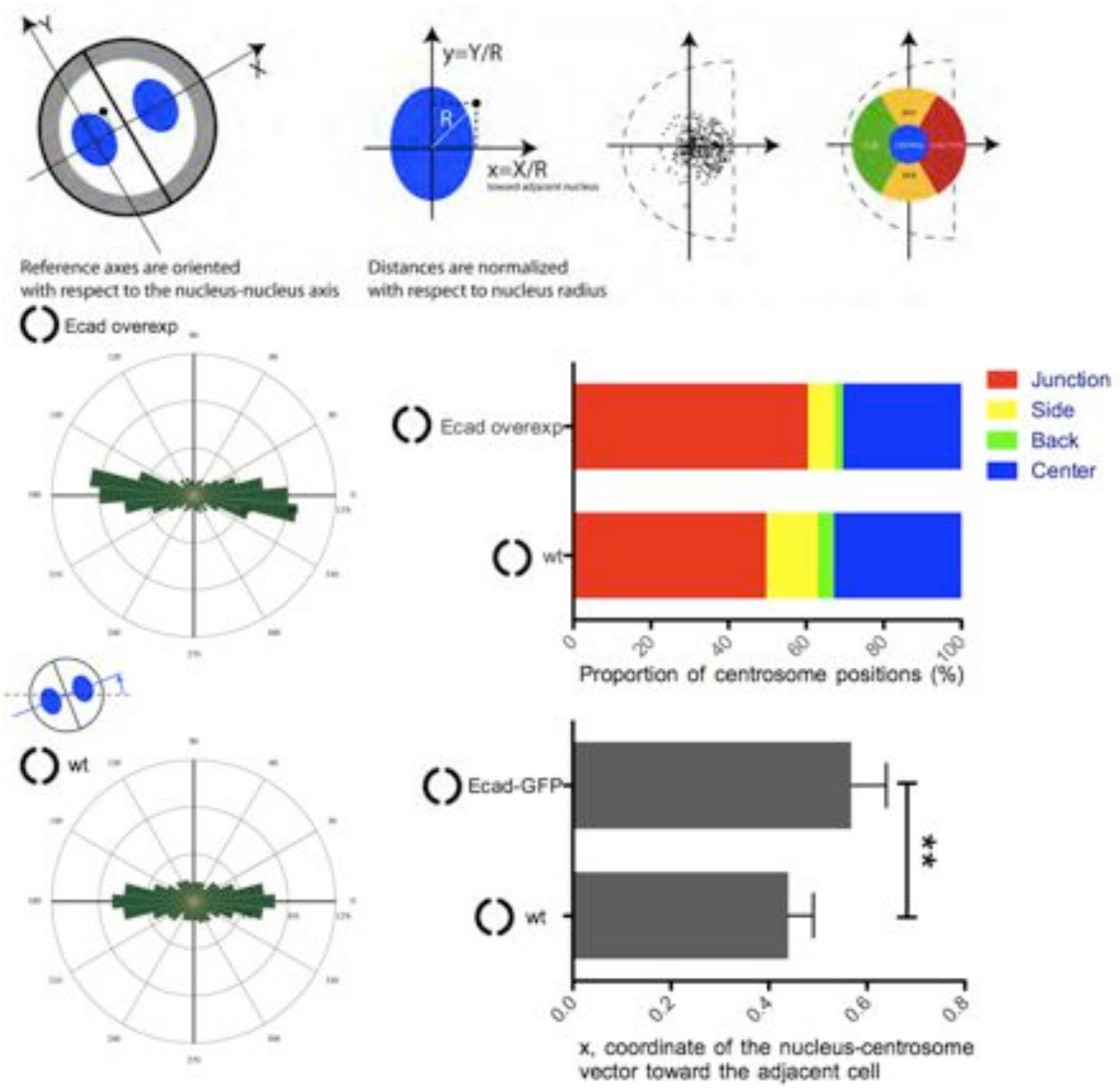

Figure 3.17: Centrosome positioning was further biased toward junction after overexpressing E-cadherin

3.5 Spatial patterning between different intercellular junction

Tight junction located apically to adherens junction

It has been reported that due to low expression level of polarity protein Crumbs3, the MCF10A cells grown as monolayer are unable to form tight junction**(Fogg et al., 2005)**. However, we still observed a small portion (~15%) of MCF10A cells within the monolayer formed continuous border of ZO-1 staining similar to the tight junction staining seen in MCF7 or MDCK monolayers(Figure3.18). We can even notice that the ZO-1 staining was positioned slightly apical to the E-cadherin staining (compare the region marked by the red box in Figure3.18). Since the tight junction complex plays a critical role in signaling epithelial polarity, and its formation and position are closely coupled with the cadherin-based adherens junction. It leads us to wonder how the positioning of the tight junctional protein, ZO-1, is related to the E-cadherin-based adheren junction.

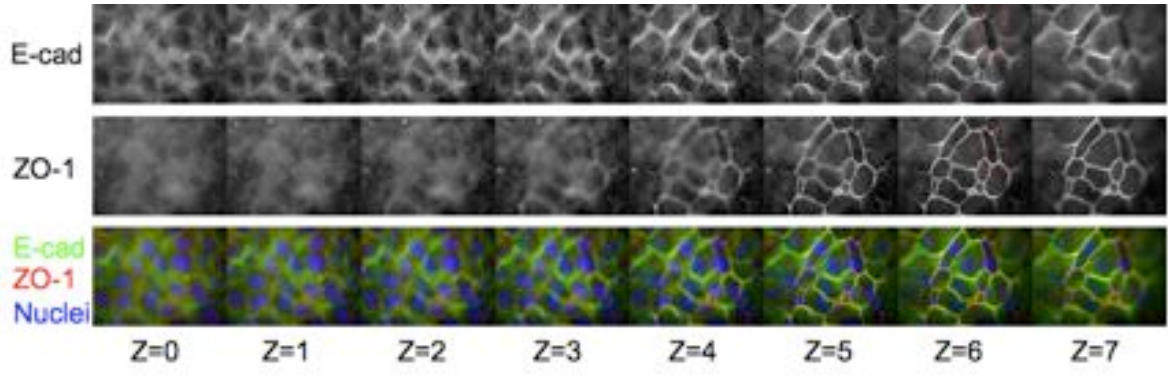

Figure 3.18: MCF10A confluent monolayer stained for E-cadherin and ZO-1

Initial positioning of tight junction

On the [I]-shaped fibronectin micropattern, most cell doublets adopt a top-down configuration along the Y-axis and placed their cell-cell junction horizontally across the midline (Figure3.10, 3.13). In such highly reproducible cell-cell positioning, it is easier to perceive minor changes of protein localization pattern. The immunofluorescent images from the bottom section (projection of z=0-1μm) of individual cell doublet showed that

tight junction protein ZO-1 was localized to the cell-cell junction similar to the staining on monolayer (Figure3.18). However, the ZO-1 was more homogenous distributed along the junction while the E-cadherin staining was more concentrated at the two extremities (Figure3.19 upper panel). This distribution pattern was further confirm on the averaged images of ZO-1 and E-cadherin staining (Figure3.19 lower panel).

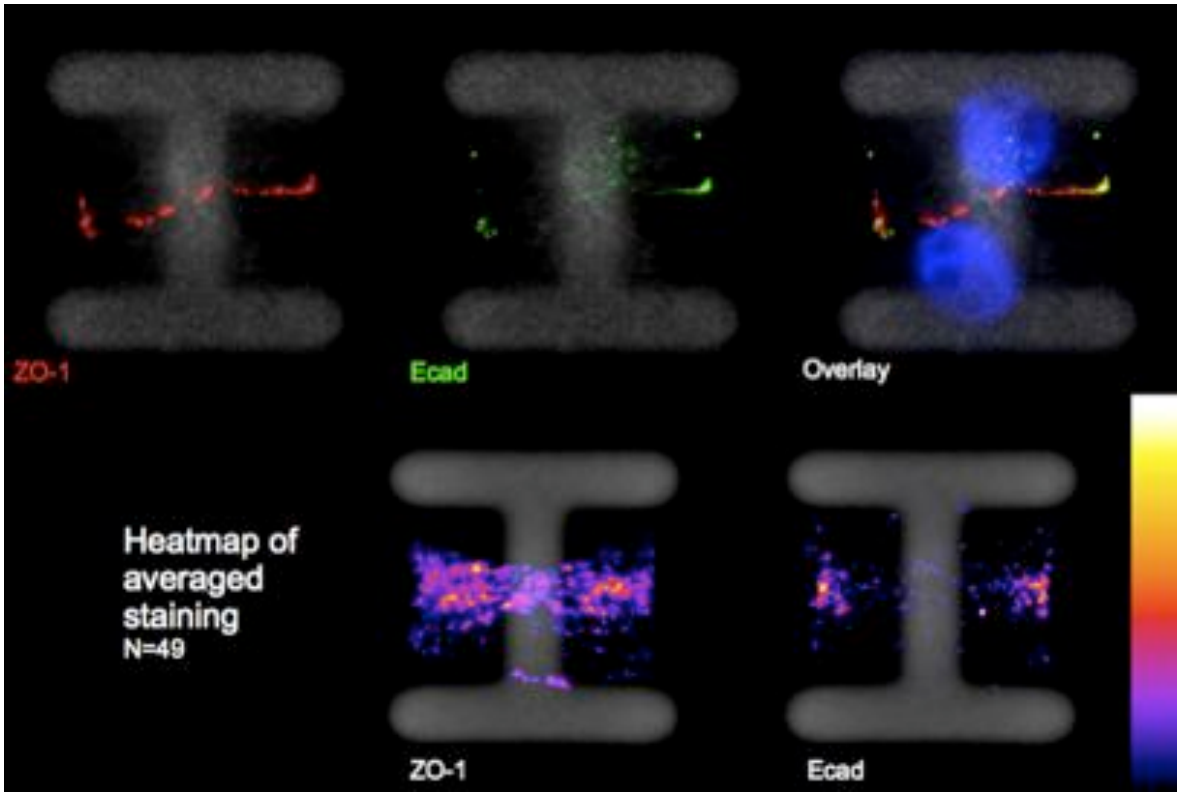

Figure 3.19: Comparison of ZO-1 and E-cadherin localization

This difference in the distribution of adherens junction component and tight junction component, prompted us to ask whether there was also a difference between bottom and top section. Even though our cell doublets had only formed their junction less then 24hr and might not have a full apical-basal polarity, the relative positioning between these two junctions at this early period can give us insight into the initial step of the spatial organization of cell-cell junctional complexes. In figure3.20, the intensity of E-cadherin diminished abruptly as the optical section moved toward cell top. On the contrary, ZO-1 intensity was highest at the middle section and persisted at the top section.

These results suggested that the spatial patterning of adherens and tight junction started shortly after the formation of initial intercellular junction. How such spatial pattern was determined remains to be answered.

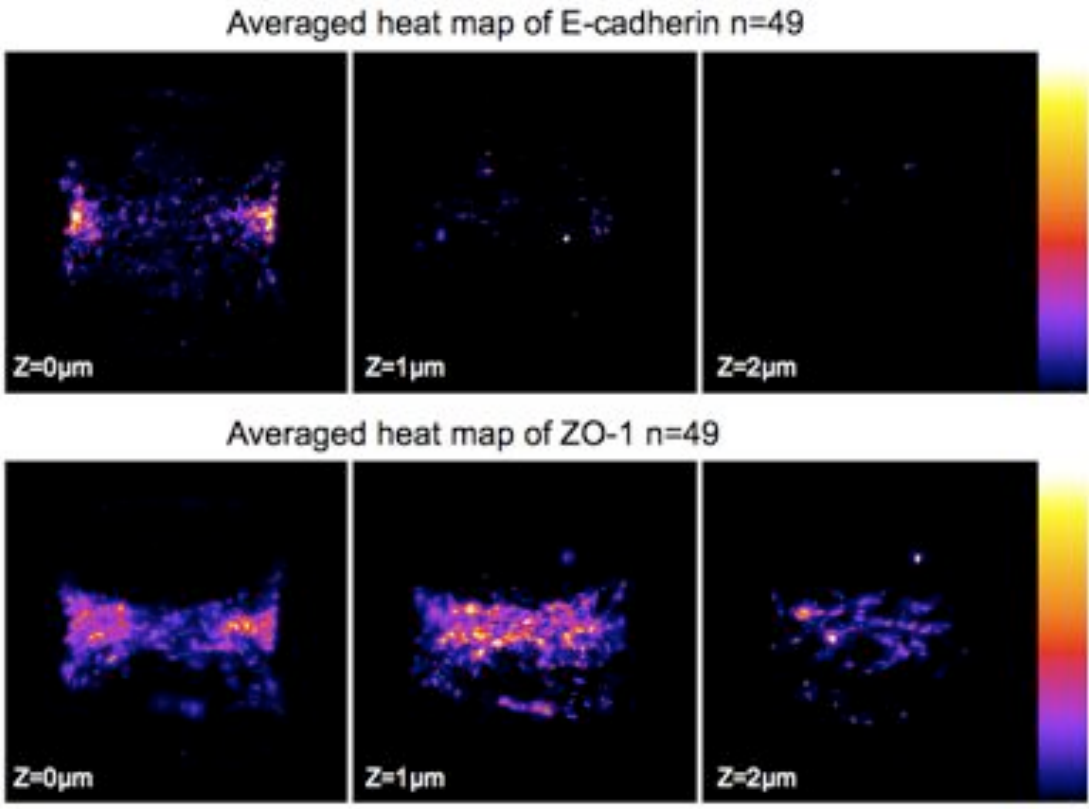

Figure 3.20: ZO-1 were located more apically than the E-cadherin shortly after the establishment of cell-cell junction (<24hr)

3.6 Discussion

Physiological context of our experimental system

Mammary epithelia is one of the few tissues that undergoes extensive postnatal development. The isolated mammary epithelial cell line thus provides a relevant *in vitro* cell culture system for epithelial development process, such as cyst formation and tubulogenesis. MCF10A is a non-malignant cell line isolated from premenopausal adult woman. Its capability to self-organize into 3D cyst and undergo tubulogenesis upon stimulation makes it a common cell type to study epithelial morphogenesis and the epithelial-mesenchymal transition. However, the mammary epithelial tissue is somehow more complex than the simple columnar or cuboidal epithelium that formed a homogeneous monolayer directly over the basal lamina matrix as depicted on the textbook. *In vivo,* there is usually a layer of myoepithelial cell forming a stellate network in between the luminal mammary epithelium and the basal lamina(Pitelka et al., 1973; Nagato et al., 1980). The successful reconstruction of mammary epithelial architecture and polarity in three dimensional culture relies a specific composition of extracellular matrix or the presence of myoepithelial cells(Gudjonsson et al., 2002; Inman et al., 2010).

In our study, epithelial cells were grown on a 2D surface composed of one specific matrix protein (fibronectin). We should therefore be specially cautious when interpreting our result in a more physiological context. Our minimum system is much more different from the *in vivo* tissue organization than the commonly used 3D culture system. We might not be able to obtain a well developed epithelial basoapical polarity nor a fully functional tight junction. Nonetheless, this simplified system permit us to gain control over many parameters that were impossible to access in other experimental systems. Thus we are able to ask specific questions that are deeply linked to the intrinsic cellular mechanisms, such as the spatial segregation and crosstalk between different adhesion systems. In addition, the geometrical control of cell shape minimized the cell to cell variability and helped to reveal obscure cellular reorganization which could be difficult to perceive under unconstrained condition.

Apical-basal polarity and centrosome polarity

In the present study, we used mainly the centrosome position to represent the internal organization of the cell. For the epithelial cell, however, the cellular polarity is more emphasized on the apical-basal polarity which involved majorly the membrane components, membrane junctional proteins, and the associated polarity complex such Par3, Par6, aPKC, and etc.. The fully developed apical-basal polarity usually takes 10-15 days to establish as for the epithelial cyst formed in 3D culture. It requires the segregation of membrane domains by a adhesion belt formed by the tight junctions, as well as a complete sorting of endocytosis and exocytosis pathways. As a result, it would be less relevant to discuss such type of polarity for the cell doublet which was maintained in culture for less than 24 hours (duration between two mitosis). In such early period, however, the dynamic modification of cellular organization upon the cell-cell contact and the intercellular junction formation shall still be reflected somewhere else.

The centrosome polarity (asymmetrical positioning of centrosome) appears to be an ideal indicator for the internal organization of cell(Bornens, 2008). Furthermore, in many epithelial cell microtubules were not only anchored to the centrosome but to the apical adherens junction(Meng et al., 2008), the desmosomes(Lechler et al., 2007), or the apical membrane surface(Mogensen, 2005). The microtubule arrays in such epithelial cell are organized as parallel arrays running apico-basally, which are essential for proper sorting of membrane components and for directing vesicle traffic(Gilbert et al., 1991) This suggested a potential interplay between the centrosome and the cortical junctional complex. The transfer of microtubule anchorage and nucleation abilities from centrosome to the apical cortex might be a crucial link between the cortical apical-basal polarity and the internal organelle polarity.

The positioning of the tight junction

The epithelial intercellular junctions *in vivo* can be made up with alternately posed adherens junctions and desmosomes, but with the tight junction invariably located at the most apical part. This configuration ensures the impermeability of the paracellular spaces and the segregation of apical membrane domain from the basal lateral membrane domain.

However, the exact mechanism governing the position of the tight junction remains elusive. Is there any preexisting polarity signals to guide this spatial organization of cell-cell junctions ? Or the initial formation of junction itself is providing polarity guidance. In *Drosophila* embryo, it has been reported that the apical localization of polarity protein is established prior to adherens junction formation. Nevertheless, the *de nov*o formation of vertebrate epithelia may proceed in a quite different way if we take into account the lack of prior patterning of polarity proteins like in the *Drosophila* embryo, and significant differences of junction organization between insect and vertebrate. It is possible the contact with ECM furnished the first cue to establish apical-basal axis, this preliminary polarity would guide further organization of cell-cell adhesions. Then, the mature polarity is reinforced and maintained by the apical formation of the tight junction which associates with a multitude of apical polarity protein complexes.

Our results implied that the apical positioning of the tight junction might occur early during the formation of multicellular assembly. In our case, it is plausible that the initial cue for the tight junction position was provided by the cell-ECM adhesion.

The physiological EMT and pathological EMT

The process of EMT was first recognized in the early 80s(Greenburg et al., 1982). It was not until the beginning of the 21th century when the similitude between this developmental process and the malignant tumor transformation process was put forward(Thiery, 2002), EMT became an intensive research field in both developmental and cancer biology. Today, when the term EMT is used, the first impression it conveys is the tumor metastasis with disruption of intercellular junction and lost of polarity. Nonetheless, we shall not forget the EMT is also a physiological event that permits multicellular organisms to have a certain degrees of plasticity during the developmental process. In such context, it is thus difficult to imagine cells undergoing EMT would “lost” their polarity rather than remodel it. While in the pathological condition, the malignant cell could have only by chance used a fraction of this highly coordinated process to acquire the invasiveness.

In our study, the EMT induced by TGFβ which is an endogenous growth and differentiation factor secreted by the embryonic cells could be interpreted as an EMT more

equivalent to physiological context. Conversely, the EMT phenotype resulted from removing a specific kinase, casein kinase 2, would be more likely a process happened under pathologic situation. The TGFβ induced EMT modulated the spatial organization of their adhesion system, hence rendered the cell-cell junction less sensitive to the presence of cell-ECM interaction. At the same time, cells still preserved the communication between cell-cell junction and centrosome which might have a certain physiological implications. While the knockdown of CK2 perturbed both the arrangement of adhesion system and the relation between junction and centrosome positioning which might be more similar to the metastatic situation.

4 Mechanical forces within cell and tissue

For living organisms, the ability to perceive physical stimuli is as important as their ability to sense chemical signals. Take examples from our body, the basic sensations of touching and hearing are purely triggered by physical forces. The physical/mechanical stimuli are transformed into chemical and electrical signals via mechanosensitive ion channels and receptors. Reciprocally, most living organisms are able to convert chemical energies into mechanical action. The most well-known example is the consumption of ATP to generate muscle contraction.

Nevertheless, it is not until recently that we start to acknowledge the crucial role physical force played in diverse cellular events. This could be partly due to the fact that many complex biological processes can not be fully understood without taking into account the physical forces. In addition, the advancements in instrumentation and technology also enabled us to probe more precisely the mechanical properties within the tissue and cell.

In this chapter, I will first review the mechanism that generate mechanical forces within the cell. Then we will go through the mechanical properties of cell and extracellular matrix, and introduce our current knowledge on the physical model of single cell as well as epithelial assembly. Afterward, I will present my studies on the contractile forces of single cell as well as the force equilibrium within multicellular arrangement.

4.1 Introduction

At the cellular level, the most manifest event that directly referring to physical forces may be the migration of cell. By coordinating the protrusion, retraction, and attachment which are all resulted from the forces generated within the cell, cells are able to translocate along their substrate. With a closer scrutiny, we will find physical forces also participate in a multitude of cellular events. For example, the active constriction force cuts apart daughter cells when cell divides; the pulling and pushing forces between neighboring cells guide the collective migration during wound healing. Even for a stationary cell within tissue, its geometry and positioning are governed by physical forces.

At a larger scale, the tissue morphogenesis is also a complex event that requires coordination of physical forces, albeit it had been predominantly described by the biochemical signaling such as growth factors, hormones, and morphogens. In fact, the idea of formulating the morphogenesis by physical terms was purposed almost a century ago(Thompson, 1917). However the overwhelming information in genetics and biochemistry had somehow marginalized the role of physical forces. In spite of that, the most fundamental physical laws always remind us that the change in shape for an object must be resulted from the force applied on them or generated by themselves. The same principle should also be true for living cells and tissues.

The origin of force

Mechanical force is generated in every scale in biological system: from the tiny force produced by the contractile sheath of bacteriophage, to the gigantic swimming stokes of whales. Although the general origin of these force can be attributed to the conformation change and self-assembly of biomolecules, the force generated by the action of motor proteins and the polymerization of cytoskeletons in eukaryotic cells will be more specifically discussed here.

Motor proteins are tiny machines that convert chemical energy into mechanical works. There are three major class of motors in the eukaryotic cell. The myosin family proteins move on the actin filament. While the kinesin and dynein families use the microtubules as tracks. The motor proteins participate in a wide spectrum of cellular functions, including the transportation of organelle and vesicle, ciliary movement, cell division, signal transduction, mRNA transportation and force generation and remodeling of cytoskeleton network(Schliwa et al., 2003).

Contrary to the case of cargo transportation by motor protein, the force generation by motor protein requires the attachment to a resistant point, such as the membrane or another cytoskeleton structure. The best-known model for this type of force generation is the muscle contraction. Nonetheless, the omnipresence of myosin throughout a wide variety of cell types has highlighted the potential mechanical functionality in non-muscle cells(Coluccio et al., 2008). For example, in the non-migrating epithelial cell, the antiparallel sliding of actin filaments by myosin generates contractile actin structures which is responsible for dramatic cell shape change like the apical constriction during the embryogenesis. The same force generation mechanism is also found on microtubule networks and the generated forces are used in ciliary beating and mitotic spindle organization(Tolić-Nørrelykke, 2008).

Besides, mechanical forces can also be generated by the polymerization of cytoskeletons. Experiments have demonstrated that cells in absence of motor activity are still capable of making membrane protrusions(Pollard et al., 2003). Moreover, a more striking evidence of the polymerization-generated forces is the motility generated by the intracellular pathogens *Listeria* where the propulsion force is purely produced by actin polymerization(Lambrechts et al., 2008). The force generation through the the

polymerization process is explained by the so-called Brownian ratchet model(Peskin et al., 1993). The ratchet mechanism is described by the intercalation of cytoskeletal monomers between the polymer end and a load which is usually the plasma membrane. The insertion of monomers at the tip eventually biases the brownian diffusion of the load toward a given direction, thus generates a protrusive force(Figure4.1).

By coordinating the motor forces and the polymerization forces, cytoskeletal network found the basis for more complex mechanical actions in the cell.

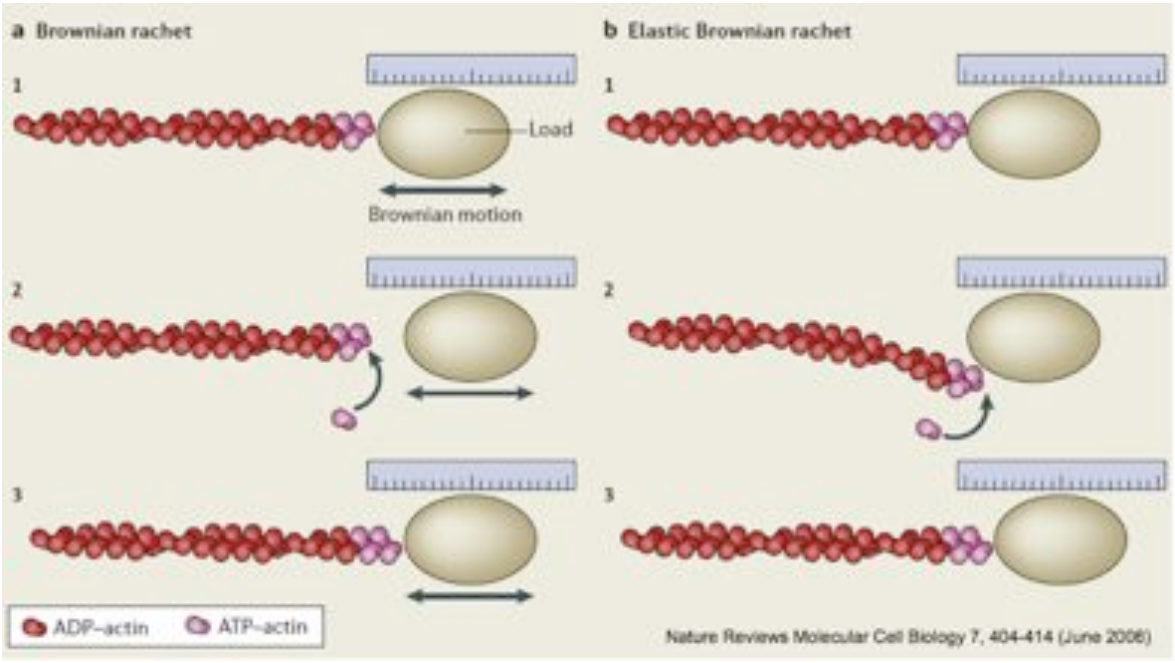

Figure 4.1: The molecular brownian ratchet model

Mechanical properties of individual cell

Since mechanical forces are widely implicated in physiological functions and cellular activities, there is a growing interest in modeling single cell mechanical properties. Clearly, it is an essential ingredient of complete physical descriptions for more complex multicellular assemblies such as tissue and organ. A prerequisite for modeling the mechanical property of cell is to describe it in appropriate physical terms. Many attempts have been made previously, either based on direct experimental measurements or formulated from the current understanding of cellular architectures.

Direct measurements of the material properties of the whole cell have been preformed by using different techniques including micropipette aspiration, atomic force microscopy, magnetic tweezer, etc.(Bao et al., 2003; Loh et al., 2007) (Figure4.2). Results show that cells possess both elastic and viscous properties, and thus are best described as viscoelastic materials(Kasza et al., 2007). Mechanical measurements have also been done on reconstituted cytoskeleton networks. It is believed that cytoskeletal networks, especially the actin filaments, are the main contributors to the mechanical properties of cell(Janmey et al., 2007).

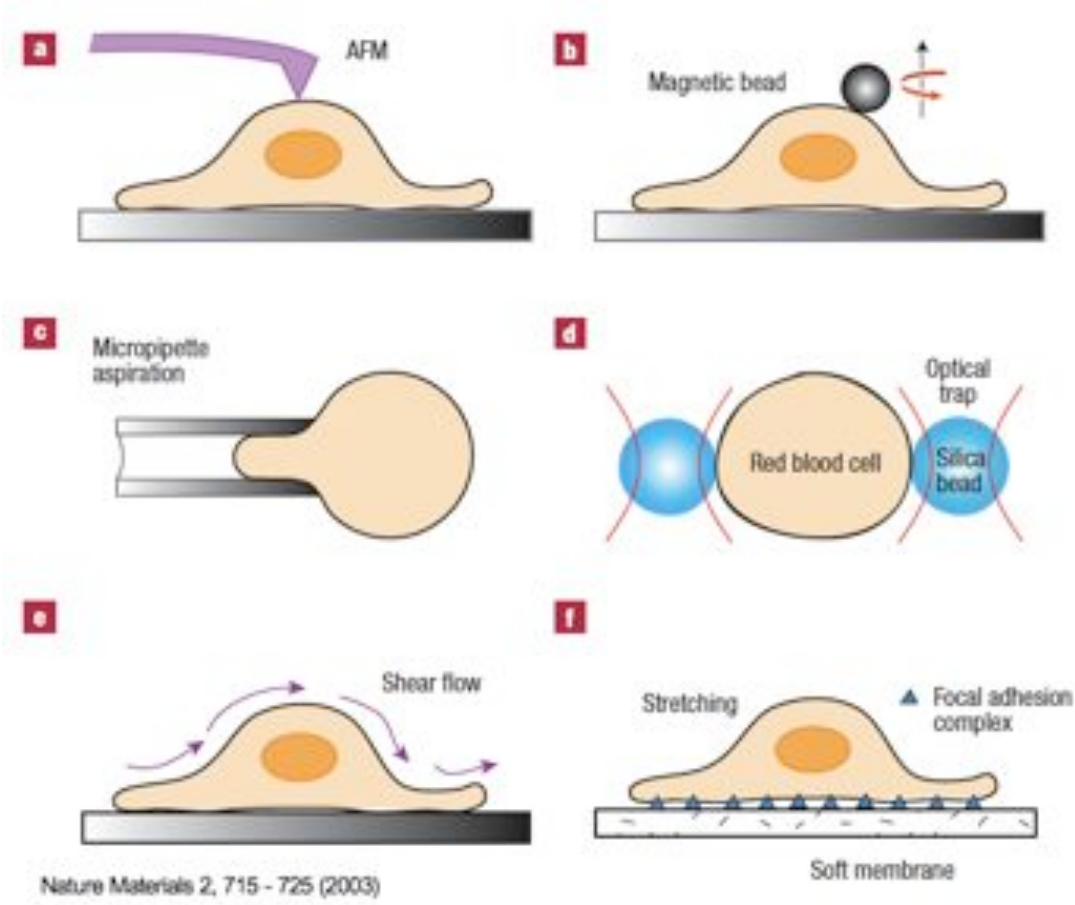

Figure 4.2: Experimental techniques to probe cell mechanical properties

These studies provided us rough ideas about the scale of the mechanical properties in cellular context, and the material features of the cell and its architectural blocks. Nevertheless, the dynamics of the living system make it difficult to build physical models of the cell simply by approximating it as a combination of inert materials. It is now recognized that the active contractile force generated by the cytoskeletal network plays a

crucial role in cellular mechanical property. For example, the whole cellular elastic property measured *in vivo* could be reproduced on the cross-linked actin network only if the network was already under tension(Gardel et al., 2006). This so-called cellular "prestress" has also been demonstrated in live cell, for example the retraction of stress fiber after laser ablation(Kumar et al., 2006; Colombelli et al., 2009); the shrinkage of cell peripheries after myosin inhibition(Théry et al., 2006);the concave contour of cell border(Bischofs et al., 2008);and the cellular traction forces exerted on the substrate(Dembo et al., 1999; Harris et al., 1980) (see section2.5). More elaborate models such as the "tensegrity", or the "soft glassy rheology" model, can better account for this prestress characteristic compared with the model composed of passive polymer network(Ingber, 1997; Bursac et al., 2005; Kasza et al., 2007).

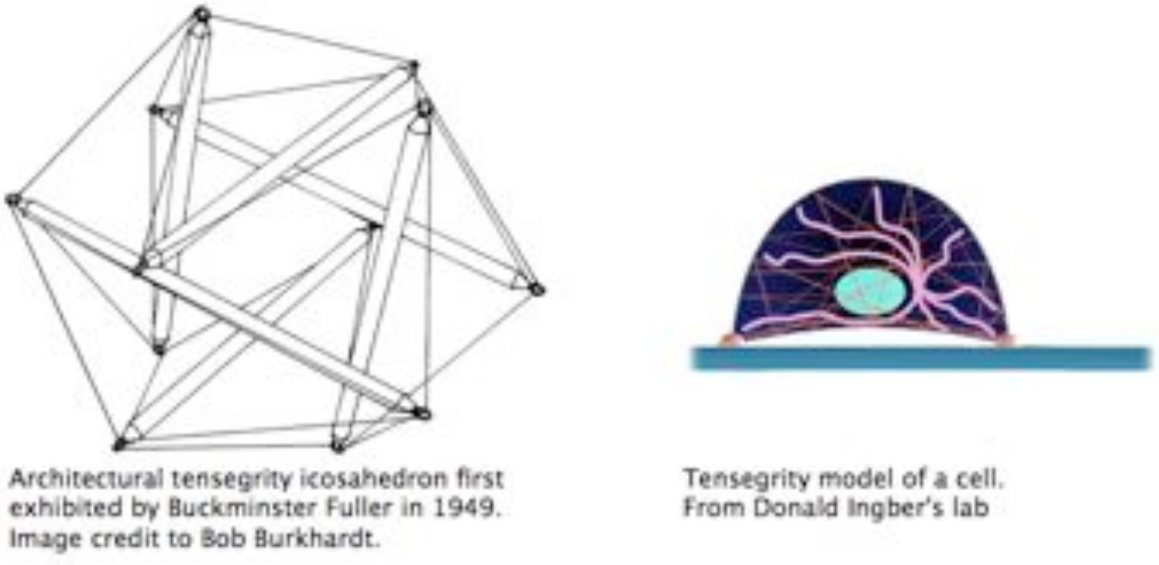

Figure 4.3: The cellular tensegrity model

Because the mechanical properties of the cell are resulting from the combination of many cellular activities, it is conceivable that pathological conditions would also be reflected on the cellular mechanical features. Indeed, the mechanical properties like elasticity, or contractile force of cell have been proposed as indicators of tumor malignancy(Munevar et al., 2001; Guck et al., 2005; Cross et al., 2007; Butcher et al., 2009).

Mechanical properties of the ECM

Within the tissue, cells have to interact with extracellular matrix and/or other cells. Consequently, the global tissue morphology and mechanical properties have to take into account the individual cellular architecture as well as the extracellular matrix and the mechanical continuum between cells and cell-matrix connected through adhesion systems.

Traditionally, the extracellular matrix was only regarded as a substrate providing chemical signals for growth and migration. However, recent studies have unveiled its diverse functionalities in cellular mechanics. It has been first demonstrated by Pelham & Wang that the mechanical properties of the matrix would affect the internal organization and the migratory behavior of the cell(Pelham et al., 1997). Afterward, a growing body of evidence has come to light suggesting that the mechanical properties of the extracellular matrix are important regulators for cellular behavior and developmental process(Janmey et al., 2009; Rozario et al., 2010)(Figure4.4). Among them, the most striking examples are that the stem cell differentiation can be guided solely by matrix rigidity(Engler et al., 2006).

The viscoelastic measurement of the extracellular matrix shows a significant difference between the matrix taken from different tissues(Ludwig et al. 2007). The fact that matrix protein is not only being secreted but also being actively restructured by the cell, further confirms the idea that mechanical properties between the extracellular matrix and tissue cells are actually coordinated(Mao et al., 2005; Larsen et al., 2006; Davidson et al., 2008; Haigo et al., 2011). The reciprocal mechanical regulation between tissue and extracellular matrix has also been shown to be crucial for the homeostasis and tumor transformation(Paszek et al., 2004; Butcher et al., 2009)(Figure4.5).

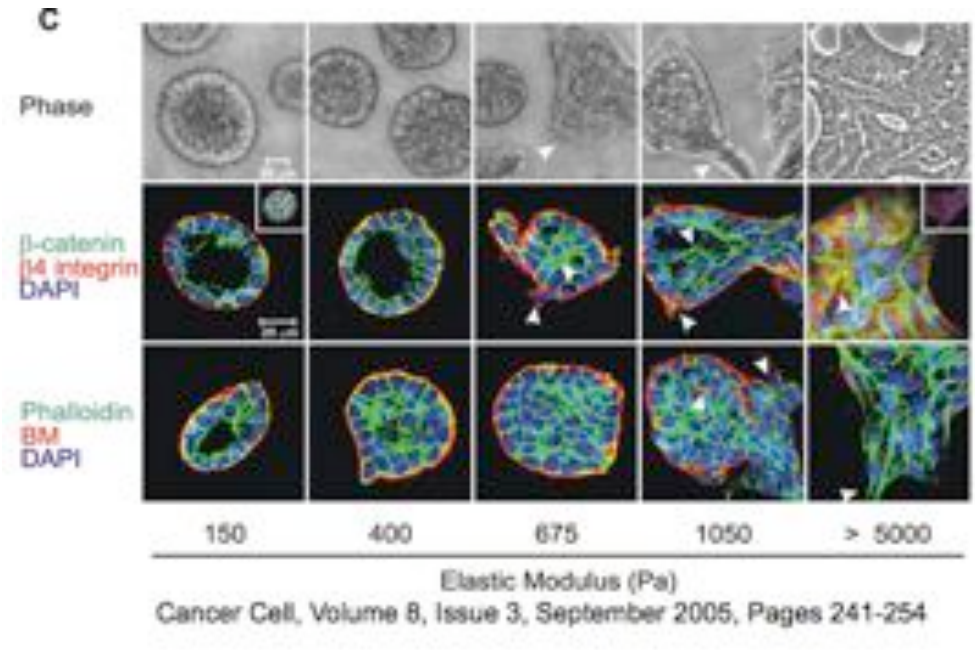

Figure 4.4: Matrix stiffness modulates mammary epithelial morphology

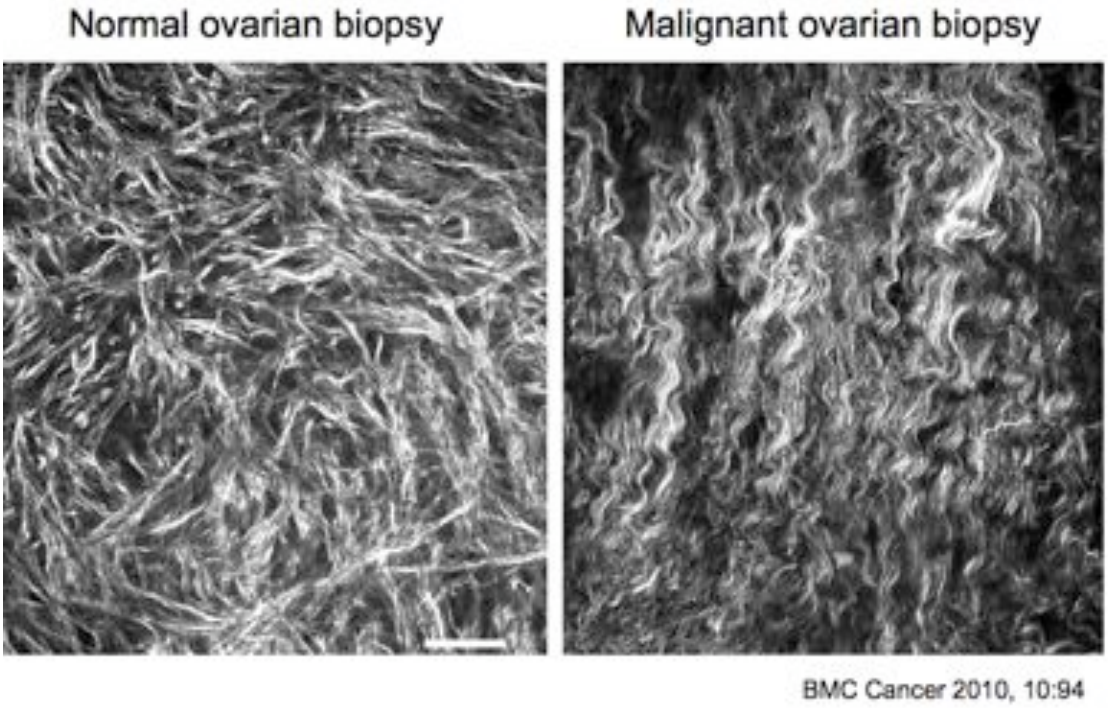

Figure 4.5: Collagen networks imaged by second harmonic generation microscopy

Mechanical forces in epithelial assembly

In physiological condition, epithelial cells grow as multicellular assemblies instead of isolated cells. They are not only interacting with the extracellular matrix but also with their neighboring cells. Even though this intercellular crosstalk have been dominantly expressed in genetic and chemical terms in the past decades, much greater importance is now attached to the implication of physical forces in a wide scope of cellular events such as embryogenesis or tumor metastasis. It is therefore a crucial issue to understand the force regulation in multicellular scale and the mechanical communication across the multicellular assembly.

The association between the adhesion complex and the cytoskeletal network implies the potential of mechanical communication through the adhesion complex. Studies have now revealed the mechanosensitivity in both cell-matrix(Balaban et al., 2001; Riveline et al., 2001) and cell-cell adhesion system(Ladoux et al., 2010; Chu et al., 2004; Yonemura et al., 2010). It further confirms the concept of mechanical integrity in multicellular level. While there are increasing evidences showing that the tissue cell and their substrate are mechanically regulating each other in a reciprocal way, how the cell regulates and communicates mechanically with their neighbor remains poorly understood. Nevertheless, it is an indispensable element to fully understand certain cell behaviors, for example the collective movement of epithelia during morphogenetic events.

There are several pioneering works attempted to deduce the mechanical forces propagating through the epithelial assembly by measuring the global traction force of the cell group. The measurements of traction forces between two or three cells have revealed substantial forces applied on the neighboring cell, and this force transmission was mediated by the cadherin-based cell-cell junction(Liu et al., 2010; Maruthamuthu et al., 2011). Experiments on larger group of cells or on the epithelial sheet also highlighted the importance of intercellular forces in the mechanical balance and collective migration(Saez et al., 2010; Trepat et al., 2009).

Physical models for epithelial assembly

The regularity of tissue cell shape and the formation of specific tissue pattern have long fascinated both biologists and physicists. It is appealing to associate fundamental physical laws to biological forms which resemble some natural structures arising from relative simple physical process. For example, the cobblestone pattern of the cell in epithelia sheet has been compared to the structure of soap foam and the honeycomb. Although a physical model may be over simplified if we considered the immense complexity at cellular level, successful simulation of the biological pattern by simple physical terms can help us to identify the most essential parameters in the whole system.

Early works of establishing physical models for the epithelial assembly were largely focused on the surface mechanics, which originates from the intercellular adhesion forces(Steinberg, 1963; Hayashi et al., 2004). The similarities between the packaging pattern of epithelia and the soap bubble was the main initiative for these models based on surface tension (Figure4.6a). Nevertheless, models based solely on the adhesion forces cannot fully describe epithelia assemblies unless the cellular contractility was taken into account(Käfer et al., 2007; Farhadifar et al., 2007). Experiments that use laser ablation to directly probe the contractility of cell in the *Drosophila* embryo further validated the role that mechanical force played in epithelial assembly(Rauzi et al., 2008; Landsberg et al., 2009; Farhadifar et al., 2007).

Albeit this growing appreciation for the mechanical forces in epithelial assembly, we are still far from a complete physical vision of multicellular assembly. How the mechanical force equilibrium governs the global geometry? How cell-cell adhesion complexes, cytoskeletons and mechanical forces interact with each other? Many questions remain to be clarified in the future.

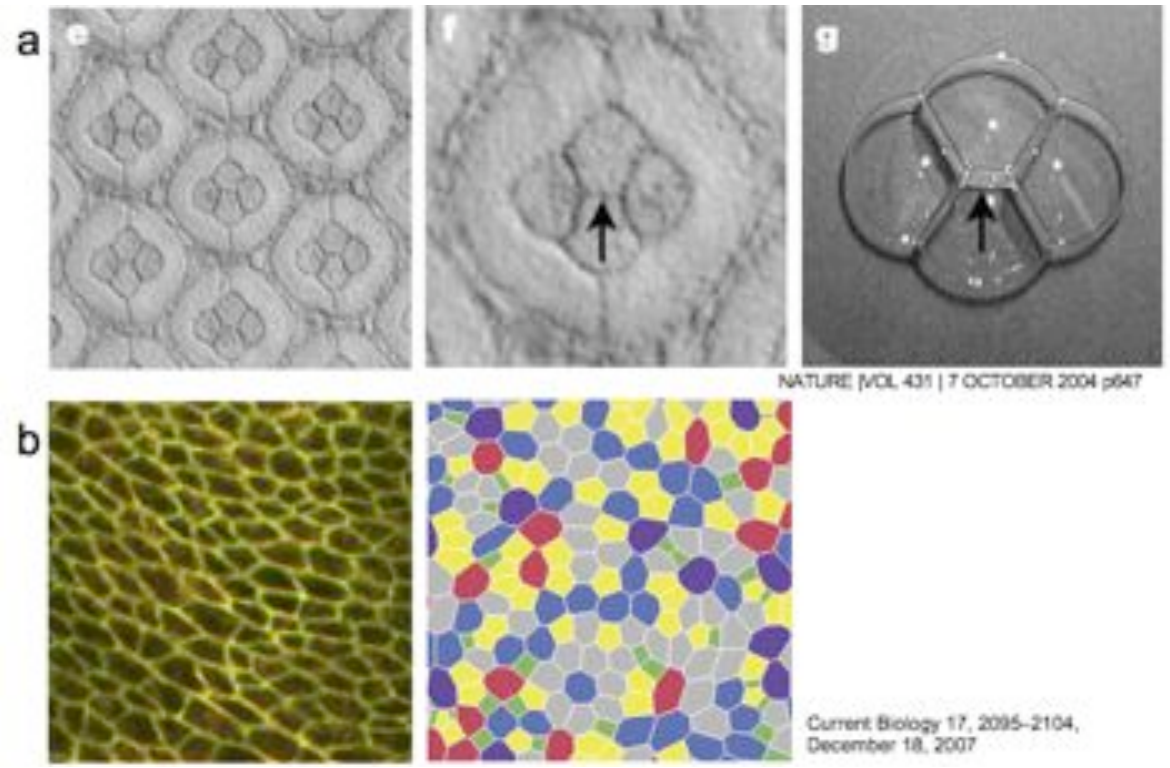

Figure 4.6: (a)Compare the regular pattern of Drosophila ommatidia with soap bubble. (b)simulation of the polygonal network of epithelia.

Motivations and objectives

Current attempts to assess the mechanical properties of single cell or multicellular assembly are frequently hindered by the heterogeneity of other physical parameters, such as the cell shape or the size and location of cell-matrix and cell-cell adhesion. It renders the analysis difficult and sometimes irreproducible. Owing to the micropatterning technique, we are able to minimize the variability in cell shape, cell size, and the location of cell-matrix adhesion. Moreover, our previous knowledge on the spatial organization of the integrin and cadherin adhesion allow us to control the positioning of cell-cell junction on specific ECM geometry. Therefore, we can now ask more precisely how the mechanical forces are regulated within the cell and across the cell. We also want to construct a physical model for the the cell-cell positioning with the mechanical terms measured experimentally. Thus we can have a deeper insight into how cells placed their junctions and positioned themselves within the epithelial assembly.

4.2 Cell contractility and tumor malignancy – (PAPER)

The paper presented here is the study of single cell contractility by using the Traction Force Microscopy (see section2.5).

It first described the development of the micropatterning techniques on the soft polyacrylamide gel(see section2.2). Then with this techniques, we demonstrated the ability to measure the global cellular contractility simply through a single measurement of the pattern length. No more particle tracking and force calculation were required. After validating the force measurement capability, we compared the single cell contractility between cells with different degrees of tumor malignancy. Contrary to the current view, our results showed that tumor transformation is not necessarily associated with higher contractility. Some transformed cell type could exhibit similar contractile level as normal cell.

Lab on a Chip

View Online
Dynamic Article Links

Cite this: DOI: 10.1039/c0lc00641f

www.rsc.org/loc

PAPER

A new micropatterning method of soft substrates reveals that different tumorigenic signals can promote or reduce cell contraction levels†

Qingzong Tseng,[a] Irene Wang,[b] Eve Duchemin-Pelletier,[c] Ammar Azioune,[d] Nicolas Carpi,[d] Jie Gao,[b] Odile Filhol,[c] Matthieu Piel,[d] Manuel Théry*[a] and Martial Balland*[b]

Received 29th November 2010, Accepted 6th April 2011
DOI: 10.1039/c0lc00641f

In tissues, cell microenvironment geometry and mechanics strongly impact on cell physiology. Surface micropatterning allows the control of geometry while deformable substrates of tunable stiffness are well suited for the control of the mechanics. We developed a new method to micropattern extracellular matrix proteins on poly-acrylamide gels in order to simultaneously control cell geometry and mechanics. Microenvironment geometry and mechanics impinge on cell functions by regulating the development of intra-cellular forces. We measured these forces in micropatterned cells. Micropattern geometry was streamlined to orient forces and place cells in comparable conditions. Thereby force measurement method could be simplified and applied to large-scale experiment on chip. We applied this method to mammary epithelial cells with traction force measurements in various conditions to mimic tumoral transformation. We found that, contrary to the current view, all transformation phenotypes were not always associated to an increased level of cell contractility.

Introduction

Geometrical and mechanical properties of cell microenvironments have a profound impact on cell morphogenesis and functions. They will impinge on cell cytoskeleton architecture, polarity, migration, division, growth, and differentiation.[1] New materials have been engineered to reveal these effects, investigate the mechanisms by which they regulate cell functions and eventually control them to design new tools for tissue engineering applications. Microenvironment geometry has been controlled with micro-patterning techniques. They were used to manipulate the localization of adhesive molecules from the extracellular matrix (ECM) and thereby control the position and shape of individual cells.[2] Microenvironment mechanics have been controlled with soft substrates. The reticulation and density of synthetic or bio-polymers were used to control their stiffness.[3,4] Both parameters, geometry and mechanics, should be controlled on the same material to faithfully reproduce the physiological conditions that cells encounter in tissues and to fully control the physical signals affecting cell morphogenesis. Cell shape control on deformable substrates has been performed using various micro-fabricated tools on either poly-acrylamide (PA) gels or arrays of micro-pillars. Micro-molded stamps,[5] stencils[6,7] or microfluidic channels[8] were used to locally deposit ECM proteins on chemically activated PA. Micro-contact printing was used to print ECM proteins on arrays of micro-pillars.[9] We developed a new, fast, efficient and robust micropatterning method on PA in which no specific microfabricated tool was required except the commercially available photomask. We validated it by controlling the shape, cytoskeleton architecture and traction force production of human mammary epithelial cells.

Microenvironment geometry and mechanics affect cell architecture and function notably by modulating the forces produced by cells. Cells attach to their microenvironment and exert traction forces *via* the myosin dependent contraction of their actin cytoskeleton. Microenvironment geometry will affect the orientation of contractile stress fibers and the location of force application sites (Fig. S1†). In spatially confined, non-migrating cells, stress fibers form along cell edges resulting in the application of traction forces at cell apices.[6,7] Stress fibers appear larger when no ECM is available for cell adhesion between cell apices.[10] Microenvironment stiffness will affect the magnitude of cell traction forces: a stiffer substrate will promote larger forces.[11,12] The sub-cellular location of traction forces affects intra-cellular organization, notably centrosome positioning,[13] primary cilium growth[14] and intra-cellular trafficking.[15] It is therefore a major regulator of cell polarity.[16] Cell contractility also governs

[a]*Laboratoire de Physiologie Cellulaire et Végétale, iRTSV, CEA/CNRS/UJF/INRA, 17 rue des martyrs, 38054 Grenoble, France. E-mail: manuel.thery@cea.fr*
[b]*Laboratoire de Spectrométrie Physique, CNRS/UJF, UMR5588, 140 Avenue de la Physique, 38402 Saint Martin d'Heres, France. E-mail: martial.balland@ujf-grenoble.fr*
[c]*Laboratoire de Transduction du Signal, iRTSV, CEA/CNRS/UJF, 17 rue des martyrs, 38054 Grenoble, France*
[d]*Institut Curie, CNRS UMR 144, 26 rue d'Ulm, 75248 Paris Cedex 05, France*
† Electronic supplementary information (ESI) available. See DOI: 10.1039/c0lc00641f

extensive cytoskeletal remodeling during cell migration,[17,18] and division.[19] In addition, cell contractility promotes cell growth[20] and directs stem cell differentiation.[11] Considering this broad impact of actin cytoskeleton contractility on cell physiology, it is not surprising that up-regulation of force production is involved in tumoral transformation.[21,22] Polarity misorientation,[14] disordered cell positioning[23,24] and amplified growth[25] are characteristic tumoral features that can be induced by increasing cell contractility. Therefore, Rho kinase inhibitors, which reduce the level of cell contractility, have been seriously considered as cancer treatment agents.[26,27] However, many pathways lead to tumoral transformation and it is not clear yet whether high levels of cell contraction are systematically associated to tumoral transformation. To investigate this issue, we took advantage of our new micropatterning method of PA to orient cell traction forces and impose them to perform a standardized exercise. With identical spreading and location of stress fibers, cells were rigorously and easily comparable to each other. We could quantify the effect of various tumorigenic treatments on human mammary epithelial cells.

Results

New micropatterning method on soft substrate

We used direct exposure of PA to deep UV (180 nm) through an optical quartz mask to rapidly achieve micropatterning, with high spatial resolution and reproducibility, on a soft substrate of controlled stiffness (see Experimental section). A drop of acrylamide solution was placed directly on the chromium side of the

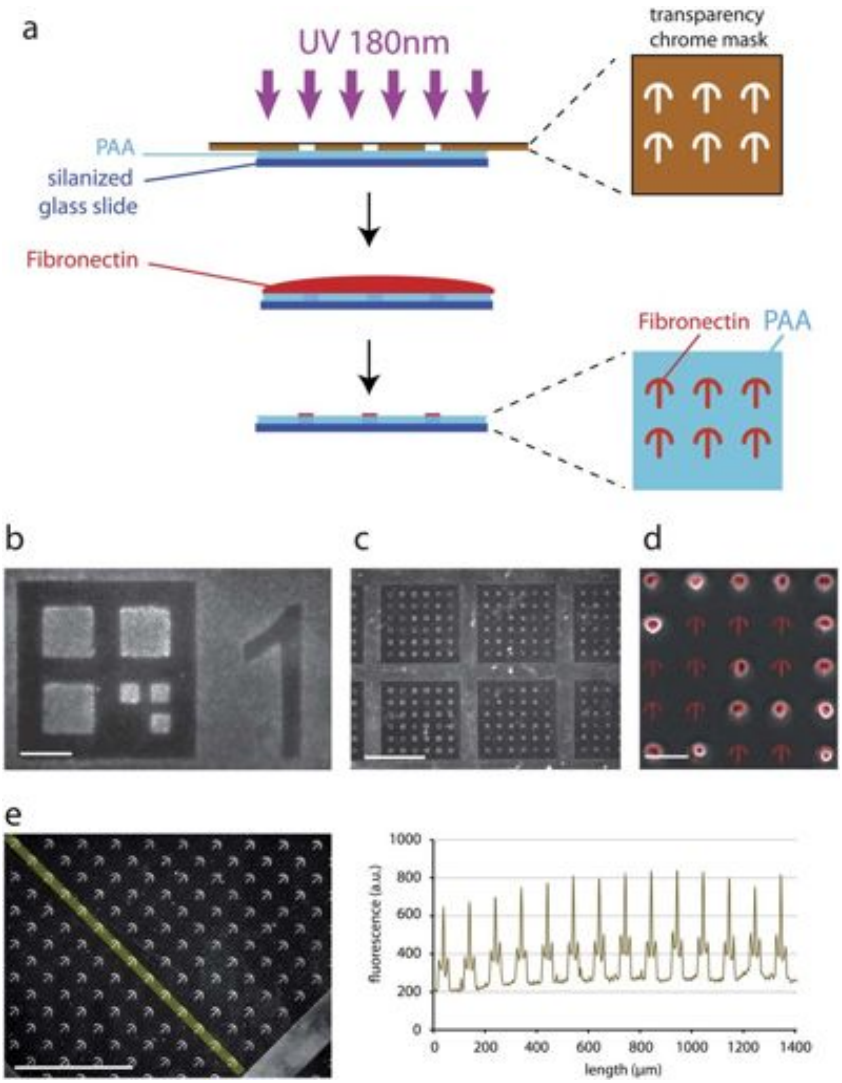

Fig. 1 Micropatterning of PA gel. (a) PA micropatterning method. The gel is polymerized on the photomask, exposed to deep UV and coated with ECM proteins. Cells attach specifically to the UV exposed regions. (b) Fibronectin and fibrinogen-A546 coating on micropatterned PA. Scale bar represents 10 μm. (c) Fibronectin and fibrinogen-A546 coating on micropatterned PA. Scale bar represents 500 μm. (d) MCF10A cells (phase contrast) plated on crossbow shaped micropattern (red) on PA. Cells specifically attach on the micropatterns. Scale bar represents 100 μm. (e) Linescan of fluorescence intensity along a 1 mm long line (yellow) showing the homogeneity of fluorescence staining and reproducibility of micropattern shapes. Scale bar represents 500 μm.

optical mask and covered with a silanized glass coverslip. After PA polymerization, the sandwich was exposed to deep UV through the micropatterned transparent regions of the optical mask. Deep UVs generate ozone which activate the PA[28–30] (Fig. 1a). The coverslip along with the PA gel was removed from the mask and coated with crosslinker and fibronectin, which adsorbed only on the UV-exposed regions. The direct contact with the optical mask during PA polymerization and UV-exposure allowed a faithful reproduction of its spatial features and ensured a good, sub-cellular, spatial resolution. 3 micron wide squares, corresponding to the minimum size we could obtain on low cost quartz mask, could be resolved on PA (Fig. 1b). The coating was quite homogeneous over the entire coverslip (Fig. 1c and e). The entire process, from PA preparation to the end of protein coating, lasts 2 h, including 1 h of PA polymerization.

Controlled localisation and focusing of force application sites

Non-tumorigenic human epithelial cells from the mammary gland, MCF10A, were plated on the micropatterned PA substrates. Cells specifically attached to the fibronectin coated micropatterns since non-exposed PA regions prevented protein adsorption (Fig. 1d). The effect of micropattern geometry on the orientation of cell traction forces was tested on various shapes: disc, pacman and crossbow (Fig. 2a). Spread cells exerted traction forces on the micropattern that could be measured by looking at the displacement of fluorescent beads embedded in the PA gel (see Fig. 2b and Experimental section). Particle image velocimetry followed by individual particle tracking were used to measure bead displacements.[31,32] Force fields were calculated from the bead displacement fields using the Fourier transform traction cytometry.[32,33] Force fields exerted by individual cells were overlaid and averaged to quantify their reproducibility (Fig. 2c and d). On homogeneously coated regions cells developed forces that were randomly distributed from one cell to the other. In cells constrained on disc shaped micropatterns, forces were still randomly oriented but their magnitudes were lowered due to reduced cell spreading.[9] In cells constrained on pacman shaped micropatterns, force distribution was geometrically biased due to enhanced cell contraction above non adhesive regions.[10] Cell ability to exert traction forces was even more stimulated on crossbow shaped micropatterns, where the total traction force per cell was higher than on any other micropattern shape (Fig. 2d and S2†). Importantly, most of the traction forces were reproducibly oriented upward, along the straight adhesive bar, on the extremity of which we measured the highest pressure (Fig. 2d and S3†). These results demonstrated that appropriate micropattern geometries can both stimulate cell contraction and orient force application. Such geometries place cells in optimal conditions to reveal potential cell contractility and measure their contraction strength.

Force field streamlining allows reproducible force-deformation relationship

Cells deform the soft micropattern when pulling on it. The local amplitude of the deformation is related to the local force application. However, when all actin cables are oriented toward a single point, as it is the case on crossbow shaped micropatterns (Fig. S1†), the local deformation could reveal the total amount of contractile forces. If so a very simple measurement of the local deformation could be a simple and direct measure of the global cell contraction level. Such a measure would be convenient for high throughput and large-scale analyses. To test this hypothesis, we used classical force field calculations with beads embedded in the PA gel (Fig. 2b) and observation of micropattern deformation (Fig. 3a) to establish the force–deformation relationship in micropatterned cells. On discs the deformation orientation was unpredictable and no good correlation could be found between the deformation along a reference axis and the total cell traction force (Fig. 3b). When the deformation was measured along the shortest, and therefore most contracted, cell axis, the correlation was improved (Fig. 3c). However this shape did not stimulate cell contraction and therefore did not fully reveal a cell contractility potential (Fig. 2d and S2†). Cell traction force magnitudes were slightly higher on pacman shapes, but force and deformation were not precisely correlated (Fig. 3d). On the crossbow, the length of the straight bar is compressed in response to oriented cell traction forces (Fig. 3a and S3†). We found a good linear correlation between crossbow bar shortening, a local measure, and total cell traction, a global cell state (Fig. 3e). Each length variation could be assigned to a defined force value. This revealed that crossbow bar length could be taken as a direct indicator of cell contraction level.

On the crossbow, a single image acquisition was sufficient to measure the bar length and read the corresponding total cell traction force using the calibration curve (Fig. 3f). It was no longer necessary to track beads in the substrate and detach the cell to recover the original bead positions in order to obtain the same measurement. Global force measurement was not only easier compared to any previous method but it also became amenable to automation.

We tested whether this linear relationship was also valid for other rigidities than the 7 kPa gels used throughout this study. On softer gels, below the range of 3 kPa, the micropattern geometry was less reproducible (Fig. S4†). So force measurements at this rigidity could not be reliably performed. With harder gels (14 kPa), the linear relationship was preserved. However, those higher rigidities naturally lead to smaller gel deformations. Thus in order to maximize the signal to noise ratio in length measurements, gels of 7 kPa were optimal, in the case of MCF10A cells, to allow reliable force measurement based on micropattern deformation.

Validation of force measurement

We validated this methodology by analyzing the well-described blebbistatin effects on cell contractility. Blebbistatin has been shown to inhibit myosin-II ATPase.[34] Cells were treated with an increasing dose of blebbistatin (Movie S1†). Crossbow bar length measurements on thresholded pictures of the fluorescent micropattern were used to estimate cell traction forces (Fig. 4a). The force inhibition profile in response to increasing dose of blebbistatin matched the myosin II inhibition profile[34] and the cellular force profile measured with other techniques.[35] Drug effects on cell contractility could thus easily and rapidly be quantified using this new methodology.

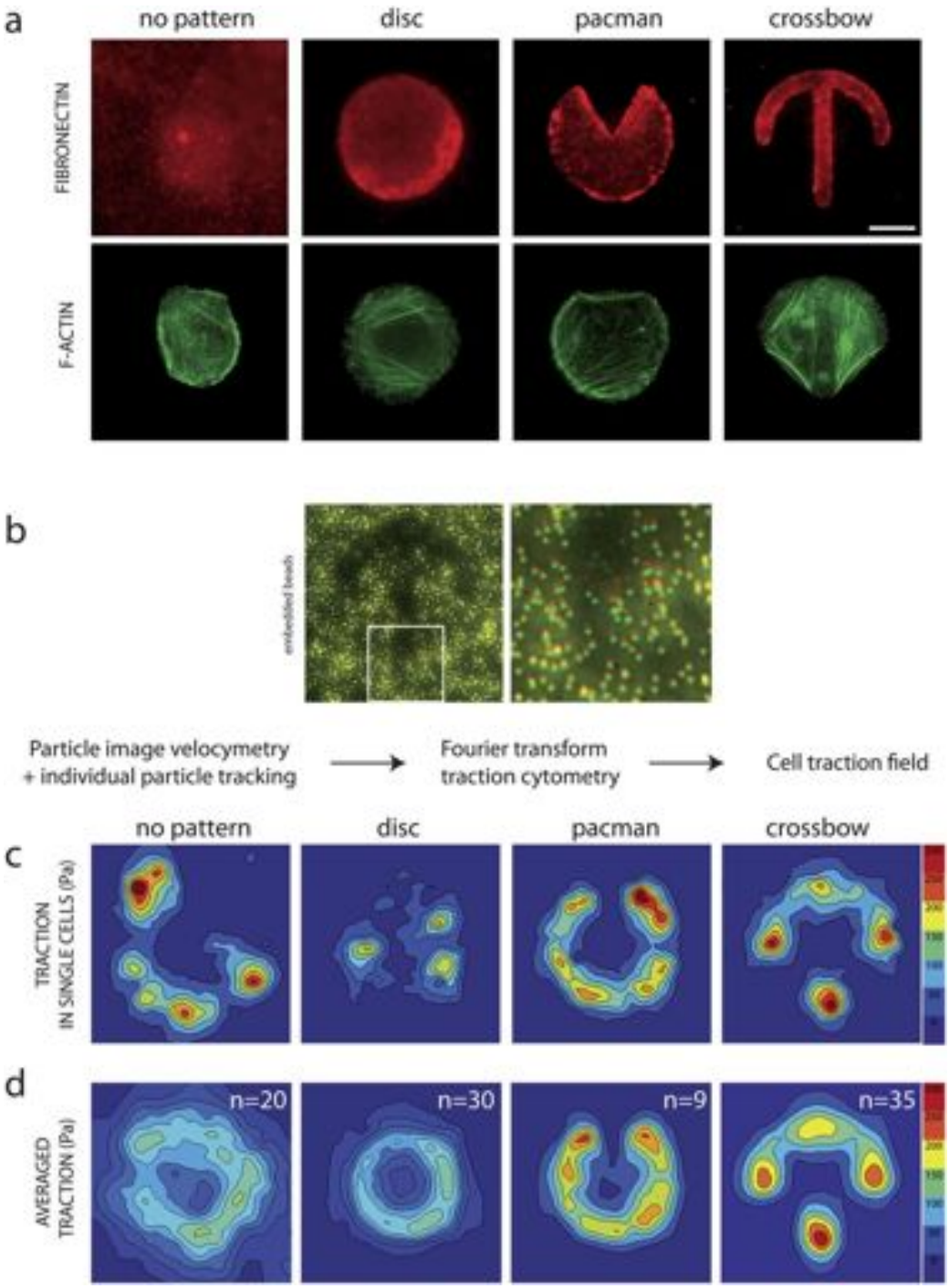

Fig. 2 Actin cytoskeleton streamlining normalizes the cell traction force field. (a) Micropattern geometry orients actin network architecture. Individual MCF10A cells plated either on non-patterned, fibronectin coated, glass slide, or on disc, pacman or crossbow shaped fibronectin micropatterns (red). Cells were fixed and stained with phalloidin to reveal F-actin filaments (green). Cells preferentially form contractile F-actin bundles, or stress fibers, above non-adhesive regions. Scale bar represents 10 μm. (b) Gel embedded beads were used to calculate the cell traction force with Fourier transform traction cytometry. Pictures of the beads were taken before (red) and after (green) cell detachment with trypsin to visualize the gel deformation upon the cell traction forces. Bead displacement was automatically detected and processed to infer the corresponding traction force field (see Experimental). (c) Traction force field calculations show that the cell exhibits an unpredictable spatial distribution of stress in non-patterned and in disc-shaped patterned cells. Cells patterned on pacman, and crossbow, develop enhanced traction forces on adhesion sites flanking non-adhesive regions. (d) Overlaying and averaging of traction force fields highlight the variability of traction force fields in non patterned cells. Non patterned cells were aligned using their nucleus position. Force fields were more precisely quantified in micropatterned cells. Crossbow shaped micropatterns reproducibly concentrate the location of cell traction forces in the bottom part of the vertical bar. Scale bar is 10 μm. Traction magnitude corresponds to the local force per area unit so it is given in Pascals.

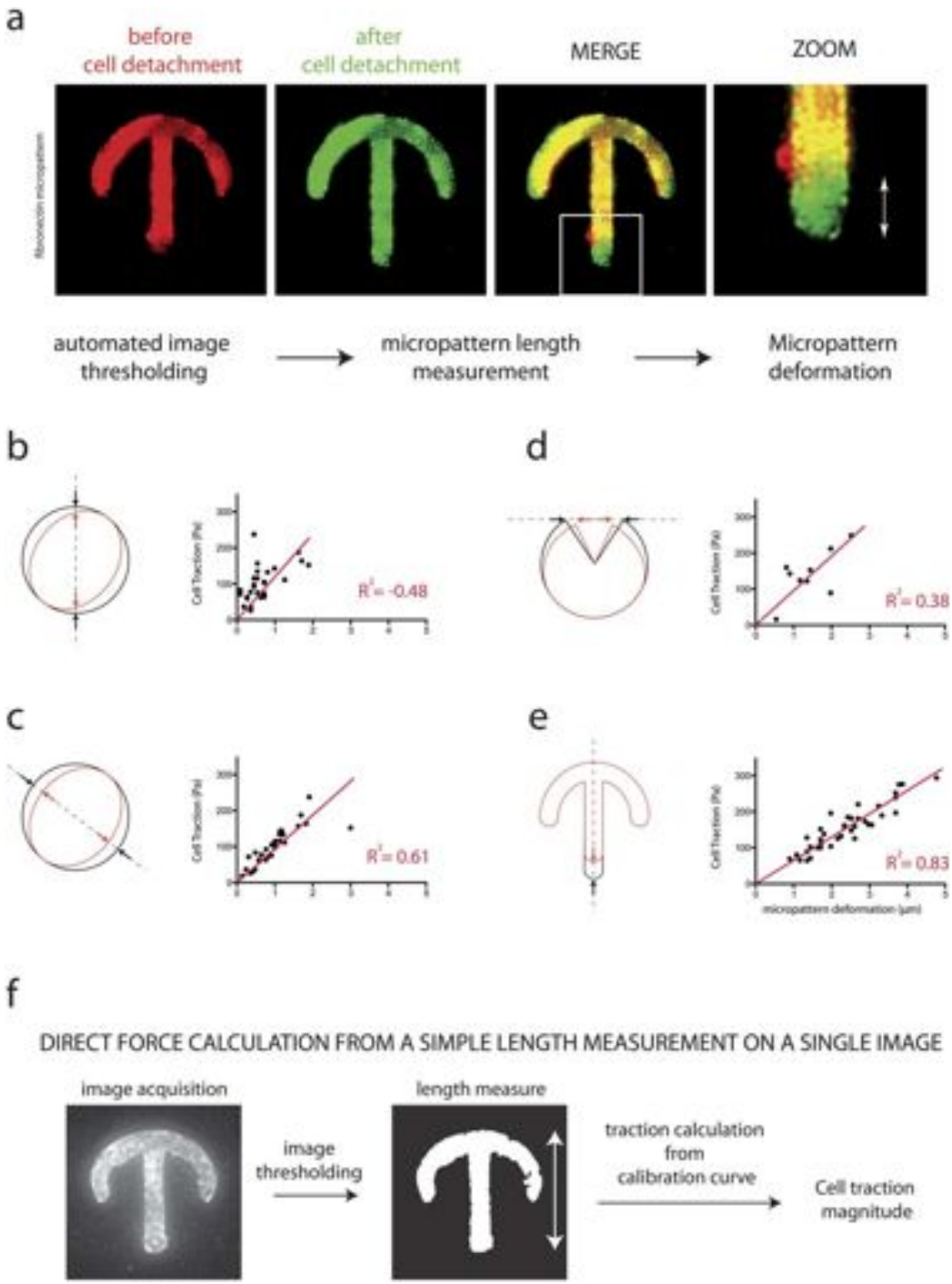

Fig. 3 Simple measurement of micropattern deformation allows easy, fast and accurate force quantification. (a) Fibrinogen-Alexa 546 coating was used to measure micropattern deformation. Pictures of micropatterns were taken before (red) and after (green) cell detachment with trypsin to visualize the micropattern deformation from the cell traction forces. (b) Red and black drawings represent micropattern shape before and after cell detachment. The micropattern deformation length corresponded to the distance between the red and black arrows. Micropattern deformation was then plotted against the total traction force exerted by the cell (normalized by cell area). Data points were fitted with a linear regression (full line). On discs, micropattern deformation could not be predicted. It was measured along an arbitrary vertical axis. The correlation in this case between total traction and micropattern deformation was not good. (c) The correlation was better when disc deformation was measured along the axis displaying the largest deformation. (d) On pacman shaped micropatterns the correlation was not optimal since the deformation was quite small and associated to large errors. (e) On crossbow shaped micropatterns the total cell traction force could be directly correlated to the micropattern deformation with a small deviation from the linear fit. This calibration curve was used in the following experiments. (f) New methodology to measure cell traction forces without bead displacement measurements or inverse problem calculation.

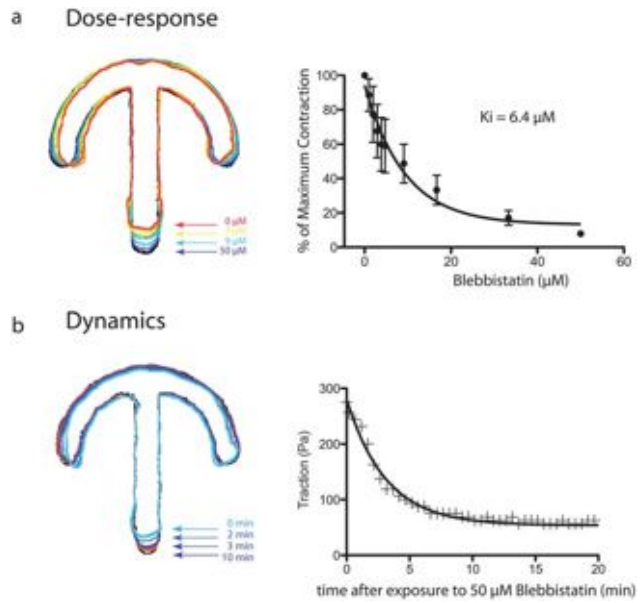

Fig. 4 Validation of simplified force measurements in response to myosin inactivation treatment. (a) Cell traction forces in response to blebbistatin, calculated by the method illustrated in Fig. 3f. Increasing drug concentrations were successively applied to 6 cells. Colored micropattern contours show a representative micropattern relaxation upon increasing drug concentrations. In the graph, the maximal cell tractions in the absence of blebbistatin were renormalized. Error bars represent the standard deviation. Data were fitted with a single exponential decay (full line) to calculate the IC50, *i.e.* drug concentration for half effect. (b) Cell traction forces over time in response to 50 µM of blebbistatin, calculated by the method illustrated in Fig. 3f. Colored micropattern contours show a representative micropattern relaxation over time. Measurements were performed on a single cell. Data were fitted with a single exponential decay (full line).

In addition we tested this new method for another application requiring numerous, and thus fast, force measurements: the analysis of force relaxation over time. We measured the force magnitude decrease in response to 50 µM of blebbistatin and found that it follows a single exponential decay (Fig. 4b).

All tumorigenic transformation do not increase cell contractility

We then used our method to compare the contraction level of wild type (WT) MCF10A cells *versus* drug treated or genetically modified MCF10A cells mimicking various forms of tumoral transformation. Indeed, tumor transformation has been shown to be associated with high levels of cell contraction.[21] This suggested that cell contraction level measurements could help in the diagnosis of cancer progression and allow the development of new and improved treatments.[36] We tested various treatments known to induce cell behaviors mimicking tumoral transformation: cell exposure to transforming growth factor beta 1 (TGFβ),[37] ErbB2 receptor activation,[38] and Protein kinase CK2 (previously known as Casein Kinase 2) inactivation.[39–43] Although already well characterized, their effect on the induction of a tumoral-like phenotype was tested here on MCF10A cells. We made two characteristic tests of tumoral-like behaviors: anchorage-independent growth[44,45] and inability to self-assemble into acini-like structures in 3D matrix.[46,47] Anchorage dependency for cell growth was tested by plating cells on soft agar.[44] Wild type MCF10A died, as revealed by the presence of black cell phantom (Fig. 5a). Inactivation of the beta subunit of CK2 as well as activation of ErbB2 receptors promoted cell growth. TGFβ treatment allowed cells to aggregate and survive (Fig. 5a). The ability to self-assemble into a mammary acini-like structure was tested by cultivating cells in Matrigel.[48] After one week, the wild type MCF10A formed the expected hollow spheres, as revealed by the reduction of nuclei in the central part of the structure (Fig. 5b). In all other conditions, cells formed irregular structures without cell clearance in the central part (Fig. 5b). These two analyses clearly confirmed that the three treatments conferred tumoral features to MCF10A cells.

MCF10A cells were treated for 2 days with 2 ng mL^{-1} of TGFβ before being plated on micropatterned PA substrates. As expected,[49] cells exhibited a significantly higher level of cell contraction as revealed by crossbow shortening (Fig. 5c). Interestingly, we found no significant changes in the level of cell contraction upon ErbB2 receptor activation (Fig. 5c). More surprisingly, in CK2b knockdown cells, the contraction level was significantly lower than in WT cells (Fig. 5c). These results show that different treatments, all inducing tumoral-like phenotypes, could either promote or reduce the level of cell contraction. They also demonstrate that our method can easily be used at larger scale to more precisely characterize this complex correlation between cell contraction and tumoral transformation.

Discussion

The use of deep UV exposure on PA in contact with the photomask is, to our knowledge, the most robust and easiest method to create homogeneous and reproducible micropatterns on soft deformable substrates. It allows a homogenous coating of ECM proteins over large micropatterned surfaces. In addition, it is faster than previous methods since it does not require any preliminary microfabrication step. These characteristics allowed this method to be adapted for large-scale production of soft micropatterned substrates. Considering the need to combine geometrical and mechanical control of cell microenvironment to recapitulate actual *in vivo* conditions for cell anchoring, we believe this new protocol will have a broad range of applications from fundamental research to tissue engineering.

The actin network streamlining and force field normalization in response to an appropriate micropattern geometry allow a precise calibration of the relationship between micropattern shape deformation and total traction forces. Thanks to the observed linear relationship between force and deformation, force measurement is simply obtained by measuring micropattern length. Classical force measurement methods are still required to obtain the calibration curve. However, afterwards, a single image acquisition is sufficient to measure micropattern length and read the corresponding traction force. The sensitive and difficult step of gel-embedded beads imaging and tracking is no longer required. Therefore, force measurement is as simple as the use of micropillars[9] without the microfabrication constraint. However since we do not consider micron-sized substrate deformations the spatial resolution is lower than the resolution that can be achieved with bead tracking.[32,50] Our method is adapted to provide an easy and fast measurement of the global

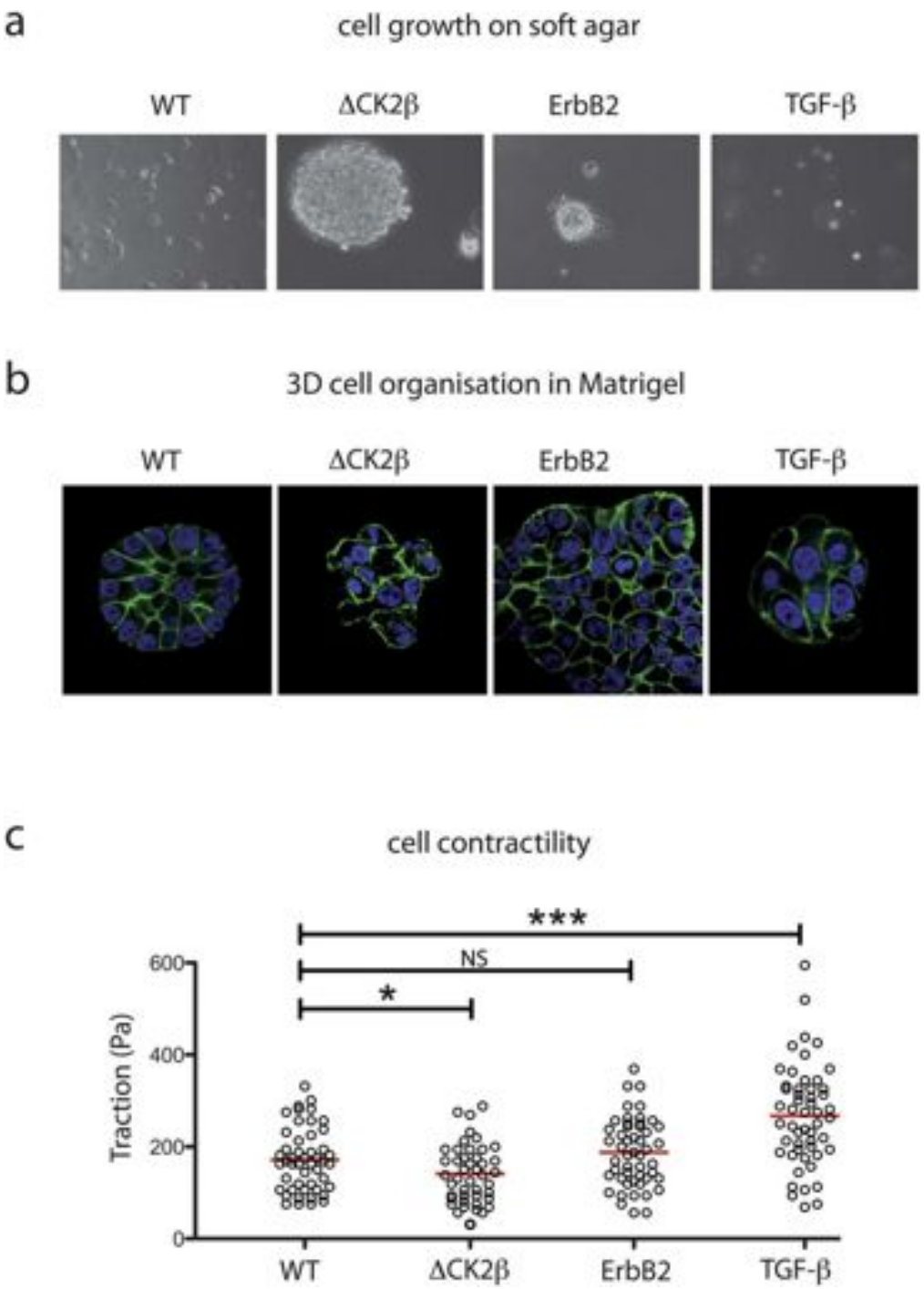

Fig. 5 Applications of large-scale force measurements to tumoral-like phenotypes. (a) Anchorage-independent growth. Cells were cultured on soft agar and imaged by phase contrast microscopy. Wild type cells died after a few days as revealed by the presence of black phantoms. CK2b knockdown cells and ErbB2 activated cells managed to grow in the absence of anchorage. TGFb1 treated cells form small aggregates (bright in phase contrast) and survived. (b) Self-assembly of 3D acini-like structures. Cells were cultured in Matrigel and stained for DNA (blue) and actin (green). Wild type cells formed spherical hollow structures as revealed by the low number of nuclei in the central part of the acini. CK2b knockdown cells, ErbB2 activated cells and TGFβ treated cells form irregular aggregates with mis-positioned cells in the central part of the structure. Pictures are 50 μm wide. (c) Cell traction forces calculated by the method illustrated in Fig. 3f in mutant or drug treated MCF10A cells mimicking tumor transformation. MCF10A WT cells were compared to CK2b knockdown cells, ErbB2 activated cells and TGFβ treated cells. Comparison between two sets of measures were performed using a student T test: two tailed, 95% interval confidence: * = $P < 0.05$ ** = $P < 0.01$ *** = $P < 0.001$.

cell contraction level with only a simple local measurement. In addition, it is easily amenable to automation since cell position and subcellular localization of force production are precisely controlled. This method paves the way to large scale and high throughput analysis of cell contraction state.

Our initial work identified characteristic tumoral-like phenotypes that were not associated to an increased level of cell contractility. High levels of contractility were observed in epithelial cells forming disorganized multicellular structures[21] or detaching from each others.[51] Such phenotypes are characteristic of advanced or late stages of tumoral transformation. ErbB2 receptor activation is a feature of early tumoral transformation that impacts on growth rate.[38] CK2 is also implicated in anti-apoptotic effect and CK2beta knockdown, specifically affecting p53-dependent cell survival.[41] Although contractility activates cell growth, early phases of cancer progression involving cell growth stimulation might not systematically be associated to a high level of contractility. It would be now necessary to more specifically analyze cell contraction levels at various phases of tumoral transformation to clarify the relationship between cancer progression and cell contraction. Mechanical property characterization of healthy and transformed cells could then be used to set up a new medical diagnosis test. Note that measurements have been performed on gels whose rigidity was about 7 kPa, but the relative levels of cell contractions for each treatment could have been different for another matrix rigidity.[52]

Conclusion

We developed a new method to micropattern poly-acrylamide gels. It associates the control of cell shape and microenvironment stiffness. This method could have a broad range of application notably in the design of new biomaterials for tissue engineering purpose. It can also be applied to the quantification of global cell contraction levels *via* the simple measurement of micropattern deformation. Our results suggested that not all cancer cells are more contracted than normal cells and that cell contraction levels may vary depending on the nature of the tumorigenic signal or the stage of cancer progression.

Experimental

PA micropatterning

25 mm round glass coverslips were first cleaned with piranha for 2 h and silanized by dipping in ethanol solution containing 2% (v/v) 3-(trimethoxysilyl)propyl methacrylate (Sigma) and 1% (v/v) acetic acid for 5 min. After cleaning with ethanol to remove excess silane residue, the coverslips were incubated at 120 °C for one hour.

Carboxylate modified polystyrene fluorescent beads (dark red 200 nm, Invitrogen F-8807) were passivated by poly(ethylene) glycol as follows: fluorescent beads were diluted 25-fold in MES buffer (10 mM pH 5.5) containing 8 mg mL^{-1} *N*-hydroxy-succinimide (NHS; Fluka) and 4 mg mL^{-1} EDC (1-ethyl-3-[3-dimethylaminopropyl]carbodiimide hydrochloride; Pierce) before 1 : 1 mixing with PLL-PEG (PLL(20)-g[3.5]-PEG(2); Susos) solution (4 mg mL^{-1} in 10 mM pH8.5 HEPES buffer). The mixture was incubated with rotation at 4 °C overnight. The beads were subsequently spun down and resuspended in HEPES buffer (10 mM pH 7.4).

The photomask was cleaned by *n*-hexane prior to use in order to maintain an hydrophobic surface. An acrylamide solution containing 6.67% acrylamide and 0.167% bis-acrylamide was mixed with passivated fluorescent beads by sonication before addition of APS and TEMED. A 35 μL drop of acrylamide solution was put directly on the chromium side of the photomask (Toppan). A silanized coverslip was placed over the drop and let it polymerize for 45 min. The sandwich was then exposed to deep UV in a UV–Ozone cleaner (Jelight) for 4 min. The coverslip, with gel, was carefully removed from the mask and incubated with 10 mg mL^{-1} EDC and 17 mg mL^{-1} NHS water solution for 15 min, and then coated with 20 ug mL^{-1} fibronectin (Sigma) and 5 μg mL^{-1} Alexa546 conjugated fibrinogen (Invitrogen) in HEPES buffer (10 mM pH 8.5) for one hour. The photomask was washed with water and then isopropanol. The gel was washed three times by PBS before seeding cells.

AFM measurement of micropatterned PA elasticity

All atomic force microscopy (AFM) measurements were carried out in PBS using a PicoPlus AFM (Agilent Technologies, USA). The spring constant of each cantilever was determined using the thermal noise method.[53] Force-indentation profiles were recorded using borosilicate sphere-tipped cantilevers with a radius, *R*, of 2.5 μm (Bioforce Nanoscience, IA, USA) and a spring constant of 60 mN m^{-1}. To delimitate insolated and non-insolated zones, topographies of 60 × 60 μm^2 were first imaged in contact mode with 512 × 512 $pixels^2$ at line rates of 0.5 Hz and with the same cantilevers. The sphere probe was then moved above the zone of interest before indentation. Young's moduli were calculated by least-square fitting of the experimental force-indentation curves. The measured Young modulus of UV exposed regions was 7.29 ± 0.42 kPa. The measured Young modulus of non-exposed regions was 6.64 ± 0.59 kPa.

Cell culture and treatments

The culture of MCF10A cells and the generation of ΔCK2β cell line was described previously.[40] The MCF10A cell expressing ligand inducible ErbB2 receptors were obtained from Ariad Pharmaceuticals.[38] Cells were seeded on the micro-patterned substrate at a density of 8 × 10^4 cm^{-2}. Cells not attaching to the adhesive region on the substrate were washed away 1–2 h after seeding. All the traction force measurements were performed 6 h after seeding to ensure a full spreading of the cells. Substrate relaxation was assessed by detaching cells with trypsin. To induce an ErbB2 cell line, AP1510 (Ariad Pharmaceuticals) was added to the culture medium to a final concentration of 1 μM, 48 h before traction force measurement.[38] TGFβ (R&D systems) was added at 2 ng mL^{-1} to the culture medium 48 h before cell plating on micropatterned PA and traction force measurement. Blebbistatin(-) (Sigma) at 100 μM was added progressively to the observation chamber to gradually obtain the specific final concentration for the drug dose-response experiment. While for the time response experiment, blebbistatin was added to directly reach a final concentration of 100 μM. Image acquisition started directly after the drug addition.

Anchorage-independent growth

Cells were detached with trypsin and resuspended in growth medium. Plates were prepared with a coating of 0.75% agarose (Cambrex) in growth medium and then overlaid with a suspension of cells in 0.45% agarose (5×10^3 cells per well). Plates were incubated for 4 weeks at 37 °C and colonies were imaged under a microscope.

Self-organization in 3D matrix

Cells (10 000) were seeded in chamber slides coated with growth factor reduced EHS ECM (Matrigel® BD Biosciences; with protein concentrations between 9 and 11 mg mL^{-1}) in assay medium (DMEM/F12 supplemented with 2% donor horse serum, 10 μg mL^{-1} insulin, 0.5 μg mL^{-1} hydrocortisone, 100 ng mL^{-1} cholera toxin, 5 ng mL^{-1} EGF (Peprotech, France). The assay medium was replaced every 3 days. When indicated, at day 6, cells were treated with 2 ng mL^{-1} TGFβ for 50 h.

Fixation and immuno-stainings

Six hours after seeding on the micropatterned gel or glass coverslip, the cells were first extracted in cytoskeleton buffer (10 mM MES, 138 mM KCl, 3 mM MgCl, 2 mM EGTA, pH 6.1) containing 0.5% Triton X-100, then fixed in 4% paraformaldehyde. 3D cell structures were fixed in 2% PFA, permeabilized in 0.5% Triton X-100–PBS. Fixed samples were wash 3 times in PBS. Afterward, samples were incubated for 1 h in PBS containing 0.1% Tween, 3% BSA, and 10 μM Phalloidin-FITC (Sigma) to stain actin filaments. On glass slides, cells were immuno labelled with primary antibodies directed against paxillin (BD Tranduction Laboratories) followed by immunolabelling with secondary Cy3-labelled antibodies (Jackson Immuno Research). All coverslips were stained with Hoechst 33342 (Sigma) to reveal cell nuclei for counting. After PBS washing, coverslips were mounted in Mowiol mounting medium.

Microscopy and Image processing

Images of fixed cells were taken with a 100× objective (NA = 1.35) on an Olympus BX-61 straight microscope, mounted with a CDD camera (HQ2, Ropper Scientific) and driven with Metamorph (Molecular Devices). Images of the 3D cell structures were performed using a Leica TCS-SP2 laser scanning confocal apparatus coupled to a Leica DMIRBE microscope. Live imaging of bead displacement and micropattern deformation were performed with a 63× objective (NA = 1.4) on an inverted 200 M Zeiss microscope, mounted with a CDD camera (HQ2, Ropper Scientific) and driven with Metamorph (Molecular Devices). Temperature and CO_2 control were ensured by the Cube and the Box from LIS Imaging.

All the acquired images were processed by ImageJ (http://rsb.info.nih.gov/ij/). Averaged fluorescent staining images were automatically aligned using micropattern images by a custom written plugin (https://sites.google.com/site/qingzongtseng/template-matching-ij-plugin). Pattern detection and length measurement were done automatically by custom written macro routines.

Traction force microscopy

Displacement fields describing the deformation of the PA substrate are determined from the analysis of fluorescent beads images before and after removal of the adhering cells with trypsin treatment. The displacement field is obtained by a two-step method consisting of particle image velocimetry followed by individual bead tracking.[32,33] A special procedure is used to evaluate displacements in the area of the adhesive pattern where gel deformation is expected to be largest. Depending on the pattern shape, traction forces may be strongly localized leading to large displacements in very small areas. In this case, failure to correctly track a few beads in such areas would significantly alter the calculated force magnitude. Therefore, the pattern area is divided into smaller windows that are allowed to overlap, before applying the cross-correlation and tracking analysis. Reducing the size of the windows makes it possible to retrieve larger displacements with cross-correlation and, using overlapped windows, we can avoid missing beads close to the windows boundaries. All image processing and analysis were performed using Matlab.[54]

To calculate cell-induced traction stress from displacement data, we have used the Fourier-transform traction cytometry (FTTC) method.[32,33] We kept the regularization parameter at small values ($\lambda < \sim 10^{-9}$) in order to maintain the best spatial resolution, which is estimated to be about 5 μm in our case.

Acknowledgements

We would like to thank Thomas Boudou, Catherine Picart, Claude Verdier and Michael Betton for AFM measurements of gel rigidities, as well as Alexandre Deshière and Laurent Blanchoin for interesting discussions. This work was supported by grants from Agence National pour la Recherche to OF and MT (ANR-PCV08_322457), from the CNRS (appel à prise de risques) to MB, from the fondation nanosciences RTRA to MB and from the Université Joseph Fourier (program SMING) to MB and MT.

References

1 M. Thery, *J Cell Sci*, 123, pp. 4201–4213.
2 D. Falconnet, G. Csucs, H. M. Grandin and M. Textor, *Biomaterials*, 2006, **27**, 3044–3063.
3 H. B. Wang, M. Dembo and Y. L. Wang, *Am. J. Physiol. -Cell Physol.*, 2000, **279**, C1345–C1350.
4 G. Blin, N. Lablack, M. Louis-Tisserand, C. Nicolas, C. Picart and M. Puceat, *Biomaterials*, 2010, **31**, 1742–1750.
5 V. Damljanovic, B. C. Lagerholm and K. Jacobson, *BioTechniques*, 2005, **39**, 847–851.
6 N. Wang, E. Ostuni, G. M. Whitesides and D. E. Ingber, *Cell Motil. Cytoskeleton*, 2002, **52**, 97–106.
7 K. K. Parker, A. L. Brock, C. Brangwynne, R. J. Mannix, N. Wang, E. Ostuni, N. A. Geisse, J. C. Adams, G. M. Whitesides and D. E. Ingber, *FASEB J.*, 2002, **16**, 1195–1204.
8 A. J. Engler, M. A. Griffin, S. Sen, C. G. Bonnemann, H. L. Sweeney and D. E. Discher, *J. Cell Biol.*, 2004, **166**, 877–887.
9 J. L. Tan, J. Tien, D. M. Pirone, D. S. Gray, K. Bhadriraju and C. S. Chen, *Proc. Natl. Acad. Sci. U. S. A.*, 2003, **100**, 1484–1489.
10 M. Théry, A. Pepin, E. Dressaire, Y. Chen and M. Bornens, *Cell Motil. Cytoskeleton*, 2006, **63**, 341–355.
11 A. J. Engler, S. Sen, H. L. Sweeney and D. E. Discher, *Cell*, 2006, **126**, 677–689.
12 J. Fu, Y. K. Wang, M. T. Yang, R. A. Desai, X. Yu, Z. Liu and C. S. Chen, *Nat. Methods*, 2010, **7**, 733–736.

13 V. Chevrier, M. Piel, N. Collomb, Y. Saoudi, R. Frank, M. Paintrand, S. Narumiya, M. Bornens and D. Job, *J. Cell Biol.*, 2002, **157**, 807–817.
14 A. Pitaval, Q. Tseng, M. Bornens and M. Théry, *J. Cell Biol.*, 2010, **191**, 303–312.
15 S. Miserey-Lenkei, G. Chalancon, S. Bardin, E. Formstecher, B. Goud and A. Echard, *Nat. Cell Biol.*, 2010, **12**, 645–654.
16 W. Yu, A. M. Shewan, P. Brakeman, D. J. Eastburn, A. Datta, D. M. Bryant, Q. W. Fan, W. A. Weiss, M. M. Zegers and K. E. Mostov, *EMBO Rep.*, 2008, **9**, 923–929.
17 C. M. Lo, D. B. Buxton, G. C. Chua, M. Dembo, R. S. Adelstein and Y. L. Wang, *Mol. Biol. Cell*, 2004, **15**, 982–989.
18 A. D. Doyle, F. W. Wang, K. Matsumoto and K. M. Yamada, *J. Cell Biol.*, 2009, **184**, 481–490.
19 A. S. Maddox and K. Burridge, *J. Cell Biol.*, 2003, **160**, 255–265.
20 E. A. Klein, L. Yin, D. Kothapalli, P. Castagnino, F. J. Byfield, T. Xu, I. Levental, E. Hawthorne, P. A. Janmey and R. K. Assoian, *Curr. Biol.*, 2009, **19**, 1511–1518.
21 M. J. Paszek, N. Zahir, K. R. Johnson, J. N. Lakins, G. I. Rozenberg, A. Gefen, C. A. Reinhart-King, S. S. Margulies, M. Dembo, D. Boettiger, D. A. Hammer and V. M. Weaver, *Cancer Cell*, 2005, **8**, 241–254.
22 J. M. Vasiliev, T. Omelchenko, I. M. Gelfand, H. H. Feder and E. M. Bonder, *Proc. Natl. Acad. Sci. U. S. A.*, 2004, **101**, 12526–12530.
23 K. P. Landsberg, R. Farhadifar, J. Ranft, D. Umetsu, T. J. Widmann, T. Bittig, A. Said, F. Julicher and C. Dahmann, *Curr. Biol.*, 2009, **19**, 1950–1955.
24 M. Rauzi, P. Verant, T. Lecuit and P. F. Lenne, *Nat. Cell Biol.*, 2008, **10**, 1401–1410.
25 S. Huang, C. S. Chen and D. E. Ingber, *Mol. Biol. Cell*, 1998, **9**, 3179–3193.
26 F. Rehfeldt, A. J. Engler, A. Eckhardt, F. Ahmed and D. E. Discher, *Adv. Drug Delivery Rev.*, 2007, **59**, 1329–1339.
27 A. J. Ridley, *Breast Cancer Res. Treat.*, 2004, **84**, 13–19.
28 A. Welle and E. Gottwald, *Biomed. Microdevices*, 2002, **4**, 33–41.
29 S. A. Mitchell, A. H. C. Poulsson, M. R. Davidson, N. Emmison, A. G. Shard and R. H. Bradley, *Biomaterials*, 2004, **25**, 4079–4086.
30 A. Azioune, M. Storch, M. Bornens, M. Thery and M. Piel, *Lab Chip*, 2009, **9**, 1640–1642.
31 W. A. Marganski, M. Dembo and Y. L. Wang, *Methods Enzymol.*, 2003, **361**, 197–211.
32 B. Sabass, M. L. Gardel, C. M. Waterman and U. S. Schwarz, *Biophys. J.*, 2008, **94**, 207–220.
33 J. P. Butler, I. M. Tolic-Norrelykke, B. Fabry and J. J. Fredberg, *Am. J. Physiol. -Cell Physol.*, 2002, **282**, C595–605.
34 A. Straight, A. Cheung, J. Limouze, I. Chen, N. Westwood, J. Sellers and T. J. Mitchison, *Science*, 2003, **299**, 1743–1747.
35 D. Mitrossilis, J. Fouchard, A. Guiroy, N. Desprat, N. Rodriguez, B. Fabry and A. Asnacios, *Proc. Natl. Acad. Sci. U. S. A.*, 2009, **106**, 18243–18248.
36 D. T. Butcher, T. Alliston and V. M. Weaver, *Nat. Rev. Cancer*, 2009, **9**, 108–122.
37 J. Massague, *Cell*, 2008, **134**, 215–230.
38 S. K. Muthuswamy, D. Li, S. Lelievre, M. J. Bissell and J. S. Brugge, *Nat. Cell Biol.*, 2001, **3**, 785–792.
39 M. R. MacPherson, P. Molina, S. Souchelnytskyi, C. Wernstedt, J. Martin-Perez, F. Portillo and A. Cano, *Mol. Biol. Cell*, 2009, **21**, 244–253.
40 A. Deshiere, N. Theis-Febvre, V. Martel, C. Cochet and O. Filhol, *Mol. Cell. Biochem.*, 2008, **316**, 107–113.
41 V. Martel, O. Filhol, P. Colas and C. Cochet, *Oncogene*, 2006, **25**, 7343–7353.
42 M. Ruzzene and L. A. Pinna, *Biochim. Biophys. Acta, Proteins Proteomics*, 2010, **1804**, 499–504.
43 J. H. Trembley, G. Wang, G. Unger, J. Slaton and K. Ahmed, *Cell. Mol. Life Sci.*, 2009, **66**, 1858–1867.
44 N. H. Colburn, W. F. Bruegge, J. R. Bates, R. H. Gray, J. D. Rossen, W. H. Kelsey and T. Shimada, *Cancer Res.*, 1978, **38**, 624–634.
45 P. J. Reddig and R. L. Juliano, *Cancer Metastasis Rev.*, 2005, **24**, 425–439.
46 J. Debnath and J. S. Brugge, *Nat. Rev. Cancer*, 2005, **5**, 675–688.
47 M. K. Wendt, J. A. Smith and W. P. Schiemann, *Oncogene*, 2010, **29**, 6485–6498.
48 J. Debnath, S. K. Muthuswamy and J. S. Brugge, *Methods*, 2003, **30**, 256–268.
49 J. Chen, H. Li, N. SundarRaj and J. H. Wang, *Cell Motil. Cytoskeleton*, 2007, **64**, 248–257.
50 J. Stricker, B. Sabass, U. S. Schwarz and M. L. Gardel, *J. Phys.: Condens. Matter*, 2010, 22.
51 J. de Rooij, A. Kerstens, G. Danuser, M. A. Schwartz and C. M. Waterman-Storer, *J. Cell Biol.*, 2005, **171**, 153–164.
52 R. W. Tilghman, C. R. Cowan, J. D. Mih, Y. Koryakina, D. Gioeli, J. K. Slack-Davis, B. R. Blackman, D. J. Tschumperlin and J. T. Parsons, *PLoS One*, 2010, **5**, e12905.
53 H. J. Butt and M. Jaschke, *Nanotechnology*, 1995, **6**, 1–7.
54 Y. X. Gao and M. L. Kilfoil, *Opt. Express*, 2009, **17**, 4685–4704.

SUPPLEMENTARY INFORMATIONS

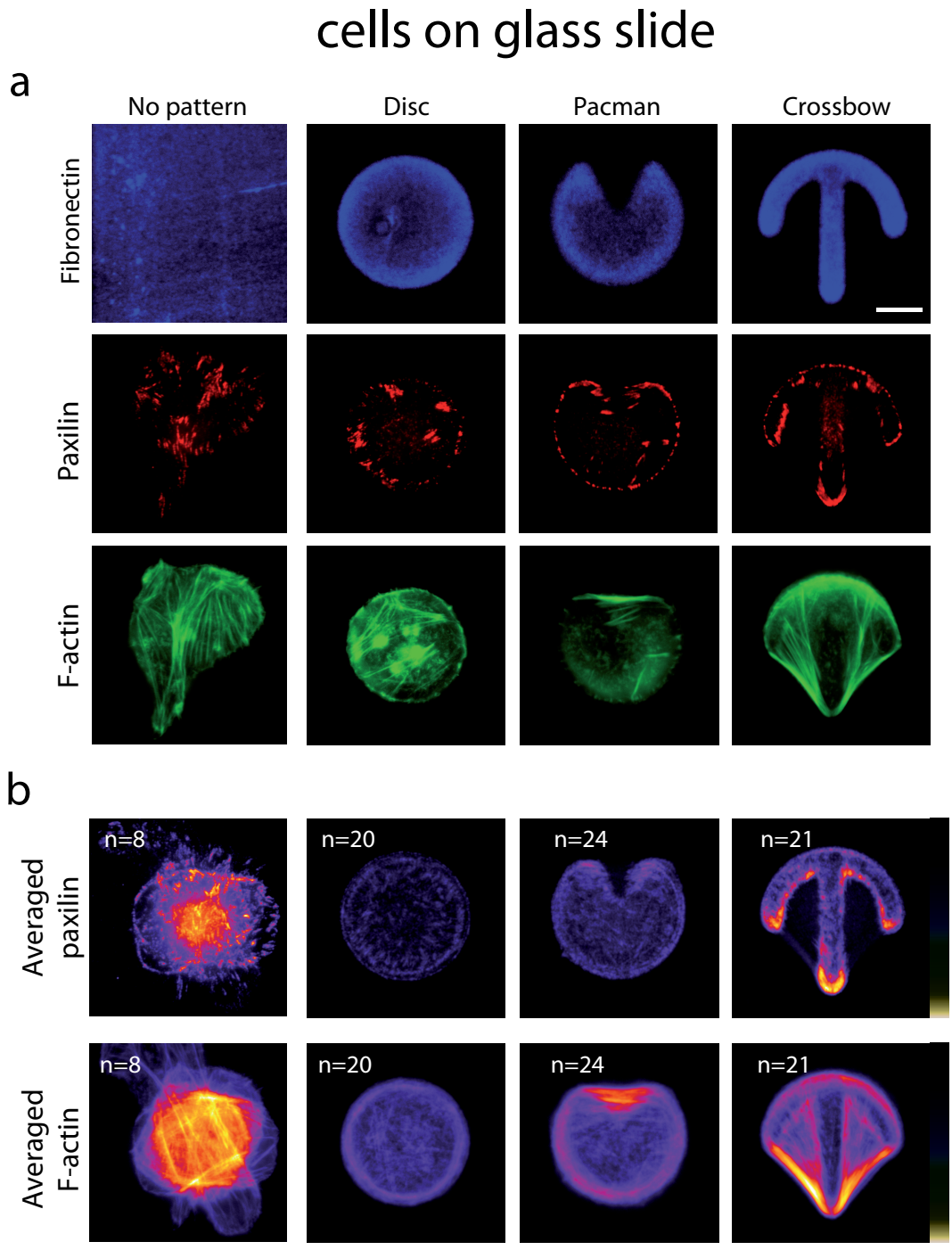

Figure S1 – Micropattern geometry orient cell actin architecture.

(a) Individual MCF10A cells plated either on non-patterned, fibronectin coated, glass slide, or on disc, or pacman or crossbow shaped fibronectin micropatterns (blue). Cells were fixed and immuno-stained for paxillin (red)

to reveal focal adhesions and phalloidin to reveal F-actin filaments (green). Scale bar is 10 µm.

(b) Paxillin and F-actin stainings were overlaid and averaged in each adhesive condition. Averaged images were color-coded with the FIRE LUT to highlight the more intense and reproducible stainings. Crossbow shapes promote the formation of reproducible stress fibers above the two non-adhesive regions. Stress fibers anchoring on focal adhesions were concentrated in the bottom of the crossbow vertical bar.

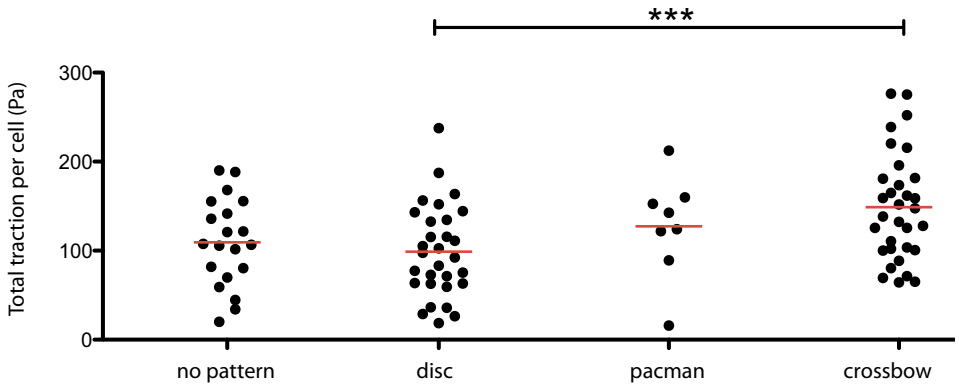

Figure S2 – Crossbow micropatterns stimulate cell contraction.

Classical traction force microscopy was used to quantify the total traction force exerted by each cell. Cells appeared to exert higher traction on crossbow shaped micropatterns. Comparison between two sets of measures were performed using a Student T test: two tailed, 95% interval confidence: *=P<0.05 **=P<0.01 ***=P<0.001.

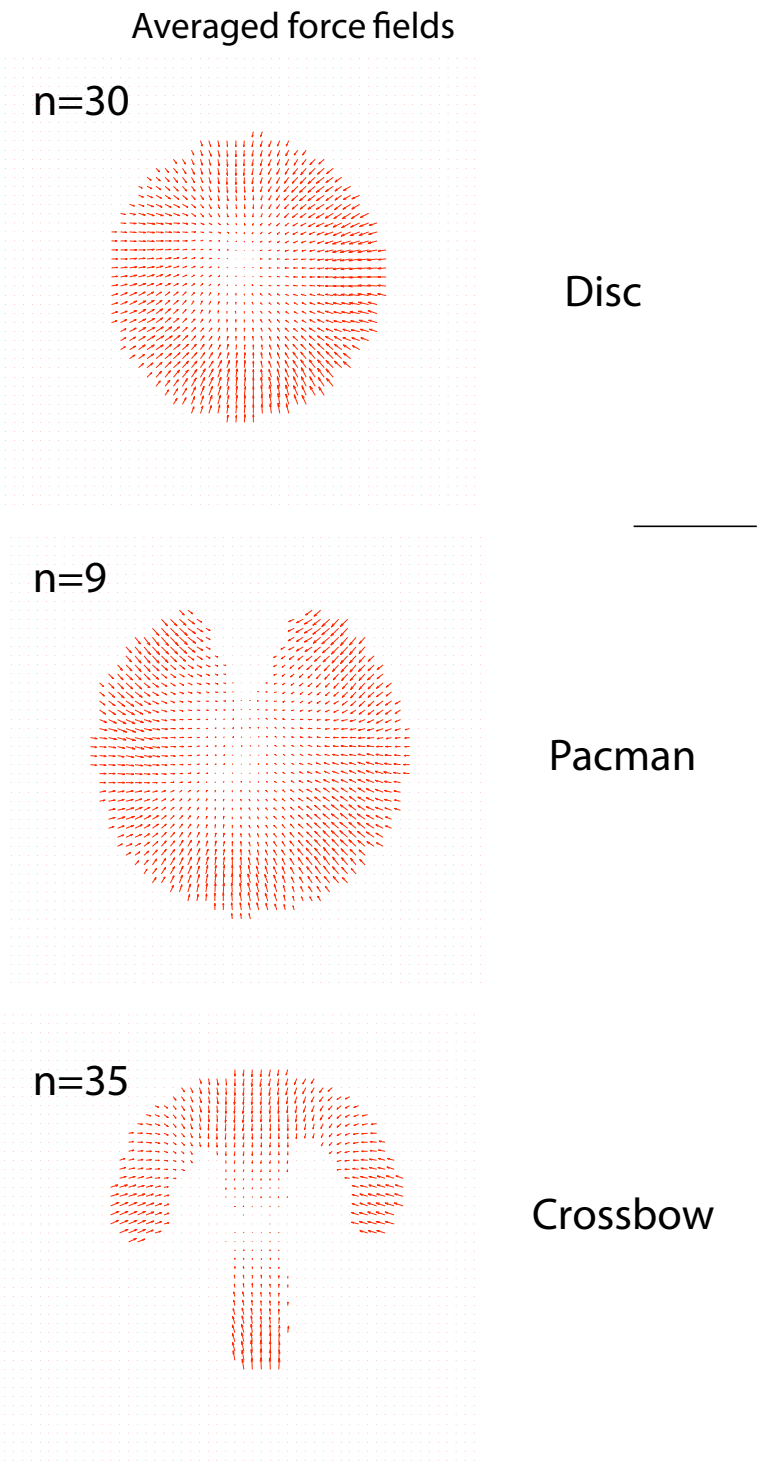

Figure S3 – Micropattern geometry orient cell traction forces.

Cells were plated on PA gels with disc, pacman or crossbow micropatterns. Classical traction force microscopy was used to reconstruct the traction vector field exerted by cells for each type of pattern. Traction fields were overlaid and averaged in each condition. Forces appeared randomly orientated in the absence of micropatterns. No preferential orientation appeared in cells plated on disc micropatterns. Forces on

crossbow shaped micropatterns were reproducibly oriented upward at the bottom of the micropattern vertical bar.

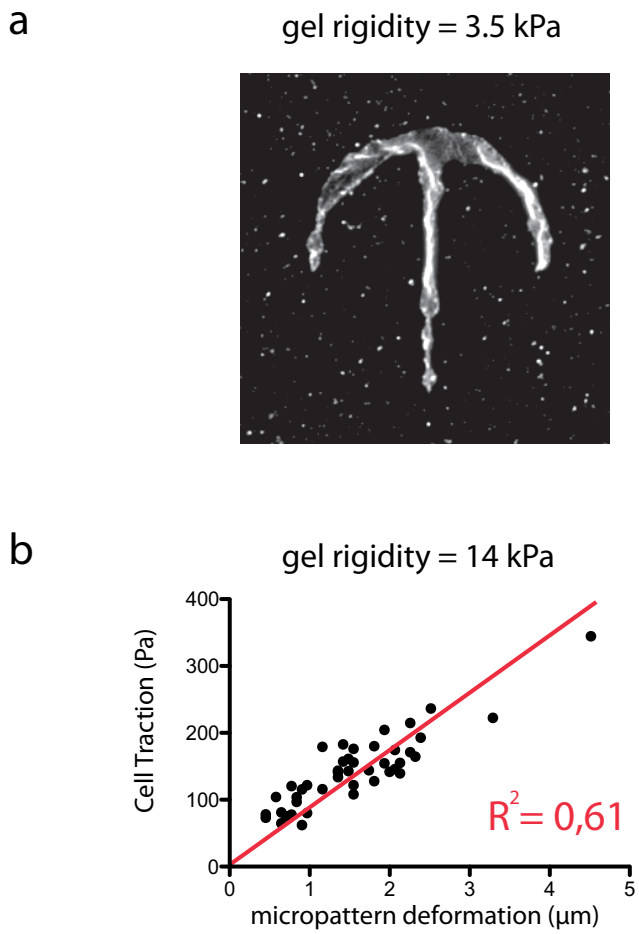

Figure S4 – Micropattern fabrication and force measurement at different rigidities

(a) Micropattern fabrication on PA gels whose rigidity is about 3 kPa. Example of a fluorescent-fibrinogen coated micropattern damaged during PA layer detachment from the optical mask.

(b) Force measurement on PA gels whose rigidity is about 14 kPa. Local micropattern deformation, measured as in figure 3e, was linearly correlated to total traction force exerted by the cells on the entire micropattern.

Movie S1

Increasing dose of Blebbistatin were added progressively on MCF10A cells plated on a crossbow shaped micropattern on PA. Pictures were taken 15 minutes after each addition of Blebbistatin. Finally the cell was detached with trypsin.

4.3 Contractility and ciliogenesis

The cellular contractility is reflecting the global state of cytoskeletal networks, thus many cellular processes are directly or indirectly associated with the cellular contractility. For example, the ciliogenesis involves the processes of centrosome positioning, membrane protrusion and polymerization of specific cytoskeletal network within the cilium.

My work on the cellular contractility has contributed to part of this paper of ciliogenesis (Pitaval et al., 2010). Apart from cell cycle dependency, we have demonstrated a direct correlation between ciliogenesis and contractility by using soft substrate, pattern confinement and myosin inhibition.

Here I will present some key results in this paper involving my studies on the cellular contractility.

Actomyosin network and ciliogenesis capability

The generation of primary cilia involves fusion of vesicle and deformation of plasma membrane(Satir et al., 2007; Rohatgi et al., 2010). As a result, this process is associated with not only the microtubule network which is the main component of the cilium , but also linked with the actomyosin network which governs the mechanical state of the membrane. The dense actin network under the membrane is often called the cortical actin. It provides anchoring point for transmembrane proteins and contribute to the mechanical integrity of the cell shape.

In the following figure, we can see by reducing the cell spreading area which mimiced the situation when cells were in confluence, the cell became less contractile (inferred by less amount of myosin)(Figure 4B). As the cellular contractility reduced, the proportion of ciliated cell increased. The same effect was also observed by reducing the contractility with Myosin inhibition.

Besides the implication in cellular contractility, there might be other mechanisms that actomyosin network regulates the ciliogenesis. For example, the treatment of Cytochalasin D, which impaired the actin polymerization has been shown to inhibit the migration of basal body and ciliary elongation(Boisvieux-Ulrich et al., 1990) Interestingly, we found after the treatment of Cytochalasin D, the proportion of ciliated cells became independent to the cell spreading area(Figure4A). This further highlights the global cellular contractility from the actin network as the major determinant for the ciliogenesis, even though the disruption of actin network would result in mislocation of cilia and impair the cilia elongation.

Contractility and cilia length

Apart from the proportion of ciliated cells, the length of each cilia is also associated with the cellular contractility. When the contractility was reduced by confining the cell spreading, we observed an increase of cilia length(Figure4A).

The most striking effect on the ciliogenesis was observed on the cells cultured on soft polyacrylamide gel, where 80% of cells were ciliated compared with 30% when cells were cultured on hard substrate(ECM-coated glass coverslips). While there was only 25% difference in the projected cell area. Furthermore, the length of the cilia was also significantly increased when cells were cultured on soft substrate(Figure 4C).

Centrosome position and ciliogenesis

The basal body of the primary cilium is derived from one of the centrioles in the centrosome. The migration of basal body and its docking to the apical membrane are crucial for the early stages of ciliogenesis. It is thus highly relevant to examine how the cellular contractility regulates the centrosome position which might be associated with this early stage of ciliogenesis.

We found that the centrosome position at the beginning of the ciliogenesis was strongly affected by the contractile state(Figure5A right, starvation). For cells on small micropattern($S=750\mu m^2$), which were less contractile, the centrosome was mainly located at the apical face and they grew cilium. While for the highly contractile cells($S=3000\mu m^2$), the centrosome was mostly located at the basal face and they failed to ciliate.

In summary, our result demonstrated that physiological cellular events such as ciliogenesis and centrosome positioning are deeply associated with the mechanical state of the cell. This mechanical state is in turn related to the mechanical property of the cellular microenvironment. For example, epithelial cells *in vivo* are usually highly compact and grow on a rather soft extracellular matrix, which render them less contractile and sensing a compliant environment. All these physical cues are crucial for the physiological functioning of the cell.

FIGURE 4

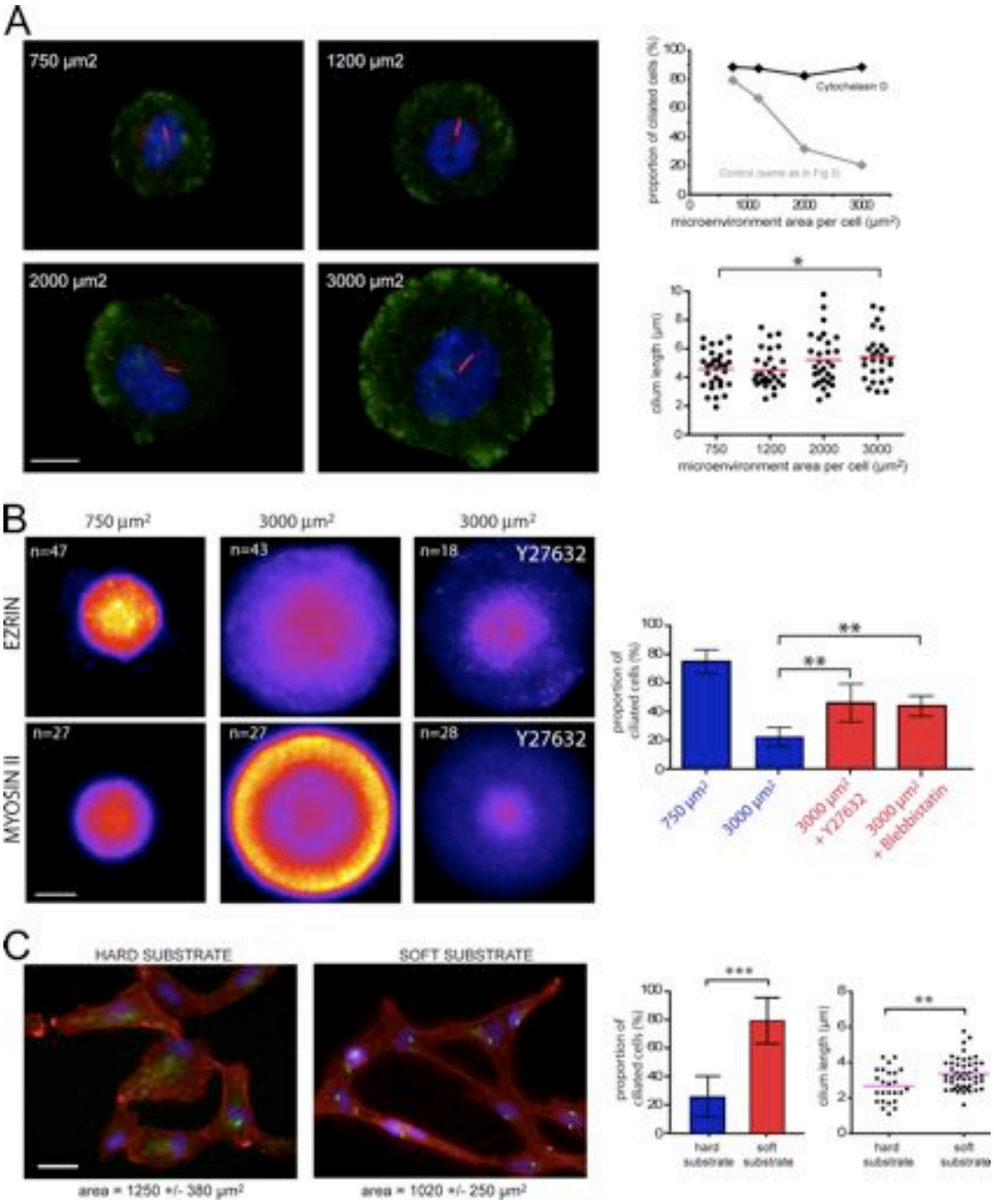
A
750 µm2
1200 µm2
2000 µm2
3000 µm2
proportion of ciliated cells (%)
Cytochalasin D
Control (same as in Fig 3)
microenvironment area per cell (µm²)
cilium length (µm)
750
1200
2000
3000
microenvironment area per cell (µm²)
B
750 µm²
3000 µm²
3000 µm²
EZRIN
MYOSIN II
n=47
n=43
n=18
Y27632
n=27
n=27
n=28
Y27632
proportion of ciliated cells (%)
750 µm²
3000 µm²
3000 µm² + Y27632
3000 µm² + Blebbistatin
C
HARD SUBSTRATE
SOFT SUBSTRATE
area = 1250 +/- 380 µm²
area = 1020 +/- 250 µm²
proportion of ciliated cells (%)
hard substrate
soft substrate
cilium length (µm)
hard substrate
soft substrate

FIGURE 5

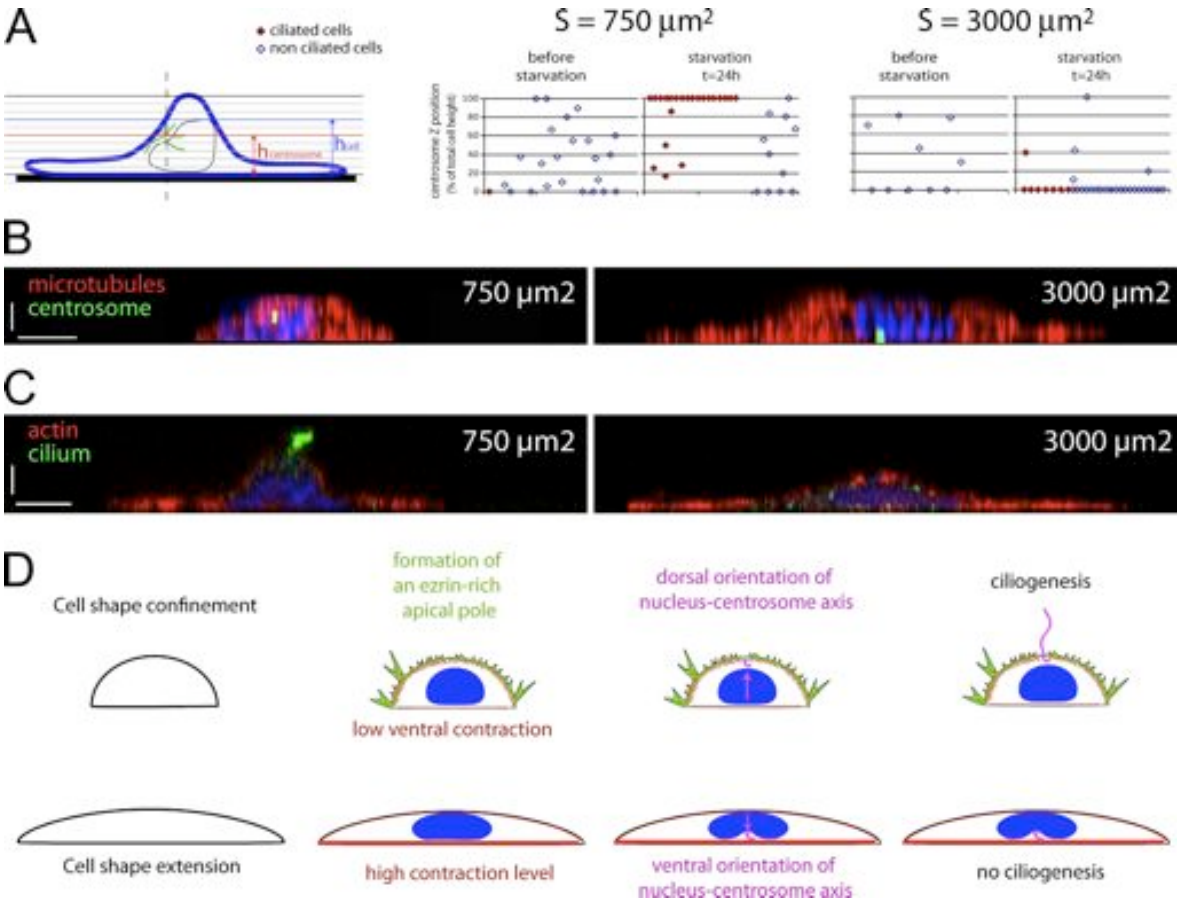
A
ciliated cells
non ciliated cells
S = 750 µm²
S = 3000 µm²
before starvation
starvation t=24h
B
microtubules
centrosome
750 µm2
3000 µm2
C
actin
cilium
750 µm2
3000 µm2
D
Cell shape confinement
formation of an ezrin-rich apical pole
dorsal orientation of nucleus-centrosome axis
ciliogenesis
low ventral contraction
Cell shape extension
high contraction level
ventral orientation of nucleus-centrosome axis
no ciliogenesis

4.4 Mechanical forces within the cell doublets

The intercellular adhesion force has long been proposed as the main driving force of progenitor cell sorting(Steinberg, 1963). Many attempts have been made to directly measure this adhesion force(Puech et al., 2006; Chu et al., 2004; Martinez-Rico et al., 2005; Ladoux et al., 2010). However, what really guides the collective cell movement and tissue deformation is the force exerted toward the surrounding cell and the force perceived by the neighboring cell. However it is difficult to have access to this force propagated across the intercellular junction.

One approach to indirectly measure this force communication is to measure the traction force the cells exerted on the substrate. Since the sum of total traction force exerted by an individual cell is zero, the unbalanced traction force can be attributed to the dragging force from the neighbor(Trepat et al., 2009; Liu et al., 2010; Saez et al., 2010). Moreover, if the cell geometry and positioning could be well controlled, the mechanical equilibrium within the cell and across the cell group can be defined more precisely.

We took advantages of the methodological tools I have developed: micropatterning on the soft substrate and the softwares for force measurement(see section2.2 and2.5). So that the mechanical forces within cell doublets as well as the effect of cell-ECM adhesion on the force equilibrium were analyzed in detail.

The force equilibrium within the cell doublets

In order to define the the force equilibrium between two cells, it will be desirable to have both cells under exactly the same condition. Furthermore, the force exerted toward their neighborhood could also be associated with their internal contractility. Since it has been suggested that the cellular contractile state was regulated by the geometry of cell-ECM adhesion(Théry et al., 2006), we will need an ECM geometry in which both the intracellular contractility and intercellular forces can be measured under similar conditions as well. In addition to above two criteria, the cell movement should also be minimized if we want to analyze the force equilibrium more relevant to the epithelial tissue where most cells are stationary, instead of analyzing the force for cell migration.

From previous result, we know that the cell doublet on a [Cross]-shaped ECM micropattern adopted a rather stable configuration with their cell-cell junction placed in the middle of the region devoid of ECM adhesion(see p.71, Figure2). It appears to be a convenient arrangement that satisfied the criteria mentioned above.

Figure4.7 shows the traction force measurement of cell doublet on a [Cross]-shaped micropattern. We can clearly see from the traction stress map that a large part of forces was applied on the four corners of the [Cross](Figure4.7b). From the traction vector map, we can also notice that there were substantial traction forces exerted toward the neighboring cell that the top cell was pulling downward whereas the lower cell was pulling upward(Figure4.7a). These forces in vertical direction were not balanced within individual cell, and could only be balanced intercellularly(Figure4.7c).

In addition, since most of the forces were applied on the four extremities and no significant counter forces along the Y direction were observed within individual cell, the X,Y components of the traction force after vector decomposition can be approximated as the forces exerted within the cell and the forces applied toward neighboring cell respectively (Figure4.7c). Another interesting observation from this single measurement was that the absolute traction values in X direction was higher than the values in Y direction. It suggests there is a force anisotropy within this configuration that cell tends to contract more within itself than pulling on its neighbor.

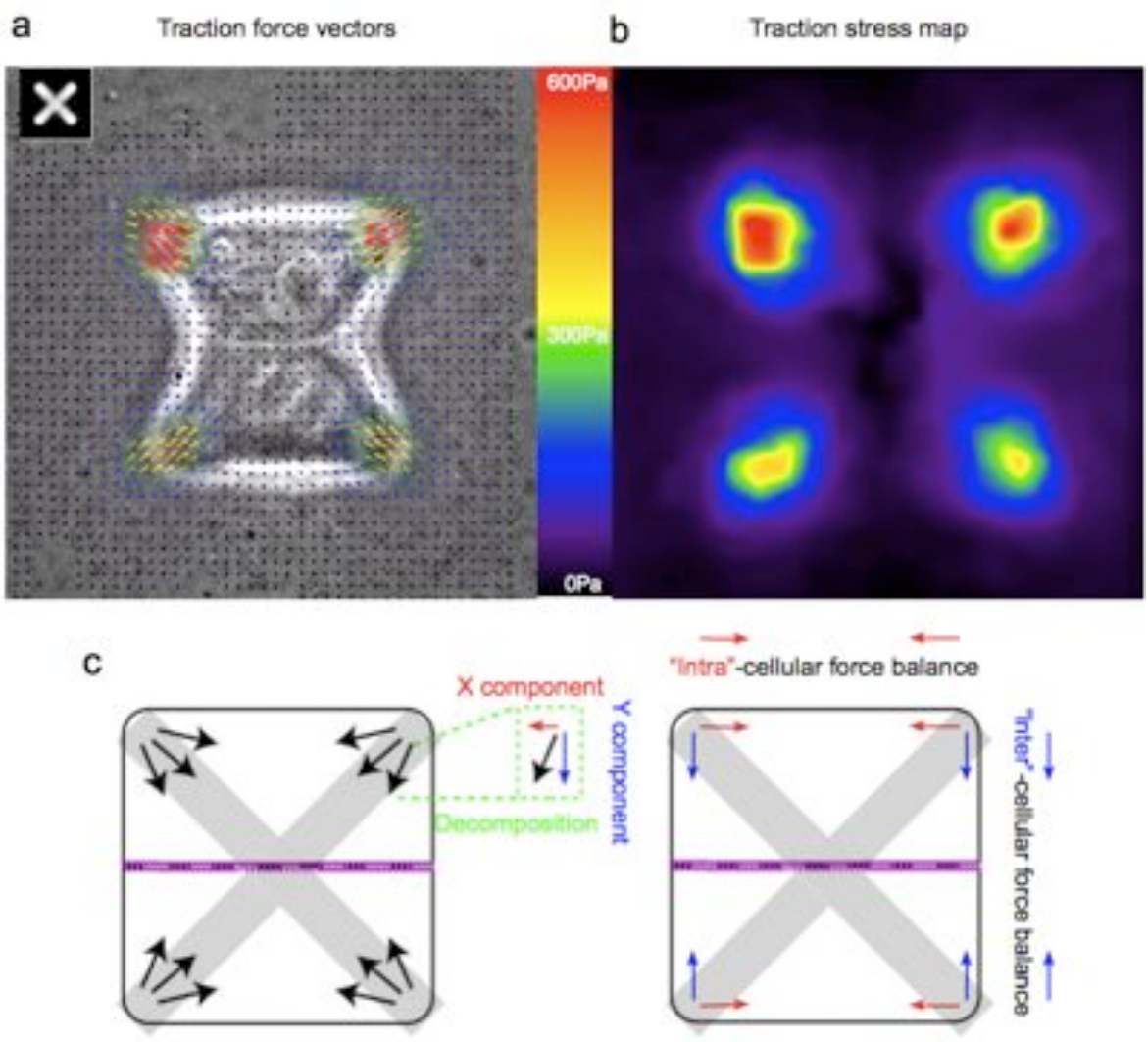

Figure 4.7: An example of traction force measurement of cell doublet on the [Cross]-shaped ECM

To further confirm what we have observed, traction force measurement was conducted on 27 cell doublets that all adopted a stable configuration as the first measurement. Indeed, the forces exerted within the cells are significantly higher than the the forces exerted toward neighboring cells, and were about 40% more important (Figure4.8a, b). Please note that the traction force is expressed in Pascal (Newton/meter^2) so that force is normalized to the surface area it applied to. Thus independent of the variation of cell size, though minor, on the [Cross]-shaped ECM.

It is intriguing to ask what is the origin of this anisotropic distribution of force of intracellular forces and intercellular forces. One explanation would be the architectural

difference between integrin and cadherin adhesion complex. Integrin adhesion connects with actin cytoskeleton in a more static manner (i.e. focal adhesion protein can bind to integrin and actin at the same time). While the cadherin adhesion's connection to actin is rather dynamic, the main cytoskeletal adaptor α-catenin cannot bind to actin and cadherin simultaneously (Drees et al., 2005; Yamada et al., 2005).

Another question arose from these measurements is whether the two neighboring cells would adapt their internal contractile level with the contractile level of their neighbor. For that purpose, we compared the intercellular (Y direction) forces and intracellular forces (X direction) between the two neighboring cells. The ratio of intercellular forces between two cells was around unity, which fits well with the assumption that the Y component of the traction force represents almost all the forces across the cells so that they have the same magnitude but in opposite direction. Surprisingly, the X component which represent the internal contractile force for each cell in the doublet could differ up to twofold (Figure4.8c).

These results suggest that even two cells have considerable difference in contractile force within themselves, they can still manage to balance the force across the cell-cell junction. It will be interesting to know if this large difference in internal contractilities between the doublet was just a transient behavior by following the force evolution over time. If so, we can envisage a scenario that the overall force equilibrium is maintained in long term (i.e. most the cell still have a similar contractile level) and it won't be perturbed by the occasional high contractile force from individual cell, since this surge of force will be damped by the force anisotropy where intercellular forces are lower than the intracellular forces. Most importantly, it implies a protective mechanism of cell-cell junction for multicellular arrangement to maintain the global mechanical equilibrium (Further discussed in section 4.7 , p.151).

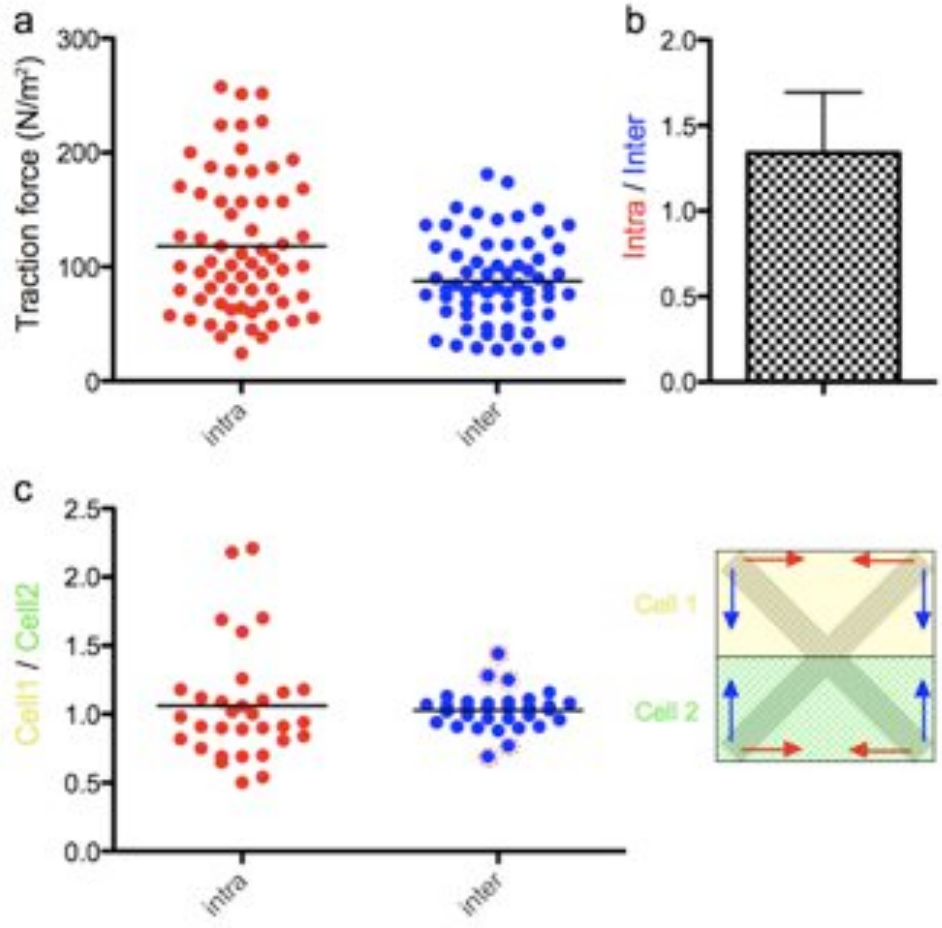

Figure 4.8: Anisotropy between intra- and inter-cellular contractilities.

The accuracy of force decomposition

The accuracy of our approach relies on the assumption that force component perpendicular to the cell-cell junction can fully represent the unbalanced traction force within individual cell. In addition, this unbalanced force should be approximately the same for the two cells (Figure4.9a). Because the only physiological origin of this unbalanced force is the pulling force coming from the other cell.

Therefore, whether this assumption is valid or not should be imperatively checked. One validation routine is to simply compare the ratio of the intercellular force as shown in (Figure4.8c). Large deviation of this ratio from unity denotes significantly unmatched forces between the two cells, which is a non-realistic situation. Another validation for our assumptions is to plot the unbalanced force against the force perpendicular to the junction. If most of the unbalanced forces which represent the *de facto* intercellular forces were resulted from the perpendicular component of the traction forces, we should obtain a well-fitted regression line with a slope value close to 1.

In figure4.8c, we can see a few points deviated from unity more than 10% (points encircled in red). These points are actually representing the measurements containing notable amount of intracellular contraction perpendicular to the junction (marked by red circles in figure4.9c). In such case, the intercellular forces cannot be fully represented by the decomposed forces. By removing these measurements that don't satisfy the above assumptions, the description of the force components will be more precise. After plotting the remaining measurements, we can see that the global trend of the force anisotropy is still conserved (Figure4.10a,b) but the approximation of intercellular force by the perpendicular component highly reliable(Figure4.10c). In the following results, only the measurements with balanced intercellular forces within the doublet would be taken into account.

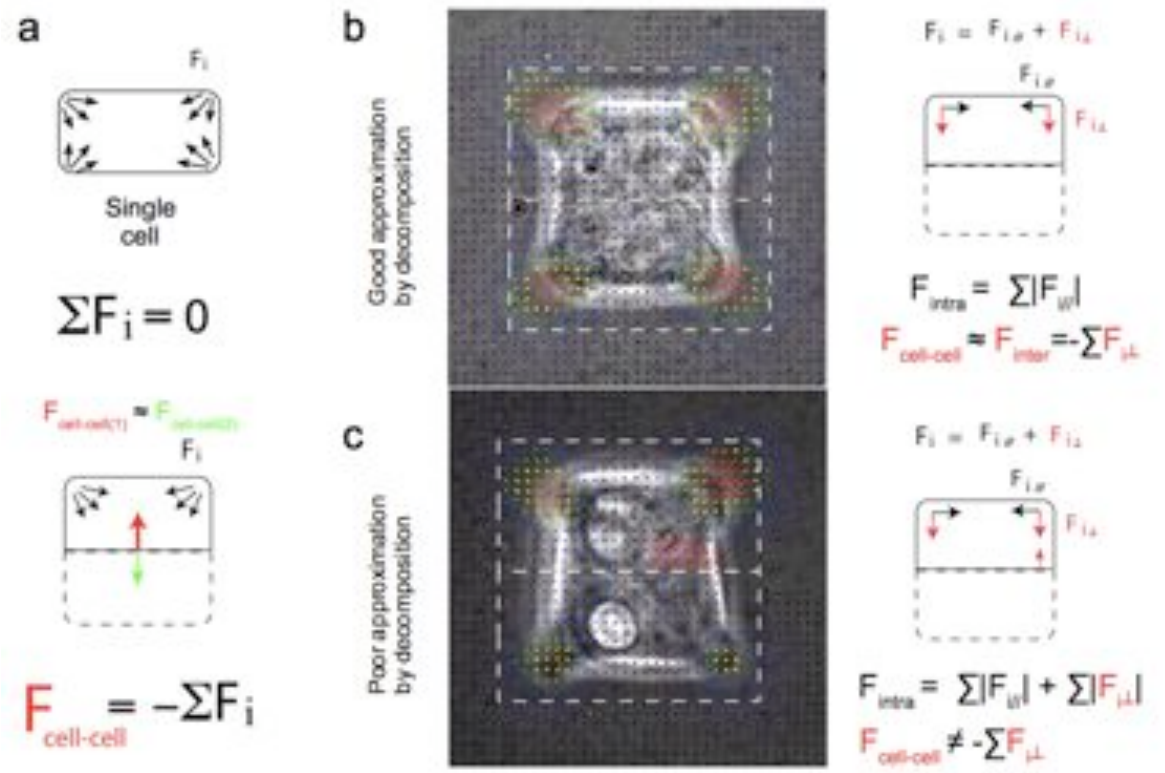

Figure 4.9: Approximate the intercellular forces by the perpendicular components

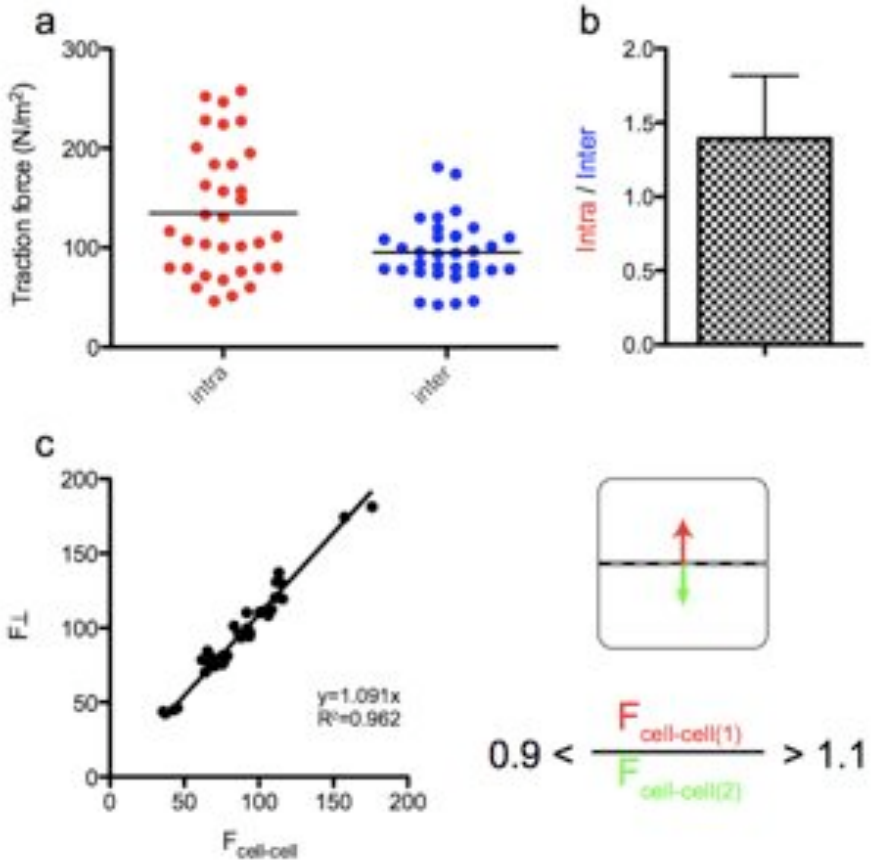

Figure 4.10: Force measurements on [X], only if the intercellular forces were matched.

ECM geometry modulates traction and intercellular forces

ECM adhesion reduced intracellular contraction

With the capability to manipulate the cell-ECM adhesion spatially, we went on to ask whether the geometry of cell-ECM adhesion could affect the traction force as well as the intercellular force. Instead of using a [Cross]-shaped ECM micropattern, we measured the forces of doublet on a [工]-shaped micropattern, on which the doublet invariably positioned their cell-cell junction horizontally. The anisotropy between intercellular forces and intracellular forces was always conspicuous (Figure4.11). Interestingly when we compared the forces on the [工] and [Cross], we have seen a lower intracellular forces on the [工]-shape (Figure4.12). This suggests that geometry of cell-ECM adhesion is affecting the traction forces. The cell tends to contract more when the matrix adhesion only happens at the extremity of the edge, like on the [Cross]-shaped ECM. While the traction forces get lower when there are continuous adhesions all along the edge, like on the [工]-shaped ECM.

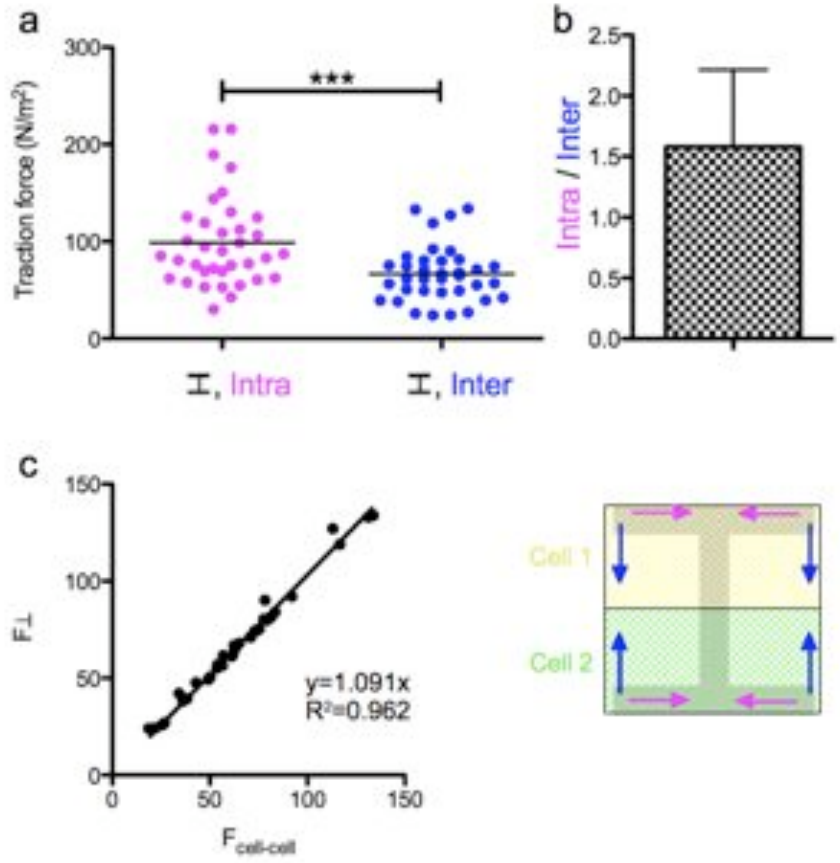

Figure 4.11: Compare inter- and intra-cellular forces of cell doublet on [H]

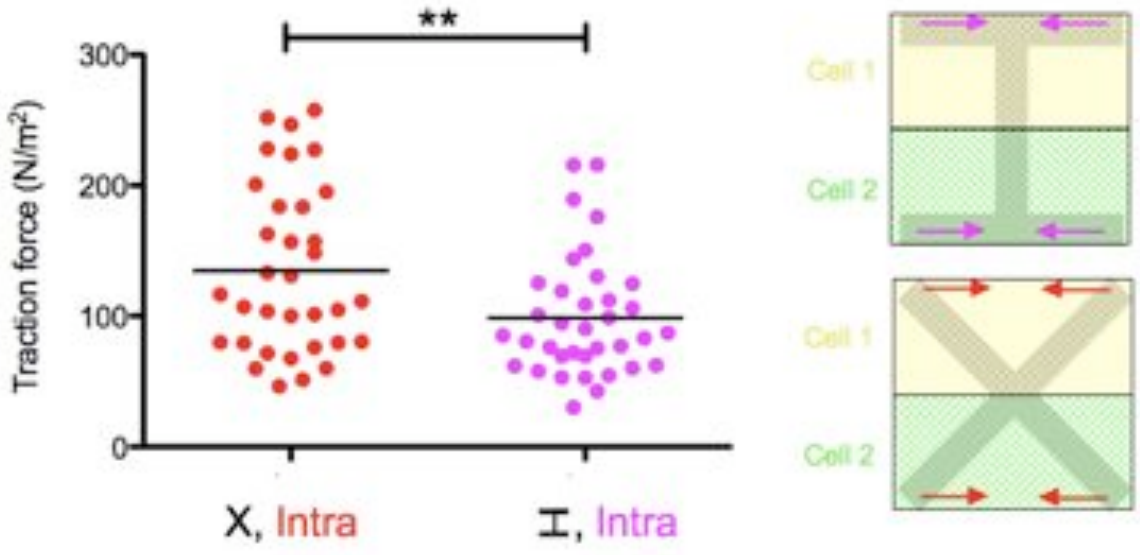

Figure 4.12: Intercellular contraction increased over non-adhesive ECM region

ECM adhesion increased intercellular contraction

The mechanical regulation through the cell-ECM adhesion may have strong consequences in the epithelial architecture. Since we have already seen the intracellular mechanical state can be modulated by the ECM geometry, we further went on to ask whether the intercellular force can be modulated by the cell-ECM adhesion as well.

On the [Square]-shaped ECM micropattern, we would have intercellular junction placed on the cell-matrix adhesion edges, instead of being placed on the non-adhesive region like on the [Cross]- or [I]-shaped pattern. Interestingly, under this configuration, we found less difference between the inter- and intra- cellular forces (Figure4.13). Moreover when we compared the measurements on the [I] and [Square], we found that the intercellular forces were significantly lower when cell-cell junction was placed over the non-adhesive edge (on the [I]) than the case when cell-cell junction was placed over the adhesive edge (on the [Square]) (Figure4.14).

In summary, we found that the spatial organization of cell-matrix adhesion could modulate both the intra- and inter-cellular contractile forces. The intracellular forces are significantly increased when there is a large region devoid of ECM and cell-ECM adhesion only occurs at the extremities (on the [Cross]). On the contrary, the intercellular forces are decreased when they are spanning across a region devoid of ECM (on the [I]). This modulation can have profound impact on the multicellular tissue architecture. For example, the increase contractile force over the ECM gap might help tissue cell to assemble ECM fibers into specific structures(Dzamba et al., 2009), or to cross the region devoid of ECM(Schwartz et al., 2006). On the other hand, the higher intercellular contractile forces near the cell-ECM adhesion(on the [Square]), might be necessary during the initial formation of cell-cell junction(Yamada et al., 2007 b). While the decreased contractile force permit the cell to gain in height, so that the more distance there is between cell-cell junction and ECM adhesion the less contractile force would be applied on them (c.f. Figure4.17, p.144). The reduced force across intercellular junction might further function as an absorber for occasional high contractile force within the multicellular assembly, so that the global mechanical equilibrium can be stably maintained. The detailed molecular mechanism for this force anisotropy deserves further investigation in the future.

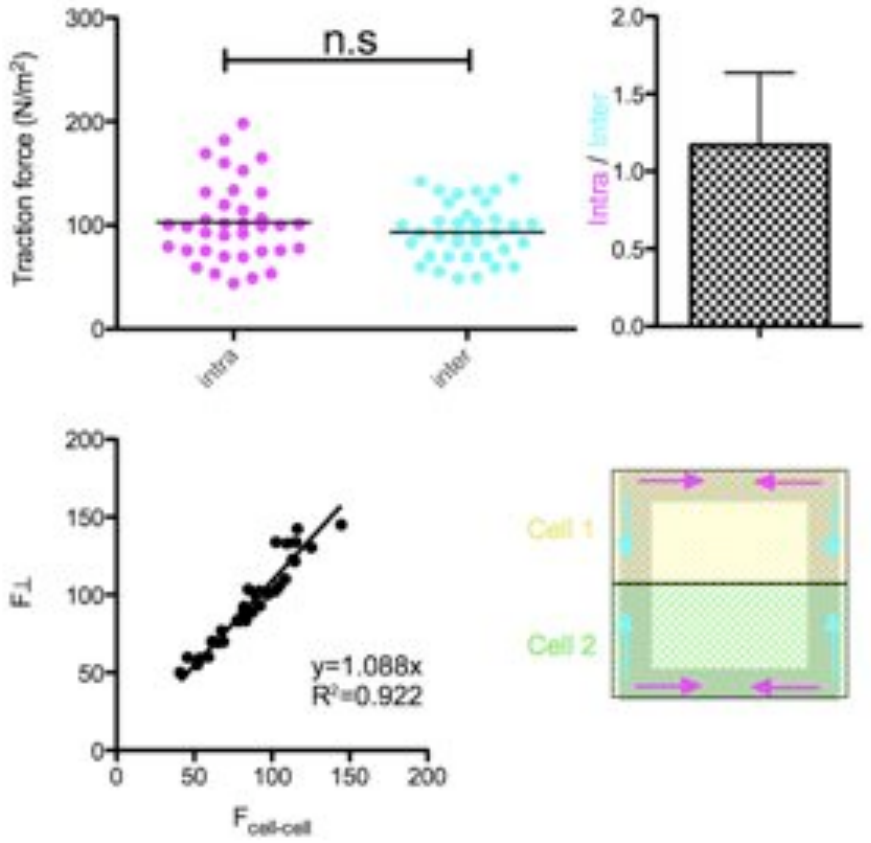

Figure 4.13: Compare inter- and intra-cellular forces of cell doublet on [Square]

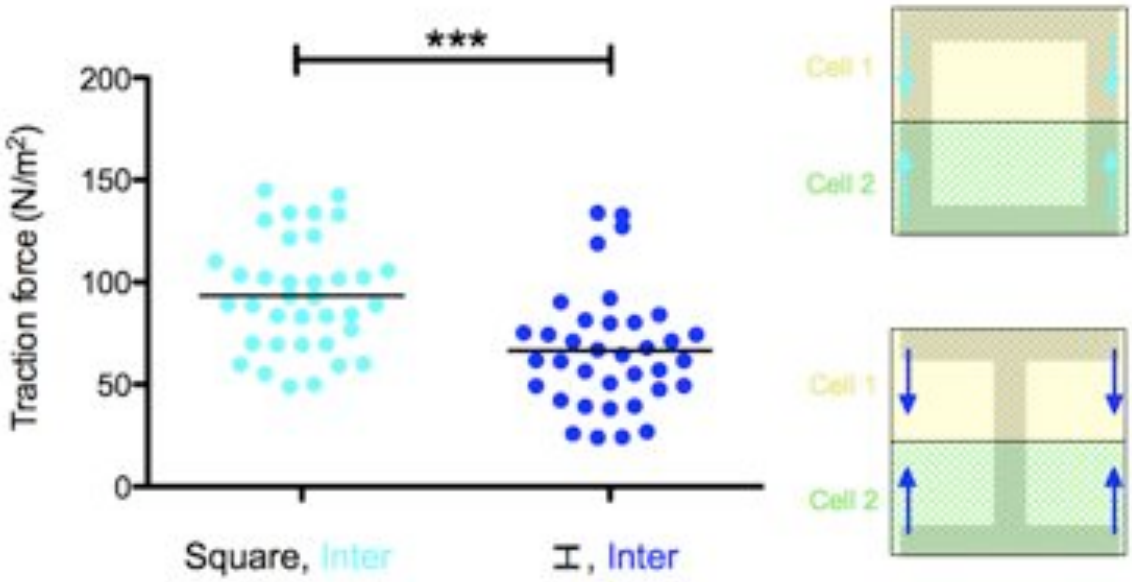

Figure 4.14: Intercellular forces were reduced over non-adhesive ECM region

4.5 Direct probing of cellular contractility

Contractile level of actin cables modulated by cell-matrix adhesion

In contrast to the measurement of cellular traction force which is an indicator of the overall forces reflected on the cell-substrate interaction, one can also estimate the cellular contractile level by breaking a tensed cytoskeletal structure, such as the actin stress fibers(Colombelli et al., 2009). Laser ablation appears to be a promising tool to perform such intracellular surgery. By focusing a pulsed laser, non-linear absorption of laser energy happens only at the focal spot where both chemical reactive species like free radicals and local plasma effect are generated. As a result, light induced damages only take place at the very vicinity of the focal point whereas the remaining of the cell stays untouched(Vogel et al., 2007).

When cell doublets were grown on the [I] and [Cross] micropatterned substrates, they developed conspicuous actin fibers at the cell periphery (Figure4.15). Intense stainings of paxillin at the corners suggested that these actin fibers were bearing mechanical forces(Riveline et al., 2001). Thus by cutting these fibers using laser ablation, we could deduce the contractile level of the fiber from the retraction velocity of the cut ends.

In collaboration with Pierre-François Lenne and Matteo Rauzi (IBDML, Marseille), we used a femtosecond infrared laser to perform nano-ablation on the actin fibers(Cavey et al., 2008). The initial maximum velocity of fiber retraction which correspond to the initial mechanical tension of the actin cable, was measured from the kymograph (Figure4.16a,b). We can see that depending on whether they are inter- or intra-cellular actin cables and the adhesiveness of the edge, actin cables displayed different levels of contractility (Figure4.16c). This result is consistent with the previous traction force measurements showing that the cellular contractile forces are indeed modulated by the geometry of cell-ECM adhesion.

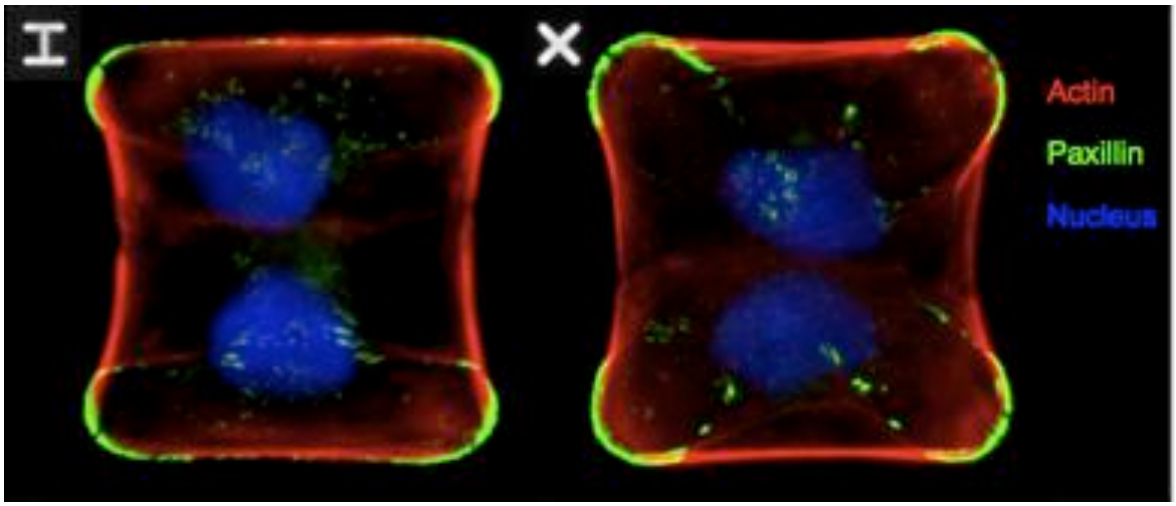

Figure 4.15: Prominent actin structures at the cell periphery.

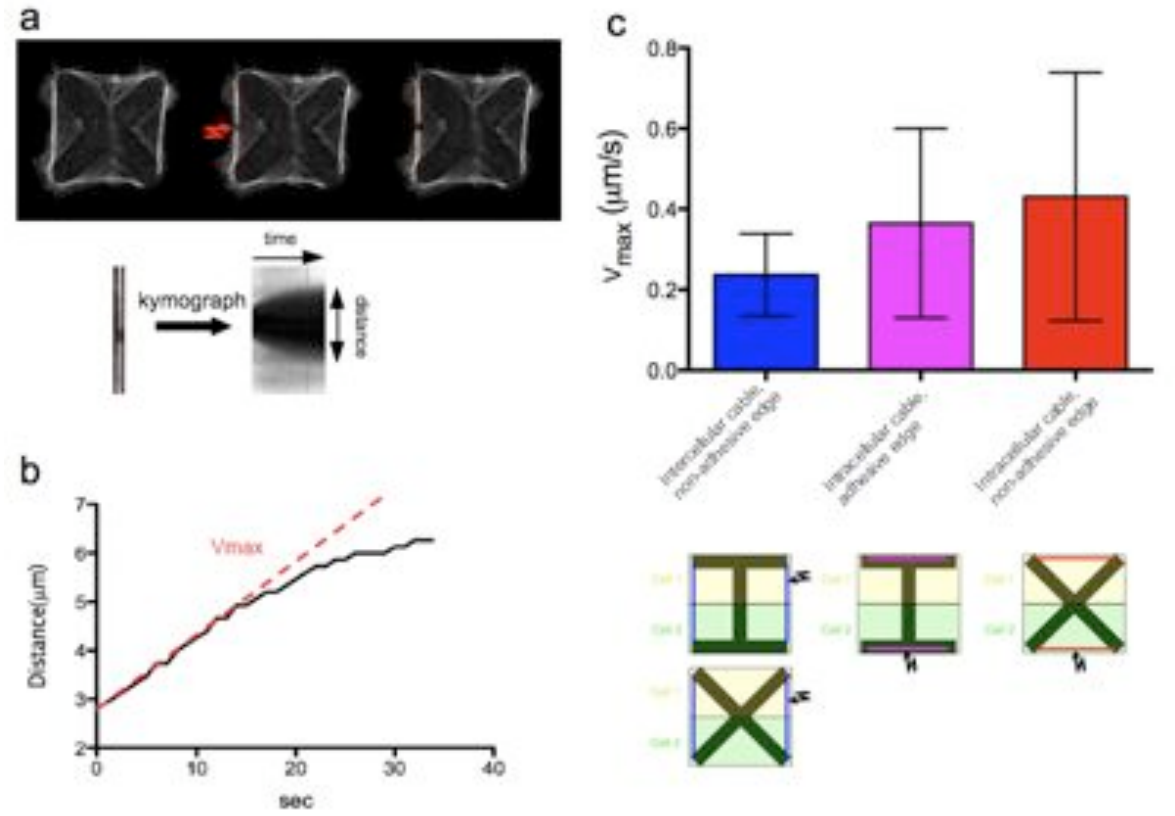

Figure 4.16: Mechanical tension probed by laser ablation of actin strucutres

Taken together, both the traction forces and the tension of actin fibers suggest that the presence of cell-cell junction over a region devoid of cell-matrix adhesion will relax the contractile force along this direction which could have crucial implication in building epithelial architecture such as stabilizing the apically positioned cell-cell junction. While

the presence of ECM gap below intracellular adhesion will provoke higher contractile force which might promote the assembly of ECM into specific structures (Figure4.17).

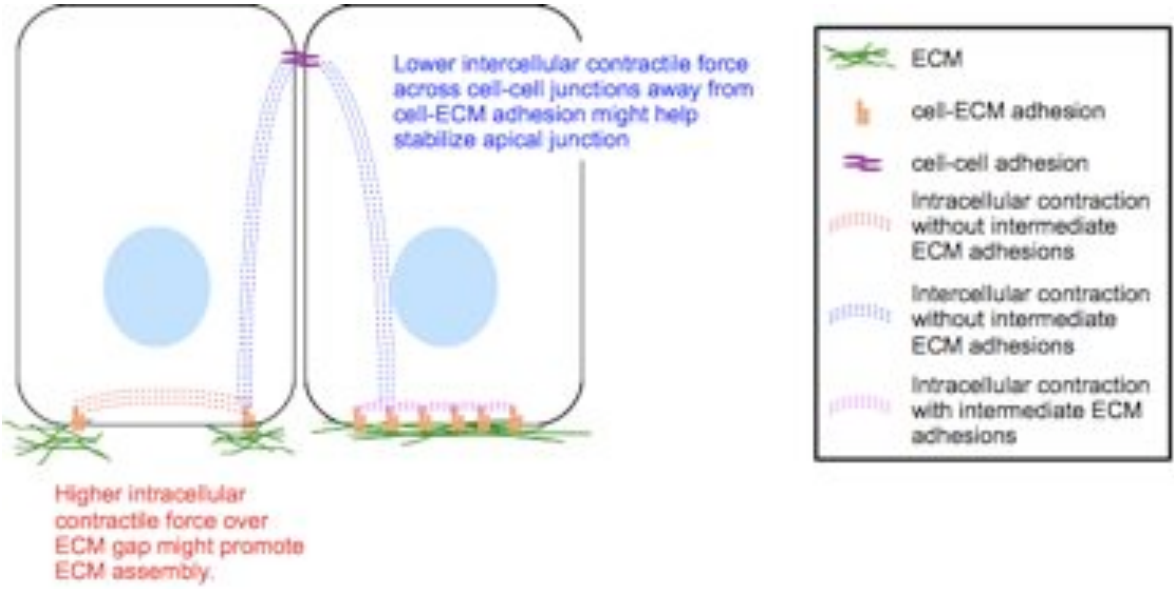

Figure 4.17: Scheme showing the mechanical consequences of the spatial organization of adhesion systems.

Cellular contractile level was globally modulated throughout the cell

The significant actin stress fibers often gave the impression that they were the main origins of cellular contractility. Nevertheless, we cannot neglect the existence of actin fine structures that are not visible under light microscope, for example the dense actin network under the membrane cortex. So it is possible that spatially distinct actin stress fibers are physically connected with each others via a global cytoskeletal network.

To test this idea, we made laser ablations consecutively on distantly located actin fibers. Interestingly, we found that the fiber retraction from second and the third cut were systematically slower than that from the first cut. This suggests that the global cellular tension was released right after the first ablation event. Despite the other actin fibers remained structurally intact, they no longer bore the same tension as they had before ablation. It confirms the idea that spatially distinct actin structures are physically linked and they are regulated under the global mechanical state of the cell.

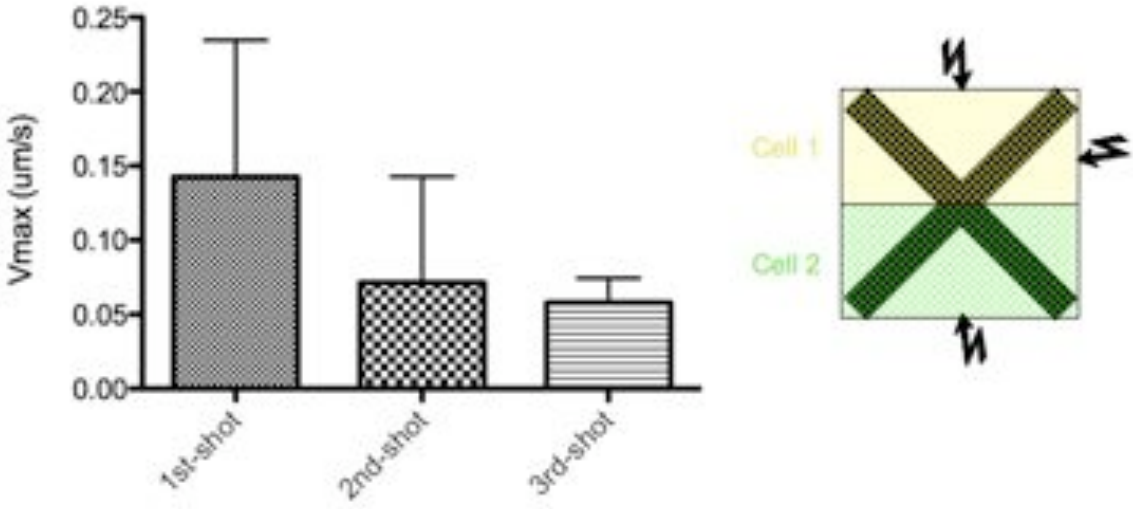

Figure 4.18: Cellular tension was released right after first ablation event.

4.6 Physical model with anisotropic contractile forces

According to the current physical models of epithelial geometry, the cell shape and positioning are governed by cell perimeter, cell area, and the cell-cell adhesion energy(Farhadifar et al., 2007; Käfer et al., 2007). Figure4.19 simply illustrated this model and the formula of energy function. The first and third terms in this function are purely elastic terms analogous to the spring equation where the potential energy is proportion to the square of deviation from natural length (or area). The second term deals with the energy along the cell-cell junction calculated by a linear relationship between the junction length and junction line tension. The line tension here is a mixed term of the cell-cell adhesion strength and the cortex tension which tends to made rounded border instead of straight junction(Lecuit et al., 2007).

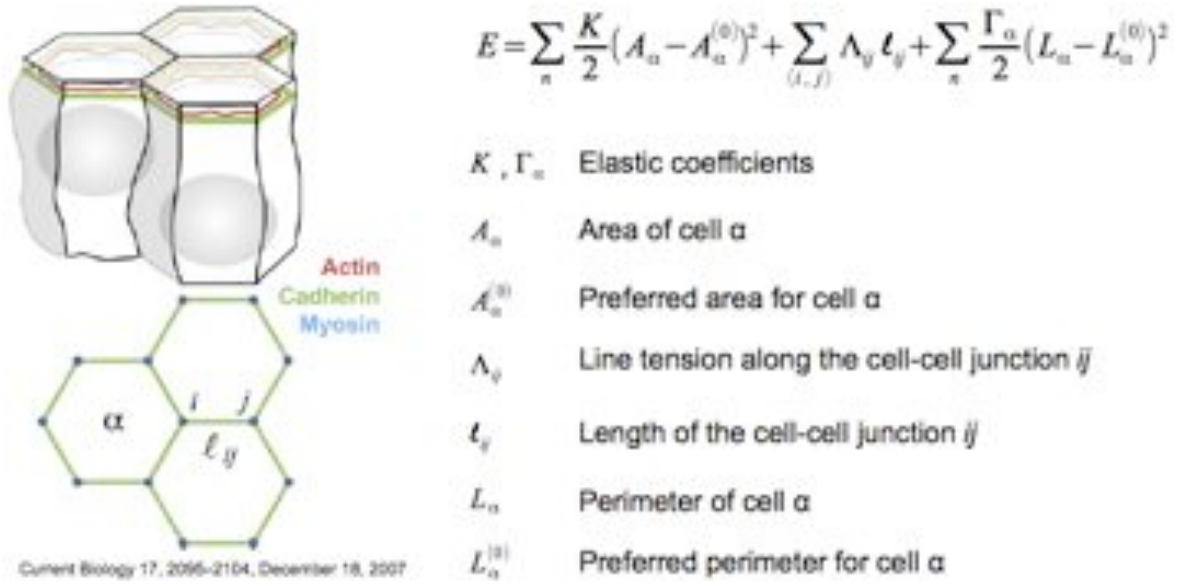

Figure 4.19: Current physical model and potential energy formula for the epithelial asseembly

Limitation of current model

In our minimum system, this model does satisfy the cell positioning on some ECM geometries. For example on the [Square]-shape the orthogonal position of cell doublet is preferred over the diagonal position. It could be explained by their difference in potential energy, since by changing to diagonal position both the cell perimeter and cell-cell junction length changed (Figure4.20a). It can also explain the positioning on the [elongated cross]-shape, where cells tends to avoid a geometry with larger cell perimeter (Figure3.14, p.85).

Nevertheless, for the other ECM geometries this model failed to explain why cell doublet preferred one configuration over another. For example on the [I]-shape ECM geometry, the cell doublet are predominantly positioned vertically (along the y-axis) instead of being positioned horizontally (along the x-axis), even though this two configurations lead to the same potential energy (Figure4.20b).

It could be argued that on the [I]-shape, the doublet was only stuck at one configuration due to the large ECM gap which might prevent cells from adopting another configuration. To avoid this complication of cell migration and ECM gap (which will be addressed later on, see section4.7 p.152) at this moment, we will take example from the [Hourglass]-shape which is only slightly different from the [Square] and don't have any gaps on the ECM. Similarly, the current model cannot explain the cell positioning on [Hourglass]-shape that have been observed experimentally (Figure4.20c) .

Obviously the geometry of ECM adhesion should be taken into account to explain our result. Our results about the force modulation by the ECM geometry urged us to do so as well.

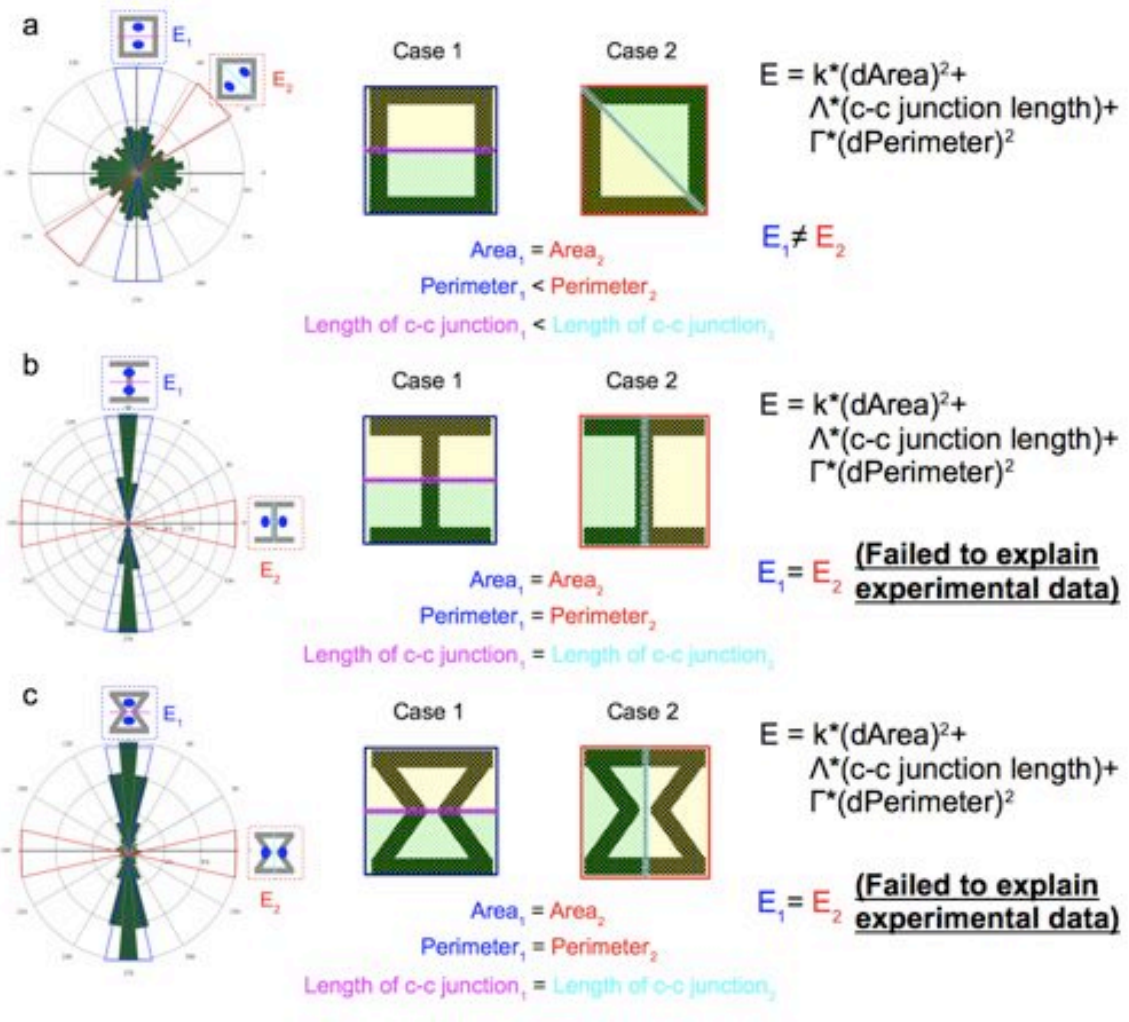

Figure 4.20: Inadequacy of current physical model in explaining our experimental data.

Modified model with anisotropic contractility over cell perimeter

The current model used a constant elastic coefficient for the contractility along the cell perimeter based on the assumption that the actomyosin network at the apical face is rather homogeneous(Figure4.19). Since we have found that cellular contractility differs depending the ECM geometry, this gives us a rationale for incorporating the anisotropic contractilities into the model (Figure4.21).

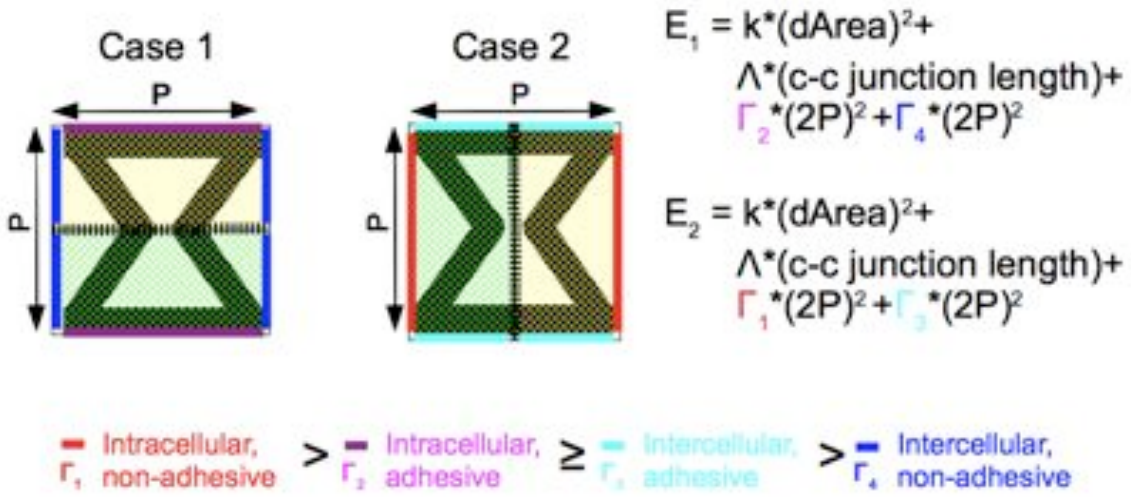

Figure 4.21: Potential energy function with anisotropic contractilities

With this modified energy function, we can easily figure out that the configuration in case2 will cost more in terms of potential energy. Because in this case, the elastic coefficients for both the intra- and intercellular peripheries are higher than those in case1(Γ_1, Γ_3 are higher than Γ_2, Γ_4 in figure4.21). This satisfies with experimental observation that case1 occurs much more frequently than case2.

Therefore, we can consider the cell doublet moving on a given ECM geometry is like probing a given potential energy profile. The higher the potential energy is, the less frequently the doublet will stay on the corresponding configuration. Even without a rigorous numerical simulation, we can already compare the frequency of each configuration with a hypothetic energy profile based on the anisotropic contractility model (Figure4.22).

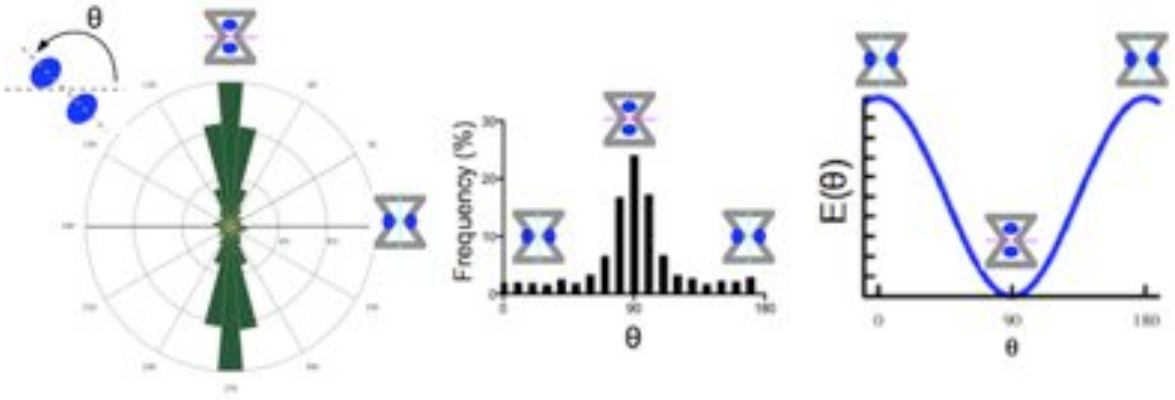

Figure 4.22: Frequency histogram from the experimental data and the hypothetic energy profile

4.7 Discussion

Collateral damaged of the laser ablation

The ablation cause by non-linear absorption of laser energy is a non-specific process. Unlike the light absorption by the fluorophore in the cases of photobleaching (FRAP) or chromophore-assisted inactivation (CALI), the local plasma and heat generated by laser pulses could breakup anything in vicinity even if they were not fluorescently labelled. Consequently, a crucial question to ask when making ablation on specific actin fibers is whether adjacent cellular structures was also damaged. An obvious pitfall would be the damage of the plasma membrane. If the membrane was damaged concomitantly with the ablation, what we have observed might be rather a result from the change of osmotic pressure than the internal mechanical tension. Even with a infrared laser which minimizes the damage along the light passage, the integrity of membrane should, nevertheless, be verified. It could be done by diffusing chromophores impermeable to plasma membrane after ablation. If a UV laser was used instead, it would be even more critical to verify the membrane integrity after each ablation event.

Correlation between traction force and actin structure

In our study, two different methods were used to probe the mechanical properties of the cell: the traction force microscopy and laser ablation of actin fiber. The measurement of traction force is a gauge for the global contractile work of the cytoskeletal network. While the ablation of actin fiber is rather a measurement of local mechanical property. Even though our results suggest the local and global mechanics are, in some way, correlated. We don't have direct evidence to attribute the traction force to individual actin fibers. Based on the observation that global tension was relaxed after the first ablation event, it is plausible that both the prominent actin stress fibers and the ensemble of the actomyosin network are equally important for the generation of traction force.

It is thus worthwhile to combine these two measurements by making ablation and traction force measurement at the same time. In this way, we can directly measure the change of traction force right after perturbing specific actin fiber. Preliminary experiments done in our lab (by Timothée Vignaud) rather support the idea that traction forces are resulted from joint work of actin stress fiber and global actin network. So that not only the traction force in proximity to the severed fiber was released, but the relaxation also occurred at location distant to the ablation site.

The dynamics in the physical model

The physical model proposed in our study did not take into account the dynamics that deal with the transition from one configuration to another. It is more a model to explain the final stable states. As a result, we can deduce the mechanisms that are associated with the steady states, such as the cell shape and contractility. Nevertheless, the dynamic movement of the cell which is more related to the kinetic energy is absent in our physical model.

If we draw a hypothetic energy profile for the cell doublet on [Cross], we will have two energy minima on this profile corresponding to the two symmetric configurations (blue profile in figure4.23). The peaks in this profile represent the unstable configuration with elevated potential energy. As a result, we need a certain degrees of dynamics for our doublet to pass from one stable position to another stable position (for example, from $\theta = 0^{\circ}$ to $\theta = 90^{\circ}$). This dynamics is a concept related to the energy dissipation from

intracellular activities. During this transition process the doublet need to gain energies in order to cross the high energetic peak of the unstable position (θ = 45°). In the physical point of view, this gain in potential energy could come from the conversion of chemical energy to mechanical force (i.e. the myosin activity). In the biological point of view, this gain in energy is resulted from the ensemble of cell activities including membrane protrusion, actin dynamics, fluctuation of cell-cell junction, and etc.. Thus the dynamic of cellular behavior determines how easy they could pass the energy barriers to another energy minimum. As a result, we could expect the transition between two state would be more difficult if the cell dynamics was diminished, for example by treating the cell with drug that perturbs the actin dynamics.

Again, we can envisage this dynamic concept on another ECM geometry. On the [Square]-shaped ECM geometry, the doublet goes more easily from one energy minimum to another (shown as green profile in figure4.23). It can be explained by the reduced difference in potential energy between the minima and the peaks. So that less energy is required to pass the barrier. The same observation can also be accounted by the continuity of the ECM along the periphery which provides paths for cell doublets to make stepwise movement from one position to another.

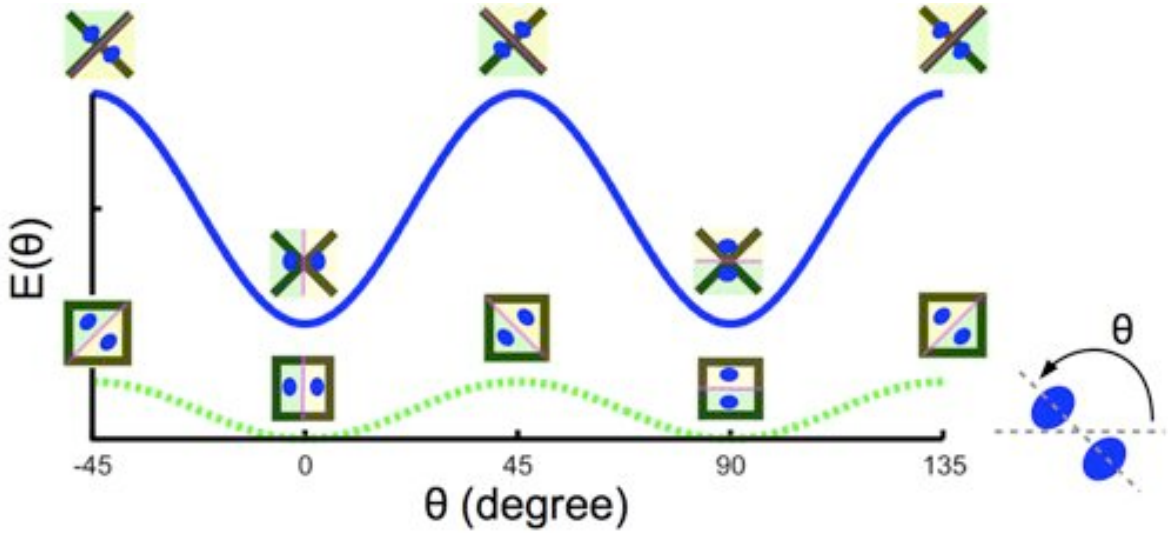

Figure 4.23: Hypothetical energy profile for the [Cross]- and [Square]-shape

The increased stability by enlarging the ECM gap can be another example for this concept (see figureS3, p.77) . When the region devoid of ECM get enlarged(red line in

figure4.24), larger fluctuations of cell-cell junction are required in order to cross this gap (θ from 90° to 45°). The ECM gap signifies more cellular dynamics are required. At the same time, the presence of ECM gap can also be regarded as the change in potential energy. According to our model, as the ECM gap below the intracellular periphery increased, it becomes more costly in terms of potential energy (compare the energy state at θ=0° and θ=45° in figure4.24, see also Figure4.21 for the model). As a result, the energy barrier gets higher as the potential energy corresponding to the intermediate state(θ=45°) increases (compare magenta and blue lines in figure4.24).

Taken together, the parameters in our physical model are indeed correlated to the physiological behaviors we have observed experimentally. The anisotropy in cellular contractility resulting from the spatial arrangement of cell-ECM adhesion can determine the final energetic state of respective multicellular geometry. On the other hand, this energy difference originated from the discontinuity of ECM adhesion can also be interpreted as obstacles for cell movement. Therefore, the ECM geometry governs both the dynamic cellular behavior such as migration, as well as the steady state stability of multicellular assembly.

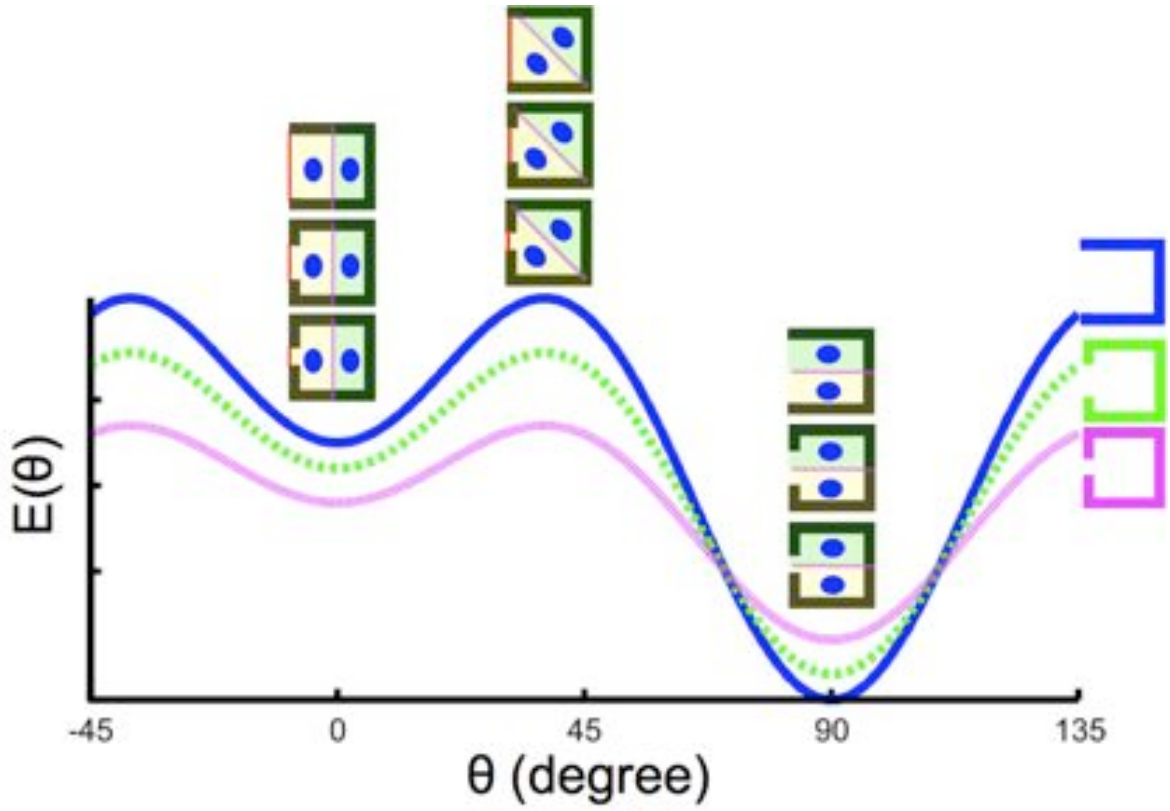

Figure 4.24: The presence of ECM gap is at the same time an obstacle for migration and higher expanse in potential energy.

The force and the cadherin junction

If we considered that the cadherin junction exhibit a mechanosensitivity analogous to the focal adhesion complex, the reduction of contractility as the cell-cell junction get distant from the cell-ECM adhesion site could be intuitively related to a diminishing of cadherin complex. Nevertheless, on the [H] shaped ECM pattern on which the intercellular contractility was the lowest, we have invariably observed a strong staining of E-cadherin at the extremities of the junction. Even though the immunostaining of E-cadherin and the force measurement were done separately on rigid glass slide and soft gel, it is appealing to speculate that the force and cadherin complex don't have a simple positive correlation as in the case of focal adhesion complex.

The nature of matrix adhesion and cell-cell adhesion could have fundamental difference. *In vivo*, integrin-based ECM adhesion have important role in shaping matrix proteins, and sense the environmental rigidity. The force dependent strengthening might be crucial for these functions. However, the cell-cell adhesion need to have a certain degrees of dynamic, so that epithelial sheet are capable to undergo morphological change such as the cell intercalation during *Drosophila* embryogenesis. It has been shown that the tension at the adherens junction need to be finely regulated(Warner et al., 2009). Hence, the increase in mechanical forces orthogonal to the junction might both recruit more adhesion complex and rupture the existing cadherin adhesion. In the case of rupture, less intercellular force would be measured. It might be a protective mechanism to prevent overshooting of intercellular contractile force.

Nevertheless, all the above speculation will need to be confirmed experimentally. With the fluorescently labeled junction protein, it is possible to measure the force and protein amount at the same time, allowing us to make detailed correlation between them.

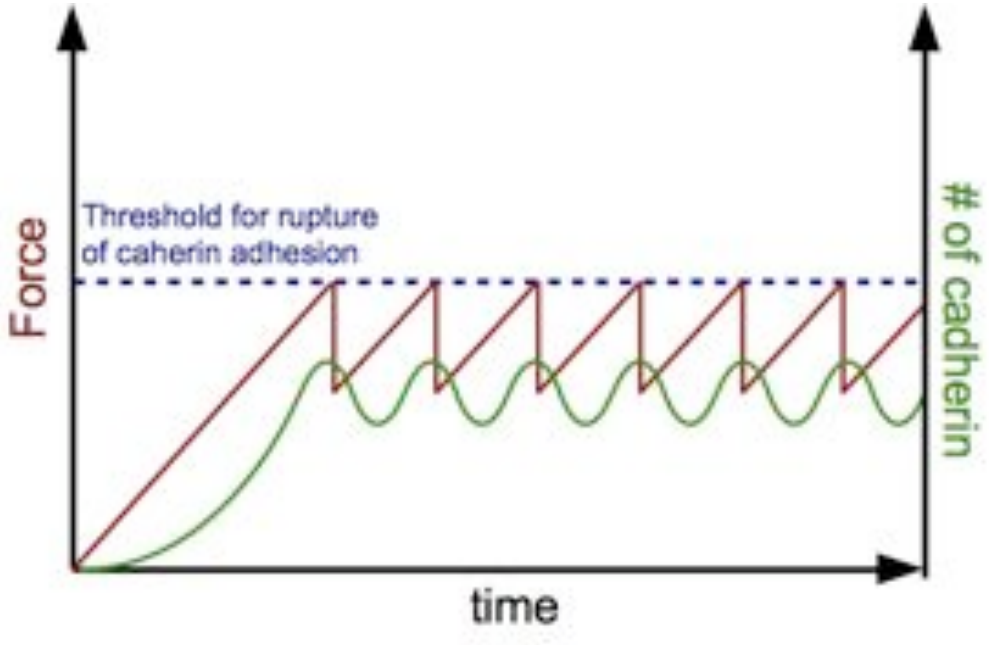

Figure 4.25: Hypothetical relationship between force and cadherin

5 Conclusion

Even though the presenting study might look like a series of curious observations on a rather artificial experimental system, I believe that is how all the biological studies proceed: starting by careful observations, introducing perturbations and observing how the system respond. With a detailed descriptive work, we are able to formulate our hypothesis and then test it by making pertinent perturbations. Constraining cells on ECM micropatterns is indeed an artificial manipulation, but it is also a controlled way to introduce perturbations to our system so that we can understand how cells reorganize themselves regarding to the changes in adhesion geometry. While conventional cell culture on petri dishes is a system we have less control over the cell adhesion and is no closer to *in vivo* conditions.

Although this study was not very focused on detailed molecular mechanisms, it did shed new light on how the epithelial architecture was constructed. By precisely controlling the cell-ECM interaction, we could clearly see that the cell-ECM adhesion played an instructive role in the localization of cell-cell junction and the final epithelial geometry. The resulting spatial arrangement of the adhesion system further governed the internal organization of the cell. This additional control over the adhesion system also revealed subtle details of the epithelial remodeling suggesting the cortical adhesion and the internal polarity might be regulated differently depending on the context of Epithelial-mesenchymal transition.

The biophysical approaches employed in this study have enriched our description of cellular system. Physical parameters such as cellular contractility are difficult to assess and intangible to pure observation. However, the manipulation of adhesion geometry, the traction force measurement, the laser ablation, and the physical modeling made these parameters more perceptible. Together with previous results from others, this study further emphasizes the contribution of mechanical forces in epithelial morphogenesis. These mechanical forces are actively modulated regarding to the spatial organization of the adhesion system and the geometry of the cell. The resulting anisotropic force distribution within the cell have profound implication in epithelial morphology as well as in mechanical equilibrium of multicellular arrangement.

Conclusion

The methodological development had a pivotal role in this study. The micropatterning technique on soft gel allowed us to control both the substrate rigidity and adhesion geometry. It also rendered traction force analysis more precise. We have also applied two patents based on this patterning technique. The automatized images analysis made it possible to survey tens of thousands of microscope images and extract useful information rapidly. Along with other image acquisition and analysis routines I have developed, the repetitive routine works could be greatly reduced. Finally, the development and implementation of the traction force microscopy software not only facilitated the force analysis in large throughput, its availability in public domain can eventually benefit many researchers interested in the physical aspect of cell biology.

ANNEXES

A Computer routines for automated image acquisition

A.1 Centering the sample

A motorized microscope stage not only allowed user to record the positions of each image been taken, but also provide a certain comforts during manipulation. One of them is moving the sample of interest to an arbitrary position in the field of view. For example, one of a common practice while taking images of cells on micropattern is to move the pattern to the center of the camera field. Although it is not a big deal if there is a good joystick with fine tuning, it becomes a burden when there are tens or hundreds of samples to take. With the motorized stage, one could simply click the center of the pattern on the off-centered image or live preview(FigureA.1), to get the distance between the clicked point which is the center of the pattern (x1,y1) and the center of the field(348,260) in pixel. Since the magnification of objectives, the pixel size and the binning of the camera are known, the distance that the stage should move in order to get the pattern at center of the field of view can be obtained. In this way, centering the sample could be done by a simple click on the screen.

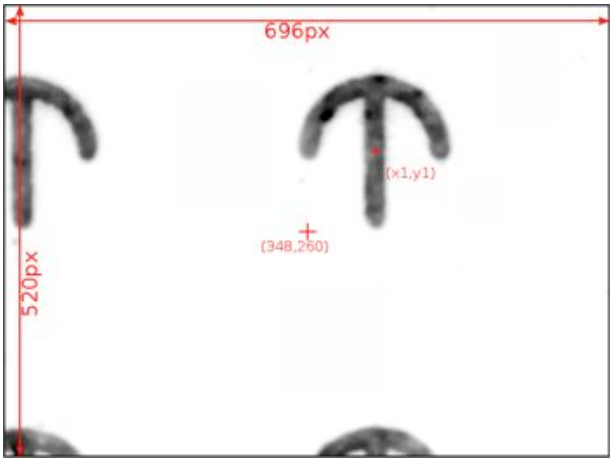

Figure A.1:

A.2 Stage calibration

The first step for the automated acquisition is to precisely locate the imaging field to each micropattern. A practical way to determine the stepping distance is to measure it directly. For example, the microscope field of view is first centered on the pattern(I.). Then, the field is centered to the pattern(II.) which is in the same line as pattern(I.). The distance (c) and (d) can be obtained by the recorded stage positions of (I.) and (II.) (FigureA.2). As a result, the distance the stage should move to reach the next pattern is c/10 in x direction and d/10 in y direction. However, this simple interpolation method relies on a fixed spacing between patterns, a distance large enough between two calibration points, and precise placement of the pattern at the same position in the microscope field of view.

Another method to calibrate the stage is to measure the tilt angle θ, which is $\tan^{-1}(d/c)$ (FigureA.2). Since the spacing between each micropattern (a) and (b) is known, the step distance between adjacent pattern can be calculated by simple trigonometric relationship using a,b and θ.

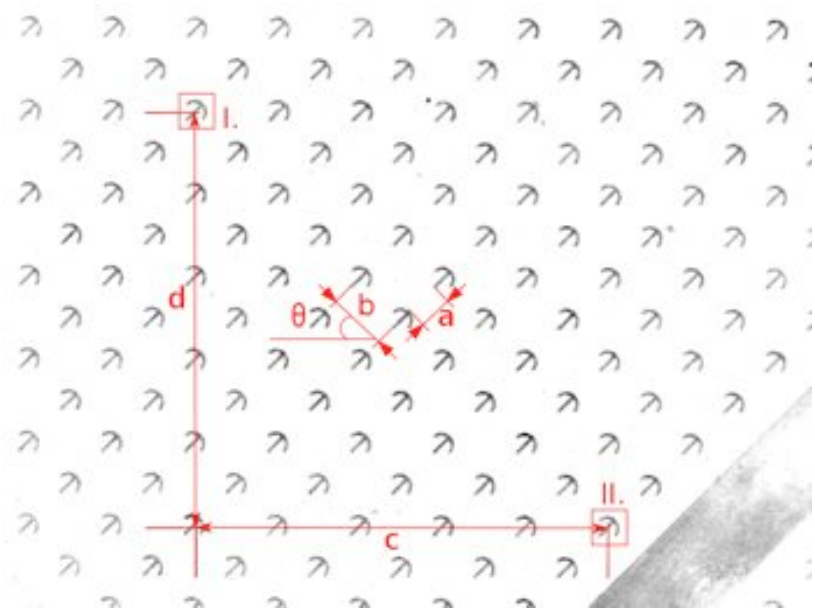

Figure A.2: Stage calibration

A.3 Keep the focus

One crucial issue in automated image acquisition is to find and keep the focus plane. This could be done through a hardware autofocus device which measures constantly the distance between objectives and the surface of coverslips, or by a software autofocus algorithm which calculates the focus qualities of each plane acquired from a certain range in the Z-axis. Although the hardware autofocus system is more straightforward and robust, it is expensive and not available for every microscope model. On the other hand, the software method requires a clearly defined object in the field as a reference to calculate the focus quality, for example the nucleus of cell(Liebel et al., 2003). With fluorescently labelled micropattern on the coverslip surface, the software autofocus method can be implemented by looking for the plane with the best focus quality of the micropattern image. There are several commonly used autofocus algorithms, and built-in "find focus" function in image acquisition software Metamorph could be used to determine the focus quality. Experimentally, the algorithm "Normalized Variance" or simply the mean pixel value of the edge-filtered image gave a rather good result to find the focus plane of fluorescently labelled pattern. During the whole acquisition period, this autofocus routine could be repeated punctually depending on how large the deviation in Z-axis between each sample.

This autofocus routine is implemented as an ImageJ plugin, and is available online:

https://sites.google.com/site/qingzongtseng/find-focus

A.4 Screening for samples of interest

Since the number of cells per micropattern is not precisely controlled but only optimized by the cell plating density on the micropatterns, it is preferable to select out the positions with desired number of cells per pattern before doing multi-channels of Z stack acquisitions. Although one could choose to do a full acquisition of the whole slide and make the screening afterward, it will take up unreasonable acquisition time and storage spaces if high magnification and large Z stack are required.

The simplest way to determine the number of cells per pattern is based on the nucleus labeling. The pattern without any cell on it can be ruled out just based on the standard deviation of the fluorescent signal. While the classification between one, two or more cells per pattern is more complicate. With appropriate threshold method (see section2.4), the nucleus image can be binarized and counted. To discern one nucleus from two or more nuclei, the size and shape factor can also be used as selection criteria, i.e. the circularity of a single nucleus is usually more closer to unity than two linked nuclei. Nevertheless, it happened very often that nuclei were touching each other, or the blurring of fluorescent signal (light from out of focus plane) overlapped. In these cases, further image processing is required to get a precise counting of nuclei (see section2.4).

B Experimental protocols

B.1 Micropatterning on glass coverslips with polystyrene precoating

1. 20 x 20 mm No.1 glass coverslip is first spin coated with adhesion promoter TI prime (MicroChemicals) at 3000rpm (acceleration= 1000rpm/sec)
2. TI prime coated coverslip is cured at 120˚C for 1min.
3. The same coverslip is again spin coated with 0.5% polystyrene (Acros Organics, 178890250) at 3000rpm (acceleration=1000rpm/sec).
4. The polystyrene coated coverslip is then oxidized by oxygen plasma (FEMTO; Diener Electronics) 10s at 30W and
5. Incubated the coverslip with 0.1 mg/ml poly-L-lysine poly-ethylene-glycol (PLL(20)-g[3.5]-PEG(2), Surface Solutions) in 10mM HEPES pH7.4 for 15min.
6. At the end of 15min incubation, remove the PEG solution by dewetting without washing. Use compressed air flow to remove the last drop of PEG solution at the corner of coverslip.
7. PEG coated coverslips could be stored in 4˚C up to 2 weeks.
8. Illuminate the coverslip through a quartz photomask by deep UV (UVO cleaner, Jelight) for 2min. The contact (spacing) between the coverslip and the mask is crucial for reproducing the mask resolution.
9. Carefully remove the coverslip and rinse it with PBS before incubating with protein solution (Fibronectin 20ug/mL+Fibrinogen-Alexa546 10ug/mL in PBS) for 30min.
10. Wash the coverslip with sterilized PBS 3 times before seeding cells.

B.2 Acryl- silanization of glass coverslip

1. Soak the coverslips in Piranha solution (add 25mL 30% H_2O_2 into 75mL 95%-97% H_2SO_4) for 20min.
2. Remove the Piranha and wash the coverslips with large amount of water 5 to 10 times.
3. Soak the coverslips in silane solution (1% Acetic acid, 2% 3-(trimethoxysily)propyl methacrylate, in 95% EtOH) for 20min.
4. Rinse the coverslips by 95% EtOH twice.
5. Dry the coverslips by air flow without leaving traces of solution.
6. Heat the coverslips at 120°C for 1hour.

B.3 Micropatterning of polyacrylamide gel

1. Throughly clean the quartz mask (or a quartz plate without any patterns) by isopropanol.
2. Smear the Mask with n-hexane by a fine tissue.
3. (optional) Adding 6uL fluorescent beads to 167uL acrylamide solution (final beads conc. = 0.04%). Sonicate for 3min.
4. Add 1uL TEMED and 1uL 10%APS to 167uL monomer solution. Mix by vortex quickly.
5. Put a drop of 30uL monomer solution directly on the mask.
6. Cover the drop with 25mm round coverslip (activated by acrylate silane), The solution should go under the coverslip instead of spreading out. (Due to the treatment by n-hexane).
7. Let the gel polymerize for at least 45min.
8. Illuminate through the mask with deep UV for 4min at a distance of 2cm.
9. Detach the gel-coverslip from the mask by soaking 1min in milliQ-water.
10. Gently remove the liquid on the gel surface by blowing with air-flow.
11. Put the coverslip (gel side down) directly on 80uL of 0.15M NHS + 0.2M EDC water solution on parafilm for 15min. Move the coverslip every 5min during incubation to remove bubbles.
12. Remove excess NHS/EDC solution by blotting edge of the coverslip against an absorbing tissue.
13. Put the coverslip (gel side down) over 100uL Fibronectin (20ug/mL, with 10ug/mL Cy3 or Cy5 conjugated fibrinogen in 10mM pH8.5 HEPES) on a parafilm.
14. Incubate at room temperature for 0.5~1hr.
15. Wash 3x times by PBS.

B.4 PEG passivation of fluorescent beads for TFM

1. Beads 20uL (stock solution is 2% solid, so 20uL equals to 0.4mg of beads) + 80uL MES buffer(10mM pH5.5), mix well.
2. Prepare 400uL 4mg/mL EDC, 2mg/mL NHS in MES (pH5.5 10mM). (4mg EDC and 2mg NHS and use 1mL MES(pH 5.5 10mM) to dissolve)
3. Prepare PLL-PEG 1~2mg in 500uL HEPES buffer(10mM pH8.5)
4. Mix 1(100uL) and 2 (400uL) (by inverting the tube during 30sec, then proceed to step 5)
5. add 3(500uL) to the mixture of 1+2

   Important!!! (if the time between 4 and 5 is too long, beads might form aggregates)
6. RT incubate rotate 2hr (or 4°C rocking overnight)
7. Spin down at 10000g 30min the beads, remove solution.
8. Resuspend in HEPES (10mM pH7.4)
9. Spin down the beads, remove solution
10. Resuspend in 2~4x original beads volume of HEPES(10mM pH7.4) (ex: 40~80uL for 20uL beads)

B.5 Molecular cloning of human E-cadherin-GFP fusion protein

1. The total RNA was extract from MCF10A confluent cell culture using QIAGEN RNeasy kit
2. 1st strand cDNA was synthesized by a oligo-d(T) primer using Superscript II ReverseTranscriptase.
3. The human E-cadherin (CDH1) mRNA fragment was PCR amplified by the primer pair: forward(F1) 5'-tgagcttgcggaagtcagttca-3' ; reverse(R1) 5'-aaccaccagcaacgtgatttct-3'
4. This PCR fragment was subsequently amplified by another set of primer containing the designed restriction sites: forward(F4) 5'-ccgctcgagccagccatgggcccttggagccgcagcc-3' ; reverse(R3)3'-ggaagatcttcgtcgtcctcgccgcctccgtacatgtc-3'
5. The sequence of this fragment was shown below. No random mutation due to PCR reaction was found.
6. This fragment was then cut by restriction enzyme BglII and XhoI and gel purified.
7. The lentivirus vector pLVX-Lifeact-mGFP was cut by restriction enzyme BamHI and XhoI and gel purified to remove the Lifeact fragment.
8. This two RE cut fragments was finally ligated and amplified in bacteria to obtain the lentivirus vector containing the E-cadherin-mGFP fusion gene.

Sequence of E-cadherin fragment

Sequence of E-cadherin fragment

Sequence of E-cadherin fragment

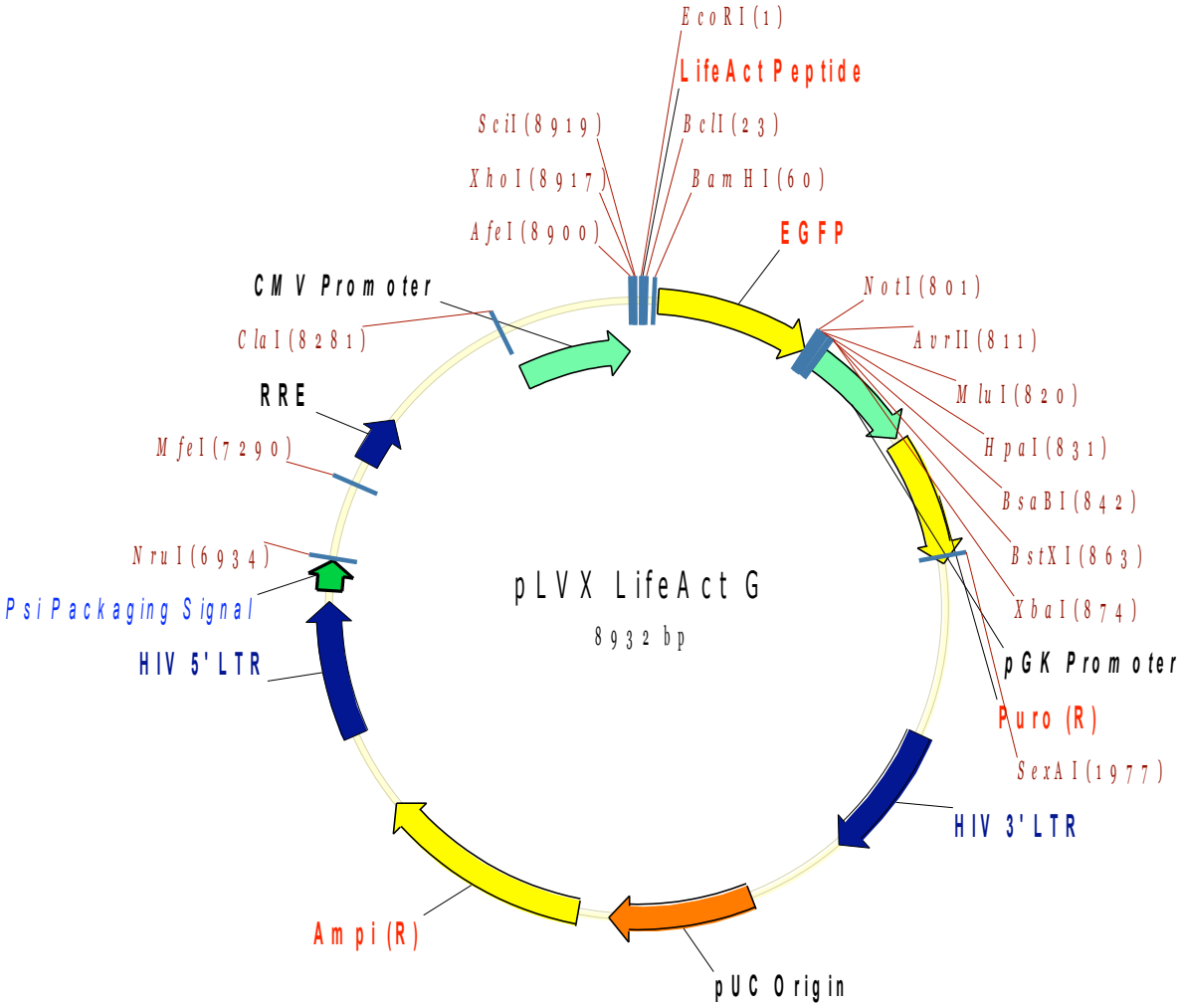

Lentivirus vector pLVX Lifeact-mGFP

Bibliography

de Anda FC, Pollarolo G, Da Silva JS, Camoletto PG, Feiguin F, and Dotti CG. (2005). Centrosome localization determines neuronal polarity. *Nature* 436: 704-708.

Ando-Akatsuka Y, Yonemura S, Itoh M, Furuse M, and Tsukita S. (1999). Differential behavior of E-cadherin and occludin in their colocalization with ZO-1 during the establishment of epithelial cell polarity. *Journal of Cellular Physiology* 179: 115-125.

Azioune, Carpi N, Tseng Q, Théry M, and Piel M. (2010). Protein micropatterns: A direct printing protocol using deep UVs. *Methods Cell Biol* 97: 133-146.

Azioune, Storch M, Bornens M, Théry M, and Piel M. (2009). Simple and rapid process for single cell micro-patterning. *Lab Chip* 9: 1640.

Balaban NQ, Schwarz US, Riveline D, Goichberg P, Tzur G, Sabanay I, et al. (2001). Force and focal adhesion assembly: a close relationship studied using elastic micropatterned substrates. *Nat Cell Biol* 3: 466-472.

Bao G, and Suresh S. (2003). Cell and molecular mechanics of biological materials. *Nat Mater* 2: 715-725.

Baumgartner W, Hinterdorfer P, Ness W, Raab A, Vestweber D, Schindler H, et al. (2000). Cadherin interaction probed by atomic force microscopy. *Proceedings of the National Academy of Sciences* 97: 4005 -4010.

Bershadsky A, Kozlov M, and Geiger B. (2006). Adhesion-mediated mechanosensitivity: a time to experiment, and a time to theorize. *Current Opinion in Cell Biology* 18: 472-481.

Bischofs IB, Klein F, Lehnert D, Bastmeyer M, and Schwarz US. (2008). Filamentous Network Mechanics and Active Contractility Determine Cell and Tissue Shape. *Biophysical Journal* 95: 3488-3496.

Boisvieux-Ulrich E, Lainé M-C, and Sandoz D. (1990). Cytochalasin D inhibits basal body migration and ciliary elongation in quail oviduct epithelium. *Cell Tissue Res.* 259: 443-454.

Bornens M. (1977). Is the centriole bound to the nuclear membrane? *Nature* 270: 80-82.

Bornens M. (2008). Organelle positioning and cell polarity. *Nat Rev Mol Cell Biol* 9: 874-886.

Braga VM, and Yap AS. (2005). The challenges of abundance: epithelial junctions and small GTPase signalling. *Current Opinion in Cell Biology* 17: 466-474.

Bryant DM, and Mostov KE. (2008). From cells to organs: building polarized tissue. *Nat Rev Mol Cell Biol* 9: 887-901.

Burakov A, Nadezhdina E, Slepchenko B, and Rodionov V. (2003). Centrosome positioning in interphase cells. *The Journal of Cell Biology* 162: 963 -969.

Bursac P, Lenormand G, Fabry B, Oliver M, Weitz DA, Viasnoff V, et al. (2005). Cytoskeletal remodelling and slow dynamics in the living cell. *Nat Mater* 4: 557-561.

Butcher DT, Alliston T, and Weaver VM. (2009). A tense situation: forcing tumour progression. *Nat Rev Cancer* 9: 108-122.

Butler JP, Tolić-Nørrelykke IM, Fabry B, and Fredberg JJ. (2002). Traction fields, moments, and strain energy that cells exert on their surroundings. *Am. J. Physiol., Cell Physiol* 282: C595-605.

Campbell ID, and Humphries MJ. (2011). Integrin Structure, Activation, and Interactions. *Cold Spring Harbor Perspectives in Biology [Internet]* 3. Available from: http://cshperspectives.cshlp.org/content/3/3/a004994.abstract

Cavey M, Rauzi M, Lenne P-F, and Lecuit T. (2008). A two-tiered mechanism for stabilization and immobilization of E-cadherin. *Nature* 453: 751-756.

Cereijido M, Contreras RG, and Shoshani L. (2004). Cell Adhesion, Polarity, and Epithelia in the Dawn of Metazoans. *Physiological Reviews* 84: 1229 -1262.

Chappuis-Flament S, Wong E, Hicks LD, Kay CM, and Gumbiner BM. (2001). Multiple cadherin extracellular repeats mediate homophilic binding and adhesion. *J. Cell Biol* 154: 231-243.

Chu Y-S, Thomas WA, Eder O, Pincet F, Perez E, Thiery JP, et al. (2004). Force measurements in E-cadherin–mediated cell doublets reveal rapid adhesion strengthened by actin cytoskeleton remodeling through Rac and Cdc42. *The Journal of Cell Biology* 167: 1183 -1194.

Colombelli J, Besser A, Kress H, Reynaud EG, Girard P, Caussinus E, et al. (2009). Mechanosensing in actin stress fibers revealed by a close correlation between force and protein localization. *J Cell Sci* 122: 1665-1679.

Coluccio LM, Conti MA, Kawamoto S, and Adelstein RS. (2008). Non-Muscle Myosin II. In: Ridley A, Frampton J, editors. Myosins. Vol. 7. Proteins And Cell Regulation. Springer Netherlands. p 223-264. Available from: http://dx.doi.org/10.1007/978-1-4020-6519-4_7

Cowan CR, and Hyman AA. (2004). Centrosomes direct cell polarity independently of microtubule assembly in C. elegans embryos. *Nature* 431: 92-96.

Cross SE, Jin Y-S, Rao J, and Gimzewski JK. (2007). Nanomechanical analysis of cells from cancer patients. *Nat Nano* 2: 780-783.

Cukierman E, Pankov R, Stevens DR, and Yamada KM. (2001). Taking Cell-Matrix Adhesions to the Third Dimension. *Science* 294: 1708 -1712.

Damljanović V, Lagerholm BC, and Jacobson K. (2005). Bulk and micropatterned conjugation of extracellular matrix proteins to characterized polyacrylamide substrates for cell mechanotransduction assays. *BioTechniques* 39: 847-851.

Davidson LA, Dzamba BD, Keller R, and Desimone DW. (2008). Live imaging of cell protrusive activity, and extracellular matrix assembly and remodeling during morphogenesis in the frog, Xenopus laevis. *Dev. Dyn.* 237: 2684-2692.

Davidson LA, Keller R, and DeSimone DW. (2004). Assembly and remodeling of the fibrillar fibronectin extracellular matrix during gastrulation and neurulation in *Xenopus laevis*. *Dev. Dyn.* 231: 888-895.

Dembo M, and Wang YL. (1999). Stresses at the cell-to-substrate interface during locomotion of fibroblasts. *Biophys J* 76: 2307-2316.

Discher DE, Janmey P, and Wang Y-li. (2005). Tissue Cells Feel and Respond to the Stiffness of Their Substrate. *Science* 310: 1139-1143.

Drees F, Pokutta S, Yamada S, Nelson WJ, and Weis WI. (2005). [alpha]-Catenin Is a Molecular Switch that Binds E-Cadherin-[beta]-Catenin and Regulates Actin-Filament Assembly. *Cell* 123: 903-915.

Dzamba BJ, Jakab KR, Marsden M, Schwartz MA, and DeSimone DW. (2009). Cadherin Adhesion, Tissue Tension, and Noncanonical Wnt Signaling Regulate Fibronectin Matrix Organization. *Developmental Cell* 16: 421-432.

Engler AJ, Sen S, Sweeney HL, and Discher DE. (2006). Matrix Elasticity Directs Stem Cell Lineage Specification. *Cell* 126: 677-689.

Etienne-Manneville S, and Hall A. (2001). Integrin-Mediated Activation of Cdc42 Controls Cell Polarity in Migrating Astrocytes through PKC[zeta]. *Cell* 106: 489-498.

Farhadifar R, Röper J-C, Aigouy B, Eaton S, and Jülicher F. (2007). The influence of cell mechanics, cell-cell interactions, and proliferation on epithelial packing. *Curr. Biol* 17: 2095-2104.

Fink J, Thery M, Azioune A, Dupont R, Chatelain F, Bornens M, et al. (2007). Comparative study and improvement of current cell micro-patterning techniques. *Lab Chip* 7: 672-80.

Fogg VC, Liu C-J, and Margolis B. (2005). Multiple regions of Crumbs3 are required for tight junction formation in MCF10A cells. *J Cell Sci* 118: 2859-2869.

Friedl P. (2004). Prespecification and plasticity: shifting mechanisms of cell migration. *Current Opinion in Cell Biology* 16: 14-23.

Gardel ML, Nakamura F, Hartwig JH, Crocker JC, Stossel TP, and Weitz DA. (2006). Prestressed F-actin networks cross-linked by hinged filamins replicate mechanical properties of cells. *Proceedings of the National Academy of Sciences of the United States of America* 103: 1762 -1767.

Garrod DR, Merritt AJ, and Nie Z. (2002). Desmosomal cadherins. *Current Opinion in Cell Biology* 14: 537-545.

Gautam KS, Schwab AD, Dhinojwala A, Zhang D, Dougal SM, and Yeganeh MS. (2000). Molecular Structure of Polystyrene at Air/Polymer and Solid/Polymer Interfaces. *Phys. Rev. Lett.* 85: 3854.

Geiger B, Spatz JP, and Bershadsky AD. (2009). Environmental sensing through focal adhesions. *Nat Rev Mol Cell Biol* 10: 21-33.

Gilbert T, Le Bivic A, Quaroni A, and Rodriguez-Boulan E. (1991). Microtubular organization and its involvement in the biogenetic pathways of plasma membrane proteins in Caco-2 intestinal epithelial cells. *The Journal of Cell Biology* 113: 275 -288.

Godsel LM, Hsieh SN, Amargo EV, Bass AE, Pascoe-McGillicuddy LT, Huen AC, et al. (2005). Desmoplakin assembly dynamics in four dimensions. *The Journal of Cell Biology* 171: 1045 -1059.

Gomes ER, Jani S, and Gundersen GG. (2005). Nuclear movement regulated by Cdc42, MRCK, myosin, and actin flow establishes MTOC polarization in migrating cells. *Cell* 121: 451-463.

Gonzalez-Mariscal L, Bruewer M, and Nusrat A. (2006). Regulation of Paracellular Transport across Tight Junctions by the Actin Cytoskeleton. In: Tight Junctions. Springer US. p 135-145. Available from: http://dx.doi.org/10.1007/0-387-36673-3_10

Green KJ, Geiger B, Jones JC, Talian JC, and Goldman RD. (1987). The relationship between intermediate filaments and microfilaments before and during the formation of desmosomes and adherens-type junctions in mouse epidermal keratinocytes. *The Journal of Cell Biology* 104: 1389-1402.

Green KJ, Getsios S, Troyanovsky S, and Godsel LM. (2009). Intercellular Junction Assembly, Dynamics, and Homeostasis. *Cold Spring Harbor Perspectives in Biology* 2: a000125-a000125.

Greenburg G, and Hay ED. (1982). Epithelia suspended in collagen gels can lose polarity and express characteristics of migrating mesenchymal cells. *J. Cell Biol* 95: 333-339.

Grier EV. (2006). Neural stem cell research. Nova Publishers.

Grill SW, and Hyman AA. (2005). Spindle Positioning by Cortical Pulling Forces. *Developmental Cell* 8: 461-465.

Grosheva I, Shtutman M, Elbaum M, and Bershadsky AD. (2001). p120 catenin affects cell motility via modulation of activity of Rho-family GTPases: a link between cell-cell contact formation and regulation of cell locomotion. *J. Cell. Sci* 114: 695-707.

Guck J, Schinkinger S, Lincoln B, Wottawah F, Ebert S, Romeyke M, et al. (2005). Optical Deformability as an Inherent Cell Marker for Testing Malignant Transformation and Metastatic Competence. *Biophysical Journal* 88: 3689-3698.

Gudjonsson T, Ronnov-Jessen L, Villadsen R, Rank F, Bissell MJ, and Petersen OW. (2002). Normal and tumor-derived myoepithelial cells differ in their ability to interact with luminal breast epithelial cells for polarity and basement membrane deposition. *J Cell Sci* 115: 39-50.

Gumbiner BM. (2005). Regulation of cadherin-mediated adhesion in morphogenesis. *Nat Rev Mol Cell Biol* 6: 622-634.

Haigo SL, and Bilder D. (2011). Global Tissue Revolutions in a Morphogenetic Movement Controlling Elongation. *Science [Internet]*. Available from: http://www.sciencemag.org/content/early/2011/01/05/science.1199424.abstract

Harris AK, Wild P, and Stopak D. (1980). Silicone rubber substrata: a new wrinkle in the study of cell locomotion. *Science* 208: 177-179.

Harris TJC, and Tepass U. (2010). Adherens junctions: from molecules to morphogenesis. *Nat Rev Mol Cell Biol* 11: 502-514.

Hartsock A, and Nelson WJ. (2008). Adherens and tight junctions: Structure, function and connections to the actin cytoskeleton. *Biochimica et Biophysica Acta (BBA) - Biomembranes* 1778: 660-669.

Hayashi T, and Carthew RW. (2004). Surface mechanics mediate pattern formation in the developing retina. *Nature* 431: 647-652.

Hong S, Troyanovsky RB, and Troyanovsky SM. (2011). Cadherin exits the junction by switching its adhesive bond. *The Journal of Cell Biology* 192: 1073 -1083.

Huveneers S, and Danen EHJ. (2009). Adhesion signaling - crosstalk between integrins, Src and Rho. *J Cell Sci* 122: 1059-1069.

Ingber DE. (1997). TENSEGRITY: THE ARCHITECTURAL BASIS OF CELLULAR MECHANOTRANSDUCTION. *Annu. Rev. Physiol.* 59: 575-599.

Inman J, and Bissell M. (2010). Apical polarity in three-dimensional culture systems: where to now? *Journal of Biology* 9: 2.

Itoh M, Nagafuchi A, Moroi S, and Tsukita S. (1997). Involvement of ZO-1 in Cadherin-based Cell Adhesion through Its Direct Binding to α Catenin and Actin Filaments. *The Journal of Cell Biology* 138: 181 -192.

Janmey PA, and McCulloch CA. (2007). Cell Mechanics: Integrating Cell Responses to Mechanical Stimuli. *Annu. Rev. Biomed. Eng.* 9: 1-34.

Janmey PA, Winer JP, Murray ME, and Wen Q. (2009). The hard life of soft cells. *Cell Motility and the Cytoskeleton* 66: 597-605.

Käfer J, Hayashi T, Marée AFM, Carthew RW, and Graner F. (2007). Cell adhesion and cortex contractility determine cell patterning in the Drosophila retina. *Proc. Natl. Acad. Sci. U.S.A* 104: 18549-18554.

Kasza KE, Rowat AC, Liu J, Angelini TE, Brangwynne CP, Koenderink GH, et al. (2007). The cell as a material. *Current Opinion in Cell Biology* 19: 101-107.

Keely PJ, Conklin MW, Gehler S, Ponik SM, and Provenzano PP. (2007). Investigating integrin regulation and signaling events in three-dimensional systems. *Meth. Enzymol* 426: 27-45.

Kumar S, Maxwell I, Heisterkamp A, Polte T, Lele T, Salanga M, et al. (2006). Viscoelastic Retraction of Single Living Stress Fibers and Its Impact on Cell Shape, Cytoskeletal Organization, and Extracellular Matrix Mechanics. *Biophysical Journal* 90: 3762-3773.

Ladoux B, Anon E, Lambert M, Rabodzey A, Hersen P, Buguin A, et al. (2010). Strength Dependence of Cadherin-Mediated Adhesions. *Biophysical Journal* 98: 534-542.

Lambrechts A, Gevaert K, Cossart P, Vandekerckhove J, and Van Troys M. (2008). Listeria comet tails: the actin-based motility machinery at work. *Trends in Cell Biology* 18: 220-227.

Landau L. (2006). Theory of elasticity. 3rd ed. Amsterdam ;;Heidelberg: Elsevier Butterworth-Heinemann.

Landsberg KP, Farhadifar R, Ranft J, Umetsu D, Widmann TJ, Bittig T, et al. (2009). Increased Cell Bond Tension Governs Cell Sorting at the Drosophila Anteroposterior Compartment Boundary. *Current Biology* 19: 1950-1955.

Larsen M, Artym VV, Green JA, and Yamada KM. (2006). The matrix reorganized: extracellular matrix remodeling and integrin signaling. *Current Opinion in Cell Biology* 18: 463-471.

Lechler T, and Fuchs E. (2007). Desmoplakin: an unexpected regulator of microtubule organization in the epidermis. *The Journal of Cell Biology* 176: 147 -154.

Lecuit T, and Lenne P-F. (2007). Cell surface mechanics and the control of cell shape, tissue patterns and morphogenesis. *Nat Rev Mol Cell Biol* 8: 633-644.

Lewis J. (1995). Fast normalized cross-correlation. In: Vision Interface. Canadian Image Processing and Pattern Recognition Society. p 120-123. Available from: http://citeseerx.ist.psu.edu/viewdoc/summary?doi=10.1.1.21.6062

Liu Z, Tan JL, Cohen DM, Yang MT, Sniadecki NJ, Ruiz SA, et al. (2010). Mechanical tugging force regulates the size of cell–cell junctions. *Proceedings of the National Academy of Sciences* 107: 9944 -9949.

Loh O, Vaziri A, and Espinosa HD. (2007). The Potential of MEMS for Advancing Experiments and Modeling in Cell Mechanics. *Exp Mech* 49: 105-124.

Ludwig T, Kirmse R, Poole K, and Schwarz US. (2007). Probing cellular microenvironments and tissue remodeling by atomic force microscopy. *Pflugers Arch - Eur J Physiol* 456: 29-49.

Mao Y, and Schwarzbauer JE. (2005). Stimulatory effects of a three-dimensional microenvironment on cell-mediated fibronectin fibrillogenesis. *J Cell Sci* 118: 4427-4436.

Martin-Belmonte F, Gassama A, Datta A, Yu W, Rescher U, Gerke V, et al. (2007). PTEN-Mediated Apical Segregation of Phosphoinositides Controls Epithelial Morphogenesis through Cdc42. *Cell* 128: 383-397.

Martinez-Rico C, Pincet F, Perez E, Thiery JP, Shimizu K, Takai Y, et al. (2005). Separation Force Measurements Reveal Different Types of Modulation of E-cadherin-based Adhesion by Nectin-1 and -3. *Journal of Biological Chemistry* 280: 4753 -4760.

Maruthamuthu V, Sabass B, Schwarz US, and Gardel ML. (2011). Cell-ECM traction force modulates endogenous tension at cell–cell contacts. *Proceedings of the National Academy of Sciences* 108: 4708 -4713.

Mège R-M, Gavard J, and Lambert M. (2006). Regulation of cell-cell junctions by the cytoskeleton. *Current Opinion in Cell Biology* 18: 541-548.

Meng W, Mushika Y, Ichii T, and Takeichi M. (2008). Anchorage of Microtubule Minus Ends to Adherens Junctions Regulates Epithelial Cell-Cell Contacts. *Cell* 135: 948-959.

Mitic LL, and Anderson JM. (1998). MOLECULAR ARCHITECTURE OF TIGHT JUNCTIONS. *Annu. Rev. Physiol.* 60: 121-142.

Mogensen MM, Malik A, Piel M, Bouckson-Castaing V, and Bornens M. (2000). Microtubule minus-end anchorage at centrosomal and non-centrosomal sites: the role of ninein. *J. Cell. Sci* 113 (Pt 17): 3013-3023.

Mogensen MM. (2005). Microtubule Organizing Centers in Polarized Epithelial Cells. In: Centrosomes in Development and Disease. Wiley-VCH Verlag GmbH & Co. KGaA. p 299–319. Available from: http://dx.doi.org/10.1002/3527603808.ch15

Munevar S, Wang Y-li, and Dembo M. (2001). Traction Force Microscopy of Migrating Normal and H-ras Transformed 3T3 Fibroblasts. *Biophysical Journal* 80: 1744-1757.

Nagato T, Yoshida H, Yoshida A, and Uehara Y. (1980). A scanning electron microscope study of myoepithelial cells in exocrine glands. *Cell Tissue Res. [Internet]* 209. Available from: http://www.springerlink.com.gate1.inist.fr/content/kw678h46m0347h32/

Ndlec FJ, Surrey T, Maggs AC, and Leibler S. (1997). Self-organization of microtubules and motors. *Nature* 389: 305-308.

Nelson WJ. (2008). Regulation of cell-cell adhesion by the cadherin-catenin complex. *Biochem. Soc. Trans* 36: 149-155.

Nelson WJ. (2009). Remodeling Epithelial Cell Organization: Transitions Between Front–Rear and Apical–Basal Polarity. *Cold Spring Harbor Perspectives in Biology [Internet]* 1. Available from: http://cshperspectives.cshlp.org/content/1/1/a000513.abstract

Neumann B, Held M, Liebel U, Erfle H, Rogers P, Pepperkok R, et al. (2006). High-throughput RNAi screening by time-lapse imaging of live human cells. *Nat Meth* 3: 385-390.

Neumann B, Walter T, Hériché J-K, Bulkescher J, Erfle H, Conrad C, et al. (2010). Phenotypic profiling of the human genome by time-lapse microscopy reveals cell division genes. *Nature* 464: 721-727.

Nichols SA, Dirks W, Pearse JS, and King N. (2006). Early evolution of animal cell signaling and adhesion genes. *Proceedings of the National Academy of Sciences* 103: 12451 -12456.

Nigg EA, and Raff JW. (2009). Centrioles, Centrosomes, and Cilia in Health and Disease. *Cell* 139: 663-678.

O'Brien LE, Jou T-S, Pollack AL, Zhang Q, Hansen SH, Yurchenco P, et al. (2001). Rac1 orientates epithelial apical polarity through effects on basolateral laminin assembly. *Nat Cell Biol* 3: 831-838.

Ohno S. (2001). Intercellular junctions and cellular polarity: the PAR-aPKC complex, a conserved core cassette playing fundamental roles in cell polarity. *Current Opinion in Cell Biology* 13: 641-648.

Parker KK, Brock AL, Brangwynne C, Mannix RJ, Wang N, Ostuni E, et al. (2002). Directional control of lamellipodia extension by constraining cell shape and orienting cell tractional forces. *FASEB J* 16: 1195-1204.

Pasdar M, and Nelson WJ. (1988). Kinetics of desmosome assembly in Madin-Darby canine kidney epithelial cells: temporal and spatial regulation of desmoplakin organization and stabilization upon cell-cell contact. II. Morphological analysis. *The Journal of Cell Biology* 106: 687 -695.

Paszek MJ, and Weaver VM. (2004). The Tension Mounts: Mechanics Meets Morphogenesis and Malignancy. *J Mammary Gland Biol Neoplasia* 9: 325-342.

Pelham RJ, and Wang Y-li. (1997). Cell locomotion and focal adhesions are regulated by substrate flexibility. *Proceedings of the National Academy of Sciences of the United States of America* 94: 13661-13665.

Perez-Moreno M, and Fuchs E. (2006). Catenins: Keeping Cells from Getting Their Signals Crossed. *Developmental Cell* 11: 601-612.

Perez-Moreno M, Jamora C, and Fuchs E. (2003). Sticky Business: Orchestrating Cellular Signals at Adherens Junctions. *Cell* 112: 535-548.

Peskin CS, Odell GM, and Oster GF. (1993). Cellular motions and thermal fluctuations: the Brownian ratchet. *Biophysical Journal* 65: 316-324.

Pitaval A, Tseng Q, Bornens M, and Théry M. (2010). Cell shape and contractility regulate ciliogenesis in cell cycle–arrested cells. *The Journal of Cell Biology* 191: 303 -312.

Pitelka DR, Hamamoto ST, Duafala JG, and Nemanic MK. (1973). CELL CONTACTS IN THE MOUSE MAMMARY GLAND. *The Journal of Cell Biology* 56: 797 -818.

Pollard TD, and Borisy GG. (2003). Cellular Motility Driven by Assembly and Disassembly of Actin Filaments. *Cell* 112: 453-465.

Puech P-H, Poole K, Knebel D, and Muller DJ. (2006). A new technical approach to quantify cell-cell adhesion forces by AFM. *Ultramicroscopy* 106: 637-644.

Radola BJ. (1980). Ultrathin-layer isoelectric focusing in 50-100 μm polyacrylamide gels on silanized glass plates or polyester films. *Electrophoresis* 1: 43-56.

Raff JW, and Glover DM. (1989). Centrosomes, and not nuclei, initiate pole cell formation in Drosophila embryos. *Cell* 57: 611-619.

Rauzi M, Verant P, Lecuit T, and Lenne P-F. (2008). Nature and anisotropy of cortical forces orienting Drosophila tissue morphogenesis. *Nat. Cell Biol* 10: 1401-1410.

Retta SF, Balzac F, and Avolio M. (2006). Rap1: A turnabout for the crosstalk between cadherins and integrins. *European Journal of Cell Biology* 85: 283-293.

Revenu C, and Gilmour D. (2009). EMT 2.0: shaping epithelia through collective migration. *Current Opinion in Genetics & Development* 19: 338-342.

Riveline D, Zamir E, Balaban NQ, Schwarz US, Ishizaki T, Narumiya S, et al. (2001). Focal Contacts as Mechanosensors: Externally Applied Local Mechanical Force Induces Growth of Focal Contacts by an Mdia1-Dependent and Rock-Independent Mechanism. *J. Cell Biol.* 153: 1175-1186.

Rodriguez-Boulan E, Kreitzer G, and Musch A. (2005). Organization of vesicular trafficking in epithelia. *Nat Rev Mol Cell Biol* 6: 233-247.

Rohatgi R, and Snell WJ. (2010). The ciliary membrane. *Current Opinion in Cell Biology* 22: 541-546.

de Rooij J, Kerstens A, Danuser G, Schwartz MA, and Waterman-Storer CM. (2005). Integrin-dependent actomyosin contraction regulates epithelial cell scattering. *J. Cell Biol.* 171: 153-164.

Rozario T, and DeSimone DW. (2010). The extracellular matrix in development and morphogenesis: A dynamic view. *Developmental Biology* 341: 126-140.

Saez A, Anon E, Ghibaudo M, du Roure O, Di Meglio J-M, Hersen P, et al. (2010). Traction forces exerted by epithelial cell sheets. *J. Phys.: Condens. Matter* 22: 194119.

Sage D, Neumann FR, Hediger F, Gasser SM, and Unser M. (2005). Automatic tracking of individual fluorescence particles: application to the study of chromosome dynamics. *IEEE Trans. on Image Process.* 14: 1372-1383.

Saraste J, and Goud B. (2007). Functional Symmetry of Endomembranes. *Mol. Biol. Cell* 18: 1430-1436.

Satir P, and Christensen ST. (2007). Overview of Structure and Function of Mammalian Cilia. *Annu. Rev. Physiol.* 69: 377-400.

Schliwa M, and Woehlke G. (2003). Molecular motors. *Nature* 422: 759-765.

Schwartz MA, and Horwitz AR. (2006). Integrating Adhesion, Protrusion, and Contraction during Cell Migration. *Cell* 125: 1223-1225.

Shin K, Fogg VC, and Margolis B. (2006). Tight Junctions and Cell Polarity. *Annu. Rev. Cell Dev. Biol.* 22: 207-235.

von Stein W, Ramrath A, Grimm A, Müller-Borg M, and Wodarz A. (2005). Direct association of Bazooka/PAR-3 with the lipid phosphatase PTEN reveals a link between the PAR/aPKC complex and phosphoinositide signaling. *Development* 132: 1675-1686.

Steinberg MS. (1963). Reconstruction of Tissues by Dissociated Cells. *Science* 141: 401 -408.

Streuli CH, Schmidhauser C, Bailey N, Yurchenco P, Skubitz AP, Roskelley C, et al. (1995). Laminin mediates tissue-specific gene expression in mammary epithelia. *The Journal of Cell Biology* 129: 591 -603.

Suzuki A, Ishiyama C, Hashiba K, Shimizu M, Ebnet K, and Ohno S. (2002). aPKC kinase activity is required for the asymmetric differentiation of the premature junctional complex during epithelial cell polarization. *J Cell Sci* 115: 3565-3573.

Théry M, Pépin A, Dressaire E, Chen Y, and Bornens M. (2006). Cell distribution of stress fibres in response to the geometry of the adhesive environment. *Cell Motility and the Cytoskeleton* 63: 341-355.

Théry M, and Piel M. (2009). Adhesive micropatterns for cells: a microcontact printing protocol. *Cold Spring Harb Protoc* 2009: pdb.prot5255.

Théry M. (2010). Micropatterning as a tool to decipher cell morphogenesis and functions. *J. Cell. Sci* 123: 4201-4213.

Thiery JP, Acloque H, Huang RYJ, and Nieto MA. (2009). Epithelial-Mesenchymal Transitions in Development and Disease. *Cell* 139: 871-890.

Thiery JP. (2003). Epithelial-mesenchymal transitions in development and pathologies. *Current Opinion in Cell Biology* 15: 740-746.

Thiery JP. (2002). Epithelial-mesenchymal transitions in tumour progression. *Nat Rev Cancer* 2: 442-454.

Thompson d'Arcy W. (1917). On growth and form. Cambridge University Press.

Tolić-Nørrelykke IM. (2008). Push-me-pull-you: how microtubules organize the cell interior. *Eur Biophys J* 37: 1271-1278.

Trepat X, Wasserman MR, Angelini TE, Millet E, Weitz DA, Butler JP, et al. (2009). Physical forces during collective cell migration. *Nat Phys* 5: 426-430.

Ueda M, Gräf R, MacWilliams HK, Schliwa M, and Euteneuer U. (1997). Centrosome positioning and directionality of cell movements. *Proceedings of the National Academy of Sciences* 94: 9674 -9678.

Vogel A, Noack J, Hüttman G, and Paltauf G. (2007). Femtosecond Plasma-Mediated Nanosurgery of Cells and Tissues. In: Phipps C, editor. Laser Ablation and its Applications. Vol. 129. Springer Series in Optical Sciences. Springer Berlin / Heidelberg. p 231-280.

Wang N, Ostuni E, Whitesides GM, and Ingber DE. (2002). Micropatterning tractional forces in living cells. *Cell Motil. Cytoskeleton* 52: 97-106.

Wang Y, Jin G, Miao H, Li JY-S, Usami S, and Chien S. (2006). Integrins regulate VE-cadherin and catenins: Dependence of this regulation on Src, but not on Ras. *Proceedings of the National Academy of Sciences of the United States of America* 103: 1774 -1779.

Warner SJ, and Longmore GD. (2009). Cdc42 antagonizes Rho1 activity at adherens junctions to limit epithelial cell apical tension. *The Journal of Cell Biology* 187: 119 -133.

Watanabe T, Sato K, and Kaibuchi K. (2009). Cadherin-mediated Intercellular Adhesion and Signaling Cascades Involving Small GTPases. *Cold Spring Harb Perspect Biol* 1.

Watt FM, Jordan PW, and O'Neill CH. (1988). Cell shape controls terminal differentiation of human epidermal keratinocytes. *Proceedings of the National Academy of Sciences of the United States of America* 85: 5576 -5580.

Weber GF, Bjerke MA, and DeSimone DW. (2011). Integrins and cadherins join forces to form adhesive networks. *J Cell Sci* 124: 1183-1193.

Wozniak MA, Desai R, Solski PA, Der CJ, and Keely PJ. (2003). ROCK-generated contractility regulates breast epithelial cell differentiation in response to the physical properties of a three-dimensional collagen matrix. *The Journal of Cell Biology* 163: 583 -595.

Wu Y, Jin X, Harrison O, Shapiro L, Honig BH, and Ben-Shaul A. (2010). Cooperativity between trans and cis interactions in cadherin-mediated junction formation. *Proceedings of the National Academy of Sciences* 107: 17592 -17597.

Yamada KM, and Cukierman E. (2007).(a). Modeling Tissue Morphogenesis and Cancer in 3D. *Cell* 130: 601-610.

Yamada S, and Nelson WJ. (2007).(b). Localized zones of Rho and Rac activities drive initiation and expansion of epithelial cell–cell adhesion. *J Cell Biol* 178: 517-527.

Yamada S, Pokutta S, Drees F, Weis WI, and Nelson WJ. (2005). Deconstructing the Cadherin-Catenin-Actin Complex. *Cell* 123: 889-901.

Yang J, and Weinberg RA. (2008). Epithelial-Mesenchymal Transition: At the Crossroads of Development and Tumor Metastasis. *Developmental Cell* 14: 818-829.

Yano H, Mazaki Y, Kurokawa K, Hanks SK, Matsuda M, and Sabe H. (2004). Roles played by a subset of integrin signaling molecules in cadherin-based cell–cell adhesion. *The Journal of Cell Biology* 166: 283 -295.

Yap AS, Brieher WM, Pruschy M, and Gumbiner BM. (1997). Lateral clustering of the adhesive ectodomain: a fundamental determinant of cadherin function. *Curr. Biol* 7: 308-315.

Yeaman C, Grindstaff KK, Hansen MDH, and Nelson WJ. (1999). Cell polarity: Versatile scaffolds keep things in place. *Current Biology* 9: R515-R517.

Yonemura S, Wada Y, Watanabe T, Nagafuchi A, and Shibata M. (2010). [alpha]-Catenin as a tension transducer that induces adherens junction development. *Nat Cell Biol 12: 533-542.*

Yu W, Datta A, Leroy P, O'Brien LE, Mak G, Jou T-S, et al. (2005). {beta}1-Integrin Orients Epithelial Polarity via Rac1 and Laminin. *Mol. Biol. Cell* 16: 433-445.

Zhang H, Landmann F, Zahreddine H, Rodriguez D, Koch M, and Labouesse M. (2011). A tension-induced mechanotransduction pathway promotes epithelial morphogenesis. *Nature* 471: 99-103.

Zhu J, Burakov A, Rodionov V, and Mogilner A. (2010). Finding the Cell Center by a Balance of Dynein and Myosin Pulling and Microtubule Pushing: A Computational Study. *Mol. Biol. Cell* 21: 4418-4427.

Yano H, Mazaki Y, Kurokawa K, Hanks SK, Matsuda M, and Sabe H. (2004). Roles played by a subset of integrin signaling molecules in cadherin-based cell–cell adhesion. *The Journal of Cell Biology* 166: 283 -295.

Yap AS, Brieher WM, Pruschy M, and Gumbiner BM. (1997). Lateral clustering of the adhesive ectodomain: a fundamental determinant of cadherin function. *Curr. Biol* 7: 308-315.

Yeaman C, Grindstaff KK, Hansen MDH, and Nelson WJ. (1999). Cell polarity: Versatile scaffolds keep things in place. *Current Biology* 9: R515-R517.

Yonemura S, Wada Y, Watanabe T, Nagafuchi A, and Shibata M. (2010). [alpha]-Catenin as a tension transducer that induces adherens junction development. *Nat Cell Biol 12: 533-542.*

Yu W, Datta A, Leroy P, O'Brien LE, Mak G, Jou T-S, et al. (2005). {beta}1-Integrin Orients Epithelial Polarity via Rac1 and Laminin. *Mol. Biol. Cell* 16: 433-445.

Zhang H, Landmann F, Zahreddine H, Rodriguez D, Koch M, and Labouesse M. (2011). A tension-induced mechanotransduction pathway promotes epithelial morphogenesis. *Nature* 471: 99-103.

Zhu J, Burakov A, Rodionov V, and Mogilner A. (2010). Finding the Cell Center by a Balance of Dynein and Myosin Pulling and Microtubule Pushing: A Computational Study. *Mol. Biol. Cell* 21: 4418-4427.

Introduction Générale *(French version)*

L'une des caractéristiques les plus remarquables des organismes multicellulaires est l'orchestration des processus de différenciation avec les mouvements morphogénétiques au cours de la formation des organes. La réalisation et le maintien de telles organisations régulières au cours du développement embryonnaire et du renouvellement des tissus adultes, sont toujours des sujets fascinants.

L'épithélium est considéré comme le tissu le plus ancien. Il est apparu précocement chez les premiers animaux (Nichols et al., 2006). L'adhérence des cellules entres elles et la polarisation des cellules sont les caractéristiques essentielles des épithélia. Elles permettent la formation d'interfaces fonctionnels entre les tissus internes et l'extérieur du corps de l'animal ainsi que le transport orienté des composés solubles (Cereijido et al., 2004). Dans les métazoaires complexes, l'épithélium participe à différentes fonctions comme la digestion, la reproduction, l'excrétion, et la sécrétion des hormones. Les épithéliums peuvent adopter de multiples morphologies plus ou moins stratifiées au sein desquels les cellules peuvent avoir des formes cuboïdales ou très allongées. Ils sont généralement constitués de motifs réguliers, notamment dans le cas de la rétine de Drosophile ou la structure tubulaire de nos reins. Les mécanismes de la morphogenèse des épithélia et de la formation de ces motifs sont des sujets intrigants en biologie comme en physique.

La morphogenèse épithéliale est souvent étudiée sur des embryons d'insectes, de vers ou de poissons. Dans ces systèmes expérimentaux, la machinerie naturelle des mécanismes morphogénétiques est intacte. De plus, les outils génétiques propres à certains organismes modèles ont facilité l'identification des composants des réseaux moléculaires impliqués dans la morphogenèse épithéliale. Cependant, la complexité de ces organismes entiers ne permet pas d'avoir un contrôle précis des paramètres expérimentaux, sans parler du coût, de la difficulté du travail et des problèmes éthique liés à l'emploi de certains embryons, ceux de mammifères en particulier.

La culture cellulaire offre un système expérimental simplifié. Bien que les cellules soient maintenues dans des conditions très différentes de celles rencontrées au sein des tissus, la maîtrise complète des paramètres expérimentaux en fait un modèle de travail

intéressant. De plus, elle permet de réduire largement les inconvénients de l'entretien, de la manipulation et de l'imagerie des organismes vivants.

Le micropatterning des protéines de la matrice extra-cellulaire permet de manipuler la distribution spatiale des interactions des cellules avec la matrice extra-cellulaire, ainsi que la forme des cellules. En réponse à des conditions limites identiques les comportements cellulaires deviennent plus reproductibles ce qui permet d'effectuer des analyses statistiques plus fiables.

L'objectif de ces travaux est d'utiliser le contrôle géométrique du microenvironnement des cellules afin d'étudier les mécanismes de régulation de l'architecture des épithélia. La modulation fine des positions des adhérences cellule-matrice et cellule-cellule devrait nous permettre de voir sous un jour nouveau les mécanismes biochimiques et mécaniques impliqués dans la morphogenèse des épithélia.

Conclusion *(French version)*

Cette étude nous a permis d'identifier un rôle majeur de la matrice extra-cellulaire dans la construction de l'architecture des épithélia. En contrôlant précisément la géométrie des interactions entre les cellules et la matrice extracellulaire, nous avons observé que la jonction cellule-cellule se plaçait systématiquement sur les zones les moins riches en matrice. Cette exclusion spatiale entre les deux systèmes d'adhérence provoque ensuite une réorganisation des compartiments internes de la cellule. De façon reproductible, dans les cellules épithéliales, on observe que le centrosome se positionne vers les jonctions cellule-cellule qui sont stabilisées à distance des adhérences cellule-matrice. Enfin, l'étude de la réorganisation de la structure des épithélium au cours de la transition épithélio-mesenchymateuse nous a montré que l'exclusion spatiales des deux systèmes d'adhérences et l'orientation de la polarité interne vers les jonctions cellule-cellule pouvaient être modifiés ensemble ou séparément selon la nature du stimulus induisant la transition.

L'utilisation de nouvelles techniques de biophysique nous a permis d'enrichir notre description des mécanismes de construction des épithélia. Les paramètres physiques comme le niveau de contractilité d'une cellule ou la distribution spatiale des forces sont difficiles à évaluer de façon quantitative par une simple observation. Néanmoins, la manipulation de la géométrie d'adhérence, les mesures des forces de traction, l'ablation laser, et les simulations numériques rendent ces paramètres plus perceptibles. Ensemble, nos résultats, et ceux d'autres laboratoires, confirme le rôle déterminant joué par les contraintes mécanique au cours de la morphogenèse épithéliale. Ces forces sont régulées avec précision en réponse à la géométrie des adhérences à la matrice extra-cellulaire et à la forme des cellules. Les forces de tension appliquées perpendiculairement aux jonctions inter-cellulaires sont plus importantes lorsque ces jonctions sont placées à proximité de la matrice extra-cellulaire. Dans un édifice multicellulaire stable, les forces interne sont donc distribuées de façon très anisotropes. Les forces de traction intra-cellulaires sont élevées au-dessus de la matrice extra-cellulaire et les forces de tension inter-cellulaires sont faibles au dessus des zones où la matrice est absente. La distribution anisotrope des forces au sein des cellules est donc profondément impliquée dans la morphologie de l'épithélium ainsi que l'équilibre mécanique de l'architecture multicellulaire.

Conclusion (French version)

Les nouveaux développements méthodologiques on eu un rôle majeur dans cette étude. Le micropatterning des supports souples nous a permis de contrôler à la fois la rigidité et la géométrie du microenvironnement des cellules. Il a aussi facilité et amélioré l'analyse des forces de traction. L'automatisation de l'analyse des images offre la possibilité de travailler sur des dizaines de milliers d'images et d'en extraire rapidement des mesures quantitatives. Le transfert de ces méthodes dans le domaine publique, à l'aide d'Image J, permettra à tous les chercheurs interessés par les mesures de force de les effectuer eux-mêmes sans connaissances spécifiques. Enfin, ces outils et tous ceux qui ont été développés pour automatiser l'acquisition et l'analyse des images ont permis de réduire considérablement les taches répétitives et de normaliser les méthodes de mesures, ce qui devrait constituer une base importante pour le futur de l'analyse quantitative en biologie cellulaire.